

Alfred-Wegener-Institut für Polar- und Meeresforschung
– Forschungsstelle Potsdam –
Arbeitsgruppe ‚Periglazialforschung‘

**Late Quaternary environmental dynamics
of the western Canadian Arctic**
– Permafrost and lake sediment archives at the eastern Beringian edge –

**Kumulative Dissertation
zur Erlangung des akademischen Grades
"doctor rerum naturalium"
(Dr. rer. nat.)
in der Wissenschaftsdisziplin "Terrestrische Geowissenschaften"**

**eingereicht an der
Mathematisch-Naturwissenschaftlichen Fakultät
der Universität Potsdam**

**von
Michael Fritz**

Potsdam, 18. Oktober 2011

Table of content

Abstract	iv
Kurzfassung.....	vi
1 Introduction.....	1
1.1 Motivation.....	1
1.2 Scientific background	2
1.2.1 Beringian environments in time and space	2
1.2.2 The eastern Beringian edge.....	6
1.2.3 Permafrost as environmental archive.....	7
1.2.4 Ground ice as environmental archive.....	8
1.2.5 Arctic lake sediments as environmental archive.....	11
1.3 Aims and approaches	12
1.4 Thesis organization	13
1.4.1 Overview of chapters	13
1.4.2 Authors' contributions	15
2 At the eastern Beringian edge: Late Wisconsinan and Holocene landscape dynamics along the Yukon Coastal Plain, Canada	17
Abstract	17
2.1 Introduction.....	18
2.2 Study area	19
2.3 Material and methods.....	23
2.4 Results.....	25
2.4.1 Litho- and cryostratigraphic properties.....	25
2.4.2 Geochronology.....	31
2.4.3 Ground ice.....	33
2.4.4 Ostracod studies at Komakuk Beach	36
2.5 Discussion.....	37
2.5.1 Late Wisconsinan landscape evolution.....	37
2.5.2 Early Holocene Thermal Maximum	41
2.5.3 Middle and late Holocene permafrost aggradation	43
2.6 Conclusions.....	44
Acknowledgements	45

3	Origin and characteristics of massive ground ice on Herschel Island (western Canadian Arctic) as revealed by stable water isotope and hydrochemical signatures.....	46
	Abstract	46
3.1	Introduction.....	47
3.2	Study site.....	48
3.3	Material and methods.....	50
	3.3.1 Stable water isotope geochemistry.....	50
	3.3.2 Hydrochemistry	50
3.4	Results.....	51
	3.4.1 TSD exposure	51
	3.4.2 HIW exposure	55
3.5	Discussion.....	58
	3.5.1 Origin of TSD massive ice (Unit A).....	58
	3.5.2 Origin of HIW massive ice	60
3.6	Conclusions.....	63
	Acknowledgements	64
	Supplementary material.....	65
4	Late glacial and Holocene sedimentation, vegetation, and temperature history from easternmost Beringia (Northern Yukon Territory, Canada)	66
	Abstract	66
4.1	Introduction.....	67
4.2	Study site and regional setting	68
4.3	Material and methods.....	69
	4.3.1 Coring and on-site sampling	69
	4.3.2 Geochronology.....	70
	4.3.3 Sediment properties	70
	4.3.4 Pollen treatment and numerical methods	72
4.4	Results.....	73
	4.4.1 Modern limnology	73
	4.4.2 Chronostratigraphy and sediment properties	73
	4.4.3 Pollen	77
4.5	Discussion.....	81
	4.5.1 Formation and development of Trout Lake in ice-marginal east Beringia	81

4.5.2 Environmental change during the late glacial–Holocene transition (~16 to 11.6 cal ka BP)	82
4.5.3 Environmental development since the early Holocene (11.5 cal ka BP to present)	84
4.6 Conclusions.....	86
Acknowledgements	87
5 Synthesis	88
5.1 Main results in a Beringian context	89
5.1.1 Glacial chronology.....	89
5.1.2 Depositional environments	91
5.1.3 Changes in hydrology and moisture.....	92
5.1.4 Ground ice development and climatic implications.....	94
5.1.5 Vegetation and temperature history	97
5.2 Potentials and limitations of the studied paleoenvironmental archives within and beyond the eastern Beringian edge	99
5.2.1 Permafrost and ground-ice archives.....	99
5.2.2 Lake sediment archives.....	102
5.3 Outlook	103
6 Bibliography	105
Acknowledgements.....	120

Abstract

Arctic regions are highly vulnerable to climatic change and are currently undergoing the most rapid environmental transition experienced on Earth, at a pace that is expected to increase over the coming decades. Instrumental records of environmental variability do not exceed the last 200 years and are therefore much too short to assess the full range of climate variability, its causes and interactions. Consequently, paleoenvironmental archives with longer datasets play a key role in our understanding of the Earth's past climate system in order to better understand current processes and to estimate future changes. *Beringia*, the continuous and unglaciated land mass between the Eurasian and North American ice sheets of the Pleistocene provides terrestrial records of natural environmental change beyond the last glacial–interglacial transition. Moreover, the eastern Beringian edge offers the possibility to comparing paleoenvironmental information of landscape development within and beyond the former ice margin in the direct proximity to the Arctic Ocean, as the major climatic module in the Arctic system.

This study seeks to reconstruct the late Quaternary environmental dynamics within and beyond the eastern margin of Beringia in the northernmost part of the Yukon Territory (Canada). Lake sediments, permafrost sequences and sub-surface ground ice within frozen deposits were investigated as paleoenvironmental archives to get an encompassing view of regional landscape genesis, with particular emphasis on permafrost and ground-ice development, and on changes in temperature and moisture conditions over time. Methods are based upon a multi-proxy approach that combines field observations, paleoecological studies, laboratory analyses of sediments and ground ice and statistics. Absolute dating methods provide chronological control in order to relate environmental changes to the stratigraphical context.

Few environmental records have been preserved along the Yukon Coastal Plain accounting on full-glacial conditions of the late Wisconsin. A lobe of the Laurentide Ice Sheet (LIS) approaching its terminal position deposited ice-thrust material to form a system of push moraines that is today partly represented by Herschel Island (69°36'N, 139°04'W) in the southern Beaufort Sea. Radiocarbon dates of permafrost and lake sediments suggest that deglaciation of the northern Yukon commenced at ~16 cal ka BP. With the help of stable water isotope analyses and hydrochemical measures, large massive ground-ice bodies and ice-rich sediments were characterized and identified to have a glacial origin, either as buried glacier ice or refrozen meltwater. Substantially colder than modern air temperatures (i.e. glacial conditions) during ice formation are inferred by $\delta^{18}\text{O}$ values below -30‰ . Beyond the ice margin, east Beringian landscapes were strongly influenced by the proximity of the LIS, which had a direct cooling effect and caused widespread aridity due to katabatic winds and a stable high pressure system over the LIS. Fossil pollen spectra contained in lake sediments from Trout Lake (68°50'N, 138°45'W;

163 m asl) indicate a sparse graminoid-herb tundra and bear witness of harsh and dry climate conditions during the latest part of the Wisconsin. Lake development in east Beringia was inhibited until glacial meltwater input and atmospheric moisture availability increased. Permafrost and ground ice re-aggraded after the ice had retreated in formerly glaciated areas. Thermal contraction cracking led to the formation of ice wedges, which exhibit an oxygen isotope signature below -26‰ . This implies still cold climate conditions and suggests in combination with low deuterium excess values ($\leq 1.7\text{‰}$) sustained dry conditions and/or different moisture pathways than today.

The transition from the last glacial period to the Holocene brought along wholesale changes in climate mode and environmental response. However the spatial-temporal characteristics across *Beringia* are still poorly understood. Pollen-derived quantitative temperature reconstructions indicate summer air temperatures up to 10°C and a rapid warming during the Bølling/Allerød interstadial (14.7–13.0 cal ka BP) in response to increasing summer insolation and a waning ice sheet. Climate amelioration during this interstadial was followed by a distinct cold reversal during the Younger Dryas (12.9–11.6 cal ka BP), which had not been reported for the northern Yukon so far. Younger Dryas cooling might have also been responsible for the first phase of ice-wedge growth along the formerly glaciated Yukon coast. Permafrost aggradation and ice-wedge formation were interrupted by higher than modern summer temperatures during the early Holocene thermal maximum ($\sim 11\text{--}7$ cal ka BP) that was driven by a summer insolation maximum based on changes in orbital parameters. Deep thaw up to ~ 1.5 m below the modern surface and well below the base of the modern active layer due to increasing air temperatures caused a regional thaw unconformity and a truncation of cryostrucures. Melt-out of ice wedges and increased thermokarst activity were accompanied by rapid peat growth and the infill of ice-wedge casts with lacustrine deposits dating to the early Holocene. A stable sedimentation history during the Holocene on flat and low-lying tundra areas are faced with very dynamic depositional environments in high-relief areas on Herschel Island in connection with retrogressive thaw slumping and coastal erosion. The available moisture increased during the middle Holocene in the northern Yukon in response to postglacial sea level rise and decreasing summer insolation, while the latter led to an extensive renewal of permafrost and ground-ice aggradation with oxygen-isotope signatures above -25‰ . Waterlogging and increased moisture favored the establishment of an alder-birch shrub tundra over the last 5000 years. The combination of results from permafrost, ground ice and palynological studies indicate a conversion of a continental Beringian landscape into a coastal-maritime environment near the Beaufort Sea.

This study highlights that landscape and environmental change in ice-marginal east Beringia is strongly dependent on its glacial and periglacial history. The past, present and future dynamics of this Arctic region are closely tied to the interactions between permafrost, vegetation, and sea-level history in response to climate change.

Kurzfassung

Arktische Regionen reagieren besonders empfindlich auf Klimaänderungen und erfahren derzeit die schnellsten Umweltveränderungen auf der Erde, und zwar in einem Tempo, das voraussichtlich in den kommenden Jahrzehnten zunehmen wird. Messreihen zur Umweltvariabilität gehen nicht über die letzten 200 Jahre hinaus und sind damit zu kurz, um das gesamte Spektrum der Klimavariabilität, dessen Ursachen und Wechselwirkungen beurteilen zu können. Folglich spielen Paläoumweltarchive mit längerfristigen Datenreihen eine Schlüsselrolle in unserem Verständnis über das Klimasystem in der Vergangenheit, die es erst ermöglichen, gegenwärtige Prozesse besser zu verstehen und zukünftige Änderungen abzuschätzen. Zwischen den eurasischen und nordamerikanischen Eisschilden des Pleistozäns existierte eine unvergletscherte und kontinuierliche Landmasse, die als *Beringia* bezeichnet wird. Dieser Großraum ist reich an Paläoumweltarchiven, die die Rekonstruktion natürlicher Umweltveränderungen über den Zeitraum des letzten Glazial-Interglazial-Zyklus hinaus zulassen. Darüber hinaus ermöglicht die Untersuchung der östlichen Randzone Beringias den Vergleich von Paläoumweltinformationen hinsichtlich der Landschaftsentwicklung innerhalb und außerhalb der ehemaligen Eisrandlage, in unmittelbarer Nähe zum Arktischen Ozean – der dominierenden Steuergröße im arktischen System.

Ziel der vorliegenden Arbeit ist es, die spätquartäre Umweltdynamik dies- und jenseits der östlichen Grenze Beringias zu rekonstruieren. Permafrostsequenzen sowie darin eingeschlossenes Grundeis und Seesedimente sind als Paläoumweltarchive im nördlichsten Teil des Yukon Territoriums (Kanada) untersucht worden, um ein umfassendes Bild der regionalen Landschaftsentwicklung zu gewinnen. Besondere Schwerpunkte lagen dabei auf der Permafrost- und Grundeisentwicklung sowie auf Veränderungen von Temperatur- und Feuchtigkeitsbedingungen seit der späten Phase des Wisconsin-Glazial vor ca. 28.000 Jahren. Die angewendeten Methoden basieren auf einem Multi-Proxy-Ansatz, welcher Feldbeobachtungen, paläoökologische Untersuchungen, Laboranalysen an Sediment und Grundeis und statistische Verfahren kombiniert. Methoden zur absoluten Altersdatierung liefern den zeitlichen Rahmen, um Umweltveränderungen in den stratigraphischen Zusammenhang zu bringen.

Entlang der Yukon-Küstenebene sind nur wenige Umweltaufzeichnungen über die eiszeitlichen Bedingungen des Spät-Wisconsin hinaus erhalten geblieben. Ein Lobus des Laurentischen Eisschildes (LIS) in seiner maximalen Ausdehnung, lagerte mit dem Eis transportiertes und gestauchtes Material in Form eines Systems von Moränenrücken ab, das unter anderem die heutige Insel – Herschel Island (69°36'N, 139°04'W) – in der südlichen Beaufortsee bildet. Radiokarbonatierungen von Permafrost- und Seesedimenten zeigen, dass die Deglaziation des nördlichen Yukon ca. 16 cal ka BP einsetzte. Mit Hilfe der Analyse von stabilen Wasserisotopen und hydrochemischen Untersuchungen wurden große massive Grundeiskörper und eisreiche Sedimente cha-

rakterisiert und identifiziert, die einen glazialen Ursprung haben. Diese bestehen entweder aus begrabenem Gletschereis oder aus rückgefrorenem Schmelzwasser. Sauerstoffisotopenwerte unter -30 ‰ lassen auf deutlich kältere Lufttemperaturen (d.h. glaziale Bedingungen) bei der Eisbildung schließen als sie heutzutage im Untersuchungsgebiet vorherrschen. Jenseits des Eisrandes waren die Landschaften im östlichen Teil Beringias stark durch die Nähe des LIS beeinflusst. Dies hatte einen direkten Abkühlungseffekt und weiträumige Trockenheit zur Folge, verursacht durch katabatische Winde und durch ein stabiles Hochdruckgebiet über dem LIS. Anhand fossiler Pollenspektren aus Seesedimenten vom Trout Lake ($68^{\circ}50'N$, $138^{\circ}45'W$; 163 m ü.NN) konnte eine spärliche und von Süßgräser sowie Kräutern dominierte Tundravegetation abgeleitet werden. Dies zeugt von sehr rauen und trockenen Klimabedingungen während des letzten Abschnitts des Wisconsin-Glazial. Die Entwicklung von Seen war in Ost-Beringia gehemmt bis sich die Verfügbarkeit von Gletscherschmelzwasser und Feuchtigkeit erhöhten. Ebenso kam es zur Neubildung von Permafrost und Grundeis nachdem sich das Eis aus zuvor vergletscherten Gebieten zurückgezogen hatte. Thermische Kontraktionsrisse führten zur Eiskeilbildung, die eine Sauerstoffisotopensignatur unterhalb von -26 ‰ aufweisen und damit kennzeichnend für kalte Klimabedingungen sind. Niedrige Deuterium-Exzess-Werte ($\leq 1,7\text{ ‰}$) in Eiskeilen deuten auf trockene Bedingungen und/oder veränderte Transportpfade für Feuchtigkeit hin.

Der Übergang vom letzten Glazial zum Holozän brachte tiefgreifende Veränderungen im Klimageschehen und darauffolgender Umweltveränderungen mit sich, die in ihrer räumlich-zeitlichen Ausprägungen in *Beringia* noch wenig verstanden sind. Anhand von Pollendaten quantitativ rekonstruierte Sommertemperaturen von bis zu $10^{\circ}C$ zeigen eine rasche Erwärmung während des Bølling/Allerød Interstadials (14,7–13,0 cal ka BP). Maßgeblich für die Temperaturerhöhung waren steigende Sommerinsolationswerte und der abnehmende Einfluss des rückschmelzenden Eisschildes mit zunehmender Distanz zum Untersuchungsgebiet. Der Klimaerwärmung während dieses Interstadials folgte eine ausgeprägte Kältephase während der Jüngerer Dryas (12,9–11,6 cal ka BP), die bislang im nördlichen Yukon nicht belegt war. Diese Abkühlung während der Jüngerer Dryas könnte auch für die erste Phase der Eiskeilbildung entlang der vormals vergletscherten Yukonküste verantwortlich sein. Permafrost- und Eiskeilbildung wurden durch ein frühholozänes Klimaoptimum ($\sim 11\text{--}7$ cal ka BP) unterbrochen. Veränderungen in den Erdbahnparametern führten zu einem Maximum der Sommerinsolationswerte und damit zu höheren Sommertemperaturen als die gegenwärtigen. Wegen steigender Lufttemperaturen kam es zu tiefreichendem Tauen bis zu $\sim 1,5$ m unter Flur. Dies wiederum führte zur Ausbildung einer regional verbreiteten Auftaudiskordanz und zur Kappung von Kryostrukturen deutlich unterhalb der Basis der aktuellen saisonalen Auftauschicht. Das Austauen von Eiskeilen und erhöhte Thermokarstaktivität waren von schnellem Torfwachstum und dem Ausfüllen von Eiskeilpseudomorphosen mit limnischen Ablagerungen aus dem Frühholozän begleitet. Dem relativ

konstanten Sedimentationsgeschehen während des Holozäns auf flachen und niedrig gelegenen Tundrangebieten stehen sehr dynamische Ablagerungsbedingungen in reliefstarken Arealen auf Herschel Island gegenüber, v.a. in Verbindung mit Küstenerosion und rückschreitenden Erosionsformen (sogen. *retrogressive thaw slumps*). Die Verfügbarkeit von Feuchtigkeit im nördlichen Yukon erhöhte sich im Laufe des mittleren Holozäns in Folge des postglazialen Meeresspiegelanstieges und der abnehmenden Insolationsintensität im Sommer. Letzteres wiederum führte zu erneuter Permafrost- und Grundeisbildung mit Sauerstoffisotopenwerten über -25% . Staunässe und höhere Feuchte förderten in den letzten 5000 Jahren die Entwicklung einer von Birken und Erlen dominierten Strauchtundren-Vegetation. Die Kombination der Ergebnisse aus Permafrost-, Grundeis- und palynologischen Studien dokumentiert den Umweltwandel von kontinentalen Bedingungen Beringias zu einer küstennahen maritimen Umwelt unweit der Beaufortsee.

Diese Studie verdeutlicht, dass die Landschafts- und Umweltentwicklung in der Randzone Ost-Beringias stark von der regionalen Glazial- und Periglazialgeschichte geprägt ist. Die vergangene, gegenwärtige und zukünftige Dynamik dieser arktischen Region ist eng an die Wechselwirkungen zwischen Permafrost, Vegetation und Meeresspiegelschwankungen als Ausdruck von Klimaänderungen geknüpft.

1 Introduction

1.1 Motivation

The high latitudes of the northern hemisphere are highly vulnerable to climatic change [ACIA, 2004]. During the past century, the Earth's surface mean annual air temperature has warmed by 0.74°C overall [IPCC, 2007]. During the same period, land areas in the Arctic have grown warmer by ~3°C [Serreze and Francis, 2006]. Widespread increase in thaw depth of permafrost [Lachenbruch and Marshall, 1986; Osterkamp, 2005] is projected to be associated with an extensive release in terrigenous carbon as additional greenhouse gases (CO₂, CH₄) [Oechel *et al.*, 1993; Walter *et al.*, 2006] and enhanced coastal erosion rates – a risk for industry, community planners and aboriginal peoples [Rachold *et al.*, 2004; Lantuit and Pollard, 2005; Forbes, 2011].

Most recently, the Arctic Council – the high-level policy forum for the Arctic countries, the European Union and indigenous peoples in the Arctic – has underscored the environmental significance of the Arctic region and has stressed its critical nature in the global climate system, and the emerging geopolitical relevance of the Arctic region [Fitzpatrick *et al.*, 2010]. The importance of developing an improved knowledge of the Earth's past and present climate and environment as well as their natural long-term cycles has been recognized by many international organizations and policy bodies.

The Arctic is particularly sensitive to a changed forcing due to powerful positive feedbacks in the Arctic climate system [Serreze *et al.*, 2009]. Instrumental records and environmental monitoring programs dedicated to resolving high-latitude climate forcing are only available for the last 200 years or less. They are, therefore, much too short to cover the full range of natural fluctuations and feedback mechanisms. Answers to the urgent questions of a future climate behavior in response to anthropogenic fossil-fuel burning must come from paleoclimate data. Paleoenvironmental records play a key role in our understanding of the Earth's past and present climate system and in predicting future environmental changes [Fitzpatrick *et al.*, 2010]. Indirect proxy methods can be used to infer these past conditions [Pienitz *et al.*, 2004]. A proxy is an environmental relict stored in an environmental archive that is used to infer past environmental conditions [NCDC, 2011]. Over the last decades a large number of paleoenvironmental approaches have been developed to reconstruct climatic and other environmental variations from natural palaeoclimate archives. These advances provided ground for the herein presented investigation of long-term environmental and landscape changes in the western Canadian Arctic, an area of particular paleoclimatic interest that has been rarely examined yet.

1.2 Scientific background

1.2.1 Beringian environments in time and space

The early David Hopkins was inspired by the observations published by Eric Hultén in 1937, who noticed that the similarity of most arctic and many boreal plant species between eastern Siberia and northern North America was likely due to an ice-free and emerged migration corridor between both subcontinents [Hultén, 1937], while much of northern North America and parts of Siberia were covered with glacial ice [Hopkins, 1967]. Hultén was the first who introduced the term “Beringia” for the vast arctic lowlands that must have been exposed during the worldwide glacial epochs, and that have been a refugium for species becoming isolated. Since the first book on Beringian paleoenvironments “The Bering Land Bridge” [Hopkins, 1967] and the volume entitled “Paleoecology of Beringia” [Hopkins *et al.*, 1982], much progress has been made in the various fields dealing with Beringian studies [Elias, 2001a]. With the end of the Cold War, scientists from North America and Russia had the opportunity to work together on this topic and to compare their findings from both realms. As a result of the 1997 Beringian Paleoenvironments workshop and in honor of D. Hopkins, a large collection of papers was published in 2001 in *Quaternary Science Reviews* (v. 20, no. 1-3) and provided an encompassing view of the state of the art research related to Beringia and the next research hot-spots within the framework for reconstructing Beringian paleoenvironments. Most recently, the passing of Andrei Sher, who played a major role in developing scientific collaboration between East and West [Kuzmina *et al.*, 2011], led to a compilation of key papers in *Quaternary Science Reviews* (v. 30, no. 17-18) as a tribute to his career.

Beringia – in nowadays usage – represents the repeatedly emerged subcontinent and adjacent lowlands that extended contiguously between the Pleistocene ice sheets of Eurasia and North America (Fig. 1.1); from Taymyr Peninsula in central north Siberia until the Mackenzie River in the northwest of Canada [e.g. Hopkins *et al.*, 1982]. This includes the dry-fallen continental shelves of the Laptev, East Siberian, Chukchi, Bering and Beaufort seas as the consequence of a globally lowered sea level during the glacial stages of the Pleistocene. While large parts of the high latitudes in Eurasia and North America were covered by ice sheets, the lowlands of Beringia remained largely ice-free, thus providing a refugium for high-latitude flora and fauna [Elias and Brigham-Grette, 2007] as well as a migration corridor for early men [Morlan and Cinq-Mars, 1982; Mason *et al.*, 2001]. It is most notable for Quaternary scientists that the uncommon presence of a vast unglaciated and contiguous landmass in the Arctic which has existed for several glacial–interglacial cycles provides us with continuous paleoenvironmental records and with one of the best

frameworks for comparing regional climate change with forcing mechanisms that include changes in insolation, sea level, and the size of ice sheets [Brigham-Grette *et al.*, 2004].

Global sea level dropped repeatedly below the sill depth of the Bering Strait (−53 m) separating the Pacific and Arctic oceans [England *et al.*, 2009] to expose large portions of the continental shelves, leading to dry land forming the Bering land bridge (Fig. 1.1a). By mapping the 120 m-isobath (of the adjacent sea floors), which approximates the lowest sea level during the last ~140 ka BP [Fairbanks, 1989; Yokoyama *et al.*, 2000; Lambeck *et al.*, 2002], it is possible to follow the outline of the formerly exposed land bridge region. In the course of this thesis, three geographic sectors of Beringia are referred to (see Fig. 1.1a).

- (1) Western Beringia comprises northeast Siberia from the Taymyr Peninsula as the westernmost end to the modern Bering and Chukchi Sea coast.
- (2) Central Beringia is the area of the Bering land bridge that is now submerged.
- (3) Eastern Beringia encompasses the unglaciated regions of Alaska and the Yukon Territory. This places the easternmost edge of Beringia along the northwest margin of the Laurentide Ice Sheet (LIS) at its maximum extent (Fig. 1.1b).

Closing the isthmus cut off the circulation between the North Pacific and Arctic ocean waters. This in turn greatly increased continentality [Elias and Brigham-Grette, 2007] by shutting down the influx of warm Pacific water masses into the Arctic basin and therefore reduced the capability of moisture advection. Beringia was also positioned ‘down-wind’ of the large Eurasian and North American ice sheets, themselves creating widespread aridity [Siegert *et al.*, 2001]. Simulations of a split jet stream during full glacial conditions with branches passing north and south of the LIS favored intensive troughing with descending dry air masses over east Beringia [Bartlein *et al.*, 1991]. Moreover, Pacific moisture transport into the interior regions of Alaska and the Yukon Territory is blocked by the Alaska Range and the system of coastal mountains that form the rim of the Gulf of Alaska [Kaufman and Manley, 2004]. This together with a lowered sea level and the presence of the Cordilleran Ice Sheet (Fig. 1.1a) would have greatly reduced the moisture availability in interior regions of east Beringia.

Robust reconstructions of temperature and sea level variations across Beringia are available at least since the last interglacial (MIS 5, Table 1.1). CAPE [2006] and Otto-Bliesner *et al.* [2006] have summarized the last interglacial summer temperatures to have been 4 to 8°C warmer than today in west Beringia [cf. Kienast *et al.*, 2011] but similar to today in east Beringia together with generally wetter conditions across the whole subcontinent [Muhs *et al.*, 2001]. At the peak of the last interglacial (MIS 5e), the eustatic sea level was about 6-7 meters higher than it is today [Chen *et al.*, 1991], corresponding to the Pelukian transgression, dated between 125-115 ka BP [Brigham-Grette and Hopkins, 1995].

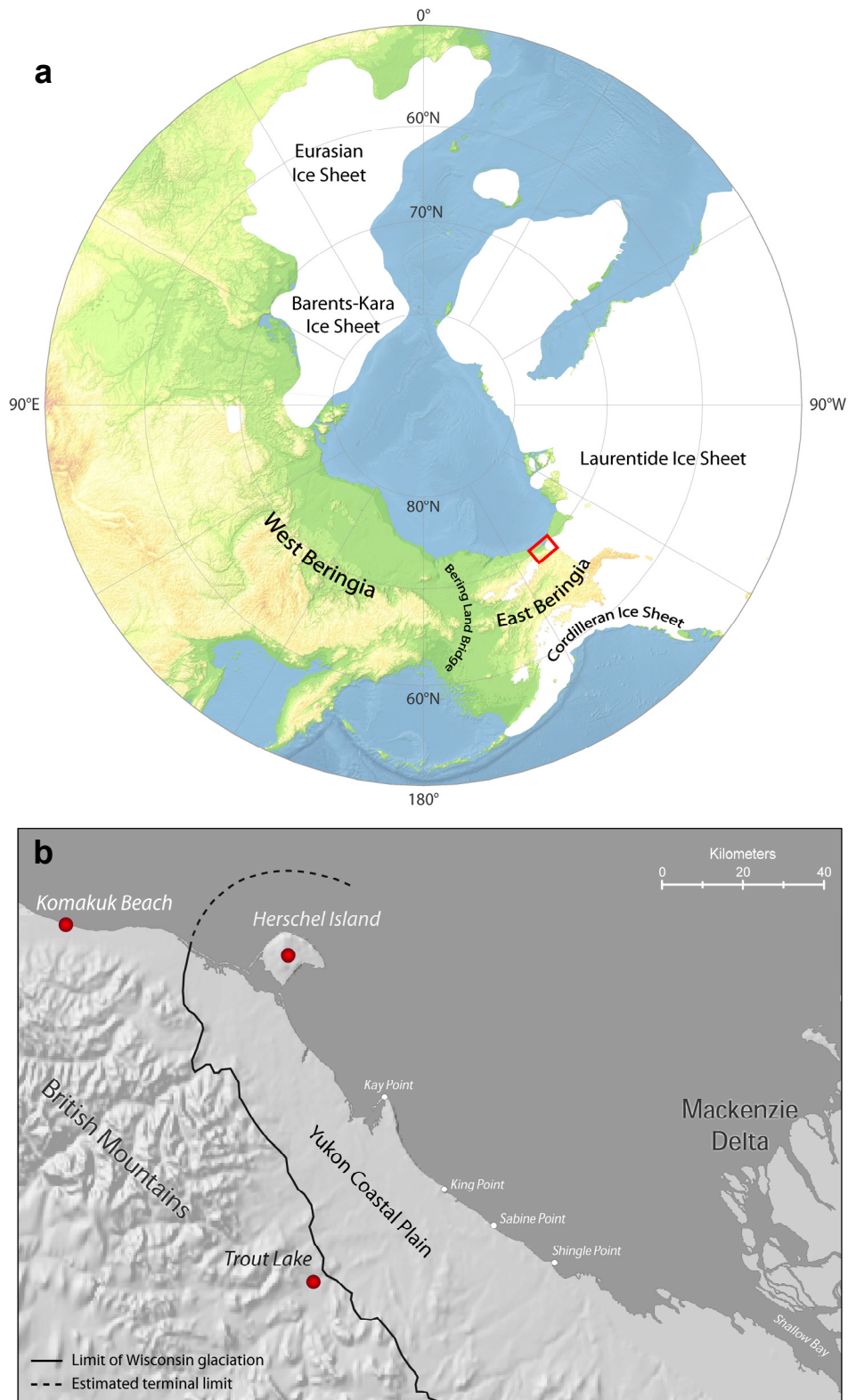


Figure 1.1: (a) Map of the northern polar regions, showing the ice sheets during the Last Glacial Maximum (LGM) and the regions of west and east Beringia, the Bering land bridge, and the exposed shelf areas during LGM sea level lowstand of -120 m. The study area (red rectangle) in the western Canadian Arctic is shown as close-up in (b). Specific study sites are marked with red dots. The extent of the Eurasian, the Laurentide, and the Cordilleran Ice Sheets as well as regional glaciations in Alaska are according to Svendsen *et al.* [2004], Dyke *et al.* [2003], and Manley and Kaufman [2002], respectively.

Table 1.1: Overview of late Pleistocene stratigraphic and climatic nomenclature for eastern Beringia.

MIS ^a	Period	Approximate age range (ka BP ^b)
1	Holocene	10–present
2	Late Wisconsin	28–10
3	Middle Wisconsin	60–28
4	Early Wisconsin	115–60
5	Sangamon (Eem)	125–115

^a MIS – Marine Isotope Stage

^b ka BP – thousand years before present (1950).

During the penultimate glaciation (early Wisconsin, MIS 4), ice caps and alpine glaciers were considerably more extensive throughout much of Beringia than during the subsequent late Wisconsin glaciation in MIS 2 [Brigham-Grette *et al.*, 2003; Kaufman and Manley, 2004; Ward *et al.*, 2008]. Paleotemperature reconstructions for MIS 4 in eastern Beringia, based on fossil beetle assemblages in Alaska and the Yukon, suggest cold summers with temperatures $\sim 6^{\circ}\text{C}$ below modern levels [Elias, 2001b]. Middle Wisconsin interstadial warming associated with MIS 3 (Table 1.1) gave rise to retreating ice sheets along the margins of Beringia [Schweger and Matthews, 1985; Dredge and Thorleifson, 1987]. Sedimentological and paleobotanical evidence as well as fossil beetle assemblages suggest that the MIS 3 interstadial was characterized by a relatively warm and moist climate, together with strong variations in environmental conditions that still remained more severe than during the Holocene (MIS 1) [e.g. Anderson and Lozhkin, 2001; Elias, 2001b; Schirmer *et al.*, 2002b; Sher *et al.*, 2005].

Beringia was extremely cold and dry during the late Wisconsin glaciation, which is equivalent to MIS 2 (Table 1.1). The lack of moisture across Beringia during the Last Glacial Maximum (LGM), in response to various environmental factors, prevented the growth of large ice masses [Elias and Brigham-Grette, 2007]. Eustatic sea level was at its lowest and large shelf areas became exposed further supporting continentality of interior regions. Beringia was surrounded by the large ice caps of the Barents-Kara Ice Sheet in Eurasia and the LIS in North America; the latter had coalesced with the Cordilleran Ice Sheet and thereby closing the corridor to the mid latitudes. Although Beringia was most likely characterized by a heterogeneous vegetation mosaic [Kurek *et al.*, 2009], large parts of the dry lowlands were dominated by a grass/herb vegetation-type, also known as the cold tundra-steppe [Guthrie, 1968, 2001]. This graminoid-herb tundra was productive enough to support the Pleistocene herbivore megafauna [Sher *et al.*, 2005]. Pollen-based climate reconstructions from the western Beringian margin, on the northern Taymyr Peninsula, suggest summer temperatures were up to 5°C colder than today and annual precipitation was ~ 100 mm less

during the LGM than at present [Andreev *et al.*, 2002, 2003, 2011]. In easternmost Beringia, paleotemperature estimates based on pollen and fossil beetle assemblages suggest average summer temperatures between 4 and 7.5°C colder than present [Elias, 2001b; Viau *et al.*, 2008]. In response to a rising sea level at the end of the last glaciation, the resubmergence of the Bering Strait re-established the circulation between the Pacific and Arctic Ocean [Elias *et al.*, 1996; 1997]. Recent finds of postglacial Pacific mollusk fauna reported by Bradley and England [2008] from the Canadian Arctic indicates an earlier inundation of the land bridge (~13 cal ka BP) than previously proposed by Elias *et al.* [1996] and Keigwin *et al.* [2006]. This date also marks the end of Beringia as a continuous land mass. Postglacial environmental change throughout Beringia brought along wholesale changes in vegetation and geography; the regional extinction of much of the Pleistocene megafauna, and the expansion of *Homo sapiens* to North American mid latitudes [Brigham-Grette *et al.*, 2001].

1.2.2 The eastern Beringian edge

The northern Yukon Territory in the western Canadian Arctic possesses several archives for studying strong environmental gradients. While the eastern part was ice-covered during the late Wisconsin (≤ 28 cal ka BP) [Dyke and Prest, 1987; Dyke *et al.* 2002], the western parts apparently remained ice-free for numerous glacial–interglacial cycles throughout the entire Quaternary [Brigham-Grette *et al.*, 2003; Brigham-Grette and Gualtieri, 2004; Duk-Rodkin *et al.*, 2004]. Therefore, the area of interest is located immediately on the interface of the formerly glaciated area to the east, the easternmost margin of Beringia to the west, and the Beaufort Sea to the north. Moreover, recent investigations by Murton *et al.* [2010] have identified a major outburst flood path from glacial Lake Agassiz to the Arctic Ocean running through the Mackenzie River system in the Canadian Arctic, accounting for the Younger Dryas cold reversal.

Despite its apparently outstanding position for the understanding of regional landscape and climate development in ice-marginal areas, the late Quaternary history of the Yukon Coastal Plain (YCP) is largely unknown and relies on few studies [Bouchard, 1974; Rampton, 1982]. Especially landscape and environmental changes in the northern Yukon, whose climatic characteristics are closely related to sea level history and coastal processes, are poorly understood [Burn, 1997]. A comprehensive assessment of arctic climate changes, their causes and feedbacks requires terrestrial records that mirror coastal changes in order to address the interaction of the upper lithosphere and the cryosphere with the arctic hydrosphere. Up to now, few studies have used permafrost sequences as environmental archive in the northern Yukon [Burn *et al.* 1986, Burn, 1997] and concepts of landscape genesis close to the ice margin since the last glacial–interglacial transition are sparse. Moreover, vegetation history and absolute temperature reconstructions in east Beringia are rare

[*Elias, 2001b; Viau et al., 2008; Kurek et al., 2009*] or do not provide conclusive evidence [*Matthews, 1975*]. In the wide tundra areas of the Arctic Coastal Plain of Alaska and the Yukon, where tree ring and ice core archives are not available, and where lacustrine records usually do not cover large timescales, ground ice contained in permafrost sequences may serve as an additional climate archive. However, up to now, only scattered information on the late Quaternary paleoclimate has been obtained from ice wedges in east Beringia [e.g. *Kotler and Burn, 2000; Meyer et al., 2008, 2010; Kanevskiy, et al., 2011*].

1.2.3 Permafrost as environmental archive

Today, approximately 24 % of the northern hemispheric landmass are affected by permafrost [*Zhang et al., 1999*], with the number being even larger for Canada, Alaska and Russia, with ~50 %, ~80 % and ~50 %, respectively [*French, 2007*] (Fig. 1.2). Permafrost or perennially frozen ground describes all earth material remaining at or below 0°C for at least two consecutive years, regardless of whether it consists of rock, unconsolidated deposits or organics [*van Everdingen, 1998*]. The most important environmental factors controlling permafrost conditions are the prevailing regional climate, topographic features, the subsurface material and its moisture content [*Washburn, 1979*]. The aggradation of permafrost reflects a negative thermodynamic balance between ground and surface temperature, which is controlled by air temperature and the geothermal gradient [*Pollard, 1998*].

Escaping extensive regional glaciations, Beringian landscapes and ice-marginal regions even in the mid latitudes of North America, Europe and Asia were instead subject to permafrost conditions during most of the Quaternary [*Kaplina, 1981; Hopkins et al, 1982; Brigham-Grette, 2004; Hubberten et al., 2004*], beginning with the onset of northern hemispheric glaciations about 2.6 Ma ago [*Jansen and Sjøholm, 1991*]. Information about climate-controlled environmental transitions in the geological record are often well-preserved in unconsolidated deposits that remained in frozen state for a considerable amount of time and have therefore been protected against redeposition and/or biological decomposition. Consequently, Quaternary permafrost sequences are excellent archives for paleoenvironmental reconstructions [e.g. *Vasil'chuk, 1991; Brigham-Grette, 2001; Schirrmeyer et al., 2002b, c, 2003; Eisner et al., 2005; Reyes et al., 2010, and references therein; Andreev et al., 2011*]. They contain a large variety of environmental proxies that, if employed within a multi-disciplinary approach, enable a comprehensive understanding of regional landscape evolution and provide insights into the interactions of climate-controlled earth systems over time.

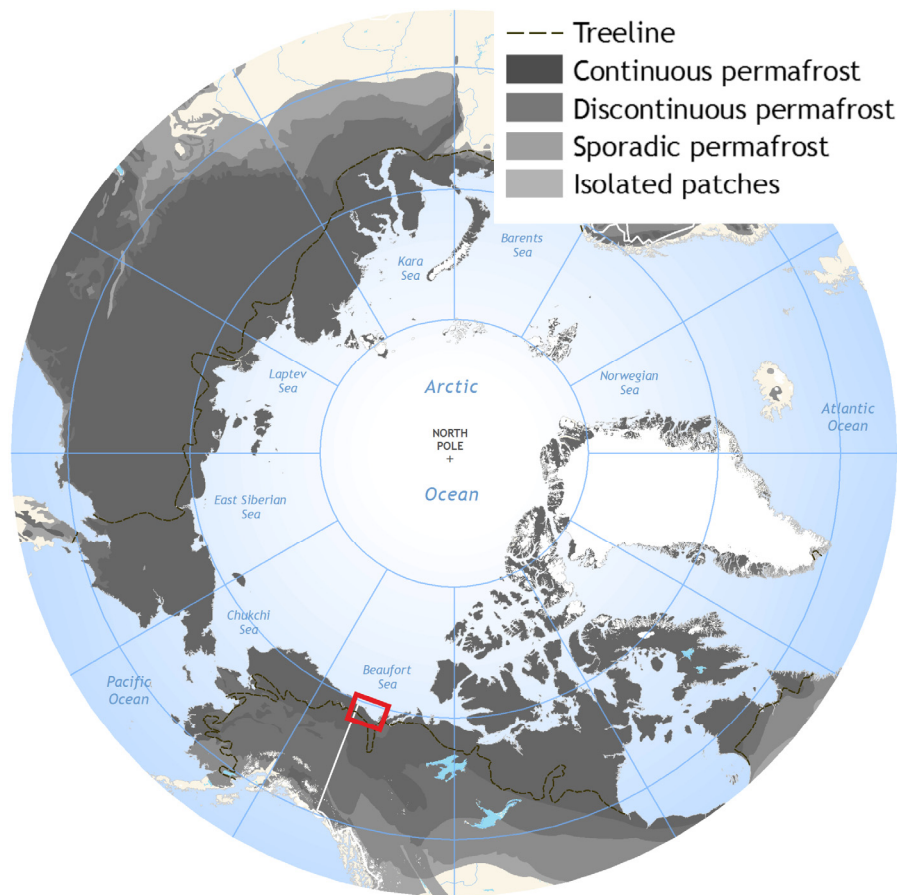


Figure 1.2: Modern permafrost distribution of the northern hemisphere [Brown *et al.*, 1998]. The study area is marked with a red rectangle (see Fig. 1.1b).

Physical sediment properties for example provide valuable information on facies conditions, depositional environments and the sediment source. Geochemical parameters from enclosed ground ice and organic matter may elucidate paleotemperature conditions and the ability of permafrost to sequester and release large amounts of carbon from different natural pools. Micro and macro fossil remains of plants and animals give hints on the composition of ancient biocoenoses and may serve as absolute paleo-temperature proxies via transfer functions due to the organisms' dependence on certain climate and temperature regimes. Absolute geochronological dating methods (e.g. ^{14}C -AMS, $^{230}\text{Th}/\text{U}$, luminescence dating, tephrochronology) are invaluable tools to relate any paleoenvironmental findings to the geological record.

1.2.4 Ground ice as environmental archive

Ground ice, defined as all types of ice contained in frozen or freezing ground [van Everdingen, 1998], is either directly fed by meteoric water sources or by recycled water (e.g. surface water, ground water) that has been subject to post-depositional transformations. Similar to glacier ice, ground ice is a natural environmental archive as it captures short-lived meteorological conditions as

well as long-term climatic trends due to its preservation potential of atmospheric precipitation, air and hydrological conditions at its source, transport pathway and place of deposition. It can be described by numerous physical, chemical and biological parameters (i.e. environmental proxies) that are related to climate and environmental conditions on different scales and allow the reconstruction of valuable information on past climate and environmental changes [NCDC, 2011]. Therefore, ground ice can be studied as a paleoenvironmental archive [Mackay, 1983; Vaikmäe, 1989, 1991; Vasil'chuk, 1991] using analytical methods similar to those applied to ice cores from glaciers and ice caps. This is especially meaningful in polar regions without current glaciation, such as the western Canadian Arctic.

One of the most promising archives for paleoclimate reconstructions are ice wedges that arise from the episodically repeated filling of thermal contraction cracks, mainly fed by snow meltwater, which percolates into the frost fissure, refreezes immediately [Lachenbruch, 1962] and therefore retains its original environmental information [cf. Michel, 1982]. Tabular massive ground ice bodies (excluding ice wedges) are defined as laterally and vertically extensive subsurface ice masses [Mackay, 1972b; 1989] with an ice content exceeding 250 % (i.e. on an ice-to-dry-soil weight basis [van Everdingen, 1998]) and are among the most striking features of permafrost areas. The occurrence of massive ground-ice bodies has often been related to the former presence of Pleistocene ice caps, since many massive ice exposures have been found within the limits of Quaternary glaciations. Since the end of the 19th century, early explorers speculated that these ice bodies consisted of relict glacier ice [von Toll, 1897; Lorrain and Demeur, 1985; Kaplyanskaya and Tarnogradsky, 1986; Astakhov and Isayeva, 1988; Ingólfsson et al., 2003; Murton et al., 2005; Fritz et al., 2011], or whether the ice has a segregation origin [Mackay, 1971, 1973; Rampton, 1991, Mackay and Dallimore, 1992], with glacial meltwater delivering the huge amount of water required for their formation [Rampton, 1988; French and Harry, 1990].

A variety of permafrost landscape features have their origin in the aggradation or degradation of ground ice (e.g. polygonal nets, pingos, thermokarst lakes, thermoerosional valleys and retrogressive thaw slumps), which is a major component of permafrost dynamics. Ground ice locally makes up to 50 % of the volume of near-surface permafrost in the western Canadian Arctic [Mackay, 1971]. Thermokarst phenomena that represent major threats for arctic infrastructure are often associated with the melting of massive ice [e.g. Murton, 2001; Burgess and Smith, 2003; Lantuit and Pollard, 2008]. Besides massive ice types there exists a variety of non-massive ice types of various origins depending on the origin of water prior to freezing and the principle process of water movement towards the freezing plane [cf. Mackay, 1972b]. For simplification this chapter uses the term “non-massive intrasedimental ice” (NMI) for all types of pore ice or segregated ice [cf. Murton and French, 1994] within surrounding permafrost-affected sediments. NMI might also be used for paleoclimatic studies [Burn et al., 1986; Vaikmäe, 1989; Schwamborn et al., 2006].

Whereas ice wedges are mainly fed by winter precipitation [Vaikmäe, 1989; Vasil'chuk, 1991], NMI often consists of refrozen water, which is a mixture of waters of various origins (i.e. summer and winter precipitation, surface water, and last season's ground water) [Schwamborn *et al.*, 2006]. Even though preservation of soil moisture in NMI occurs in a complex way, i.e. through repeated seasonal freeze and thaw that adds numerous cycles of phase change and therefore promotes isotopic fractionation, it can still reflect environmental and climatic changes [Schwamborn *et al.*, 2006]. Murton and French [1994], Vardy *et al.* [1997], Kotler and Burn [2000], and Schwamborn *et al.* [2006] have shown that major changes in paleotemperature and hydrology can be resolved by interpreting the NMI record.

Pioneering work in the field of paleoclimate studies based on ground ice has primarily involved ice wedges and focused on oxygen isotope ($\delta^{18}\text{O}$) variations as an indicator for winter temperature changes [Michel, 1982; Mackay, 1983; Vaikmäe, 1989; Vasil'chuk, 1991]. This was later amended by mutual considerations of $\delta^{18}\text{O}$, δD and deuterium excess (*d*-excess), which provided additional information for paleotemperature reconstruction, for the identification of the precipitation source, and for unravelling post-depositional fractionation processes [Dansgaard, 1964; Merlivat and Jouzel, 1979; Souchez, 2000; Meyer, 2002a, b; Lacelle *et al.*, 2004; Lacelle, 2011; Opel *et al.*, 2011].

We adapted the approach from Bradley [1999] that is based on ice cores towards ground ice in order to obtain paleoenvironmental information. This involves the analysis (1) of the ice's physical characteristics, (2) of stable water isotopes, (3) of dissolved and particulate matter and (4) of entrapped gas bubbles.

- (1) Physical characteristics of the ice such as ice content, sediment inclusions and cryostratigraphic relationships to the surrounding deposits constrain a distinct ice origin and enable the identification of thaw unconformities [Mackay, 1971, 1989; Burn *et al.*, 1986, 1997; Murton and French, 1994; Murton *et al.*, 2004, 2005].
- (2) The stable water isotope composition of precipitation is strongly temperature-dependent [e.g. Dansgaard, 1964; Rozanski *et al.*, 1993] and can therefore be used as a proxy for local to regional temperature regimes [e.g. Mackay, 1983; Kotler and Burn, 2000; Meyer *et al.*, 2002a, b, 2010]. Additional information on moisture origin, water source and freezing conditions can be obtained that way [e.g. Michel, 1986; Lacelle *et al.*, 2004, 2007, 2009b; Fritz *et al.*, 2011; Lacelle, 2011].
- (3) Analyses of the dissolved ion content and radiocarbon dating of particulate organic matter can be used for the distinction of water sources [e.g. Mackay and Dallimore, 1992; Fritz *et al.*, 2011] and for providing a chronological context of environmental change deduced from ground ice [Vasil'chuk and Vasil'chuk, 1997; Vasil'chuk *et al.*, 2000, 2001; Meyer *et al.*, 2010; Opel *et al.*, 2011].

- (4) Air bubbles in ground ice may represent samples of a former atmospheric composition if they derive from buried glacier ice that consists of firn and allows the direct analyses of the paleo-atmosphere during ice formation. In this context, though not being a topic of this study, *Cardyn et al.* [2007] have shown that analyzing molar gas ratios of air entrapped in ground ice (O_2/Ar and N_2/Ar) may provide a powerful tool for clearly distinguishing between atmospheric gas in glacial ice and gases from intrasedimental ground ice to determine the origin of relict massive ground-ice bodies.

1.2.5 Arctic lake sediments as environmental archive

A characteristic feature of most arctic landscapes is the large number of lakes. The sediments accumulating in each of these lakes contain information that potentially offers a sensitive record of past environmental change [*Smol and Cumming, 2000*]. Paleolimnology, which is the study of the physical, chemical and biological information stored in lake sediments [*Smol, 2002; Cohen, 2003*] offers considerable potential for reconstructing the long-term trends in environmental and climatic conditions. Lake sediments are ideal archives for studying the patterns of paleoenvironmental change [*PARCS, 1999*] on an annual to millennial time scale and resolution for three main reasons [cf. *Pienitz et al., 2004*].

- (1) Lacustrine deposits are sources of paleoenvironmental records with high temporal resolution, similar to ice cores and tree rings. In contrast to trees, which are absent north of the treeline, in extreme regions or on high elevations, and in contrast to ice caps, which are limited in geographic distribution, lakes have an excellent spatial coverage in arctic regions.
- (2) Many lake basins contain considerable sedimentary records which, given sufficient dating control, allow the continuous reconstruction of environmental change extending back thousands or even millions of years (e.g. Lake El'gygytgyn, Lake Pingualuit).
- (3) The arctic circumpolar regions are of the least densely populated areas on earth and therefore contain some of the most pristine environments suitable for investigating natural environmental change. Paleoecological reconstructions from lake sediments are likely to be more reliable if derived from areas with little impact from local human activities such as industry, forestry, agriculture and municipal pollution.

Overpeck et al. [1997] and *Bradley* [1999] have summarized paleoenvironmental information in several regional and circumpolar composite records and demonstrate the valuable perspective that lacustrine sedimentary records can provide. It is the diversity of possible proxy records contained in lacustrine sediments that has led to considerable progress in different research areas. Macro- and microfossils and other biogenic indicators are widely utilized to document ecosystem changes. However, the relatively low bioproductivity found in many high latitude environments

frequently results in lacustrine deposits that are dominated by inorganic material, primarily derived from the lake catchment. Thus, lacustrine sedimentary records that use physical and chemical information are important research tools for reconstructing environmental conditions [Pienitz *et al.*, 2004].

1.3 Aims and approaches

The overarching goal of this thesis is to reconstruct the late Quaternary landscape evolution and environmental dynamics along the easternmost margin of Beringia in northwest Canada. Due to its glacial–deglacial history, the northern Yukon comprises environmental archives of different temporal range and geographic coverage. Permafrost deposits are ubiquitous in the northern Yukon but are rarely accessible over wide areas without the use of drilling devices. Therefore, coastal exposures at the Yukon mainland coast near Komakuk Beach (69°36'N, 140°30'W; Fig. 1.1b), which is located beyond the margin of the late Wisconsin glaciation, and retrogressive thaw slumps on Herschel Island (69°36'N, 139°04'W; Fig. 1.1b), which is a direct product of glacier ice thrust, were studied. Coastal bluffs are easier to enter and stratigraphic relationships can be pursued over long distances. For the same reasons ground ice was sampled along naturally exposed outcrops as described above. Because this study seeks to establish a continuous record of environmental change until the late Pleistocene, Trout Lake (68°49.73'N, 138°44.78'W), which is located beyond the glacial limit at the foot of the British Mountains, was drilled (Fig.1.1b). Finding a structurally controlled lake beyond the glacial limit was essential for the perspective of a long-term environmental record, because on the one hand lakes are common in the formerly glaciated areas of the YCP, but on the other hand they merely contain environmental information since the ice sheet has left the area. Sediment records from thermokarst lakes on the unglaciated part of the YCP are likewise limited in their temporal range; most likely to the onset of Holocene thermokarst.

Working within and beyond the margin of the late Wisconsin glaciation and using different environmental archive types provided the means to address the following research questions and target-aimed objectives in order to fill the gap in paleoenvironmental studies in the northern Yukon Territory.

(1) How did landscapes evolved on both sides of the former LIS margin along the YCP since the late Wisconsin and how is this development linked to permafrost aggradation and degradation through time? To answer the first question permafrost studies within this thesis:

- provide solid evidence of the timing and the spatial extent of late Wisconsin glaciation in the northern Yukon;

- compare paleoenvironmental proxy data from both sides of the Wisconsin glacial margin; and
 - characterize the climatic, hydrological and deposition conditions that prevailed since the late Wisconsin in both realms.
- (2) Which processes led to the formation of large massive ground-ice bodies within permafrost sequences in ice-marginal terrain and how can ground-ice studies contribute to paleoenvironmental reconstructions in deglacial areas? To answer the second question this study seeks to:
- determine the water source feeding large massive ground-ice bodies;
 - distinguish between different massive ground-ice bodies by its cryostratigraphic characteristics; and
 - link ground-ice formation and degradation to certain climate periods.
- (3) How did vegetation and lake sedimentation respond to the climate evolution in the unglaciated northern Yukon (east Beringia) since the late Wisconsin? To answer the third question a lake sediment core from Trout Lake was used to:
- characterize variations in summer temperature and depositional environments;
 - elaborate if the timing of vegetation change in the northern Yukon is synchronous with other records from east Beringia; and
 - reconstruct the vegetation-inferred moisture patterns that correspond to LIS retreat and Holocene warming.

In order to answer these research questions a multidisciplinary approach was applied on permafrost sediments and the enclosed ground ice obtained from coastal outcrops as well as on the lake sediment core. Figure 1.3 gives an overview of the studied archives, analyzed proxies, and methods applied to address the main research questions. Details on methodologies are given in chapter 2, 3, and 4.

1.4 Thesis organization

1.4.1 Overview of chapters

This thesis represents a cumulative dissertation that consists of an introductory chapter (chapter 1) providing scientific background and the aims and objectives of this thesis, followed by three main chapters addressing the research questions formulated in chapter 1.3, and a synthesis (chapter 5) to meet the overarching aim. The three main chapters (chapters 2, 3, 4) consist of

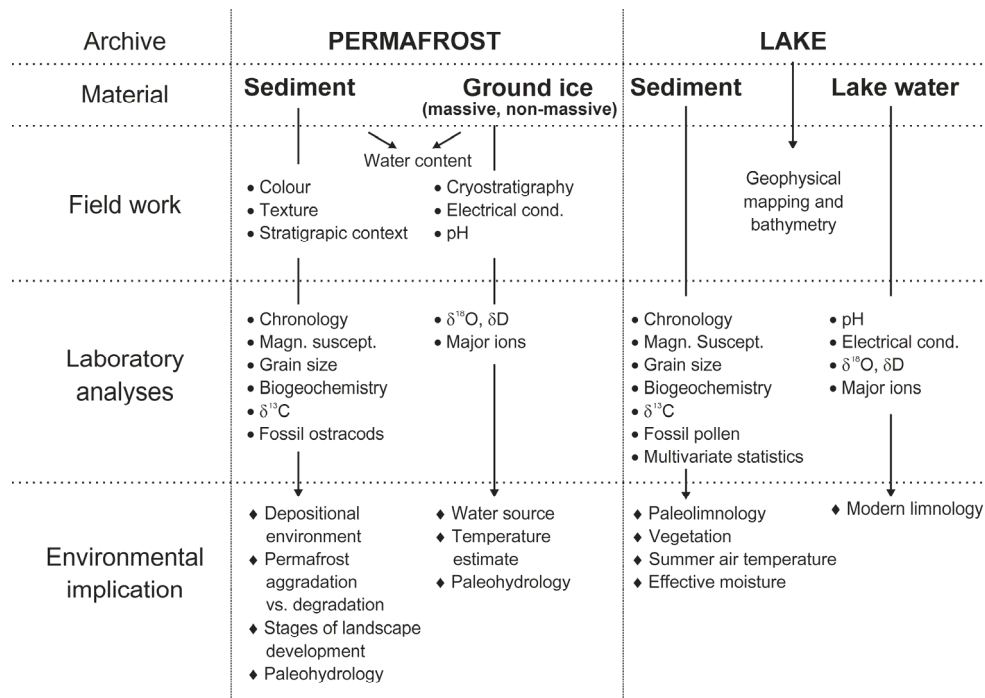


Figure 1.3: Flowchart of studied paleoenvironmental archives and methodical approach used in this thesis.

original research articles, which are structured and designated for publication in international peer-reviewed journals (Table 1.2). These articles are either under review in the journals *Palaeogeography*, *Palaeoclimatology*, *Palaeoecology* (Palaeo3; chapter 2) and *Quaternary Research* (QR; chapter 4) or published in the journal *Permafrost and Periglacial Processes* (chapter 3).

Chapter 2 deals with terrestrial permafrost archives from northwest Canada that are used to reconstruct landscape development and environmental change since the late Wisconsin along the interface of unglaciated Beringia and the formerly glaciated part of the YCP [Fritz *et al.*, under review in Palaeo3]. On the basis of field studies and multidisciplinary laboratory analyses applied to frozen deposits and ground ice, it is shown how glacial-interglacial landscape dynamics are interconnected with the local glacial history, sea-level variations, and permafrost development over time.

Chapter 3 focuses on large massive ground-ice bodies within permafrost deposits on Herschel Island (northern Yukon) and their use as paleoenvironmental archive. Stable water isotope and hydrochemical investigations, together with cryostratigraphic observations in the field seek to unravel the genetic origin of the studied ground-ice bodies. The article provides information on water source, freezing conditions and postburial landscape development in order to expand the scope of ground ice-studies in ice-marginal areas [Fritz *et al.*, 2011].

Table 1.2: Overview of publications presented within this thesis.

Chapter	Publication
2	Fritz, M, Wetterich, S., Schirrmeister, L., Meyer, H., Lantuit, H., Preusser F., Pollard, W.H., (under review). At the eastern Beringian edge: Late Wisconsinan and Holocene landscape dynamics along the Yukon Coastal Plain, Canada. <i>Palaeogeography, Palaeoclimatology, Palaeoecology</i> .
3	Fritz, M., Wetterich, S., Meyer, H., Schirrmeister, L., Lantuit, H., Pollard, W.H., 2011. Origin and characteristics of massive ground ice on Herschel Island (western Canadian Arctic) as revealed by stable water isotope and hydrochemical signatures. <i>Permafrost and Periglacial Processes</i> 22, 26-38. doi:10.1002/ppp.714
4	Fritz, M, Herzsuh, U., Wetterich, S., Lantuit, H., De Pascale, G.P., Pollard, W.H., Schirrmeister, L., (under review). Late glacial and Holocene sedimentation, vegetation, and temperature history from easternmost Beringia (Northern Yukon Territory, Canada). <i>Quaternary Research</i> .

Chapter 4 is designed to establish a continuous palaeoenvironmental record based on a lake sediment core from Trout Lake (northern Yukon), which is located beyond the Wisconsin glacial limit in east Beringia (Fig. 1.1b). We applied an interdisciplinary approach using geophysical, sedimentological, and palynological analyses together with multivariate statistics to get a comprehensive understanding of the sedimentation, vegetation, and temperature history in the proximity of the LIS. The record covers the last 16,000 years in an area where continuous palaeoenvironmental records are rare [Fritz *et al.*, under review in QR].

In chapter 5, the main results and implications of the individual thesis articles are synthesized and discussed. Moreover, this chapter provides an outlook on prospective palaeoenvironmental investigations in east Beringia and in the northern Yukon Territory, thereby critically reviewing the used research approach.

1.4.2 Authors' contributions

As first author, I initiated the scientific ideas, conducted all data analyses and interpretations, unless otherwise stated, and wrote and coordinated all manuscripts. For data acquisition I participated in three expeditions, which I partly organized and conducted. The co-authors participated in field work, contributed data, and critically reviewed and/or discussed earlier versions of the manuscripts. Lutz Schirrmeister and Sebastian Wetterich contributed to the organization of the three manuscripts and provided valuable feedback throughout the writing process. Hugues Lantuit led the expeditions this study is based on, acquired substantial third-party funding and contributed to the GIS-related data. Wayne Pollard as the Canadian counterpart of this

study provided access to the study area, helped with his regional and site-specific knowledge and added logistical support. Hanno Meyer helped with the stable water isotope analyses in the laboratory for the first and second manuscript (chapters 2, 3). Ulrike Herzschuh conducted the statistical analyses on the fossil pollen spectra for quantitative temperature reconstructions in chapter 4. Frank Preusser carried out infrared stimulated luminescence age determinations and Sebastian Wetterich identified the fossil ostracod spectra presented in chapter 2. Gregory De Pascale conducted geophysical investigations at Trout Lake presented in chapter 4.

2 At the eastern Beringian edge: Late Wisconsinan and Holocene landscape dynamics along the Yukon Coastal Plain, Canada

Michael Fritz¹, Sebastian Wetterich¹, Lutz Schirrmeister¹, Hanno Meyer¹, Hugues Lantuit¹, Frank Preusser², Wayne H. Pollard³

¹ *Alfred Wegener Institute for Polar and Marine Research, Potsdam, Germany*

² *Stockholm University, Department of Physical Geography and Quaternary Geology, Stockholm, Sweden*

³ *Department of Geography and Global Environmental and Climate Change Centre, McGill University, Montreal, Canada*

under review in Palaeogeography, Palaeoclimatology, Palaeoecology

Abstract

Terrestrial permafrost archives along the Yukon Coastal Plain in northwest Canada have recorded landscape development and environmental change since the Late Wisconsinan at the interface of unglaciated Beringia and the margin of the Laurentide Ice Sheet. The objective of this paper is to elaborate comparative stages in landscape development based on two study sites with different geomorphic settings; within the terminal limit of the Laurentide Ice Sheet (Herschel Island) and beyond it on the mainland coast (Komakuk Beach). Analyses were based on a multi-proxy approach including sedimentology, cryostratigraphy, palaeoecology of invertebrates, stable water isotopes in ground ice, and hydrochemical measures that were supported by radiocarbon and infrared stimulated luminescence age determinations. Grain-size distribution and fossil ostracod assemblages indicate that deglaciation of the Herschel Island ice-thrust morainic ridge was accompanied by alluvial, proluvial, and eolian sediment supply to the unglaciated Yukon Coastal Plain until ~11 cal ka BP during a period of low glacio-eustatic sea level. Late Wisconsinan ice wedges with sediment-rich fillings on Herschel Island are strongly depleted in heavy oxygen isotopes (mean $\delta^{18}\text{O}$ of -29.1‰); this, together with low *d*-excess values, indicates colder than modern winter temperatures and probably reduced snow depths. The late Glacial–Holocene transition was marked by higher-than-modern temperatures leading to permafrost degradation that began no later than 11.2 cal ka BP and caused a regional thaw unconformity. Cryostructures and

ice wedges were truncated while organic matter was incorporated and soluble ions were leached in the thaw zone. Thermokarst evolved into ice-wedge casts and started to fill with lacustrine deposits which were subsequently covered by rapidly accumulating peat during the early Holocene Thermal Maximum. A rising permafrost table, reduced peat accumulation, and extensive ice-wedge growth resulted from climate cooling starting in the middle Holocene and evolving towards modern environmental conditions. The reconstruction of palaeolandscapes on the Yukon Coastal Plain and the eastern Beringian edge may contribute to unraveling the cross-linkages between ice sheet, ocean, and permafrost that have existed since the Late Wisconsinan.

2.1 Introduction

When the global sea level was about 120 m lower than it is today during the Last Glacial Maximum (LGM) ca. 22-19 cal ka BP [Fairbanks, 1989; Yokoyama *et al.*, 2000], Alaska and the Yukon became the easternmost province of an unglaciated zone called Beringia that extended westwards beyond the Bering land bridge towards Siberia [Hultén, 1937; Hopkins, 1982]. The region was affected by periglacial processes during the late Quaternary, creating environmental features that can be used to reconstruct Glacial-Interglacial dynamics in landscape and climate. The Yukon Coastal Plain (YCP), in the western Canadian Arctic, is situated at the interface of the formerly glaciated realm and the easternmost margin of Beringia to the west. It contains a sedimentary record that is preserved in permafrost, which has recorded strong environmental gradients in the past. Some parts were ice-covered during Wisconsinan times (115–10 ka BP), but others apparently remained ice-free even though they were in the near vicinity of the Laurentide Ice Sheet (LIS) to the east. Despite its outstanding position and relevance for the understanding of the regional landscape development near the ice sheet margin, the region and its late Quaternary history are only known from a few records based on permafrost deposits [Bouchard, 1974; Rampton, 1982; Harry *et al.*, 1988].

Several studies have been carried out since the 1970s focusing on lake sediments in the northern Yukon [e.g. Rampton, 1971; Cwynar, 1982; Ritchie and Cwynar, 1982; Lacourse and Gajewski, 2000; Pienitz *et al.*, 2000; Kurek *et al.*, 2009; Vermaire and Cwynar, 2010], in the Northwest Territories [e.g. Ritchie and Hare, 1971; Ritchie *et al.*, 1983; Spear, 1993; Cwynar and Spear, 1995], and in adjacent Alaska [e.g. Anderson, 1985, 1988; Eisner and Colinvaux, 1990; Anderson *et al.*, 1994; Berger and Anderson, 1994; Ager, 2003; Abbot *et al.*, 2010] to reconstruct climate-driven vegetation changes and past temperature regimes. Permafrost and ground-ice studies have attempted to reconstruct past environmental dynamics such as ground ice origin [e.g. Mackay, 1971; Pollard and Dallimore, 1988; Pollard, 1990; Mackay and Dallimore, 1992; Lacelle *et al.*, 2004, 2007, 2009b; Murton *et al.*, 2004, 2005], sediment transport processes [e.g. Carter, 1981;

Lauriol *et al.*, 2002; Bateman and Murton, 2006; Murton and Bateman, 2007], peatland development [e.g. Eisner, 1991; Vardy *et al.*, 1997, 1998, 2000; Eisner *et al.*, 2005], or vertebrate and invertebrate palaeoecology [e.g. Matthews, 1975; Delorme *et al.*, 1977; Nelson and Carter, 1987; Matthews *et al.*, 1990; Hamilton and Ashley, 1993; Hamilton *et al.*, 1993; Zazula *et al.*, 2009]. However, most of these studies have been conducted at sites (Fig. 2.1 and Table 2.1) that are either located within the LIS margin and are therefore unsuitable for the investigation of Beringian landscapes, or that lie far inland and beyond the influence of the Arctic Ocean, one of the main factors driving the environment of the YCP and the adjacent Arctic Coastal Plain of Alaska [Ayles and Snow, 2002].

The aim of this study is to ascertain and to compare the Late Wisconsinan and Holocene landscape development on both sides of the former LIS margin along the YCP based on permafrost deposits and ground ice. The specific objectives of this paper are:

- (1) to trace permafrost aggradation and degradation (thermokarst) history through time under changing depositional environments along the Late Wisconsinan terminal limit of the LIS, and
- (2) to differentiate and to compare significant stages in landscape development within (Herschel Island) and beyond (Komakuk Beach) the LIS limit.

2.2 Study area

The YCP is the landward extension of the Beaufort continental shelf and is covered with Pleistocene and Holocene unconsolidated deposits assigned to the Gubik Formation [Black, 1964]. The YCP extends about 200 km from the Mackenzie Delta in the southeast to the Yukon-Alaska border in the northwest where it gives way to the Arctic Coastal Plain of Alaska. In the western Canadian Arctic, the LIS probably reached its maximum extent during the Late Wisconsinan (23-18 cal ka BP), and at that time the ice shelf extended into the offshore zone [Dyke and Prest, 1987; England *et al.*, 2009] (Fig. 2.1). Even at the LIS maximum, however, parts of the YCP remained ice-free and escaped Quaternary glaciations entirely [Barendregt and Duk-Rodkin, 2004; Duk-Rodkin *et al.*, 2004]. The LIS is believed to have extended into the study area slightly west of Herschel Island, to beyond the modern Firth River [Mackay, 1959; Rampton, 1982] (Fig. 2.2).

The study site near Komakuk Beach at 69°36'12.3"N, 140°30'11.8"W is located between two alluvial fans in the unglaciated western part of the YCP (Fig. 2.2). The studied exposure is part of a coastal bluff with a height of 8-10 m above sea level (asl) and faces the Beaufort Sea to the north. A sub-horizontal and well-developed mesic polygonal terrain, which is generally vegetated with cottongrass tussock tundra, characterizes the hinterland of the coastal zone. West of the Firth River, the area is almost flat and consists of fluvial deltas and alluvial fans associated with many creeks

and streams (e.g. Malcolm River) that incise the British Mountains and flow northwards into the Beaufort Sea (Fig. 2.2).

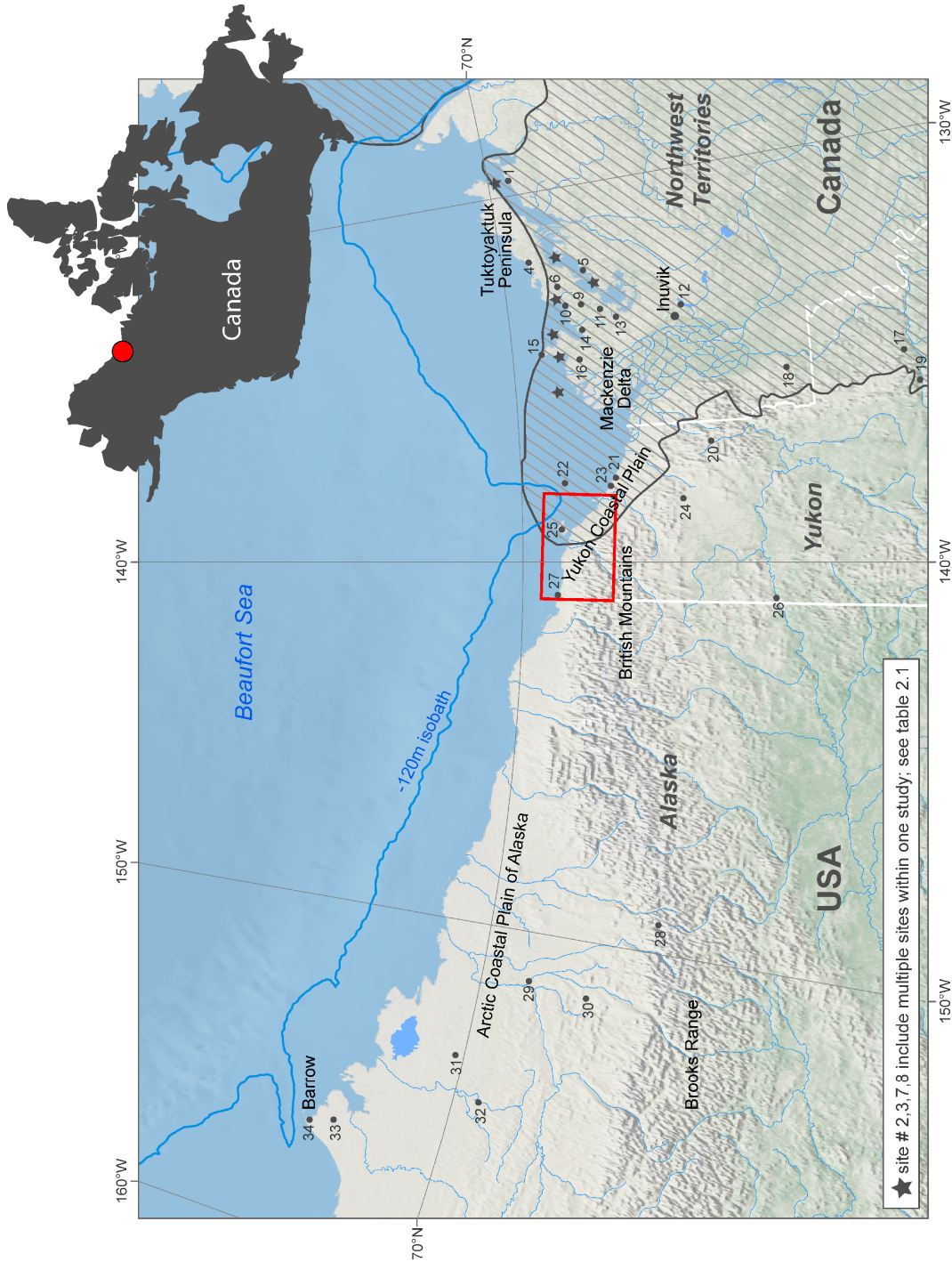


Figure 2.1: Location map of the western Arctic. Striated area indicates LGM Laurentide ice limit and follows that of Dyke and Prest [1987]. Minimum LGM sea level lowstand is shown by the -120 m isobath of the Beaufort continental shelf [Jakobsson et al., 2008]. The study area is marked with a rectangle and shown as a close-up in Figure 2.2. Site numbers are keyed to Table 2.1.

Table 2.1: Key to Figure 2.1 and references mentioned in the text to show the distribution and age range of palaeoenvironmental archives related to findings from the Yukon Coastal Plain.

Site ID	Site name	Long [°W]	Lat [°N]	Archive type	Proxy (predominant)	Age of record [ka]	Citation
1	Cliff Point	129.15	69.80	Permafrost	Geochronology	~24 (OSL)	Murton et al. (2007)
2	Tuktoyaktuk Coastlands (multiple sites)	129.25-134.38	69.07-69.83	Permafrost	Cryostratigraphy, $\delta^{18}\text{O}$, δD	> 15 cal	Murton et al. (2004, 2005)
3	Tuktoyaktuk Coastlands (multiple sites)	130.09-134.07	69.59-69.86	Permafrost	Stratigraphy, geochronology	~60 (OSL)	Bateman and Murton (2006)
4	Bluffers Pingo	131.89	69.74	Permafrost	Plant macrofossils, pollen	10.9 cal	Spear (1993)
5	Reindeer Lake	132.32	69.17	Lake sediment	Pollen	17.6 cal	Spear (1993)
6	Kukjuk Peatland	132.67	69.49	Permafrost	Pollen, plant macrofossils, $\delta^{18}\text{O}$	8.1 cal	Vardy et al. (1997)
7	Tuktoyaktuk Coastlands (multiple sites)	132.76-135.66	69.07-69.68	Permafrost	$\delta^{18}\text{O}$, δD	n.a.	Mackay (1983)
8	Tuktoyaktuk Coastlands (multiple sites)	133.04-135.66	69.40-49.60	Permafrost	Geochronology, cryostratigraphy	~9 cal	Burn (1997)
9	Campbell Creek Peatland	133.25	69.28	Permafrost	Pollen, plant macrofossils, $\delta^{18}\text{O}$	10.3 cal	Vardy et al. (1998)
10	Peninsula Point	133.37	69.39	Permafrost	$\delta^{18}\text{O}$, δD , hydrochemistry	~17 cal	Mackay and Dallimore (1992)
11	Tuktoyuktuk 5	133.40	69.10	Lake sediment	Pollen	15.6 cal	Ritchie and Hare (1971)
12	Twin Tamarack Lake	133.42	68.30	Lake sediment	Pollen	15.9 cal	Ritchie et al. (1983), Spear (1993)
13	Parsons Lake	133.75	68.75	Permafrost	Ostracods, mollusks, pollen	11.5 cal	Delorme et al. (1977)
14	Sleet Lake	133.82	69.29	Lake sediment	Pollen	14.6 cal	Ritchie et al. (1983), Spear (1993)
15	North Head	134.44	69.72	Permafrost	Cryostratigraphy	> 15 cal	Murton (2005)
16	Richards Island	134.50	69.33	Permafrost	Lithostratigraphy, seismostratigraphy	~22 (OSL)	Murton (2009)
17	Richardson Mts.	135.10	66.03	Permafrost	Ostracods, mollusks, pollen	17.5 cal	Delorme et al. (1977)
18	Ft. McPherson	135.23	67.27	Permafrost	Ostracods, mollusks, pollen	11.5 cal	Delorme et al. (1977)
19	Lateral Pond	135.93	65.95	Lake sediment	Pollen	~19 cal	Ritchie and Cwynar (1982)
20	Aklavik Plateau	137.00	68.08	Permafrost	$\delta^{18}\text{O}$, δD	~10 cal	Lacelle et al. (2004)
21	Sabine Point	137.74	69.07	Permafrost	Cryostratigraphy	~17 cal	Harry et al. (1988)
22	Mackenzie Trough	137.87	69.56	Marine sediment	Foraminifera	7.0 cal	Schell et al. (2008)
23	King Point	137.98	69.10	Permafrost	Cryostratigraphy	> 10 cal	Harry et al. (1985)
24	Hanging Lake	138.38	68.38	Lake sediment	Pollen, chironomids	33 ¹⁴ C (17 cal)	Cwynar (1982), Kurek et al. (2009)
25	Herschel Island	138.85	69.57	Fossil vertebrates	Geochronology	> 53 ¹⁴ C	Zazula et al. (2009)
26	Old Crow area	140.87	67.42	Permafrost	Mollusks, pollen	18.1 cal	Lauriol et al. (2002)
27	Clarence Lagoon	140.87	69.62	Permafrost	Ostracods, pollen	12.8 cal	Matthews (1975)
28	Imnavit Creek	149.33	68.38	Permafrost	Pollen	17.7 cal	Eisner (1991)
29	Itkillik River	150.87	69.57	Permafrost	Sedimentology, geochronology	>48 ¹⁴ C	Kanevskiy et al. (2011, in press)
30	Ahaliorak Lake	151.35	68.90	Lake sediment	Pollen	>35 ¹⁴ C	Eisner and Collinvaux (1990)
31	Ikkipuk sand sea	153.00	70.20	Permafrost	Geochronology	>36 ¹⁴ C	Carter (1981)
32	Ikkipuk River	154.88	69.72	Permafrost	Plant macrofossils, fossil beetles	10.6 cal	Nelson and Carter (1987)
33	Barrow	156.40	71.07	Permafrost	Pollen	9.0 cal	Eisner et al. (2005)
34	Barrow	156.67	71.30	Permafrost	$\delta^{18}\text{O}$, δD , geochronology	14.5 cal	Meyer et al. (2010)

Herschel Island (69°36'N, 139°04'W) is located 3 km offshore in the southern Beaufort Sea, about 100 km west of the Mackenzie Delta and 60 km east of Komakuk Beach (Figs. 2.1 and 2.2). The island is part of an ice-thrust moraine resulting from a push of the LIS [Mackay, 1959]. Large parts of the Herschel Island coast are dominated by steep cliffs up to 50 m high. Coastal slopes are subject to intense thermo-erosional activity, including numerous large retrogressive thaw slumps and active-layer detachment slides [Lantuit and Pollard, 2008]. The interior of Herschel Island (up to 185 m asl) has been subject to permafrost heave and subsidence, melt-out of ice wedges, and formation of thermokarst ponds with local peat accumulation, thermoerosion valleys, and ice-wedge polygons. Up to 50 % of the near-surface permafrost volume is made up of ground ice [Mackay, 1971].

Sediments on Herschel Island are classified as preglacial, glacial, and postglacial deposits [Bouchard, 1974]. (1) Preglacial deposits include sediment types associated with ice-thrust deformation features, which are the most common and most intricate stratigraphic units on the island. Although sediments affected by glacial ice-thrust are glacial deposits in the sense of their genesis, they are considered as preglacial in order to reflect their primary deposition, which

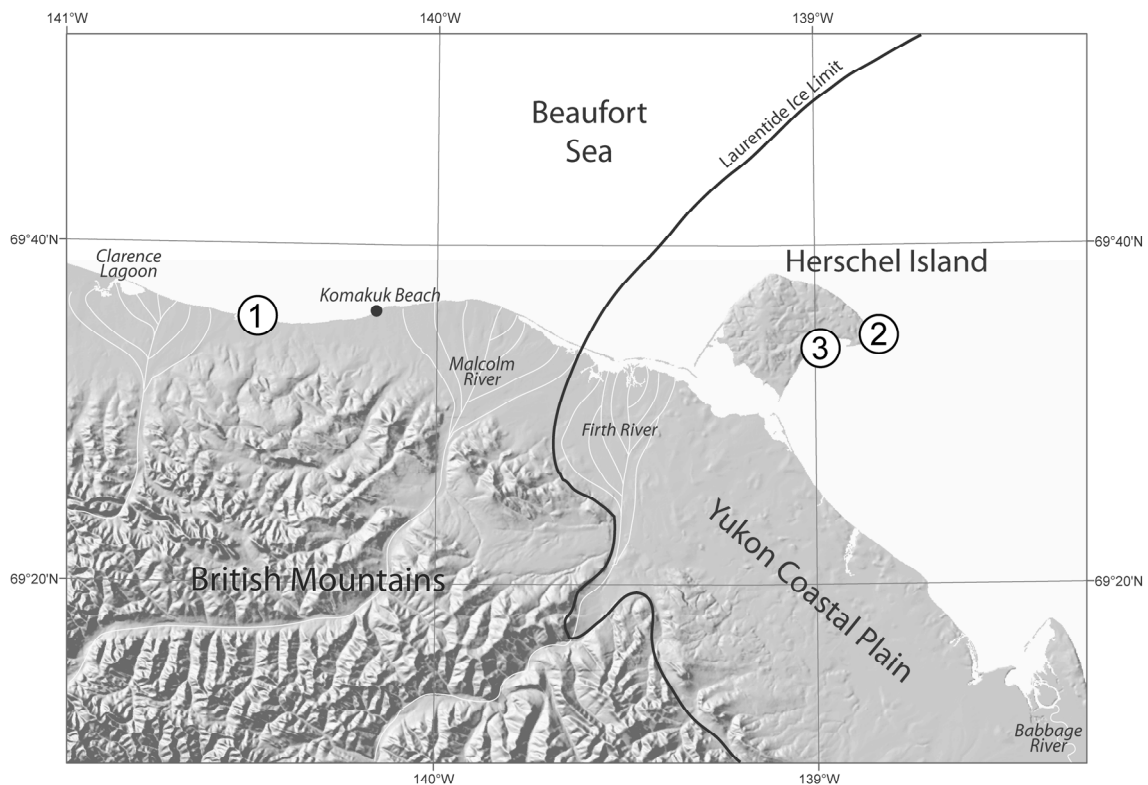


Figure 2.2: Location map of the study area along the Yukon Coastal Plain with position of the study site near (1) Komakuk Beach, and the two study sites on Herschel Island: (2) Collinson Head (COL), and (3) thaw slump D (TSD).

predated glaciation. They are categorized in terms of the environment in which they formed as marine, terrestrial, and mixed sediments [Bouchard, 1974]. (2) Glacial deposits include thin veneers of meltout till and erratic boulders scattered throughout the surface up to the highest points of the island with a distant source provenance [Bouchard, 1974]. (3) Postglacial deposits are usually related to the accumulation of peat and to littoral as well as to alluvial processes.

We studied the headwall exposures of two retrogressive thaw slumps in the southern and southeastern parts of Herschel Island (Fig. 2.2); one at Collinson Head (henceforth termed COL) and the second termed TSD for “thaw slump D”.

2.3 Material and methods

Sedimentological and cryolithological characteristics were studied at two exposures at Komakuk Beach and on Herschel Island (Fig. 2.2). Vertical sediment profiles were sampled at 0.2 to 1.0 m intervals. Field description of the sediments included color, sediment texture and bedding, organic matter occurrence, and cryostructures. The gravimetric ice content in frozen sediments, expressed as weight percentage (wt%), was determined as the mass ratio of ice to dry sample according to *van Everdingen* [1998]. Additionally, ice wedges were sampled using a chain saw, ice screw, or ice axe, depending on the accessibility of the exposures. Samples were thawed in closed plastic bags, then decanted and stored cool in airtight flasks. Electrical conductivity (EC) was measured on thawed ground-ice samples using a WTW Cond340i conductometer in order to assess the total ion content.

A laser particle analyzer (Coulter LS 200) was used for grain-size analyses. These analyses were carried out on organic-free subsamples of the < 2 mm fraction. Total carbon (TC), total organic carbon (TOC), and total nitrogen (TN) contents were measured with a carbon-nitrogen-sulphur (CNS) analyzer (Elementar Vario EL III) and are given as weight percent (wt%). The C/N ratio is expressed by the quotient of TOC and TN values. Percent carbonate content was calculated as $(TC - TOC)/0.12$, where 0.12 is the molar fraction of carbon in $CaCO_3$. Stable carbon isotope ratios ($\delta^{13}C$) of TOC were measured on carbonate-free samples with a Finnigan DELTA S mass spectrometer. The values are expressed in delta per mil notation (δ , ‰) relative to the Vienna Pee Dee Belemnite (VPDB) standard.

Supernatant water from thawed sediments was extracted, and thawed ice-wedge samples were subsampled for stable O-H isotope and hydrochemical analyses. The hydrogen and oxygen isotope composition (δD , $\delta^{18}O$) of ice wedges and segregated ice was determined with a Finnigan MAT Delta-S mass spectrometer, using the equilibration technique [Horita *et al.*, 1989]. Values are given as per mil difference from Vienna Standard Mean Ocean Water (VSMOW) standard, with internal 1σ errors of better than 0.8 and 0.1 ‰ for δD and $\delta^{18}O$, respectively [Meyer *et al.*, 2000]. The

results are presented in δD - $\delta^{18}O$ diagrams with respect to the Global Meteoric Water Line (GMWL; $\delta D=8\delta^{18}O+10$; Craig, 1961) and to the modern Local Meteoric Water Line (LMWL) derived from long-term observations in Inuvik ($7.3\delta^{18}O-3.5$; $R^2=0.98$; IAEA, 2006). In general, the most negative $\delta^{18}O$ and δD values reflect the coldest temperatures during vapor formation and deposition [Dansgaard, 1964]. Second-order parameters such as the linear δD - $\delta^{18}O$ regression slope and the deuterium excess (d -excess = $\delta D-8\delta^{18}O$; Dansgaard, 1964) provide insight into (i) the water source of the initial precipitation, and (ii) the presence or absence of secondary non-equilibrium fractionation processes.

The major cation and anion contents of the water samples from segregated ice were determined by inductively coupled plasma – optical emission spectrometry (ICP-OES, Perkin-Elmer Optima 3000 XL) and ion chromatography (IC, Dionex DX-320), respectively. Hydrogen carbonate concentrations were measured by titration with 0.01 M HCl using an automatic titrator (Metrohm 794 Basic Titrino).

Remains of fossil calcareous ostracod shells were retrieved from wet-sieved sediment samples (> 250 μm fraction) of the Komakuk Beach profiles. The ostracod species identification followed North American nomenclature as given by Swain [1963], Delorme [1968], and Smith and Delorme [2010]. Fossil plant fragments were removed from sediment samples under a stereo microscope and radiocarbon-dated at the Leibniz Laboratory for Radiometric Dating and Stable Isotope Research (Christian Albrechts University, Kiel, Germany) and the Poznan Radiocarbon Laboratory (Adam Mickiewicz University, Poznan, Poland) using accelerator mass spectrometry (AMS). Calibrated ages (cal ka BP) were calculated using “CALIB 6.0” [Stuiver and Reimer, 1993; Data set: IntCal09: Reimer et al., 2009] and we chose the 2-sigma range with the highest probability. Radiocarbon dates taken from other studies were recalibrated accordingly.

Additionally, samples for infrared stimulated luminescence (IRSL) dating were acquired using a handheld drilling machine (HILTI TE 5 A) to recover undisturbed horizontal sediment cores from frozen deposits. We used a core chamber equipped with a drill head that holds an opaque plastic cylinder to protect the samples from light. Sample preparation and IRSL analyses were conducted in the luminescence laboratory at the Institute of Geological Sciences, University of Bern, Switzerland [cf. Preusser, 2003]. The material used for equivalent dose (D_e) determination was chemically pre-treated using 10 % hydrogen chloride, 30 % hydrogen peroxide, and sodium oxalate. The 4-11 μm fraction was enriched by sedimentation according to Stokes' law. D_e was determined using the modified Single-Aliquots Regenerative (SAR) dose protocol for feldspar using a BG39 and a 410 nm interference filter. Samples were preheated at 290°C for 10 s prior to all IRSL measurements. Since storage tests identified only a minor signal loss (1 g per decade); no fading correction was carried out. Determination of dose-rate-relevant elements (K, Th, U) was done by high-resolution low-level gamma spectrometry [Preusser and Kasper, 2001]. The average

water content was estimated by using present sediment moisture and adding 10 % uncertainty for the age calculation to account for potential past changes in the hydrological conditions.

2.4 Results

2.4.1 Litho- and cryostratigraphic properties

Komakuk Beach

Four sediment units (A, B, C₁, C₂) were defined according to their different characteristics from field and laboratory data (Figs. 2.3 and 2.4). The lower three meters of the coastal cliff were covered by slumped debris and compacted snow.

The lowermost exposed sediments (4.0 to 4.5 m below surface; unit A) were composed of greenish-gray sandy silt with minor clay content and occasional cobbles up to 1 cm in diameter (Figs. 2.4 and 2.5). Black organic-rich spots and oxidation bands were rarely present. These massive fine-grained deposits had a parallel fine lens-like cryostructure (ice lenses up to 1 mm thick) and an ice content of 20 to 25 wt%. They contained little organic carbon (TOC <1 wt%) but were rich in CaCO₃ (>10 wt%), although calcareous ostracod shells and undetermined mollusk remains occurred as individual findings only. C/N ratios and $\delta^{13}\text{C}$ values were the lowest of the whole sequence at around 9 and -25 ‰, respectively (Fig. 2.5). Plant remains in this unit were sparse and showed signs of strong mechanical reworking.

Unit A was conformably overlain by ~1.5 m of the unbedded yellowish-brown to yellowish-gray fine-grained deposits of unit B (Fig. 2.3). Sedimentary properties of unit B such as bedding, grain size distribution, CaCO₃ content, and cryostructures were fairly comparable to those of unit A, but ice (up to 75 wt%) and TOC contents (up to 4.6 wt%) were clearly higher; and TOC increased to the top (Figs. 2.4 and 2.5). C/N ratios varied between 8 and 14, and $\delta^{13}\text{C}$ values (-28 to -26 ‰) were slightly depleted compared to those of unit A. Sediment grains were sometimes agglutinated by oxidation crusts. Reworked organic fragments occurred together with well-preserved seeds and chitin remains. Ostracods and mollusk shell fragments were found occasionally.

An ice-wedge cast up to 7 m wide and 3 m thick (unit C₁) filled a thermokarst depression (Figs. 2.3b and 2.3c). The ice-wedge cast contained lacustrine sediments consisting of alternating beds, from a few millimeters up to several centimeters thick, of peaty brownish plant detritus and gray fine-sandy silt layers containing clay (Figs. 2.3e and 2.5). The TOC contents were about 6 to 12 %, C/N ratios decreased upwards from 20 to about 11, and $\delta^{13}\text{C}$ values were uniform at -28 to -27 ‰. Complete gastropod and ostracod shells were frequently found. The lowermost horizon underlying the ice-wedge cast contained gray silty deposits similar to the unit A deposits.

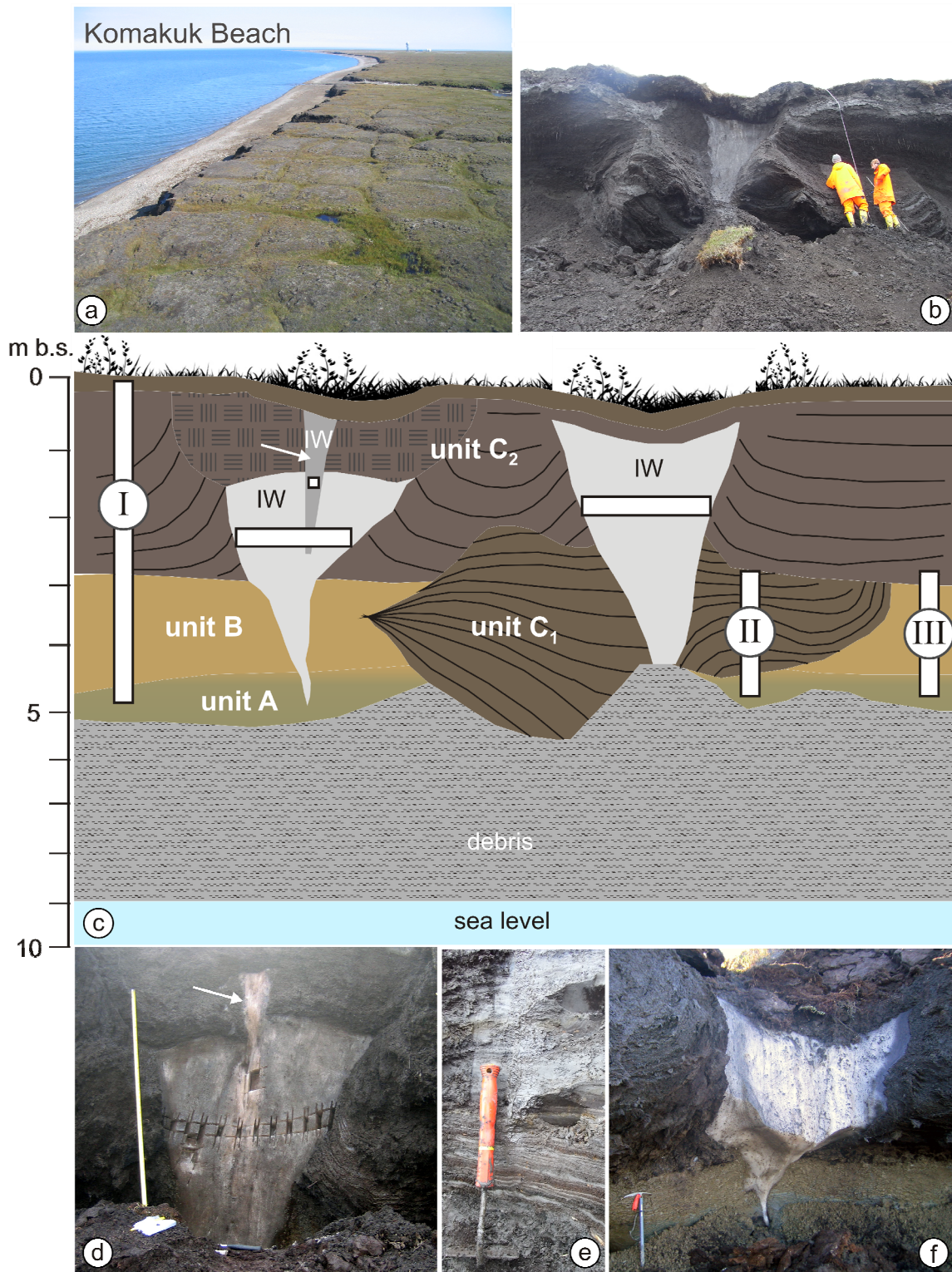


Figure 2.3: Late Glacial and Holocene sequence at the mainland coast of the Yukon Coastal Plain near Komakuk Beach (69°36'12"N; 140°30'11"W) (a) Overview photograph of high-centered polygonal tundra along the coast near Komakuk Beach; (b) Overview photograph of the studied exposure; (c) Exposure scheme with position of studied subprofiles in sediments (I, II, III) and ice wedges (IW) which are marked with white bars; (d,f) Ice wedges that penetrate the exposed sequence. Younger ice-wedge generation penetrating into an older inactive ice wedge is marked with white arrow; (e) Laminated lacustrine ice-wedge cast deposits of subprofile II (see Fig. 2.3c).

Ice-wedge cast deposits of unit C₁ were overlain by organic-rich peaty sediments of unit C₂ that were up to 3 m thick and comprised the uppermost part of the coastal outcrop (Fig. 2.3). Unit C₂ was composed of layered brownish-black moss peat at the basal part, and covered the silty sediments of unit B apart from the ice-wedge cast (Figs. 2.3c and 2.3f). The boundary between unit C₂ and B was characterized oxidation crusts, brown mottles around individual particles and highly-decomposed organic matter. Further upwards in unit C₂, peat layers with large wood fragments up to 3 cm in diameter alternated with gray sandy-silt layers 0.2 to 1.0 cm thick. The uppermost meter of the peaty sediments was weakly bedded and contained occasional particles of fine-sandy silt. TOC contents within unit C₂ varied between 11 and 46 %, C/N ratios were stable between 17 and 20, rising slightly in the uppermost meter, and $\delta^{13}\text{C}$ values reached their minimum (-29‰) towards the surface (Fig. 2.5). Unit C₂ was largely free of carbonate and calcareous fossils, likely due to acidic pH conditions within the peat. Coarse lens-like cryostructures with ice lenses between 2 and 5 cm thick and high ice contents (120 to 540 wt%) were present in unit C₂, reflecting conditions of water supersaturation prior to freezing as well as ice accumulation at the freezing front during permafrost aggradation.

Ice wedges up to 2.5 m long and 1.0 m wide penetrated the whole sedimentary sequence (Figs. 2.3c, 2.3d, and 2.3f). They cut through units A and B as epigenetic ice wedges; they became broader to the top, and probably grew syngenetically with the accumulating peat deposits as polygon fillings whose strata were often squeezed upwards (Fig. 2.3d). These wedges were usually truncated about 1 m below surface. Narrow ice wedges about 25 cm wide grew as a younger generation within the older ones, and terminated at the base of the modern active layer, which had a thickness of 30–40 cm (Fig. 2.3d). The peaty deposits and the underlying sediment units that were described could be traced between Clarence Lagoon and the airstrip at Komakuk Beach during helicopter surveys between 2006 and 2009 along the coast of the Yukon mainland. We therefore assume that the sampled locations are representative of the whole area.

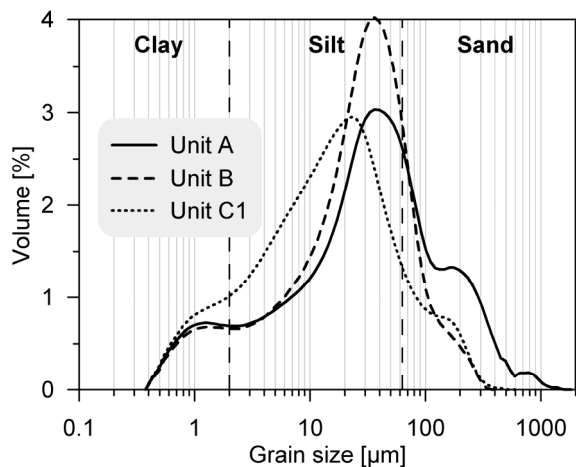


Figure 2.4: Average grain-size distribution of units A, B, and C1 from Komakuk Beach.

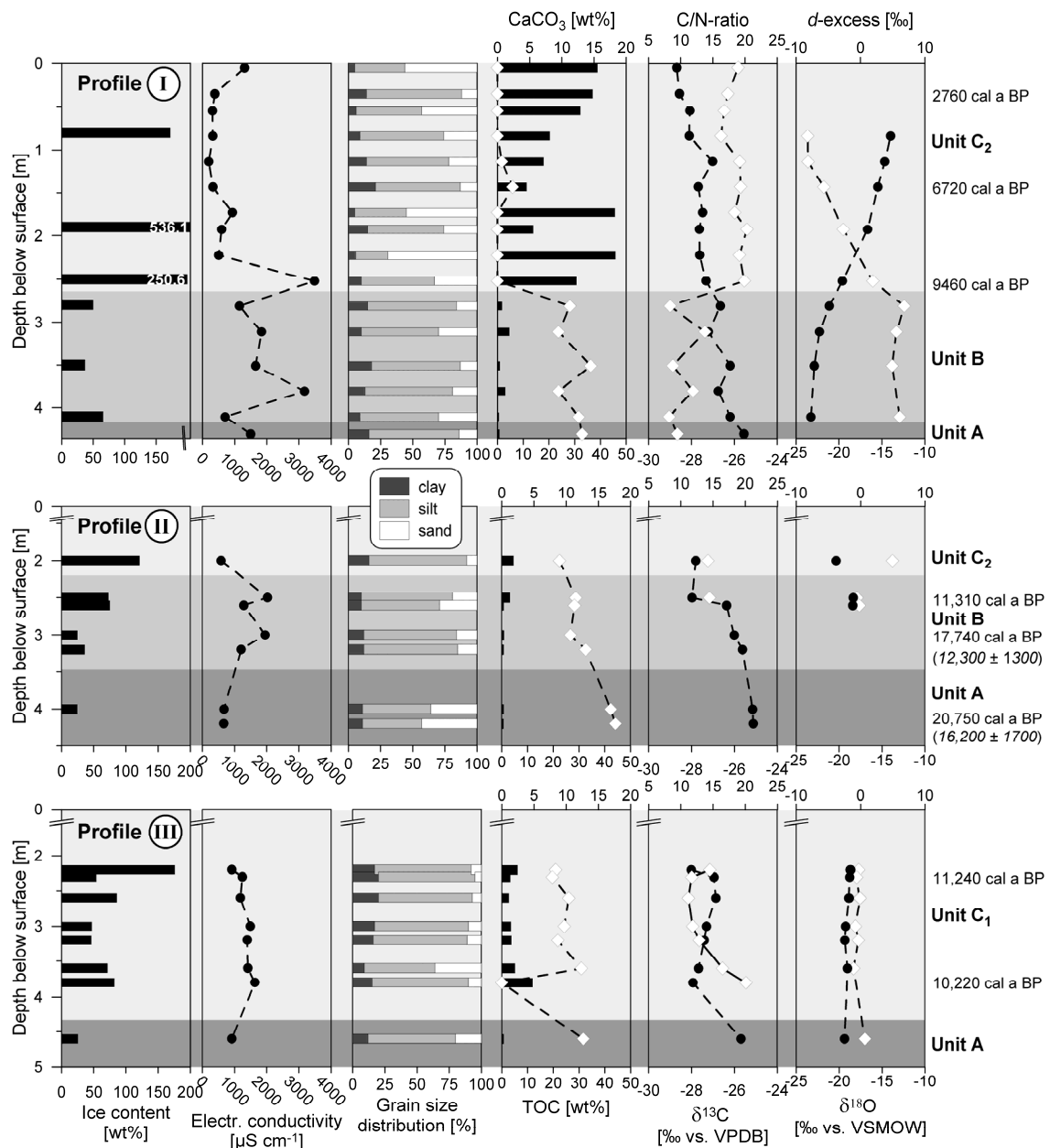


Figure 2.5: Summary of sedimentological, elemental, cryolithological, and stable isotope parameters for the different subprofiles at Komakuk Beach. Age determinations are annotated next to each horizon and are reported as calibrated years BP (IRSL ages in brackets). Parameters running down-axis (CaCO₃, C/N-ratio, d-excess) are shown as white diamonds.

Herschel Island

At the TSD site, a tabular massive ice body (unit 1, Fig. 2.6), 400 m wide, was observed in the headwall of the whole slump [cf. Fritz *et al.*, 2011]. The massive ice was unconformably overlain by a dark gray to pale gray ice-rich clayey diamicton (unit 2, Fig. 2.6) with an alternating pattern of thick ice lenses (2 to 20 cm long) and sediments with a coarse lens-like reticulate cryostructure.

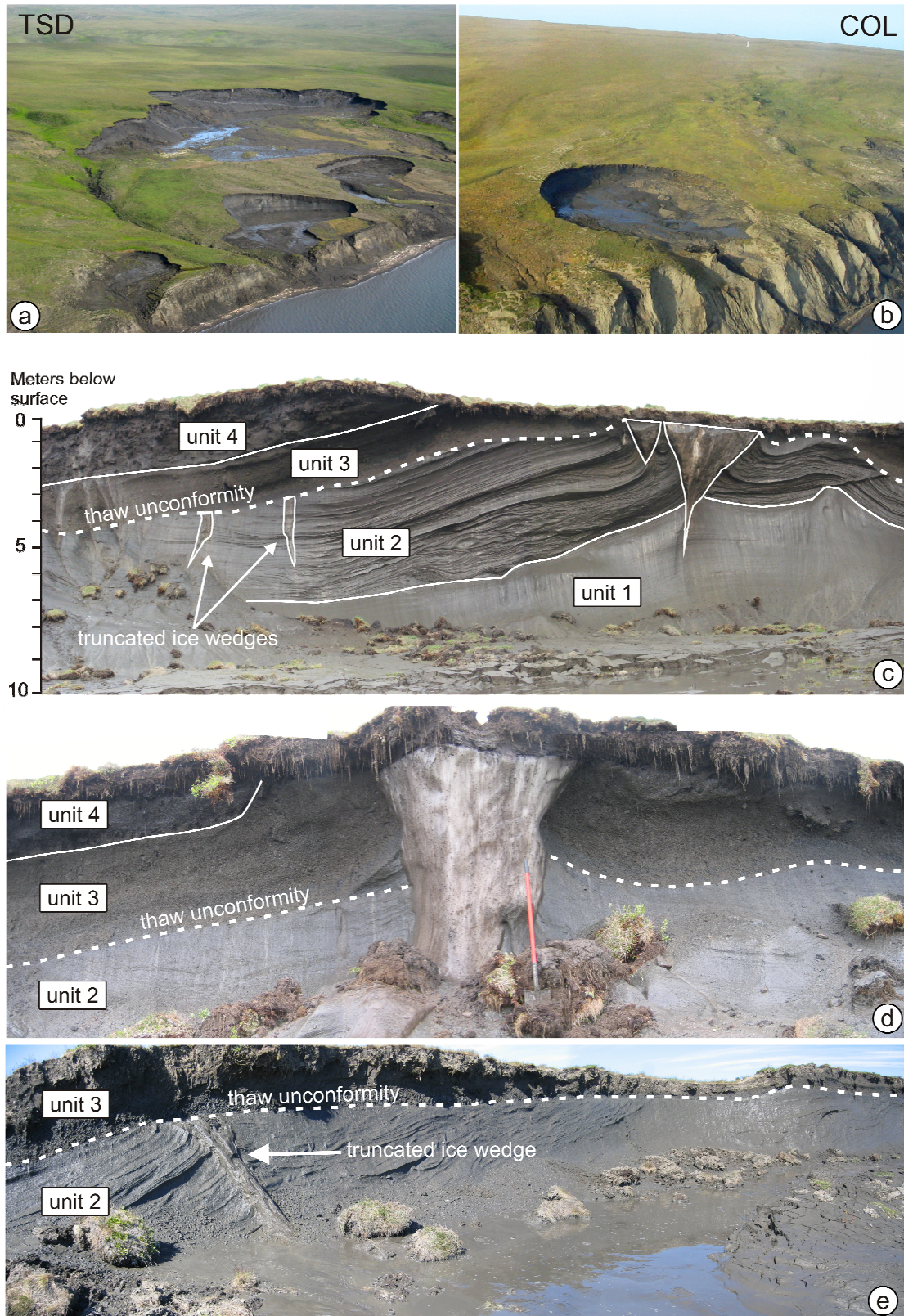


Figure 2.6: Study sites and exposures on Herschel Island (69°36'12"N; 140°30'11"W). (a) and (b) show overview photographs of retrogressive thaw slumps (TSD and COL sites); (c) Exposure of TSD site with position of thaw unconformity (dashed line); (d) Close-up view of TSD exposure with large epigenetic ice wedge penetrating thaw unconformity; shovel is 1.5m high; (e) Exposure at Collinson Head (COL site). Arrow points to a truncated ice wedge below the thaw unconformity.

Subangular rounded pebbles up to three centimeters in diameter and remains of mollusks as well as dispersed plant fragments were present throughout the unit. The main sediment fraction (< 2 mm) was characterized by a polymictic grain size distribution (Fig. 2.7). Sediments of units 1 and 2 had uniformly low TOC (0.6 to 1.6 wt%) and TN (0.1 wt%) contents. They were rich in CaCO₃ with an average of 9.2 wt% (Fig. 2.8). C/N ratios were low with values around 12, and δ¹³C values plotted within a narrow range between -26.6 and -25.9 ‰. At both sites (TSD and COL), ice-rich sediments (ice content >50 wt%) up to 5 m thick exhibited strong evidence of deformation, such as recumbent folds and boudinage structures. The upper contact of unit 2 was discordantly truncated towards unit 3 as indicated by truncated cryostructures and relict ice wedges that penetrated into the diamictic sediments and also into the deformation structures (Figs. 2.6c and 2.6e). This boundary was visible in the headwalls of both slumps (COL and TSD) and represents a thaw unconformity corresponding to the maximum depth of active-layer development in the past [cf. *Burn et al.*, 1986].

Unit 3 was composed of a grayish-brown diamicton up to 3 m thick (Fig. 2.6). It contained, on average, less ice than the underlying units (ice content ≥30 wt%), and was characterized by a lens-like reticulate to irregular reticulate cryostructure. The grain-size distribution of unit 3 was very similar to that of units 1 and 2 (Fig. 2.7), but TOC increased to 17.5 wt% in the vicinity of peat inclusions and averaged between 2 and 5 wt% (Fig. 2.8). CaCO₃ was usually depleted in unit 3, likely due to leaching by humic acids, and was absent in peaty horizons. C/N ratios showed a wide range between 11 and 23, with higher values reflecting less decomposition in organic-rich parts (Fig. 2.8).

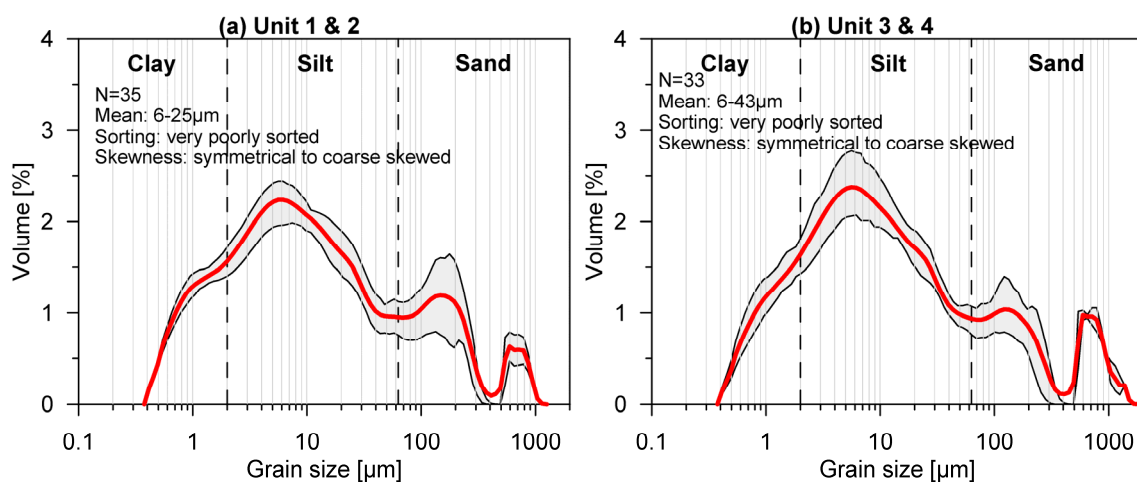


Figure 2.7: Grain-size distribution below (a) and above (b) the thaw unconformity of Herschel Island sediments. Thick line shows average grain-size distribution; gray-shaded area covers 25% and 75% percentile. Secondary grain-size parameters were calculated according to *Inman* [1952].

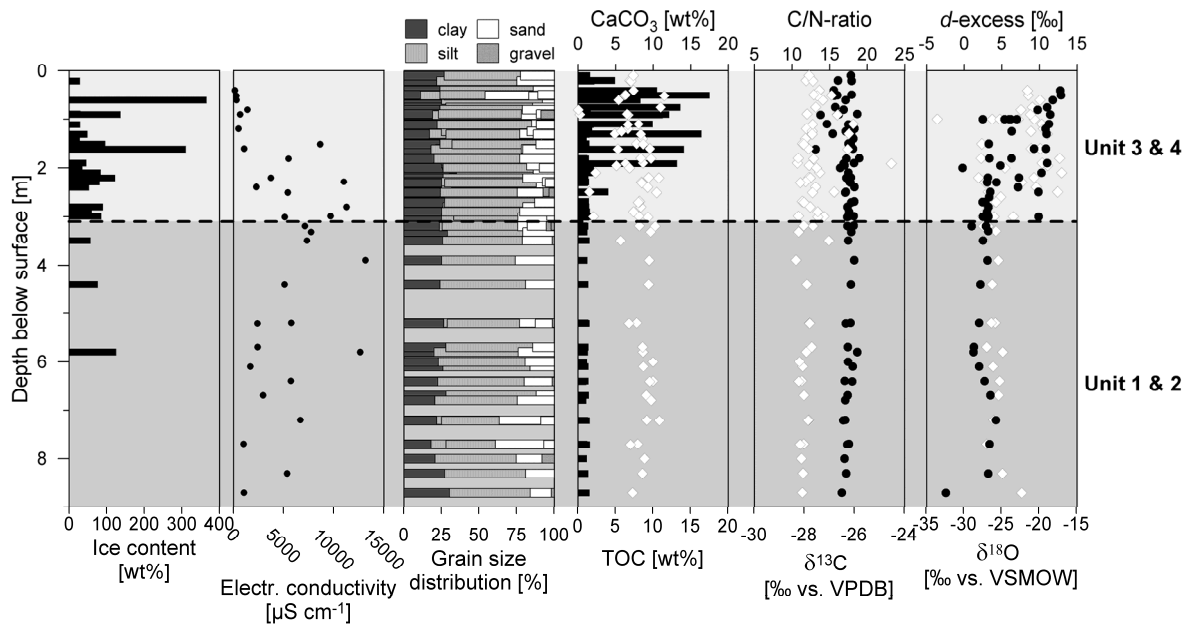


Figure 2.8: Composite plot of sedimentological, elemental, cryolithological, and stable isotope parameters for the different subprofiles on Herschel Island that combines the COL and TSD sites. Parameters running down-axis (CaCO_3 , C/N-ratio, d-excess) are shown as white diamonds. Dashed line delineates lowermost position of the thaw unconformity.

Unit 4 (Figs. 2.6c and 2.6d) was present in former depressions of a polygonal tundra only, and represents the filling of low-center ice-wedge polygons during stable surface conditions. Thick peat lenses (~50 cm) and organic-rich boggy sediments up to 2.5 m thick conformably covered the polymictic sediments of unit 3.

Inactive ice wedges up to 2.5 m wide and up to 5 m long penetrated downwards through units 2 and 3 and sometimes also into the massive ice of unit 1 (Fig. 2.6c). The very-poorly-sorted diamictic sediments on Herschel Island (Fig. 2.7) are polygenetic in character and consist of glacially-reworked marine, near-shore marine, and terrestrial deposits [Mackay, 1959; Bouchard, 1974] that have been partially redeposited during periglacial environmental conditions.

2.4.2 Geochronology

Twenty-one samples in total were AMS radiocarbon dated (Table 2.2). Nine samples originated from Komakuk Beach, eight samples from the TSD site, and four from the COL site. According to these data, the silty and fine-sandy sediments of units A and B at Komakuk Beach accumulated during Late Wisconsinan times between 20.7 and 11.3 cal ka BP. These radiocarbon dates were supported by parallel IRSL age determinations of two samples from the same units. The obtained IRSL ages of 16.2 ± 1.7 and 12.3 ± 1.3 ka (Table 2.3) fit very well with the corresponding radiocarbon ages, even though IRSL ages were slightly younger for samples of similar depth. An

age of 48.4 ka BP obtained from unit A is not taken into account for the stratigraphic interpretation because the dated material was probably some old redeposited woody fragments that occurred in this sample. The bedded peaty and boggy deposits of unit C₂ yielded Holocene ages between 9.5 and 2.8 cal ka BP and the ice wedge cast deposits of unit C₁ were dated to 11.2 and 10.2 cal ka BP.

The ages of Herschel Island sediments varied widely, from infinite to modern post-bomb ages, and age inversions within each unit were frequent. Dates below the thaw unconformity between units 2 and 3 were generally older than 16.2 cal ka BP; several samples were near the radiocarbon determination limit or of infinite age. Unit 3 deposits above the cryostratigraphic unconformity yielded ages younger than ~12 cal ka BP except for one older date of 32.0 cal ka BP directly above the transition from unit 2 to 3 at 1.8 m below surface. Additionally, two samples for IRSL dating were taken below the COL site from bedded sandy deposits with gravel bands and marine mollusk remains, stratigraphically underlying oxidized gravel beds with mollusk remains about 40 m asl. Regarded as preglacial near-shore facies sediments [Bouchard, 1974], they gave IRSL ages of 87 ± 11 ka and 74 ± 8 ka (Table 2.3).

Table 2.2: Summary of AMS ¹⁴C results. HI: Herschel Island, KOM: Komakuk Beach, LW: Late Wisconsinan, EH: Early Holocene, MH: Middle Holocene, LH: Late Holocene.

Location	Unit	Depth below surface [m]	Dated Material	Uncalibrated ¹⁴ C ages [yr BP]	Calibrated age range [cal yr BP], 2σ	Midpoint 2σ-age [cal yr BP]	Lab no. ^a	Stratigraphical assignment
KOM	C2	0.3	peat	2637 ± 31	2792-2725	2759	KIA32230	LH
KOM	C2	1.4	peat	5890 ± 40	6798-6634	6716	Poz-36431	EH / MH
KOM	C2	2.5	peat	8405 ± 45	9522-9394	9458	KIA32229	EH
KOM	B/C2	2.5	plant detritus	9890 ± 50	11,407-11,203	11,305	Poz-36432	LW / EH
KOM	B	3.0	plant detritus	14,620 ± 80	18,056-17,413	17,735	Poz-36433	LW
KOM	A	4.2	plant detritus	17,370 ± 100	21,184-20,309	20,747	Poz-36435	LW
KOM	A	4.3	wood fragments	48,400 +3270/-2320	–	–	KIA32228	^b
KOM	C1	2.3	peat	9810 ± 60	11,355-11,124	11,240	Poz-36436	EH
KOM	C1	3.8	peat	9050 ± 50	10,297-10,151	10,224	Poz-36437	EH
HI	3	0.8	plant detritus	9840 ± 60	11,400-11,161	11,281	Poz-36438	above unconformity
HI	3	0.9	plant detritus	1110 ± 35	1084-933	1009	KIA32232	above unconformity
HI	3	0.8	plant detritus	2290 ± 30	2353-2030	2192	KIA32236 ^c	above unconformity

Table 2.2: (continued)

Location	Unit	Depth below surface [m]	Dated Material	Uncalibrated ¹⁴ C ages [yr BP]	Calibrated age range [cal yr BP], 2σ	Midpoint 2σ-age [cal yr BP]	Lab no. ^a	Stratigraphical assignment
HI	3	1.1	plant detritus	625 ± 35	661-550	606	KIA32234 ^c	above unconformity
HI	3	1.8	plant detritus	27,660 ± 350	32,811-31,264	32,038	Poz-36430	above unconformity
HI	3	2.0	plant detritus	8660 ± 50	9744-9532	9638	Poz-36439	above unconformity
HI	3	2.3	plant detritus	>1954 A.D.	–	–	KIA32233 ^c	above unconformity
HI	3	3.0	plant detritus	10,190 ± 50	12,076-11,704	11,890	KIA32235	above unconformity
HI	2	3.2	plant detritus	> 48,000	–	–	Poz-36429	below unconformity
HI	2	3.5	plant detritus	50,770 +3800/-2570	–	–	KIA32231	below unconformity
HI	2	6.1	plant detritus	37,400 ± 1000	43,751-40,419	42,085	Poz-36440	below unconformity
HI	2	7.7	plant detritus	13,300 ± 70	16,781-15,609	16,195	Poz-36441	below unconformity

^a KIA = Christian Albrechts University Kiel. POZ = Poznan Radiocarbon Laboratory.

^b not used for interpretation for reasons see in the text.

^c from *Lantuit et al.* [under review].

Table 2.3: Summary of IRSL dating results. HI: Herschel Island, KOM: Komakuk Beach, D_e: equivalent dose, D_{rate}: dose rate.

Location	Deposit type	Lab no.	Depth below surface [m]	D _e [Gy]	D _{rate} [Gy/ka]	IRSL age [ka]
KOM	see unit B	KOM1	3.0	33.4 ± 0.7	2.72 ± 0.28	12.3 ± 1.3
KOM	see unit A	KOM2	4.0	45.2 ± 1.4	2.79 ± 0.28	16.2 ± 1.7
HI	bedded sand, unfrozen	COL2	1.5	239.2 ± 14.6	2.75 ± 0.30	87 ± 11
HI	bedded sand, unfrozen	COL1	1.9	205.2 ± 7.9	2.77 ± 0.28	74 ± 8

2.4.3 Ground ice

Stable water isotopes of tabular massive ice, ice wedges, and segregated ice

Table 2.4 summarizes the results for the different locations and ice types. The stable O-H isotope composition from tabular massive ground ice (unit 1) exposed in TSD was described in detail by *Fritz et al.* [2011]. These samples gave the lowest δ¹⁸O values of all studied ice types, ranging from –34.2 to –31.3 ‰ (Table 2.4). With a δD-δ¹⁸O regression slope value of 7.0 (R²=0.98)

and an average d -excess of 7.2 ‰, the massive ice samples lie slightly below the GMWL. Ice wedges at Komakuk Beach and on Herschel Island can be differentiated into two major groups based on their O-H isotope composition and their stratigraphic relationship (Table 2.4). $\delta^{18}\text{O}$ values from Komakuk Beach ice wedges ranged between -24.8 and -20.5 ‰ (Fig. 2.9a). The mean d -excess of 7.1 ‰ and δD - $\delta^{18}\text{O}$ regression slope of 7.1 ($R^2=0.99$) indicate that these samples lie slightly below the GMWL. Ice wedges from Herschel Island plotted in a similar range for $\delta^{18}\text{O}$ (-25.6 to -19.4 ‰) and d -excess (mean: 9.7 ‰), and along a regression slope of 7.7 ($R^2=0.99$) which is very close to the GMWL (Fig. 2.9a). A small number of truncated ice-wedge roots were encountered below the distinct thaw unconformity that was found between 1.5 and 3 m below the surface on Herschel Island (Figs. 2.6c and 2.6e). These deeply-truncated ice wedges could not be found at Komakuk Beach. Brownish sediment-bearing ice wedges exhibited low mean $\delta^{18}\text{O}$ values of -29.1 ‰ (Fig. 2.9a) and a low mean d -excess of 0.1 ‰, and therefore plot beneath the GMWL along a regression slope value of 7.8 ($R^2=0.99$).

Even though preservation of pore water as segregated ice occurs via a wide range of processes, Mackay [1983], Murton and French [1994], Kotler and Burn [2000], and Schwamborn *et al.* [2006] have shown that stable O-H isotopes in segregated ice can still reflect environmental and climatic changes when considered with caution. Peat deposits at Komakuk Beach showed relatively high $\delta^{18}\text{O}$ values between -19.6 and -14.0 ‰ and low d -excess values between -8.2 and 1.9 ‰; lower $\delta^{18}\text{O}$ values were accompanied by higher values for d -excess and vice versa (Figs. 2.4 and 2.9b).

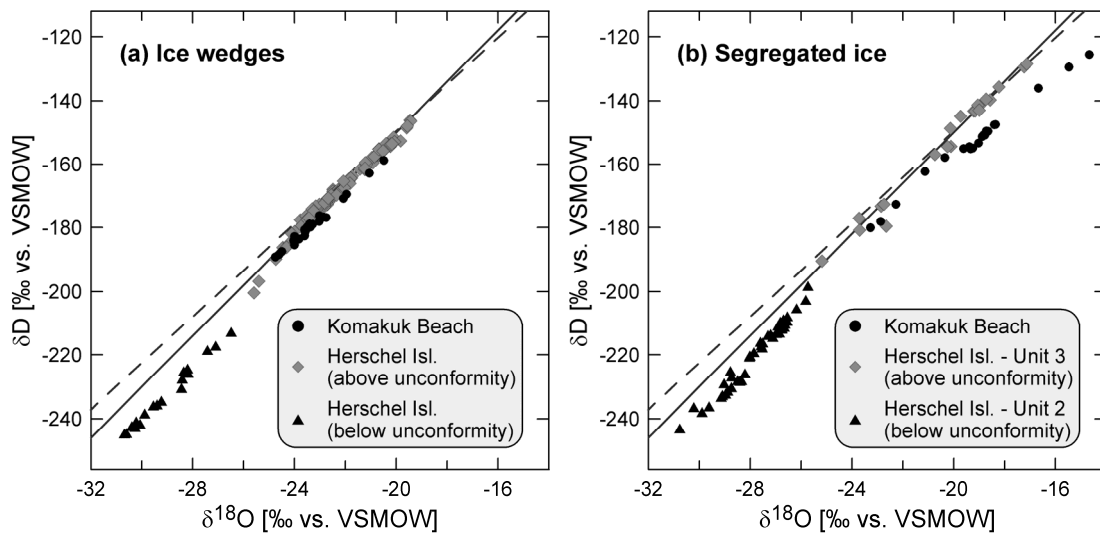


Figure 2.9: δD - $\delta^{18}\text{O}$ diagrams for (a) ice wedges and (b) segregated ice for Komakuk Beach and Herschel Island. Solid line: GMWL ($\delta\text{D}=8\delta^{18}\text{O}+10$; Craig, 1961); dashed line: LMWL for Inuvik ($\delta\text{D}=7.3\delta^{18}\text{O}-3.5$; $R^2=0.98$; IAEA, 2006).

Table 2.4: Stable isotope ($\delta^{18}\text{O}$, δD and d -excess) minimum, mean, and maximum values, as well as slopes and linear regression coefficients of the δD - $\delta^{18}\text{O}$ relationship for the different ice types sampled. HI: Herschel Island, KOM: Komakuk Beach.

Location	Ice type	N	$\delta^{18}\text{O}$ [‰]			δD [‰]			d -excess [‰]			Slope	R^2	Stratigraphic affiliation
			Min	Mean	Max	Min	Mean	Max	Min	Mean	Max			
KOM	Ice wedge	25	-24.8	-23.3	-20.5	-189	-179	-159	5.1	7.2	9.2	7.1	0.99	Holocene
HI	Ice wedge	105	-25.6	-22.1	-19.4	-200	-167	-146	4.4	9.7	12.6	7.7	0.99	above unconformity; (unit 3 & 4) Holocene
HI	Ice wedge	18	-30.7	-29.1	-26.5	-245	-232	-213	-2.8	0.1	1.7	7.8	0.99	below unconformity; (unit 2) Late Wisconsinan
KOM	Segregated ice	21	-23.3	-19.0	-14.0	-180	-152	-120	-8.2	0.1	6.8	6.3	0.99	Late Wisconsinan to sub-recent
HI	Segregated ice	21	-25.2	-20.3	-17.1	-190	-153	-129	1.6	9.5	12.9	8.0	0.98	above unconformity; (unit 3 & 4) Holocene
HI	Segregated ice ^a	44	-30.8	-27.8	-25.7	-243	-219	-198	-1.3	2.8	7.7	8.8	0.97	below unconformity; (unit 2) Late Wisconsinan
HI	Tabular massive ground ice ^a	40	-34.2	-33.0	-31.3	-265	-258	-244	5.3	7.2	9.3	7.0	0.98	Late Wisconsinan (unit 1)

^a includes data from *Fritz et al.* [2011].

Ice within the fine-grained sediments of unit A and B had $\delta^{18}\text{O}$ values of -22.2 ± 1.1 ‰ and an average d -excess of 5.9 ± 0.9 ‰. The stable O-H isotope composition of Herschel Island segregated ice mirrors the general cryostratigraphy of two zones. At the COL and TSD sites, $\delta^{18}\text{O}$ values beneath the thaw unconformity averaged below -26 ‰, with a minimum of -30.8 ‰ and an average d -excess of 2.8 ‰. A large range in $\delta^{18}\text{O}$ (-25.2 to -17.1 ‰) and d -excess (1.6 to 12.9 ‰) occurred in deposits above the unconformity (Fig. 2.9b).

Hydrochemistry of segregated ice

Table 2.5 summarizes the hydrochemical results of segregated ice for the different locations and stratigraphic units. The major ion composition of segregated ice along Komakuk Beach can be subdivided according to the described stratigraphic units. Lowermost unit A with an EC between 5000 and 7000 $\mu\text{S}/\text{cm}$ was dominated by Na^+ (52 %) and Cl^- (67 %), with second-order proportions of Ca^{2+} , Mg^{2+} , and SO_4^{2-} ; HCO_3^- was almost absent. The pore water hydrochemistry of unit B was highly variable, with EC values that ranged between 2700 and 17,800 $\mu\text{S}/\text{cm}$. This unit showed high loads of Ca^{2+} (48 %) and SO_4^{2-} (40 %); HCO_3^- was almost absent. Samples in which EC was highest were enriched in Na^+ and Cl^- ions and depleted in Ca^{2+} and SO_4^{2-} . Segregated ice from the ice-wedge cast deposits of unit C₁ showed average proportions of 51 % and 32 % for the dominant cations Ca^{2+} and Mg^{2+} ; anion proportions were highly variable, i.e. SO_4^{2-} (10-70 %),

Table 2.5: Summary of major ion composition and total ion content indicated by the electrical conductivity (EC) of segregated ice. Absolute ion contents are presented in mg/l. The percentages of individual anion and cation species are given as per cent of the total anion or cation population.

Profile		Electrical conductivity	Cl ⁻	SO ₄ ²⁻	HCO ₃ ⁻	Ca ²⁺	K ⁺	Mg ²⁺	Na ⁺	Cl ⁻	SO ₄ ²⁻	HCO ₃ ⁻	Ca ²⁺	K ⁺	Mg ²⁺	Na ⁺	
			[%]	[%]	[%]	[%]	[%]	[%]	[%]	[%]	[mg/l]	[mg/l]	[mg/l]	[mg/l]	[mg/l]	[mg/l]	[mg/l]
			[μS/cm]	[%]	[%]	[%]	[%]	[%]	[%]	[%]	[mg/l]	[mg/l]	[mg/l]	[mg/l]	[mg/l]	[mg/l]	[mg/l]
Komakuk Beach (unit A)	Mean	6083	66.5	28.2	5.3	21.0	0.4	26.2	52.4	1592	838	205	258	10.5	199	758	
	Min.	4990	42.4	17.4	3.2	16.9	0.4	26.1	45.9	838	578	133	224	8.64	177	590	
	Max.	7010	79.4	49.4	8.1	27.5	0.5	26.3	56.3	1996	1324	276	308	11.8	227	920	
Komakuk Beach (unit B)	Mean	8308	54.7	40.4	4.9	48.1	0.3	26.5	25.1	2464	885	196	667	8.15	289	599	
	Min.	2660	6.1	0.8	1.4	27.5	0.2	21.4	9.1	88.4	51.5	139	509	4.23	115	93.0	
	Max.	17770	97.8	88.3	8.6	69.2	0.4	31.8	40.5	6475	1729	293	885	15.0	620	1495	
Komakuk Beach (unit C ₁)	Mean	4280	36.6	47.8	15.5	51.2	0.4	31.6	16.7	713	1134	379	514	8.39	200	201	
	Min.	1808	15.6	10.2	2.6	40.6	0.4	26.2	11.3	139	275	121	255	4.36	79.1	88.8	
	Max.	6420	76.1	69.9	41.9	60.3	0.5	34.9	25.2	1506	1917	735	755	11.7	288	346	
Komakuk Beach (unit C ₂)	Mean	929	18.1	5.8	76.1	69.0	0.2	22.8	8.0	159	119	162	115	0.72	26.4	36.8	
	Min.	206	1.9	0	0.1	51.4	0	14.6	3.1	1.61	<0.1	4.73	23.7	<0.2	7.47	2.56	
	Max.	5170	60.8	39.1	98.1	77.6	0.5	36.2	23.7	1204	1050	247	516	2.91	150	273	
Herschel Island below thaw unconformity (unit 2) ^a	Mean	6635	86.7	7.4	5.9	5.6	1.9	11.8	80.7	2132	214	177	83.9	47.1	118	1293	
	Min.	949	25.0	0.1	1.6	1.5	1.2	6.5	44.6	213	5.50	44.1	6.91	7.24	6.47	164	
	Max.	14610	97.8	47.2	27.8	24.6	3.6	27.1	89.6	4671	1328	480	419	109	375	2715	
Herschel Island above thaw unconformity (unit 3 & 4)	Mean	4563	47.1	12.5	40.4	28.5	2.5	22.3	46.7	1290	376	215	168	25.9	107	703	
	Min.	136	5.4	0	1.9	8.5	0.9	12.2	8.4	6.05	<0.1	65.3	13.3	2.92	4.48	7.25	
	Max.	14300	90.2	39.5	94.6	58.7	4.9	34.0	73.7	4751	2019	396	540	75.0	354	2505	

^a includes data from *Fritz et al.* [2011].

HCO₃⁻ (3-42 %), and Cl⁻ (16-76 %), which decreased upwards. EC values of Unit C₂ were generally lower than 800 μS/cm and were dominated by Ca²⁺ (69 %) and HCO₃⁻ (76 %); SO₄²⁻ was nearly absent. One exception was the lowermost peat horizon (EC = 5200 μS/cm) just above the underlying clastic-dominated unit B. Cl⁻ and SO₄²⁻ ions were enriched in this horizon, HCO₃⁻ was completely absent, and notable contents of manganese (Mn²⁺: 11.0 mg/l) and nitrate ions (NO₃⁻: 113.5 mg/l) were present.

The major ion composition of segregated ice derived from Herschel Island is dominated by Na⁺ and Cl⁻ ions and high EC values of up to 14,000 μS/cm (Table 2.5). Values above the thaw unconformity showed a larger variability and higher concentrations of Mg²⁺, Ca²⁺, and HCO₃⁻. This hydrochemical pattern reflects the marine origin of host sediments on Herschel Island [*Fritz et al.*, 2011]

2.4.4 Ostracod studies at Komakuk Beach

Eight ostracod taxa were identified to species level, one to genus level, and one taxon to its subfamily level. An overview is given in Table 2.6. All identified taxa belong to freshwater habitats. Few specimens of juvenile *Cypria exsculpta* and juvenile Candoninae were found in unit A sediments. Juvenile Candoninae were present, although rarely, throughout unit B sediments. The highest ostracod occurrence and diversity could be observed at the transition between Unit B and the overlying peat of unit C₂. In this zone the assemblage comprised nine taxa including the species

Table 2.6: Freshwater ostracod taxa from sediment samples of the Komakuk profiles. Species nomenclature follows *Swain* [1963], *Delorme* [1968] and *Smith and Delorme* [2010].

Ostracod taxa	Occurrence in unit
<i>Cytherissa lacustris</i> (SARS, 1863)	C ₁
juvenile Candoninae	A, B, C ₁ , C ₂
<i>Candona candida</i> (MÜLLER, 1776)	C ₁ , C ₂
<i>Candona rectangulata</i> (ALM, 1914)	C ₂
<i>Fabaeformiscandona caudata</i> (KAUFMANN, 1900)	C ₂
<i>Cypria exsculpta</i> (FISCHER, 1855)	A, C ₁ , C ₂
<i>Limnocythere camera</i> (DELORME, 1967)	C ₂
<i>Limnocytherina sanctipatricii</i> (BRADY and ROBERTSON, 1969)	C ₂
<i>Limnocythere</i> sp.	C ₂
<i>Ilyocypris biplicata</i> (KOCH, 1838)	C ₁ , C ₂

Ilyocypris biplicata, *Cypria exsculpta*, *Limnocythere camera*, *Limnocytherina sanctipatricii*, *Candona candida*, *C. rectangulata* and *Fabaeformiscandona caudata*. Ehippia (resting eggs) of *Daphnia* sp. and mollusk shell fragments were also found. No other peat samples contained ostracod remains. Ice wedge cast deposits (unit C₁) contained *Cytherissa lacustris*, *Candona candida*, *Cypria exsculpta*, *Ilyocypris biplicata*, and juvenile Candoninae, along with mollusk shells and water plant macrofossils of *Potamogeton* sp. and *Hippuris* sp.

2.5 Discussion

2.5.1 Late Wisconsinan landscape evolution

Glacial chronology

Several attempts have been made to ascertain the formation age of Herschel Island and therefore the timing of the maximum LIS extent along the YCP during Wisconsinan times. It is difficult to establish a consistent stratigraphy on Herschel Island because of the island's ice-thrust nature in general [*Mackay*, 1959; *Bouchard*, 1974], the deformation of preglacial marine clays, near-shore and terrestrial deposits in particular as well as periglacial reworking due to thermokarst processes, and sequential unloading where tabular massive ground ice is present [*Fritz et al.*, 2011] (Fig. 2.10a). Radiocarbon dating of entrapped CO₂ in supposedly glacially-deformed massive ground ice on Herschel Island, ice that is probably equal in age to the massive ice of unit 1, yielded an age of 20.9 cal ka BP [*Moorman et al.*, 1996]. This date, together with a date of 19.2 cal ka BP for a fossil Yukon horse (*Equus lambei*) cranium that was probably found *in situ* [*Harrington*, 1989], may provide a reasonable interval for deglaciation of the Herschel Island ice-thrust ridge.

Zazula *et al.* [2009] pointed out that the absence of Herschel Island vertebrate remains that have been radiocarbon-dated to between 42.1 and 20.4 cal ka BP and the frequent occurrence of findings yielding infinite ages give a valuable indication that the all-time maximum of the LIS in the Herschel Island area occurred towards the Late Wisconsinan. This is in good agreement with evidence from the Tuktoyaktuk Coastlands [Dallimore *et al.*, 1997; Murton *et al.*, 1997; Bateman and Murton, 2006; Murton *et al.*, 2007], Banks Island [England *et al.*, 2009], the Richardson Mountains, and the Mackenzie Mountains [Duk-Rodkin and Hughes, 1995; Duk-Rodkin *et al.*, 1996; Dyke *et al.*, 2002] for a Late Wisconsinan maximum for the entire northwest margin of the LIS [Zazula *et al.*, 2009; Kennedy *et al.*, 2010]. Our IRSL ages of 74 ± 8 ka and 87 ± 11 ka on likely glacially-upthrust marine beach deposits, which predate the formation of the Herschel Island ice-thrust ridge, assign the onset of the local glaciation towards the Early Wisconsinan or younger.

Depositional environment

As was suggested for the Tuktoyaktuk Coastlands by Murton *et al.* [1997], deglaciation may have supplied a large amount of meltwater to the unglaciated parts of the YCP and adjacent dry shelf areas west of Herschel Island. A sandur-like accumulation plain with braided meltwater channels in combination with alluvial and proluvial sediment supply from the gentle foothill slopes of the Buckland Hills and the British Mountains probably led to deposition of a distal sequence of fines represented by unit A along Komakuk Beach dated to 20.7 cal ka BP (AMS) and 16.2 ± 1.7 ka (IRSL) (Fig. 2.10a). A freshwater facies is supported by the occurrence of freshwater invertebrate fossils and by $\delta^{13}\text{C}$ values that indicate a terrestrial carbon source. We infer low bioproductivity according to organic matter parameters and the sparseness of ostracods, which could be due either to running water or to harsh climate conditions. Moderately enriched ion contents probably originated from sediments similar to the ion-rich deposits that presently occur on Herschel Island.

As the meltwater input ceased due to further retreat of the LIS margin, eolian input of loess-like calcareous fine-sandy silt – identified by a more pronounced peak in the coarse silt fraction and a relatively high CaCO_3 content (Fig. 2.5) – onto a still-existing wetland during harsh and dry climate conditions may have become a more pronounced sediment source for deposition of unit B between 17.7 and 11.3 cal ka BP (Fig. 2.10b). Strong eolian activity during late-glacial times is recorded from the Tuktoyaktuk Coastlands [Murton *et al.*, 1997; Bateman and Murton, 2006; Murton *et al.*, 2007], the interior Yukon [Lauriol *et al.*, 2002], and Northern Alaska [Carter, 1981, 1983; Dinter *et al.*, 1990]. The source area of deflation may have been the exposed shelf areas and proglacial fields, which were characterized by fine-grained calcareous deposits similar to upthrust Herschel Island sediments. Higher ion contents of marine-related elements in unit B support this view (Table 2.5). In contrast to the large sand seas and dune fields in Northern Alaska and the

Tuktoyaktuk Coastlands [Carter, 1981; Murton, 2009], substantial areas along the YCP may have been protected from eolian transport by cohesive diamictic sediments [Bateman and Murton, 2006]. Moreover, the source area for eolian sediment supply in this region was probably never as large as in other parts of the Arctic Coastal Plain due to a narrow shelf close to the Mackenzie Trough that existed even during the LGM sea level lowstand (Fig. 2.1). The polygenetic sediments of unit A and B at Komakuk Beach are completely structureless, probably as a result of permafrost and ground ice aggradation in moist deposits.

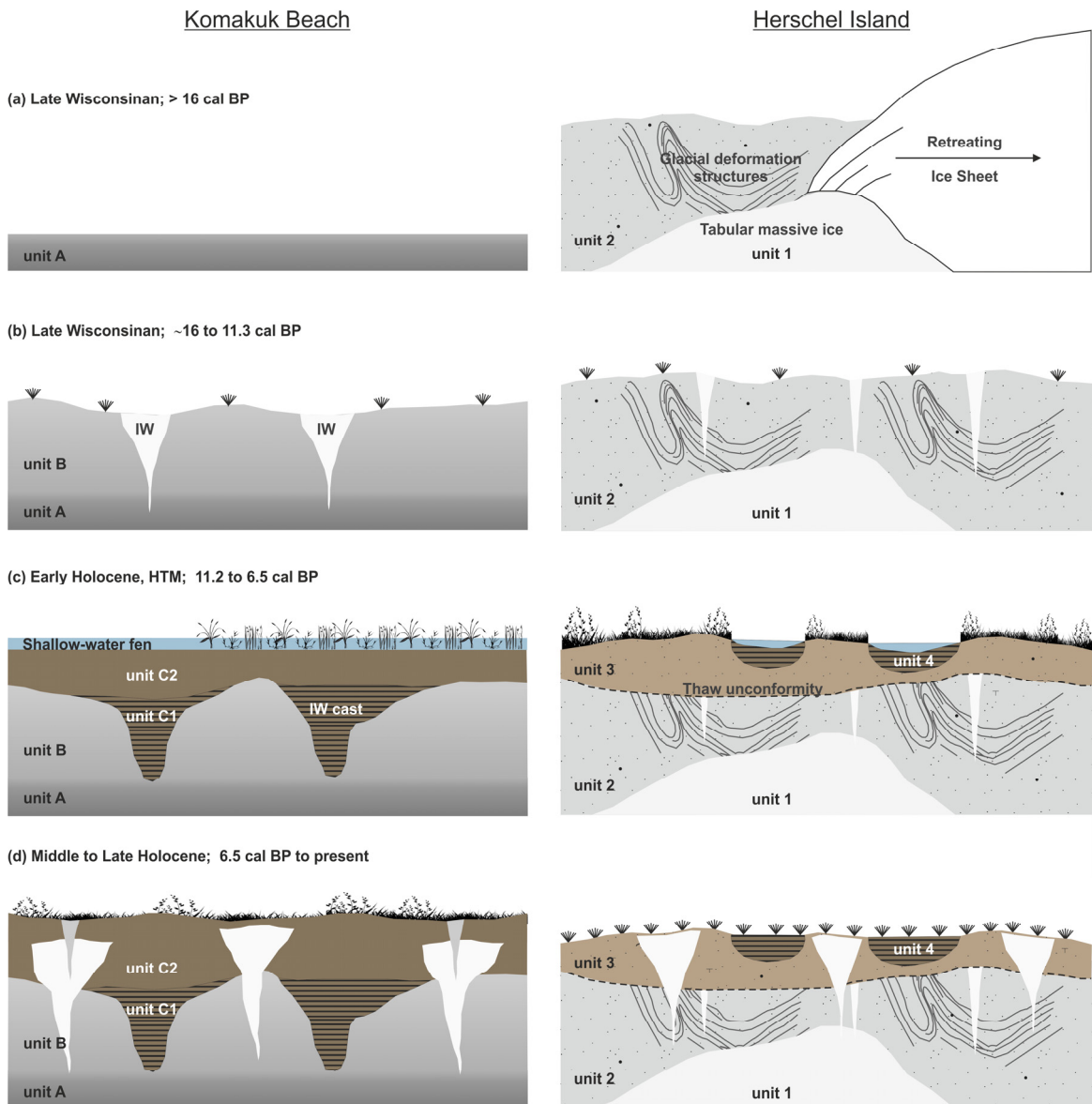


Figure 2.10: General scheme of Late Wisconsinan–Holocene landscape dynamics showing the main stages of sediment deposition, ground-ice formation, and degradation beyond the LIS maximum extent (Komakuk Beach) and within the LIS extent (Herschel Island).

Ground ice development

Ice-wedge formation and permafrost aggradation along Komakuk Beach occurred simultaneously with the deposition of unit B as indicated by ice-wedge cast deposits that must have accumulated after the melt-out of ice wedges from unit B (Figs. 2.10b and 2.10c). Ice-wedge formation occurred for some time during the late glacial, probably prior to the end of the Younger Dryas cold interval [Meyer *et al.*, 2010] at about 11.3 cal ka BP when thermokarst, peat accumulation, and organic-rich lacustrine deposition began to occur. Although completely degraded along Komakuk Beach, remnants of Late Wisconsinan ice wedges (Figs. 2.10b and 2.10c) have been preserved in Herschel Island deposits [cf. Michel, 1990] older than 16.2 cal ka BP, so that these truncated ice wedges are considered to be younger. Narrow ice-wedge roots with silty ice fillings and truncated by a distinct thaw unconformity show a $\delta^{18}\text{O}$ signature, which is depleted by 5-7 ‰ and *d*-excess values that are 7-9 ‰ lower than those of Holocene ice wedges that vary between -25.5 and -20.5 ‰. Similar low $\delta^{18}\text{O}$ values, generally below -26 ‰ and as low as -32 ‰, for pre-Holocene ice wedges were reported from Herschel Island [Michel, 1990], the Tuktoyaktuk Peninsula [Mackay, 1983], the central Yukon [Burn *et al.*, 1986; Kotler and Burn, 2000], and Barrow in Alaska [Meyer *et al.*, 2010]. The observed isotopic difference suggests greatly reduced winter air temperatures during snow formation. Although winter air temperatures had been increasing since around 16 cal ka BP, lower than modern January temperatures persisted in east Beringia at least until ~13 cal ka BP [Viau *et al.*, 2008]. Ice wedges and fossil beetle assemblages from northern Alaska have recorded a large-scale cooling of winter and summer temperatures between 12.8 and 11.5 cal ka BP, coincident with the Younger Dryas cold interval [Elias, 2000; Meyer *et al.*, 2010].

The limited occurrence of Late Wisconsinan ice wedges was probably caused by low moisture supply in winter [Kotler and Burn, 2000] triggered by an extensive sea-ice cover on the Beaufort Sea until ~9 cal ka BP [Schell *et al.*, 2008] in combination with a lowered glacio-eustatic sea level [Bateman and Murton, 2006; Murton and Bateman, 2007]. Murton [1996] concluded that a trend from sediment-rich fillings of Wisconsinan ice wedges to sediment-poor Holocene ice wedges [cf. Kanevskiy *et al.*, 2011] may record an environmental change from polar-desert-like conditions of the Late Wisconsinan to moister tundra during the Holocene. The proposed dry winter conditions could have also been responsible for a lowered *d*-excess in Wisconsinan ice wedges because a relatively large water loss by sublimation from a thin snow cover (kinetic fractionation) would lead to a loss of light isotopes in a snow pack that becomes successively depleted in ^{16}O compared to the initial precipitation [Meyer *et al.*, 2002a]. Another or even a concurrent possibility is a moisture source region that deviates from the present one. North Pacific winter sea surface temperatures (SSTs) control the moisture content and temperature of air masses that move in from the Pacific towards northwest Canada [Bartlein *et al.*, 1991], and therefore exhibit the potential to change the

d-excess signal. Mann and Hamilton [1995] suggested that a cooling of North Pacific waters during the LGM and the Younger Dryas may have intensified the Polar Front as well as the Aleutian Low and shifted them southward. Higher humidity in a more southerly moisture source region and/or lower SSTs as a consequence of a southward displacement of the sea-ice boundary that probably prevailed until late glacial times would have led to reduced *d*-excess values.

2.5.2 Early Holocene Thermal Maximum

Regional evidence

A precession-driven summer insolation maximum around 12-10 cal ka BP in combination with the waning LIS led to a warmer-than-modern period across large parts of the western Arctic [Ritchie *et al.*, 1983; Kaufman *et al.*, 2004] that is known as the Holocene thermal maximum (HTM). Western arctic Canada experienced maximum summer warmth beginning around 10.6 cal ka BP [Kaufman *et al.*, 2004] with a cooling to near-modern conditions between 6.7 and 5.6 cal ka BP [Cwynar and Spear, 1995]. A rapidly transgressing sea from its regional minimum of about 140 m below present sea level during the LGM [Hill *et al.*, 1985] and a decreasing sea ice cover [Schell *et al.*, 2008] might have attenuated increasing summer temperatures [Burn, 1997] and delivered more moisture into a formerly continental area that evolved into a coastal maritime environment [Kaufman *et al.*, 2004]. However, bathymetric charts show a relatively narrow continental shelf near Herschel Island and a shoreline position only 4 to 15 km north of the island in the early Holocene [Matthews, 1975]. This therefore implies that arctic maritime effects were already influencing the climate of Herschel Island in the early Holocene.

Nevertheless, evidence for warmer and moister conditions than today's are widespread at both study sites, as discussed below; and fall into line with previous investigations of thermokarst terrain, permafrost conditions, peatland development, and vegetation shifts in the western Canadian Arctic and on the Alaska North Slope. For example, palynological data and dated spruce stumps found *in situ* on the Tuktoyaktuk Peninsula indicate that the treeline was 75-100 km north of its present position from approximately 10.2 to 5.7 cal ka BP [Ritchie, 1984]. Dates on *Populus* wood from northern Alaska and northwestern Canada that was found beyond its present range and peaks in *Populus* pollen percentages from lake sediments suggest that *Populus* trees, which indicate substantially warmer conditions than today, had expanded into the area between 11.4 and 8.1 cal ka BP [Cwynar, 1982, Nelson and Carter, 1987; Anderson, 1988; Vermaire and Cwynar, 2010], and probably as early as 13.4 cal ka BP on favorable sites [Mann *et al.*, 2002]. Matthews [1975] described an insect fauna from an autochthonous peat lens 7 km east of Clarence Lagoon (Fig. 2.2) dated at 12.8 cal ka BP that is indicative of warmer-than-modern climatic conditions. These results are comparable with other fossil beetle and ostracod assemblages from the early

Holocene and even from the end of the late-glacial period in Eastern Beringia [Delorme *et al.*, 1977; Elias, 2001].

Thermokarst and thaw unconformity

Melt-out of ice wedges due to active layer deepening and peat growth along Komakuk Beach started around 11.2 cal ka BP as indicated by dated organic-rich material and basal peat samples (unit C₂) which cover late-glacial silty material (unit B) (Fig. 2.10). Organic-rich detritus layers containing freshwater mollusks and ostracods within an ice-wedge cast (unit C₁) yielded ages between 11.2 and 10.2 cal ka BP, supporting a rapid transition from a sandur-like landscape unfavorable for plant growth and organic matter preservation into a wetland tundra with permanently standing water in thermokarst ponds or lakes (Fig. 2.10c) [Vardy *et al.*, 1997]. Peat growth along Komakuk Beach was extensive at least until 6.7 cal ka BP, gradually slowing down afterwards.

Rampton [1982, 1988] argued that higher summer air temperatures and increased effective moisture led to the onset of thermokarst on the YCP and the Tuktoyaktuk Coastlands that peaked between 12.1 and 10.3 cal ka BP. Ice-wedge growth was probably reduced or absent [Mackay, 1992; Murton and Bateman, 2007; Murton, 2009] during a period of deep thaw and thermokarst lake/pond development. Active layer deepening to as much as 1.5-3.0 m below the modern surface is recorded on Herschel Island (Figs. 2.6 and 2.10c) and in the western Canadian Arctic by truncated ice wedges and a prominent cryostructural unconformity, which is a thaw unconformity [e.g. Burn *et al.*, 1986; Harry *et al.*, 1988; Murton and French, 1994]. Burn [1997] estimated that the palaeoactive layer reached its maximum depth around 10 to 9 cal ka BP and was up to 2.5 times thicker than modern active-layer depths. On Herschel Island, Moorman *et al.* [1996] reported radiometric dates from the base of peat deposits to be 12.8 and 10.4 cal ka BP, and Rampton [1982] dated peat in a drained thaw pond to 10.7 cal ka BP. This coincides with three dates of this study between 11.7 and 9.5 cal ka BP near the base of the palaeoactive layer on Herschel Island. Rising TOC contents in diamictic sediments on Herschel Island occur above the thaw unconformity (unit 3) and suggest that organic material was incorporated during deep thaw, cryoturbation, and mass movement (Fig. 2.10c) [Kokelj *et al.*, 2002].

Ground ice and hydrochemistry in the palaeoactive layer

Higher $\delta^{18}\text{O}$ values within a large range in segregated ice above the early Holocene thaw unconformity point either to fractionation processes during multiple freeze-thaw cycles in unfrozen material prior to conservation, or to mixed water sources [Mackay, 1983; French, 1998]. We assume that as the active layer deepened under warmer climate conditions, Holocene summer and winter precipitation mixed in the thaw zone above the unconformity with the Pleistocene meltwater

which was depleted in ^{18}O [Lacelle *et al.*, 2004; Fritz *et al.*, 2011] to form a $\delta^{18}\text{O}$ isotope composition between -25.2 and -17.1 ‰. A reduced influence of marine-derived Na^+ and Cl^- from upthrust marine sediments in favor of terrestrial ions such as Ca^{2+} , Mg^{2+} , and HCO_3^- , which occur above the thaw unconformity, support mixing with surface waters during the deep thaw period. Kokelj and Burn [2005] reported similar hydrochemical trends in freshwater depositional environments overlying brackish deposits in the Mackenzie Delta.

2.5.3 Middle and late Holocene permafrost aggradation

Evidence from northern Alaska and northwestern Canada indicates re-initiation of ice-wedge growth, permafrost aggradation, and thaw-lake drainage, presumably occurring as a response to climate cooling that followed the HTM [Ritchie, 1984; Mackay, 1992; Eisner *et al.*, 2003]. The northernmost treeline shifted southwards, reaching its present position at about 4.5 cal ka BP [Ritchie, 1984]. Cwynar and Spear [1995] noted that green alder and black spruce pollen increased in abundance throughout the northern Yukon between 6.5 and 6.0 cal ka BP. The mid-Holocene spread of both taxa was probably promoted by cooler and moister climates, leading to paludification and rising permafrost tables [Cwynar and Spear, 1995].

Since the middle Holocene, both study sites have been dominated by the formation of extensive ice wedges with $\delta^{18}\text{O}$ values centered around -23 to -22 ‰ that are aligned close to the GMWL, indicating stable conditions in terms of moisture source, frost-crack infill, and signal preservation [St-Jean *et al.*, 2011]. This is in close agreement with the observation by Michel and Fritz [1982] and Mackay [1983] who noted that ice wedges in the Tuktoyaktuk Coastlands tend to have a by 3 to 5 ‰ lower $\delta^{18}\text{O}$ value than does mean annual precipitation. This is approximately the composition of groundwater in the modern active layer (i.e. -20 to -18 ‰; Michel and Fritz, 1982).

Continuously upward-rising $\delta^{18}\text{O}$ values, from -20.3 to -14.0 ‰, of segregated ice within peat deposits (unit C₂) along Komakuk Beach, accompanied by a *d*-excess decreasing from 4.9 to -8.2 ‰, point toward strong kinetic fractionation effects. Non-equilibrium evaporation results in the enrichment of heavy isotopes (^{18}O , ^2H), and concurrently reduces the *d*-excess of the remaining water along a so-called evaporation line with a slope value significantly lower than the GMWL [Dansgaard, 1964; Gat, 1996]. The resulting regression slope of 6.0 ($R^2=0.99$) might be due to decreasing water availability as a consequence of changed hydrological conditions together with a higher selective water loss by evaporation. Vardy *et al.* [1997] suggested that organic matter accumulation and continued ground-ice growth probably raised the surface of the Kukjuk Peatland (Tuktoyaktuk Peninsula). The changing isotopic signature within the peat at Komakuk Beach may indicate an environmental change that supported the development of the modern ombrogenous

peatland surface [Vardy *et al.*, 1998]. The former low-centered polygons were converted into high-centered polygons, with improved drainage into the ice-wedge troughs. Lower summer air temperatures in response to a long-term regional cooling [Viau *et al.*, 2008; Bunbury and Gajewski, 2009] and permafrost aggradation [Vardy *et al.*, 1997] may have led to reduced peat growth and lower carbon accumulation rates during the last 4 ka [Vardy *et al.*, 2000; Eisner *et al.*, 2005].

The recent permafrost conditions are probably best explained by the occurrence and size of rejuvenated ice-wedge stages along Komakuk Beach. There, the tops of the primary wedges (~1 m below surface) mark the base of a former permafrost table that is most likely a thaw unconformity of unknown age. The upward aggradation of permafrost led to ice-wedge rejuvenation, indicated by new growth stages extending upwards to the modern frost table [Harry *et al.*, 1985]. This renewed growth has probably developed in response to a climate cooling trend [Mackay, 1976], and the small size of these ice veinlets (0.25 m) suggests that active layer thinning is a relatively recent phenomenon in this area [Harry *et al.*, 1985].

2.6 Conclusions

The following conclusions can be drawn from this study:

1. Late Wisconsinan Laurentide ice most likely left the Herschel Island ice-thrust ridge later than ~20 ka ago.
2. While Herschel Island was ice-covered during the Late Wisconsinan, the westernmost part of the YCP represented the easternmost edge of Beringia. During late-glacial times (~21 to 11.3 cal ka BP) this part of Beringia developed from a bare sandur-like accumulation plain in close vicinity to the degrading LIS and with actively aggrading permafrost into a wet thermokarst landscape, which has probably existed since the end of the Younger Dryas.
3. Warmer-than-modern temperatures during the HTM (11.2 to 6.5 cal ka BP) resulted in thaw of near-surface permafrost and melt-out of ice wedges. Thermokarst processes were accompanied by lacustrine deposition in shallow water-filled depressions that have been preserved as ice-wedge casts. Extensive peat growth on a low-centered polygonal tundra landscape proceeded until the middle Holocene.
4. Different ice-wedge generations serve as a palaeoenvironmental indicator of certain episodes of permafrost aggradation while ice-wedge casts, thaw unconformities, and truncated ice wedges record permafrost degradation along the YCP since the Late Wisconsinan.
5. Pre-Holocene and Holocene ice wedges coexist on Herschel Island and are clearly differentiated by their stable water isotope composition and ground-ice stratigraphy. Oxygen

isotope and *d*-excess values of Late Wisconsinan ice wedges reflect greatly reduced air temperatures during snow formation, and probably dryer conditions than those that have occurred from the middle Holocene until today.

6. Permafrost aggradation and extensive ice-wedge growth in the western Canadian Arctic resulted from the mid-Holocene climate cooling, and locally they became recently renewed.

In summary, we conclude that the glacial-interglacial landscape dynamics along the YCP (eastern Beringia) are closely linked to LIS history, sea-level variations, and permafrost development over time in general, as well as to ground-ice aggradation and thermokarst processes in particular.

Acknowledgements

The authors wish to express their thanks to the Yukon Territorial Government, the Yukon Parks (Herschel Island Qiqiktaruk Territorial Park), and the Yukon Department of Renewable Resources for their support during this project. We acknowledge the support of the Polar Continental Shelf Program (PCSP/ÉPCP publication number 001-08) and the Aurora Research Institute (ARI) for the field component. This study was partly funded by the German Science Foundation (DFG, Project No. LA 2399/3-1), the German Federal Ministry of Education and Research (BMBF, Project No. CAN 08/A07, CAN 09/001) and by a doctoral fellowship awarded to M. Fritz by the German Federal Environmental Foundation (DBU). Analytical work received great support from A. Eulenburg, U. Bastian, B. Plessen, C. Funk, and L. Schönicke. N. Couture, N. Arkell, and M. Angelopoulos assisted in the field. C. O'Connor is thanked for language revision.

3 Origin and characteristics of massive ground ice on Herschel Island (western Canadian Arctic) as revealed by stable water isotope and hydrochemical signatures

Michael Fritz¹, Sebastian Wetterich¹, Hanno Meyer¹, Lutz Schirrmeister¹, Hugues Lantuit¹, Wayne H. Pollard²

¹ *Alfred Wegener Institute for Polar and Marine Research, Potsdam, Germany*

² *Department of Geography and Global Environmental and Climate Change Centre, McGill University, Montreal, Canada*

Permafrost and Periglacial Processes 22, 26-38. doi:10.1002/ppp.714

Abstract

Herschel Island in the southern Beaufort Sea is a push moraine at the northwestern-most limit of the Laurentide Ice Sheet. Stable water isotope ($\delta^{18}\text{O}$, δD) and hydrochemical studies were applied to two tabular massive ground ice bodies to unravel their genetic origin. Buried glacier ice or basal regelation ice was encountered beneath an ice-rich diamicton with strong glaciotectonic deformation structures. The massive ice isotopic composition was highly depleted in heavy isotopes (mean $\delta^{18}\text{O}$: -33 ‰; mean δD : -258 ‰) suggesting full-glacial conditions during ice formation. Other massive ice of unknown origin with a very large $\delta^{18}\text{O}$ -range (from -39 to -21 ‰) was found adjacent to large, striated boulders. A clear freezing slope was present with progressive depletion in heavy isotopes towards the centre of the ice body. Fractionation must have taken place during closed-system freezing, possibly of a glacial meltwater pond. Both massive ground ice bodies exhibited a mixed ion composition suggestive of terrestrial waters with a marine influence. Hydrochemical signatures resemble the Herschel Island sediments that are derived from near-shore marine deposits upthrust by the Laurentide Ice. A prolonged contact between water feeding the ice bodies and the surrounding sediment is therefore inferred.

3.1 Introduction

Bodies of tabular massive ground ice (hereafter termed: massive ground ice), defined as ground ice with a gravimetric ice content exceeding 250 % are some of the most striking features of permafrost areas. They can form laterally extensive exposures of ice in coastal outcrops or riverbanks and are associated with thermokarst processes. Both the spatial distribution and origin of massive ground ice have long been investigated and debated. Many massive ice exposures are within the limits of Pleistocene glaciations of the Laurentide and the Eurasian Ice Sheets. In the late 1800s, explorers speculated that these ice bodies consisted of relict glacier ice [*von Toll, 1897*]. However, the most commonly accepted theory in North America is that these tabular ice bodies consist of segregated or segregated-intrusive ice, and that glacial melt supplied the large volumes of water required for their formation [*Mackay, 1971; Rampton, 1988; French and Harry, 1990*].

Segregated and glacier ice in the modern environment can be mutually distinguished on the basis of diagnostic criteria such as crystallography and stable water isotope geochemistry, hydrochemistry, and the nature of the contacts between the ice body and the surrounding sediments [*Mackay, 1989; French, 1998; Cardyn et al., 2007*]. However, bodies of massive ground ice have often undergone postburial hydrochemical and cryostructural alteration, as well as deformation, making interpretation a challenge [*French and Harry, 1990*]. In the western Canadian Arctic, *French and Harry [1990]* and *Pollard [1990]* suggested that massive ice resulting from segregation or intrusion (or a mixture of both processes) and buried glacier ice can exist in close proximity to one another and are difficult to differentiate with only field criteria and stratigraphic appraisals. In reality, no single method can be used to assess the origin of massive ground ice with certainty; and recent studies have involved multiple analytical methods [e.g. *Lacelle et al., 2004, 2007, 2009a*]. Many previous investigations using the isotopic composition of ground ice to infer its origin have been based on $\delta^{18}\text{O}$ data only [*Lorrain and Demeur, 1985; Vasil'chuk and Vasil'chuk, 1997; Brezgunov et al., 2001*] and there is a paucity of studies which have analysed both stable water isotope and hydrochemical properties [e.g. *Mackay and Dallimore, 1992*]. Simultaneous examinations of $\delta^{18}\text{O}$, δD and hydrochemical properties allow more detailed information to be obtained on the water source and the secondary processes affecting the build-up of ground ice [*Meyer et al., 2002a*].

In this study, we look at two massive ground ice bodies sampled during joint Canadian-German expeditions in 2006, 2008 and 2009 to Herschel Island in the northern part of the Yukon Territory. We use $\delta^{18}\text{O}$, δD and hydrochemical analyses to investigate these ice bodies with the goals of determining the different processes that led to their formation and of identifying their water sources.

3.2 Study site

Herschel Island (69°36'N, 139°04'W), also known as *Qikiqtaruk*, is located offshore of the Yukon Coastal Plain in the southern Beaufort Sea, about 100 km west of the Mackenzie Delta (Fig. 3.1). The island has a surface area of about 108 km² with maximum dimensions of 8 by 15 km and a maximum elevation of 185 m above sea level (asl). Herschel Island is an ice-thrust moraine resulting from a push of the Laurentide Ice Sheet (LIS) during the Wisconsin glaciation [Mackay, 1959]. The LIS advanced at least twice along the Yukon Coastal Plain [Mackay, 1972a; Duk-Rodkin et al., 2004]. Rampton [1982] postulated that only the oldest advance (termed the Buckland Glaciation) reached Herschel Island during the early to middle Wisconsin. However, there exists some debate regarding the timing of the LIS advance.

Permafrost thicknesses can be more than 600 m along the Yukon Coastal Plain [Smith and Burgess, 2000]. Large areas of the coastline along Herschel Island are dominated by steep cliffs/bluffs up to an elevation of 50 m, fronted in places by very narrow beaches. Coastal slopes are subject to intense thermokarst activity including the development of retrogressive thaw slumps [Lantuit and Pollard, 2008]. The presence of numerous thaw slumps along the coast is an indicator

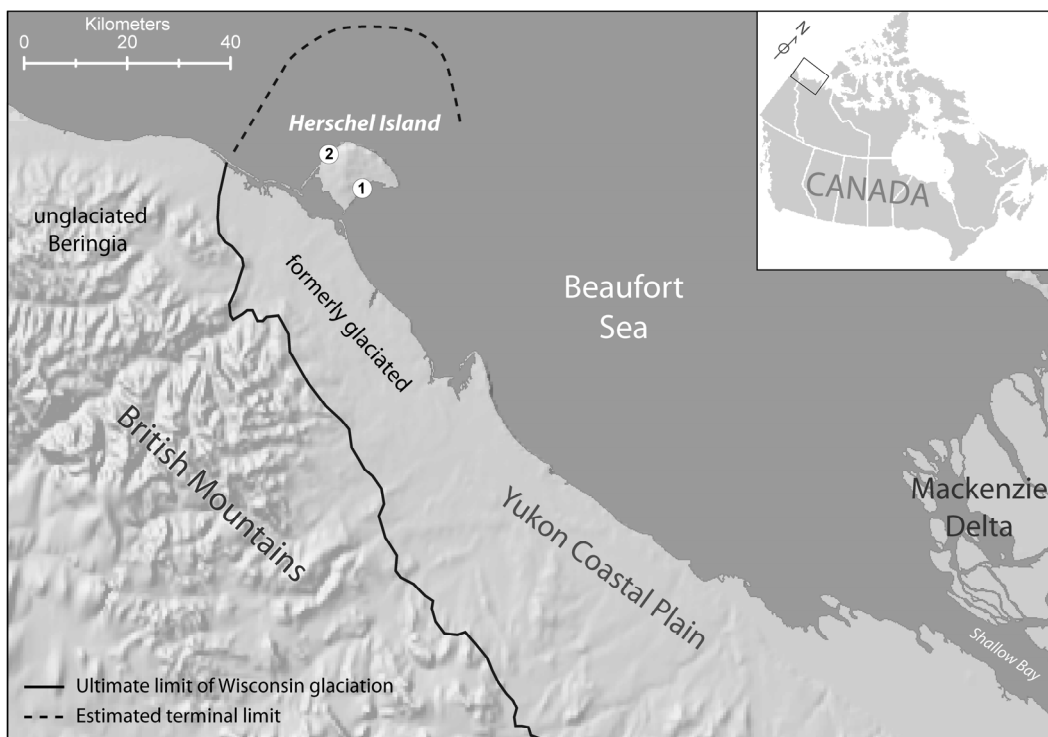


Figure 3.1: Location of Herschel Island and position of the two study sites: (1) thaw slump D (TSD massive ice) and (2) Herschel Island West massive ice (HIW massive ice). The limit of the Wisconsin glaciation was redrawn according to Smith et al. [1989], and adapted from Rampton [1982] and Dyke and Prest [1987].

that massive ground ice bodies underlie most of the island, and may constitute up to 50% of the volume of the near-surface permafrost [Mackay, 1971]. The massive ground ice bodies studied are at opposite ends of the island (Fig. 3.1). The first is in the southeast at $69^{\circ}35'52.1''\text{N}$, $139^{\circ}13'56.8''\text{W}$, at an elevation of 50 m asl (Fig. 3.2a). Here, the ground ice body is exposed within the headwall of a coastal retrogressive thaw slump called D (henceforth termed “TSD”, see *Lantuit and Pollard, 2005*). The second site is located along the northwest coast of the island ($69^{\circ}38'27.9''\text{N}$, $139^{\circ}05'41.0''\text{W}$ at approximately 20 m asl) where an exposure adjacent to an eroding valley revealed a large heterogeneous body of massive ground ice (Fig. 3.2b). This site is referred to as HIW massive ice (Herschel Island West).

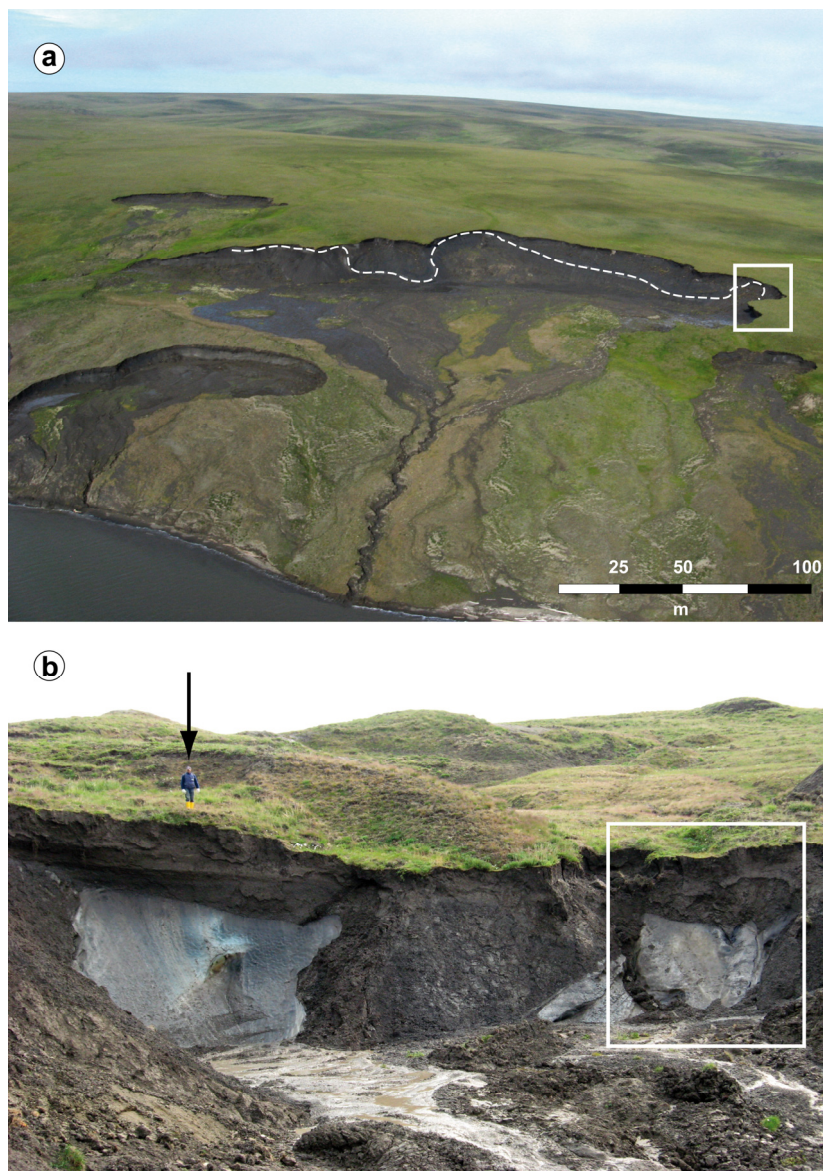


Figure 3.2: Overview photographs of (a) retrogressive thaw slump D (TSD) on the southeastern coast of Herschel Island and (b) Herschel Island West massive ice exposure (HIW). The dashed line delineates the orientation of the massive ice body which is non-conformable with the overlying surface. White rectangles indicate sampling locations. Arrow points to the person standing above the HIW exposure for scale.

3.3 Material and methods

Samples were obtained from the TSD and HIW massive ice sites and from non-massive intrasedimental ice at TSD. The vertical profile heights of the exposed sections were measured with a tape measure and the headwall was cleaned of thawed material. A detailed description and characterisation of each profile provided an overview of sedimentary and cryolithological features and their stratigraphic relationships. A chain saw and ice screws were used to cut transects across the exposed massive ice. The outer layer of the ice samples was discarded to avoid contamination by surface runoff. A total of 50 ground ice samples were collected from the TSD exposure and 91 samples from the HIW exposure.

3.3.1 Stable water isotope geochemistry

The samples were analysed for stable water isotopes ($\delta^{18}\text{O}$, δD) and hydrochemistry at the Alfred Wegener Institute for Polar and Marine Research (Potsdam, Germany). Ice samples were thawed in the field and stored cool in narrow-mouth PE-bottles until they were analysed. We measured the electrical conductivity (EC) directly in the field on the melted samples using a handheld multi-parameter instrument (WTW 340i, Tetracon 325, Weilheim, Germany). Stable water isotope analyses were carried out with a mass spectrometer (Finnigan MAT Delta-S, Bremen, Germany) using the water-gas equilibration technique (for further information see *Horita et al.*, 1989). The isotopic composition is expressed in delta per mil notation (δ , ‰) relative to the Vienna Standard Mean Ocean Water (VSMOW) standard. The reproducibility derived from long-term standard measurements is established with 1σ better than ± 0.1 ‰ for $\delta^{18}\text{O}$ and 0.8 ‰ for δD [*Meyer et al.*, 2000].

3.3.2 Hydrochemistry

A representative selection of the ice samples used for the determination of stable isotope ratios were split for hydrochemical measurements (ca. every second sample). Samples for ion analysis were passed through cellulose-acetate filters (pore size 0.45 μm) in the field. Samples for the cation analyses were acidified with HNO_3 to prevent microbial conversion processes, whereas samples for anion analysis were kept cool. The cation content was analysed by Inductively Coupled Plasma-Optical Emission Spectrometry (ICP-OES, Perkin-Elmer Optima 3000 XL, Waltham, Massachusetts, USA), while the anion content was determined by Ion Chromatography (IC, Dionex DX-320, Sunnyvale, California, USA). Hydrogen carbonate concentrations were determined by titration with 0.01 M HCl using an automatic titrator (Metrohm 794 Basic Titrino, Filderstadt, Germany). The detection limit for the different ions is 0.1 mg/l for Cl^- , SO_4^{2-} , Ca^{2+} and Mg^{2+} ,

0.2 mg/l for K^+ and Na^+ , and 3.05 mg/l for HCO_3^- . A standard error of $\pm 10\%$ is taken for all values.

3.4 Results

3.4.1 TSD exposure

Stratigraphy

This retrogressive thaw slump is more than 400 m wide, features a vertical headwall up to 10 m high and a more gently sloping headscarp 15–20 m in height where the massive ice body is exposed (Fig. 3.2a). The massive ice can be traced laterally across the headwall by an undulating milky white ice band (Fig. 3.2a) and exhibits synclinal and anticlinal structures (Fig. 3.3c), while it appears dome-shaped further north (Fig. 3.3b). A generalised stratigraphy of the exposure is shown in Figure 3.3a.

Unit A of TSD (Figs. 3.3a, b, c) is a massive ice body of almost pure ice with a thickness of more than 10 m. It is mainly composed of clear to milky white ice. Sediments are present in a dispersed form and as sediment bands with a variable frequency and a thickness of 5 mm to several centimetres. Layers of a matrix-based diamicton (with occasional cobbles) are deformed together with the ice, leading to anticlinal and synclinal as well as vertically- and horizontally-bedded structures (Figs. 3.3b, c). These gentle folds are open and either upright or inclined. Subangular rounded cobbles (diameters up to 5 cm) are incorporated into the ice. Gas bubbles are up to 5 mm in diameter and are not oriented within the ice, in contrast to the sediment inclusions that are elongated and oriented in the same direction as the inclination of folds. The lower contact of the massive ice was not exposed. The upper contact of the massive ice is unconformable. In some parts of the exposure, the massive ice is unconformably overlain by an ice-rich clayey diamicton (unit B, Fig. 3.3a) with an alternating texture of thick ice lenses (2–20 cm) and sediments. Samples of non-massive intrasedimental ice were taken from this unit. Subangular rounded pebbles, cobbles and the remains of molluscs as well as dispersed plant remains are present throughout the unit. In some places the overlying ice-rich sediments exhibit deformation structures like recumbent isoclinal folds and boudinage structures indicative of a strong linear shear stress and plastic deformation of a competent material. The upper contact of unit B has been discordantly truncated towards unit C, as indicated by cut cryostructures and truncated tails of ice wedges that penetrate into the diamictic sediments and the deformation structures of unit B.

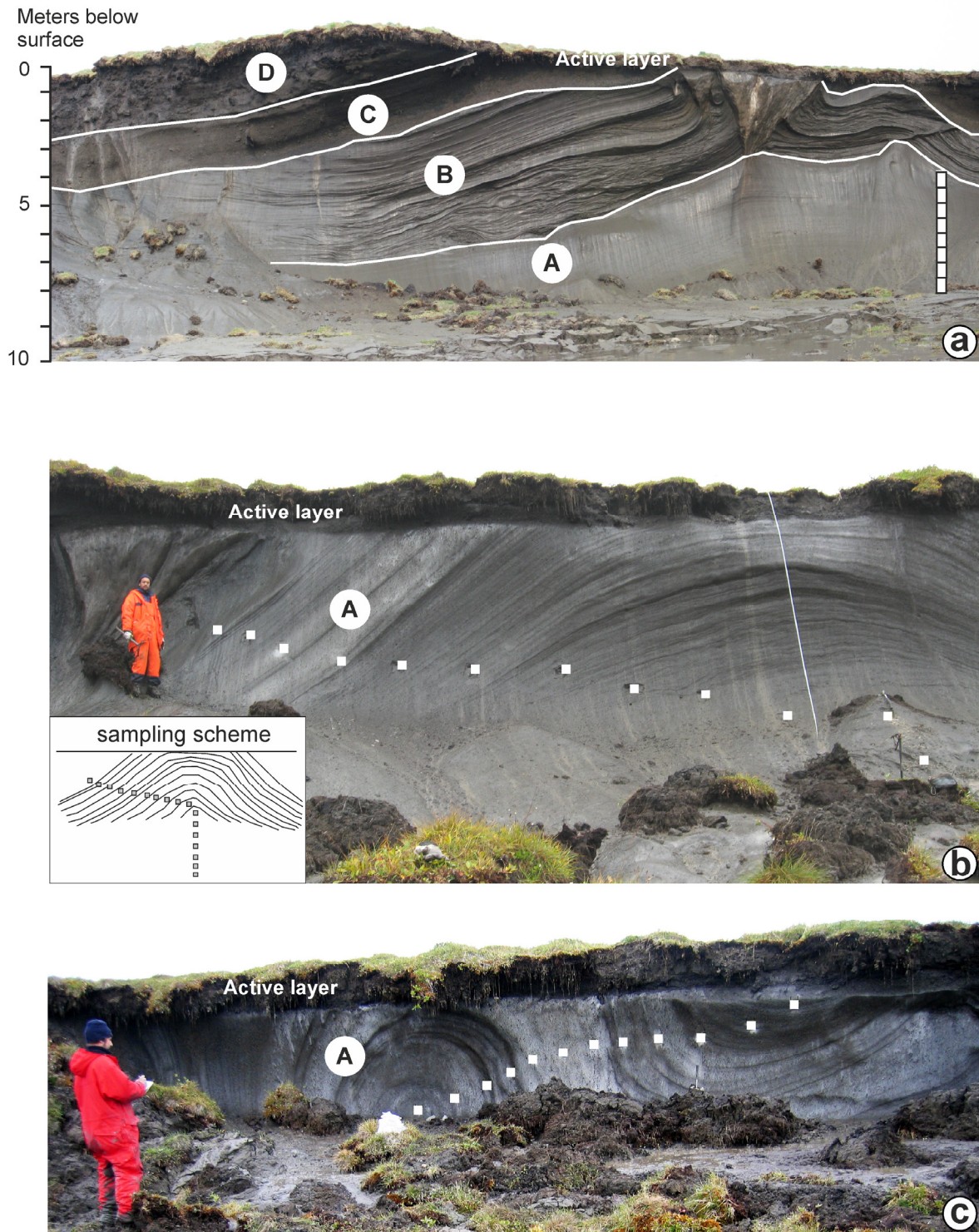


Figure 3.3: Stratigraphic units (A to D) and sampling points (white squares) of the thaw slump D massive ice (unit A) in 2006, 2008 and 2009. (a) shows a generalised stratigraphy of the exposure, (b) illustrates the dome-shaped nature of the ice body, and (c) shows its synclinal and anticlinal structures. Unit A: massive ice body with sediment bands that are deformed together with the ice; unit B: clayey diamicton with an alternating pattern of thick ice lenses (2-20 cm); unit C: clayey diamicton with a lens-like reticulate to irregular reticulate cryostructure; unit D: peaty silt with lens-like reticulate cryostructure and inactive ice wedges. Note the persons standing in front of the exposure for scale.

Unit C comprises a greyish-brown diamicton up to 3 m thick (Fig. 3.3a). It is less ice-rich and is characterised by a lens-like reticulate to irregular reticulate cryostructure without deformation structures. The sediment texture of unit C is comparable to that of unit B but has a higher content of organic remains and exhibits some peat inclusions. Unit D (Fig. 3.3a) is present in the former depressions of a polygonal tundra and represents the infill of low-centre ice-wedge polygons during stable surface conditions. Peat is up to 2.5 m thick while relict ice wedges up to 3 m wide and up to 5 m long penetrate downwards through units B and C and sometimes also into the massive ice (Fig. 3.3a).

Stable water isotopes

The stable water isotope composition of massive ground ice (unit A) exposed in TSD has $\delta^{18}\text{O}$ values ranging from -34.2 to -31.3 ‰ and δD values from -265 to -244 ‰ (Fig. 3.4; Table 3.1). With an average deuterium excess of 7.2 ‰ and a δD - $\delta^{18}\text{O}$ regression slope value of 7.0 ($R^2=0.98$), samples from the massive ice body lie slightly below the Global Meteoric Water Line (GMWL, $\delta\text{D} = 8 \delta^{18}\text{O} + 10$; Craig, 1961). Values for d vary from 5.3 to 9.3 ‰. Neither the isotopic signature nor the deuterium excess exhibits any spatial trend across the profiles through the ice body. Intrasedimental ice within unit B shows higher isotopic values ranging from -28.7 ‰ to -25.8 ‰ for $\delta^{18}\text{O}$ (Fig. 3.4, Table 3.1) indicating fractionation processes during multiple freeze-thaw cycles in an active layer before permafrost aggradation, or mixed water sources, or that it formed under warmer climate conditions. The deuterium excess of the intrasedimental ice samples ranges between 3.0 and 5.1 ‰ without showing any trend with depth. The isotopic composition of ice in Unit B overlying the massive ice is dissimilar to that of the massive ice in unit A, indicating differing conditions during the formation of the two ice types (Fig. 3.4; Table 3.1).

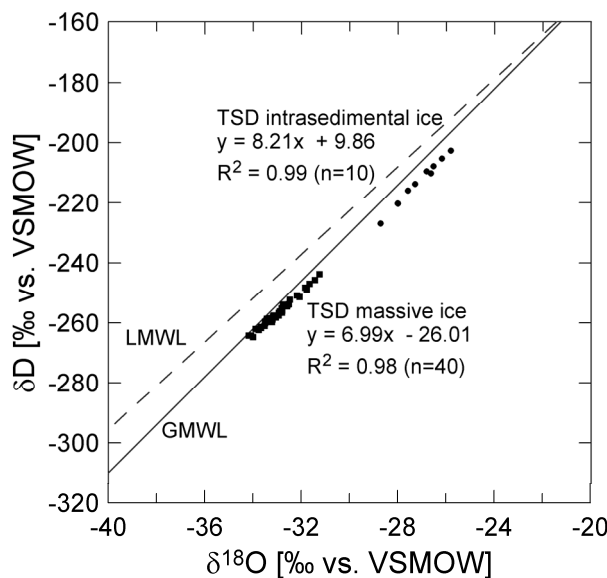


Figure 3.4: $\delta^{18}\text{O}$ - δD diagram of thaw slump D (TSD) massive ice (unit A, squares) and TSD non-massive intrasedimental ice of adjacent sediments (unit B, dots). GMWL = global meteoric water line; LMWL = local meteoric water line for Inuvik [IAEA, 2006]: $\delta\text{D}=7.3\delta^{18}\text{O}-3.5$, $R^2=0.98$; VSMOW = Vienna Standard Mean Ocean Water.

Table 3.1: Stable isotope ($\delta^{18}\text{O}$, δD and d) minimum, mean and maximum values, as well as slopes and linear regression coefficients of the $\delta\text{D}-\delta^{18}\text{O}$ relation for the different ice types sampled.

Profile	N	$\delta^{18}\text{O}$			δD			d			Slope	R^2
		Min.	Mean	Max.	Min.	Mean	Max.	Min.	Mean	Max.		
TSD massive ice	40	-34.2	-33.0	-31.3	-265	-258	-244	5.3	7.2	9.3	7.0	0.98
TSD texture ice	10	-28.7	-27.2	-25.8	-227	-213	-203	3.0	4.2	5.1	8.2	0.99
HIW massive ice	91	-39.0	-31.2	-21.0	-286	-237	-169	-3.9	6.9	25.3	5.9	0.99

TSD = Thaw slump D; HIW = Herschel Island West.

Hydrochemical composition

The electrical conductivity (EC) of the melted ice samples shows a wide range, from 20.6 to 1294 $\mu\text{S}/\text{cm}$ (mean: 406 $\mu\text{S}/\text{cm}$, Table 3.2). Higher EC-values accompany higher sediment contents and we therefore assume ion exchange processes between the sediment particles and the ice. However, we cannot eliminate the possibility that further dissolution of soluble salts from enclosing sediments occurred after thawing of the samples, so interpretations of the hydrochemical results are tentative. The entire massive ice body is dominated by HCO_3^- for the anion composition (53 %) followed by Cl^- and SO_4^{2-} (Fig. 3.5). Cation concentrations are dominated by Na^+ , accounting for 50 %, followed by Ca^{2+} , Mg^{2+} and K^+ (Fig. 3.5). No vertical or horizontal trend in the major ion distribution is apparent. The hydrochemical properties of intrasedimental ice within the overlying sediments (unit B) differ significantly from the massive ice body directly below (unit A). The EC of intrasedimental ice averages 3957 $\mu\text{S}/\text{cm}$ with maximum values above 5500 $\mu\text{S}/\text{cm}$. Na^+ and Cl^- ions are dominant (Fig. 3.5), representing more than 84 % of the total ion composition. NaCl waters clearly reflect a marine signature and therefore indicate a strong ion exchange process between porewater and the solute-rich diamicton in which the segregated ice formed.

Table 3.2: Summarised values of two major ion ratios for the different profiles and ice types.

Profile	N	$(\text{Na}^+ + \text{K}^+)/\text{Ca}^{2+}$ ratio*				$\text{Cl}^-/\text{HCO}_3^-$ ratio*			
		Mean	Median	Min	Max	Mean	Median	Min	Max
TSD massive ice	34	3.47	1.77	0.30	23.1	0.69	0.53	0.10	2.03
TSD intrasedimental ice	10	24.6	26.1	8.63	45.7	15.1	11.2	7.12	29.8
HIW massive ice	30	4.71	1.88	0.33	21.4	0.96	0.82	0.04	2.37

*Note: $(\text{Na}^+ + \text{K}^+)/\text{Ca}^{2+}$ and $\text{Cl}^-/\text{HCO}_3^-$ -ratios greater than unity indicate an enrichment of ions with a likely marine origin derived from salt spray or dissolution from sediments with a marine influence. TSD = Thaw slump D; HIW = Herschel Island West.

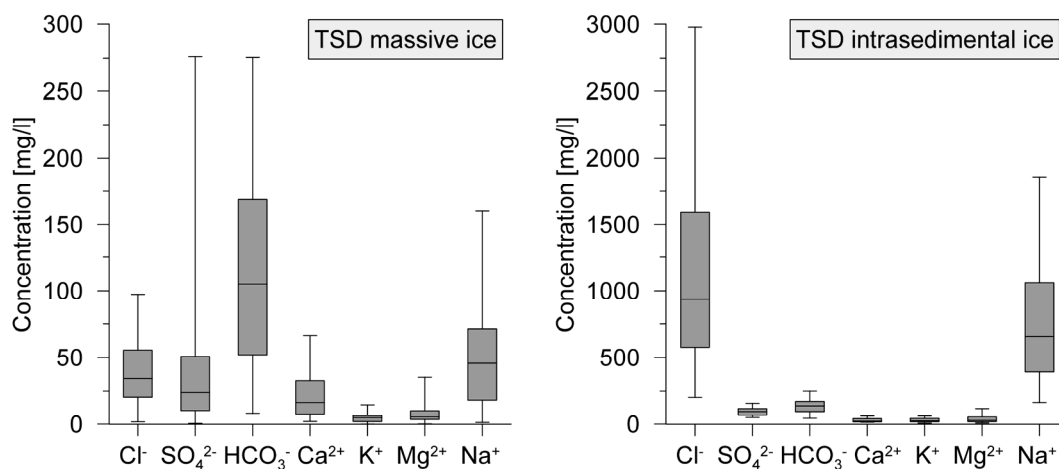


Figure 3.5: Boxplots of cation and anion concentrations (absolute in mg/l) of thaw slump D (TSD) massive ice and TSD non-massive intrasedimental ice of surrounding sediments. Note different scales for ion concentrations of TSD massive and intrasedimental ice. Plots show the minimum, maximum, median, 25 per cent-quartile and 75 per cent quartile.

3.4.2 HIW exposure

Stratigraphy

The HIW massive ice body measures between 4 and 8 m high, is unconformably overlain by several meters of sediments and shows a sharp boundary (i.e. no sediment incorporation into melted margins) between massive ice and sediments (Fig. 3.6). To the east, the ice is overlain by ~6 m of dark grey clay (unit B), itself covered by brownish-grey fine-grained deposits with a significant content of plant macrofossils (unit C). The cryostructure of units B and C is coarse lens-like reticulate with ice lenses 0.5–1 cm thick, likely indicating re-freezing after deposition. The clayey sediments are generally ice-poor with cobbles and plant remains. A notable feature is the occurrence of large striated boulders more than 1 m in diameter at the mouth of a narrow valley located ten meters further west at approximately the same elevation as the massive ice body. The HIW ice body is not homogeneous. Its different parts have distinctive cryolithological characteristics (Fig. 3.6). The outer part of HIW ice body (A-1, Fig. 3.6), which makes up the largest portion, consists of very clear ice with few gas bubble inclusions and without any sediment inclusions. The central part of the ice body is composed of milky white ice (A-2, Fig. 3.6) with sometimes fine-dispersed sediment inclusions and an apparently high gas content. Spherical gas bubbles are up to 4 mm in diameter, not oriented, and occur either dispersed or in clusters. The uppermost part of HIW (A-3, Fig. 3.6) is regarded as a transition zone between part A-1 and A-2. It has few sediment and gas inclusions and a bluish-cloudy appearance.

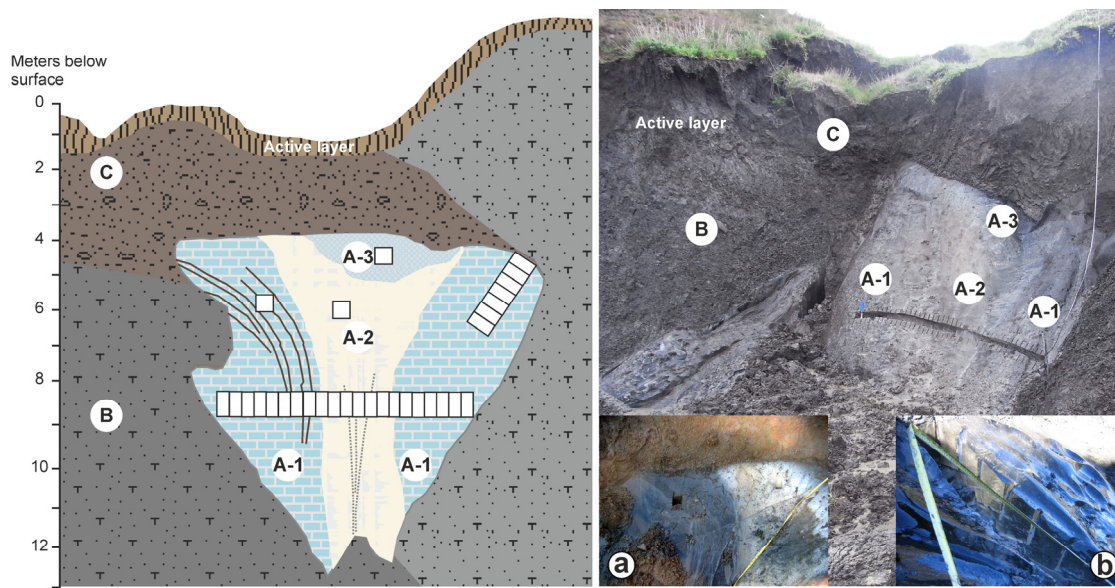


Figure 3.6: Stratigraphic units (A to C) and sampling points (white squares) of Herschel Island West massive ice (unit A). Unit A-1: Transparent ice without bubbles and without sediment inclusions; unit A-2: milky white ice, bubble-rich; unit A-3: transition zone between A-1 and A-2 with bluish cloudy appearance, few sediment inclusion and bubbles; unit B: dark grey clay; unit C: brownish-grey, fine-grained sediments with plant remains and peaty inclusions. Inset (a) illustrates the sharp transition between transparent (unit A-1) to milky white ice (unit A-2). Inset (b) shows the very clean and transparent character of Unit A-1 ice.

Stable water isotopes

Although one compact ice body was encountered, the δD and $\delta^{18}O$ composition varies from -39.0 to -21.0 ‰ for $\delta^{18}O$ and from -286 to -169 ‰ for δD (Fig. 3.7; Table 3.1). The deuterium excess also ranges widely between -3.9 to 25.3 ‰ (mean of 6.9 ‰). The $\delta^{18}O$ values show a decreasing trend from -21.0 to -39.0 ‰ towards the centre of the ice body, whereas d values increase towards the centre. In its interior, $\delta^{18}O$ is generally less than -33.0 ‰ down to its minimum of -39.0 ‰ (Fig. 3.7; Table 3.1). The very clear ice forming the outer parts of the ice body close to the sediment contact shows negative d values slowly increasing inwards. The δD - $\delta^{18}O$ regression slope of 5.9 (Fig. 3.7) is lower than the slope typically assumed for water or ground ice from meteoric sources that has not undergone secondary fractionation.

Hydrochemical composition

The total ion content of the ice is generally low with an electrical conductivity of 212 $\mu S/cm$ on average. The massive ice body is generally dominated by HCO_3^- (55 %) and Cl^- (37 %) for the anion composition with absolute contents usually less than 40 mg/l each (Fig. 3.8). The cation composition is dominated by Na^+ , accounting for 58 % and followed by Ca^{2+} with 30 % on average. Hydrochemical studies of this ice body show the same continuous trend in ion

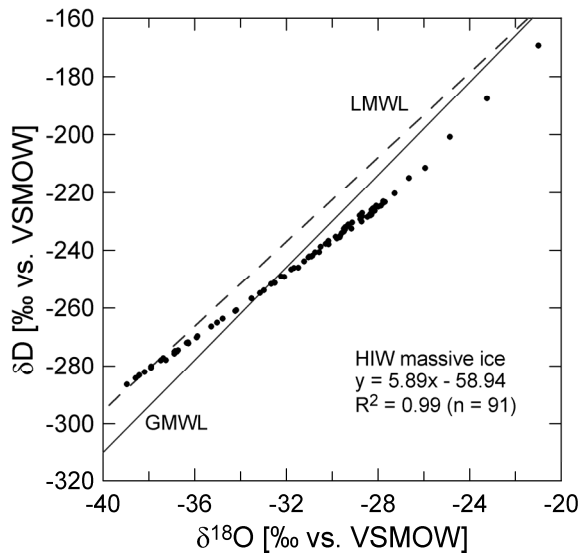


Figure 3.7: $\delta^{18}\text{O}$ - δD diagram of Herschel Island West (HIW) massive ice. GMWL = global meteoric water line; LMWL = local meteoric water line for Inuvik [IAEA, 2006]: $\delta\text{D}=7.3\delta^{18}\text{O}-3.5$, $R^2=0.98$; VSMOW = Vienna Standard Mean Ocean Water.

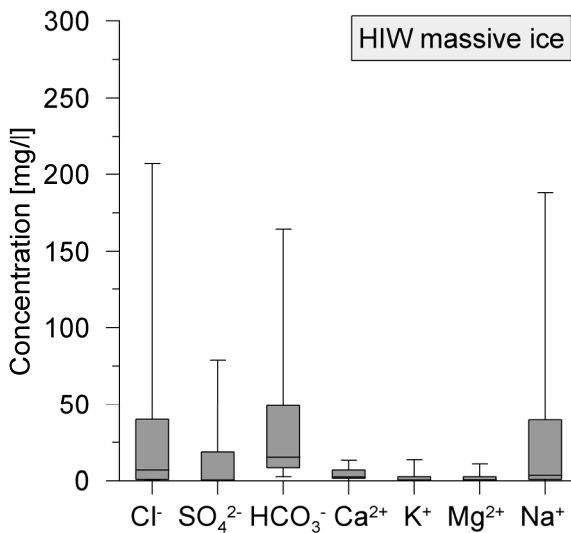


Figure 3.8: Boxplots of cation and anion concentrations (absolute in mg/l) of Herschel Island West (HIW) massive ice. Plots show the minimum, maximum, median, 25 per cent quartile and 75 per cent quartile.

concentration from the ice margins towards the centre as observed for $\delta^{18}\text{O}$ and δD . The very clear and transparent ice comprising the outer parts of the massive ice body (A-1 in Fig. 3.6) have the lowest ion contents. As one moves further into the centre of the ice body, electrical conductivity rises gradually (up to $1000\ \mu\text{S}/\text{cm}$) and so does the ion content. The milky white central part of the ice exhibits comparably high values of Cl^- (207 mg/l), HCO_3^- (164 mg/l), and Na^+ (188 mg/l) (Fig. 3.8).

3.5 Discussion

3.5.1 Origin of TSD massive ice (Unit A)

The negative $\delta^{18}\text{O}$ isotopic composition of the TSD massive ice ($\delta^{18}\text{O}$ between -34 and -31 ‰) indicates that the water contributing to ice formation originated in a cold climatic environment, likely during the Wisconsin under full-glacial conditions. Similar isotopic ratios have been determined for possibly late Pleistocene massive ground ice [e.g., *Michel and Fritz, 1978, 1983; Mackay 1983; Moorman et al., 1998*], non-massive intrasedimental ice [*Kotler and Burn, 2000*] and remnants of Pleistocene glacier ice or basal regelation ice [*Dansgaard and Tauber, 1969; Hooke and Clausen, 1982; Lorrain and Demeur, 1985; Zdanowicz et al., 2002*]. We assume a single water and/or moisture source because of the narrow isotopic range that may have been derived from glacier ice or glacial meltwater [*Rampton, 1988; 2001; French and Harry, 1990*] with a strongly depleted isotopic signature.

The $\delta\text{D}-\delta^{18}\text{O}$ regression slope of 7.0 is somewhat lower than that of the GMWL ($S = 8$) but in close agreement with the slope of the closest modern local meteoric water line (LMWL) for Inuvik, about 200 km east of Herschel Island. However, a slope of 7.0 does not necessarily point to a meteoric origin but could account for a freezing of liquid water, as well. During equilibrium freezing, the value of the $\delta\text{D}-\delta^{18}\text{O}$ regression slope differs from that of the GMWL because of different isotopic fractionation coefficients (for D and ^{18}O). During equilibrium freezing, the value of the $\delta\text{D}-\delta^{18}\text{O}$ regression slope differs from that of the GMWL because of different isotopic fractionation coefficients (for D and ^{18}O) during the water-ice-phase change than it is the case for the water-vapour fractionation. Using the fractionation coefficients for the ice-water phase change by *Suzuoki and Kimura [1973]* of $\alpha(\text{D}_{\text{i-w}}) = 1.0206$ and $\alpha(^{18}\text{O}_{\text{i-w}}) = 1.0028$, the theoretical freezing slope becomes 7.29. Consequently, ice derived from equilibrium freezing should plot along a regression slope below or equal to the theoretical freezing slope.

The deuterium excess analyses of the massive ice body do not provide conclusive evidence. An average d value of 7.2 ‰ plots well below the GMWL ($d=10$) and the LMWL ($d=14.9$), respectively (Fig. 3.9). There is no strong negative relation between d and δD which would suggest the existence of a freezing slope. However, this could mean that freezing occurred under non-equilibrium conditions. Frequent regelation, adfreezing and sediment incorporation at the glacier sole could cause mixing with groundwater and kinetic fractionation as well [*Souchez et al., 1990, 2000*]. The hydrochemistry of basal regelation ice can be strongly affected by interactions between water, ice, and solutes from basal and englacial debris [*Knight, 1997*]. Given the assumption that the enclosed sediments have been incorporated by some freezing process of liquid water, a solution

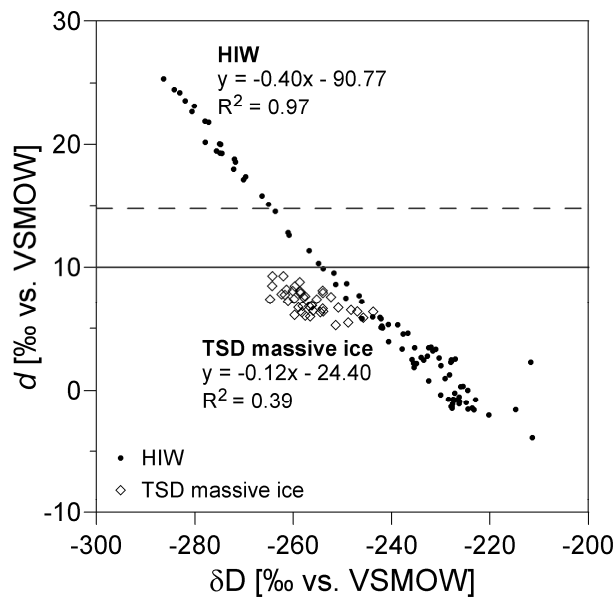


Figure 3.9: Relationship between δD and deuterium excess (d) of the two massive ice types: thaw slump D (TSD) and Herschel Island West (HIW). The horizontal solid line represents d of the global meteoric water line ($d=10$). The dashed line shows the d value of the local meteoric water line for Inuvik ($d=14.9$; IAEA, 2006). VSMOW = Vienna Standard Mean Ocean Water.

equilibrium between water and sediment may have been established prior to freezing. Artificial thaw of the ground ice for conducting the analyses could change this equilibrium, but should not completely change the ion composition as the artificial meltwater is the same water that formed the ice. Regelation ice with prolonged contact with the surrounding sediments would lose its hydrochemical purity due to ion exchange processes and the tendency to balance differences in concentration. Incorporated debris would leave its hydrochemical imprint on the ice. On Herschel Island, glacially upthrust near-shore marine deposits [Mackay, 1959; Bouchard, 1974] containing both marine and terrestrial fossils, are presumed to be the major ion source for any kind of ground ice that had contact with them in a liquid or frozen state. A recharge of groundwater by glacial meltwater leading to the formation of tabular massive ice bodies has been described by Moorman *et al.* [1998]. This takes into account that the ice should reflect both the hydrochemical signature of the glacial meltwater and that of the sediments it travelled through. The ratios of $(Na^+ + K^+)/Ca^{2+}$ and Cl^-/HCO_3^- were calculated (Table 3.2) including the two main ions in sea water Na^+ and Cl^- and those typical of terrestrial waters (HCO_3^- , Ca^{2+}). Alkali ions dominate the massive ice but to a lesser degree than is the case for the intrasedimental ice. Furthermore, HCO_3^- is dominant in the massive ice giving a clear terrestrial signature.

Alternating layers of debris-rich ice and debris-poor but bubble-rich ice were found. These features may be ascribed to either segregation or glaciotectionic structures as observed in deformed marginal or basal glacier ice [e.g. Sudgen *et al.*, 1987; Knight, 1997; Knight *et al.*, 2000; Murton *et al.*, 2005]. Density inversions between the more than ten meters of almost pure ice and the sediment cover with a higher density could lead to updoming of the underground ice in zones of weakness [Harris, 1989] over the millennia since deglaciation. This would lead to the large-scale

undulating and updoming pattern observed in the ice body. Gradational contacts are typical for massive segregated ice (also segregated-intrusive ice) [Mackay, 1989] but they should not exist for buried ice and in this case an unconformable upper contact was present while the lower contact was hidden. There is strong evidence that Pleistocene basal glacier (or basal regelation ice) was incorporated into glacial diamicton or became buried by supraglacial meltout till [see Murton *et al.*, 2005]. However, we cannot rule out the possible origin as massive segregated (-intrusive) ice as both types can contain significant quantities of stratified debris [e.g. French and Harry, 1990; Knight, 1997; Knight *et al.*, 2000; Murton *et al.*, 2005]. The question remains, whether the ice body aggraded as massive segregated (-intrusive) ice and was then deformed by glaciotectonic processes, or if the ice was originally basal regelation ice forming part of the Laurentide Ice lobe that became buried by a till.

3.5.2 Origin of HIW massive ice

A large isotopic range of about 18 ‰ (for $\delta^{18}\text{O}$) occurs within the ice body HIW together with extremely low values in its centre (-39.0 ‰). As far as we know, this range accompanied by the very low $\delta^{18}\text{O}$ values is unique in the literature on massive ground ice. Figure 3.10 shows the progressive symmetrical depletion in heavy isotopes inwards; towards the most negative values near the centre of the ice body; and the strong solute enrichment in the same direction.

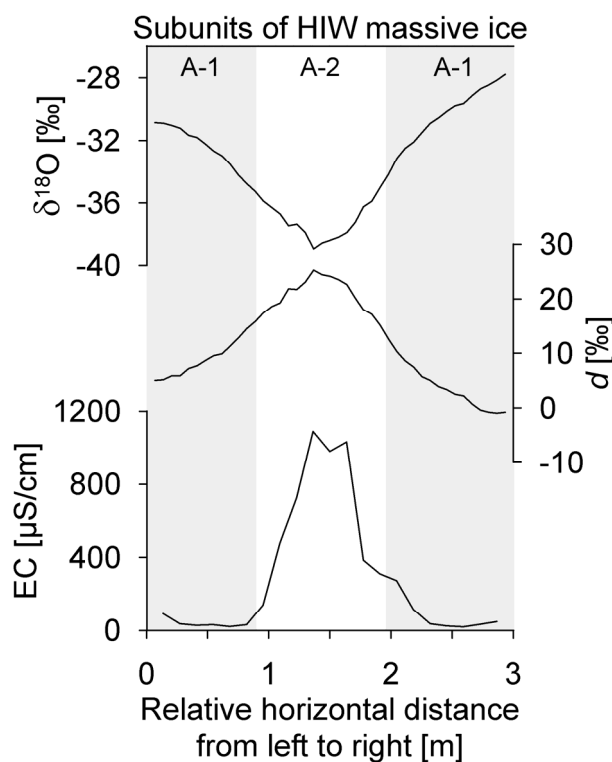


Figure 3.10: $\delta^{18}\text{O}$, deuterium excess (d) and total ion content (expressed as electrical conductivity, EC) across a horizontal transect in Herschel Island West (HIW) massive ice (see also Fig. 3.7).

We infer that the ice body was formed under closed-system conditions as a result of complete freezing of a single water body with a mixed terrestrial-marine hydrochemical signature (Table 3.2) for the following reasons. When water freezes under equilibrium conditions it follows the Rayleigh-type fractionation between water and ice. Written in the delta-notation, the Rayleigh equation becomes [Lacelle, 2011]:

$$\delta_i = (\delta_0 + \ln \alpha_{i-w} \cdot 1000 \cdot \ln f) + \ln \alpha_{i-w} \cdot 1000$$

with δ_i as the resulting isotope composition of the ice, δ_0 as the initial isotope composition of the parent water; and f is the remaining water fraction during freezing. The first part of a water reservoir to freeze in a closed system will produce ice that is isotopically enriched by about 2.8 ‰ relative to the source water [Craig, 1961; Michel, 1986]. As freezing continues, the shrinking reservoir becomes increasingly depleted in heavy isotopes (Fig. 3.11). In contrast, dissolved solutes (and bubbles) are concentrated towards the centre of the ice [Kotler and Burn, 2000] as a result of ionic segregation during freezing. The first fraction to freeze would be closest to the initial ion composition of the parent water. An average EC of < 50 $\mu\text{S}/\text{cm}$ for the whole water body is half or less of what is found in recent surface water bodies on Herschel Island fed by precipitation [S. Wetterich, AWI Potsdam, Germany, unpublished data].

When plotted on a $\delta\text{D}-\delta^{18}\text{O}$ diagram, the ice samples form a straight line with a regression slope of 5.89. During equilibrium freezing of water, the resultant ice samples are aligned along a *freezing slope* that will be lower than the GMWL (Fig. 3.7). Jouzel and Souchez [1982] observed that the slope of the freezing line depends on the initial isotopic composition, with the more depleted waters producing a lower slope value. The initial δ -value of the parent water is the intercept between the freezing slope and the GMWL [Jouzel and Souchez, 1982; Knight, 1997; Souchez et al., 2000]. We prefer to use the GMWL, as the LMWL for Inuvik reflects contemporary climate conditions and circulation patterns and there is no reconstructed Pleistocene meteoric water line for the area. Following the approach of Jouzel and Souchez [1982] and with calculated initial δ values of -251 ‰ and -32.7 ‰ (for $\delta_i\text{D}$ and $\delta_i^{18}\text{O}$) the theoretical freezing slope [$S = S_0 (1000 + \delta_i\text{D}) / (1000 + \delta_i^{18}\text{O})$] becomes 5.64. This is close to the observed slope value of 5.89 in the massive ice body. Similarly low freezing slopes attributed to regelation and closed-system freezing have been reported in other studies [e.g., Lorrain and Demeur, 1985; Michel, 1986; Clark and Lauriol, 1997; Souchez et al., 2000; Lacelle et al., 2004, 2009a; Murton et al., 2005].

Interpretation of the slope alone to explain ground ice genesis could be misleading if freezing did not occur under equilibrium conditions [D. Lacelle, University of Ottawa, Canada, personal communication]. An examination of the d - δD relation may provide further information. Figure 3.10

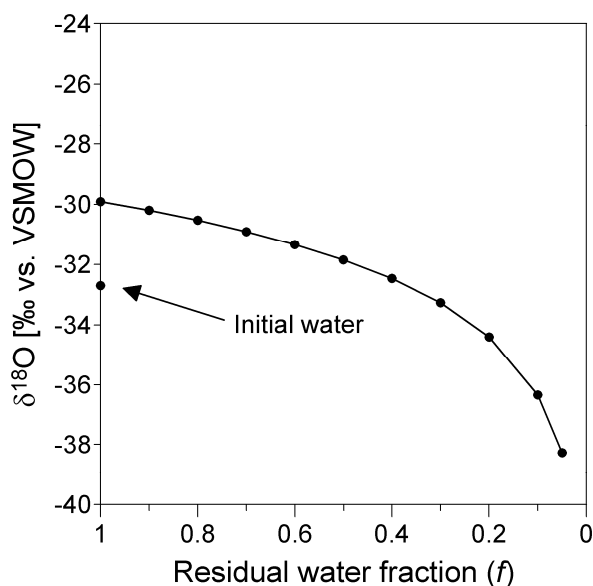


Figure 3.11: Rayleigh distillation model for the evolution of $\delta^{18}\text{O}$ during equilibrium successive freezing of water. Fractionation coefficients between ice and water are those of *Suzuoki and Kimura* [1973]. Initial δ values are -32.7‰ and -252‰ for $\delta^{18}\text{O}$ and δD , respectively. VSMOW = Vienna Standard Mean Ocean Water.

shows that as heavy isotopes become progressively depleted towards the centre of the ice body, d values rise in the same way. A negative relation between d and δD during equilibrium freezing is expected [*Souchez et al.*, 2000] because the freezing slope has a lower value than the GMWL. In the case of freezing water, deuterium excess variability is a result of the freezing conditions (freezing rate, boundary layer thickness, percentage of freezing of the reservoir [*Souchez et al.*, 2000]). Figure 3.9 shows that as freezing progresses, the δD values of the ice become progressively lower. This is accompanied by a concurrent increase in d values (Fig. 3.9) and therefore does account for closed-system freezing. However, the enriched δD and $\delta^{18}\text{O}$ values for the outermost portion of the massive ice body are less negative than the isotopic enrichment factor determined by *Suzuoki and Kimura* [1973] would suggest under Rayleigh-type fractionation. The increasingly negative δ -values are in good agreement with the theoretical Rayleigh fractionation curve (Fig. 3.11). The deviation from the Rayleigh curve may be due to (i) isotope exchange processes with porewater of the surrounding sediment or (ii) kinetic fractionation that occurs during regelation [*Zdanowicz et al.*, 2002]. This would imply a semi-closed system freezing for the outermost part of the ice body. Sediment incorporation at one edge of the ice body argues at least for the occurrence of some regelation at its margin after ice formation. This is consistent with a heavier isotopic composition at the ice-sediment interface and its deviation from the linear regression slope. The water feeding the ice body definitely formed during colder climatic conditions than today. It seems likely that the ice body was derived from glacial meltwater in a proglacial area with a retreating glacier front. We infer that a freezing front moved laterally from two sides (Fig. 3.10).

Unconformable upper and lateral contacts indicate burial [*Mackay*, 1989]. We suggest that a

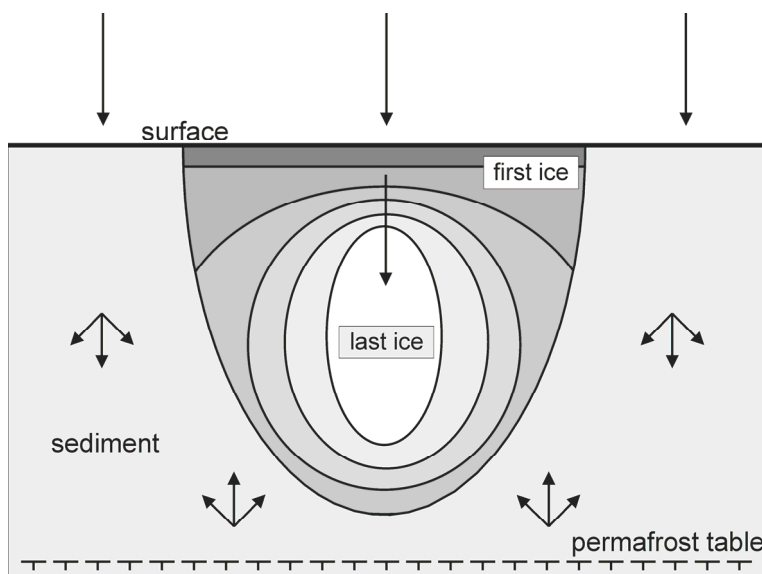


Figure 3.12: Simplified model of slow closed-system freezing of an enclosed water body under a downward moving freezing front. Different grey levels of the water body show successional freezing. The arrows indicate freezing direction. Already frozen sediments promote the cold wave into the unfrozen water. Multilateral freezing of the remaining water occurs.

network of ice-covered proglacial meltwater ponds existed. As the ice cap retreated, permafrost aggraded and enabled slow freezing of the water body from the outside inwards (Fig. 3.12) accompanied by ionic segregation and kinetic fractionation at its margins. Already-frozen sediments propagated the freezing front laterally into the more slowly freezing water body. The highly water-saturated diamicton, typical for Herschel Island sediments, could easily have been mobilised in a high-relief glacier forefield to cover frozen water bodies and enable their complete freezing and long-term preservation.

3.6 Conclusions

The following conclusions can be drawn from this study:

1. Stable isotope ($\delta^{18}\text{O}$, δD , d) and hydrochemical investigations, together with cryostratigraphical and cryolithological observations on massive ground ice bodies can expand the scope of ground ice studies in ice-marginal areas. They provide valuable information on water sources, freezing conditions and postburial landscape development where continuous records are generally rare.
2. Stable isotope signatures indicate a full-glacial water source feeding both the massive ground ice bodies examined on Herschel Island.
3. The TSD site massive ice is interpreted as originating as basal regelation glacier ice, evidenced by glaciotectonic deformation structures of an ice-rich diamicton and ice facies similar to those from basal ice layers of contemporary Arctic ice caps. However, an origin as glacially deformed segregated or segregated-intrusive ice cannot be entirely excluded.

4. Basal regelation ice and massive segregated-intrusive ice might coexist in ice-marginal areas. Large parts of the Yukon Coastal Plain may have been characterised by stagnant glacier ice and high porewater pressures in meltwater-saturated sediments while the glacier front disintegrated.
5. Combined stable isotope and hydrochemical investigations demonstrate a complete freeze through of water leading to the formation of massive ground ice at the HIW site. It is characterised by (a) a Rayleigh-type fractionation; (b) a distinct freezing slope as consequence of (a); and (c) ionic segregation towards its centre. The range of $\delta^{18}\text{O}$ values measured in this single body of massive ground ice appears to be unprecedented.

Acknowledgements

We wish to express their thanks to the Yukon Territorial Government, the Yukon Parks (Herschel Island Qiqiktaruk Territorial Park) and the Yukon Department of Renewable Resources for their support during this project. We acknowledge the support of the Polar Continental Shelf Programme (PCSP/ÉPCP publication number # 001-08) and the Aurora Research Institute (ARI) for the field component. This study was partly funded by the German Science Foundation (DFG, Project No. LA 2399/3-1), the German Federal Ministry of Education and Research (BMBF, Project No. CAN 08/A07, CAN 09/001) and by a doctoral fellowship awarded to Michael Fritz by the German Federal Environmental Foundation (DBU). Analytical work at AWI Potsdam was greatly supported by A. Eulenburg and L. Schönicke. We thank A. Lewkowicz (editor), D. Lacelle, and an anonymous reviewer for their helpful comments that improved the manuscript.

Supplementary material

Summary of major ion composition and total mineralisation indicated by the electrical conductivity. Absolute ion contents are presented in mg/l. As calculation basis and for better comparability amongst the different ions their concentration is stated in $\mu\text{mol}(\text{eq})/\text{l}$.

Profile	Electrical conductivity [$\mu\text{S}/\text{cm}$]	Cl ⁻ [mg/l]	SO ₄ ²⁻ [mg/l]	HCO ₃ ⁻ [mg/l]	Ca ²⁺ [mg/l]	K ⁺ [mg/l]	Mg ²⁺ [mg/l]	Na ⁺ [mg/l]	Cl ⁻ [$\mu\text{mol}(\text{eq})/\text{l}$]	SO ₄ ²⁻ [$\mu\text{mol}(\text{eq})/\text{l}$]	HCO ₃ ⁻ [$\mu\text{mol}(\text{eq})/\text{l}$]	Ca ²⁺ [$\mu\text{mol}(\text{eq})/\text{l}$]	K ⁺ [$\mu\text{mol}(\text{eq})/\text{l}$]	Mg ²⁺ [$\mu\text{mol}(\text{eq})/\text{l}$]	Na ⁺ [$\mu\text{mol}(\text{eq})/\text{l}$]	
																Mean
TSD massive ice	Mean	406	37.1	40.7	115	20.7	4.97	7.96	49.5	1047	846	1892	1035	127	655	2153
	Median	385	34.0	24.1	105	16.4	5.1	5.5	45.7	960	501	1724	818	129	450	1986
	Min	20.6	1.73	0.55	8.24	2.06	< 0.2	0.24	1.30	48.8	11.4	135	103	< 5.12	19.4	56.6
	Max	1294	97.2	276	275	66.5	14.7	35.1	160.0	2742	5745	4518	3318	376	2889	6960
	SD	257	24.1	50.7	71.6	14.88	3.33	6.85	38.15	681	1054	1174	743	85.4	564	1660
TSD rasedimental ice	Mean	3957	1248	100	144	31.4	31.3	43.0	827	35,181	2089	2362	1565	802	3540	35,961
	Median	4145	1223	98.4	144	24.7	28.8	37.1	807	34,498	2046	2358	1230	737	3049	35,105
	Min	1006	222	51.4	44.1	15.0	7.24	9.28	164	6262	1069	723	749	185	764	7134
	Max	6660	2977	159	250	61.6	62.0	118	1860	83,951	3311	4095	3074	1587	9711	80,910
	SD	1965	751	35.3	60.3	15.9	15.1	29.5	465	21,188	734	989	791	386	2426	20,246
HIW massive ice	Mean	212	35.2	15.3	38.1	4.13	2.30	2.14	32.3	992	318	625	206	58.8	176	1406
	Median	48.7	6.81	0.50	15.1	2.38	0.43	0.61	3.53	192	10.3	248	119	10.9	50.4	154
	Min	4.10	0.17	< 0.1	< 3.05	< 0.1	< 0.2	< 0.1	< 0.2	4.79	< 2.1	< 50	< 4.99	< 5.12	< 8.32	< 8.7
	Max	1090	206.9	78.9	164	13.2	13.6	10.9	188	5833	1641	2697	659	348	897	8178
	SD	318	58.78	24.81	47.6	3.96	3.77	3.16	54.5	1658	516	781	198	96.5	260	2369

Note: This table is available as supporting online material to the original article: [<http://onlinelibrary.wiley.com/doi/10.1002/ppp.714/supinfo>].

4 Late glacial and Holocene sedimentation, vegetation, and temperature history from easternmost Beringia (Northern Yukon Territory, Canada)

Michael Fritz¹, Ulrike Herzschuh^{1,2}, Sebastian Wetterich¹, Hugues Lantuit¹, Gregory P. De Pascale³, Wayne H. Pollard⁴, Lutz Schirrmeyer¹

¹ Alfred Wegener Institute for Polar and Marine Research, Potsdam, Germany

² Potsdam University, Institute of Earth and Environmental Sciences, Potsdam-Golm, Germany

³ University of Canterbury, Department of Geological Sciences, Christchurch, New Zealand

⁴ Department of Geography and Global Environmental and Climate Change Centre, McGill University, Montreal, Canada

under review in *Quaternary Research*

Abstract

Lake sediments from the northern Yukon Territory have recorded sedimentation, vegetation, and summer temperature changes since ~16 cal ka BP in the easternmost part of unglaciated Beringia. Depositional environments changed rapidly during the late glacial–Holocene transition near the collapsing Laurentide Ice Sheet and were triggered by a late-glacial drainage diversion of the Babbage River, probably leading to episodic spillovers of Laurentide meltwater into bedrock-controlled lake basins. Depositional conditions remained relatively stable during the Holocene and became decoupled from vegetation changes responding to climatic change. Herb-dominated tundra persisted until ~14.7 cal ka BP with mean July air temperatures ~5°C colder than today. Temperatures rapidly increased during the Bølling/Allerød interstadial towards modern conditions, favoring establishment of a *Betula-Salix* shrub tundra. Pollen-inferred temperature reconstructions recorded a pronounced Younger Dryas stadial in east Beringia with a temperature drop of ~1.5°C but show little evidence of an early Holocene Thermal Maximum. Northern Yukon Holocene moisture availability increased in response to a retreating Laurentide Ice Sheet, postglacial sea level rise, and decreasing summer insolation that in turn led to establishment of an *Alnus-Betula* shrub tundra from ~5 cal ka BP until present, and conversion of a continental into a coastal-maritime climate near the Beaufort Sea.

4.1 Introduction

During the late Wisconsin, the Bering land bridge connected the unglaciated parts of Alaska and the Yukon Territory with northeastern Siberia to form an extensive continuous landmass known as Beringia [Hopkins, 1982]. Beringian environments are of particular interest because they served as glacial refugia for various taxa [Hultén, 1937; Guthrie, 2001] and enabled the migration of plants, animals, and early men between Eurasia and North America [Morlan and Cing-Mars, 1982; Mason *et al.*, 2001]. The northern Yukon became the easternmost boundary of Beringia in close vicinity to the Laurentide Ice Sheet (LIS) and has undergone distinct changes in climate, landscape evolution, and ecology after the late glacial–Holocene transition that includes the latest part of the late Wisconsin, the late glacial warming known as the Bølling/Allerød (B/A) interstadial, the Younger Dryas (YD) stadial, and the early Holocene thermal maximum (HTM). Paleoenvironmental evidence for the YD is found in terrestrial and lake sediment records [e.g. Elias, 2000; Brubaker *et al.*, 2001; Briner *et al.*, 2002; Hu *et al.*, 2002; Yu *et al.*, 2008] as well as in ground ice from Alaska [Meyer *et al.*, 2010]. However, the regional paleoclimate dynamics during the late glacial–Holocene transition and the YD in general and in the northern Yukon in particular are poorly understood [Hu *et al.*, 2006; Viau *et al.*, 2008].

Although a number of paleoenvironmental investigations have been undertaken in east Beringia, hitherto only one lake sediment record is available from the northern Yukon that provides a continuous record of vegetation change (Hanging Lake; Cwynar, 1982). The Hanging Lake record was supposed to cover full-glacial times since the Last Glacial Maximum (LGM) and beyond until about ~ 33 ^{14}C ka BP [Cwynar, 1982]. This age estimate was recently revised by Kurek *et al.* [2009] to be significantly younger with ~ 17 cal ka BP. Even though there is a general acceptance that unglaciated late glacial landscapes were a heterogeneous mosaic of vegetation communities [Kurek *et al.*, 2009], little is known about vegetation and temperature dynamics northwest of the collapsing LIS close to the Arctic Ocean. Several studies have focused on biologic proxies like pollen, chironomids, and ostracods to reconstruct air temperatures [Bunbury and Gajewski, 2009; Kurek *et al.*, 2009], vegetation history [e.g. Rampton, 1971; Cwynar, 1982; Ritchie, 1984; Cwynar and Spear, 1995; Lacourse and Gajewski, 2000; Vermaire and Cwynar, 2010], and changes in available moisture and lake level [Pienitz *et al.*, 2000; Kurek *et al.*, 2009]. However, only few studies have investigated the late Pleistocene and Holocene sedimentation history or have taken into account lake-basin evolution and limnogeological succession [Engstrom *et al.*, 2000].

The aim of this study was, therefore, to gain a comprehensive understanding of the timing of landscape and environmental changes in the unglaciated northern Yukon since the late Wisconsin using lake sediments from Trout Lake in order to answer the following specific questions:

1. How did lake sedimentation respond to the late glacial–Holocene transition and the YD stadial in close vicinity to the collapsing LIS?
2. Is the timing of vegetation change in the northern Yukon synchronous with that seen in other records from east Beringia?
3. What have been the mean July air temperature magnitudes in ice-marginal east Beringia since the late glacial–Holocene transition?
4. How did pollen-inferred moisture pattern correspond to LIS retreat and Holocene warming?

4.2 Study site and regional setting

Trout Lake (68°49.73'N, 138°44.78'W) is located 163 m above sea level in the foothills of the British Mountains, approximately one kilometer west of the Babbage River and about 42 km south of the Beaufort Sea (Fig. 4.1a). The lake has a measured maximum depth of 10.2 m and is roughly rectangular with an area of 0.84 km². The catchment is small; steep bedrock slopes rise from the lake in the south and east, while a gently rolling plateau is located to the north and west of the lake where a small outlet stream and three smaller lakes occur (Fig. 4.1b). Trout Lake is located about 40 km north of the modern treeline [Welsh and Rigby, 1971] within the zone of continuous permafrost. The surrounding bedrock is dominated by Jurassic to Lower Cretaceous shale and siltstone [Norris, 1977]. The northern British Mountains form extensive pediments of gentle gradient [French and Harry, 1992] down towards the Yukon Coastal Plain (YCP) to the north. The study area lies beyond the maximum limit of Pleistocene glaciations (Fig. 4.1); Hughes [1972] and Rampton [1982] have pointed out that the last major ice advance (Buckland Glaciation of Wisconsin age) was restricted to the YCP to the north and northeast.

The modern climate of the northernmost part of the Yukon is subarctic maritime in summer during the open-water season of the southern Beaufort Sea, and continental in winter with pronounced anticyclonic influence [Wahl et al., 1987]. The mean annual temperature (1971–2000) is –9.9°C at Shingle Point, the closest weather station ~50 km northeast of Trout Lake, with an average July maximum of 11.2°C [Environment Canada, 2000]. Mean annual precipitation of 254 mm per year is low and is almost equally shared between rain and snow [Environment Canada, 2000]. The modern catchment vegetation is dominated by heath tundra and fellfield communities, including boreal taxa like *Alnus crispa*, *Betula glandulosa* and *Salix*, and herbs like *Empetrum nigrum*, *Vaccinium uliginosum*, *Vaccinium vitis-idaea*, *Arctous alpina* and *Anemone* sp. [Welsh and Rigby, 1971; F. Kienast, personal communication, 2011].

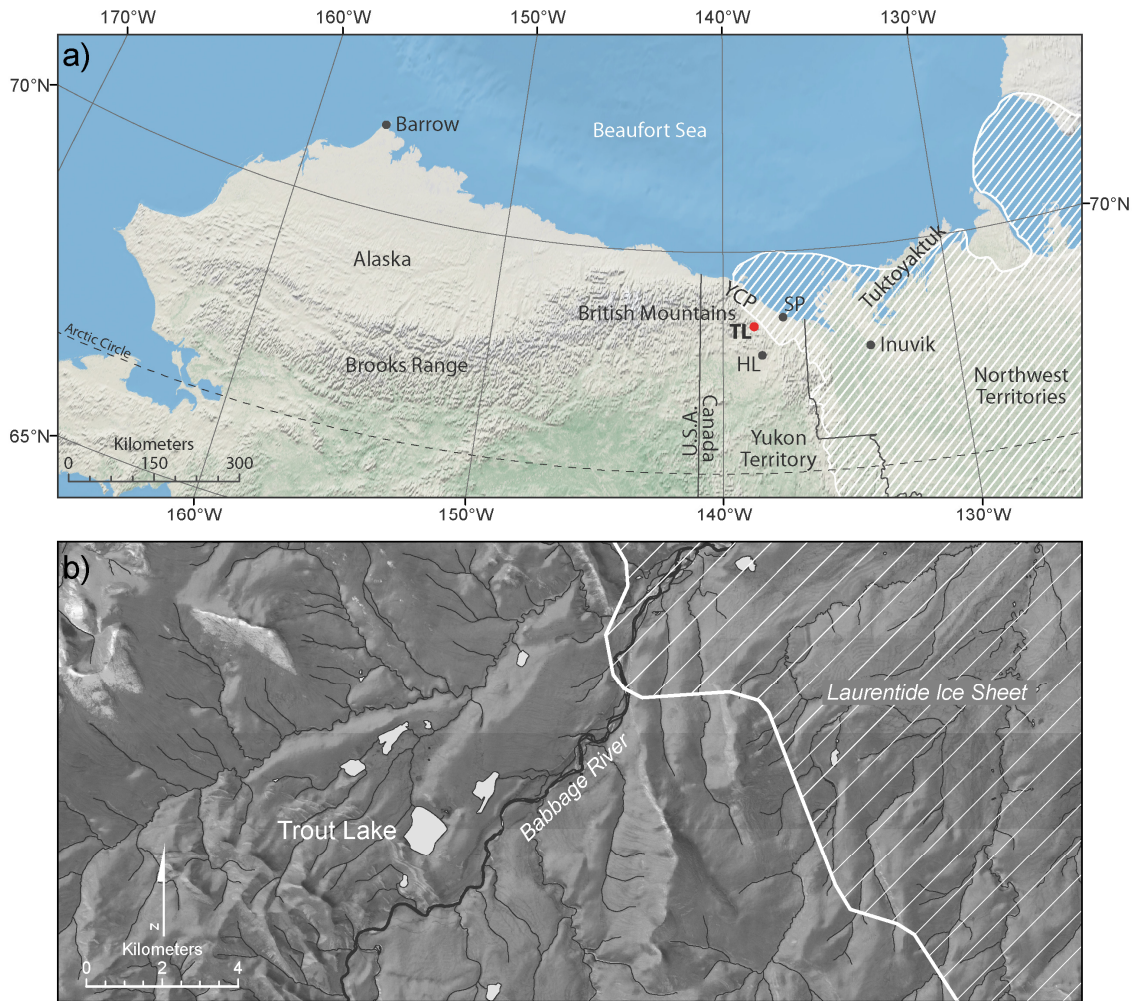


Figure 4.1: (a) Location map of the western Arctic. Striated area indicates Last Glacial Maximum (LGM) Laurentide ice limit and follows *Dyke and Prest* [1987]; TL – Trout Lake, HL – Hanging Lake, SP – Shingle Point, YCP – Yukon Coastal Plain. (b) Trout Lake study site and surrounding area with local drainage and hydrology. Trout Lake is shown in close-up in Figure 4.2. The background map is based on a Rapideye satellite image (red band, stretched and displayed in greyscale, 5 m resolution) overlain with the Yukon Digital Elevation Model (30 m resolution).

4.3 Material and methods

4.3.1 Coring and on-site sampling

The selection of the coring site was based on bathymetric profiling and ground penetrating radar (GPR) surveys carried out in August 2008 and April 2009, respectively. Bathymetric profiling was undertaken via boat in August and through drill holes in the lake ice in April. A MALÅ GPR system with both 50 MHz and 100 MHz unshielded rough-terrain antennas (RTA) was used to map the lake bathymetry, lakebed sediments (Fig. 4.2), and surrounding stratigraphy of Trout Lake during April 2009. GPR data were processed with REFLEXW software using direct-

coupling wave horizontal filtering to remove noise. In April 2009 a 405 cm-long sediment core was retrieved from the deepest basin of the lake at a water depth of 8.70 m. Coring was carried out from a tripod mounted on the two-meters-thick lake ice using a UWITEC piston corer. Bedrock at the base of the sediments prevented further penetration of the corer. Upon recovery, the overlapping sediment cores were cut into segments up to 100 cm in length which were stored cool (but above freezing) in dark conditions. In the laboratory sediment cores were split in half, photographed, and described, and 1 cm slices were sampled at 5 cm intervals for further destructive analyses. For characterization of the recent limnology, surface and bottom water samples were taken in both field seasons for determination of stable water isotopes ($\delta^{18}\text{O}$, δD), electrical conductivity, pH, dissolved O_2 , and the major anion and cation composition.

4.3.2 Geochronology

Core samples were wet-sieved ($>250\ \mu\text{m}$) to isolate plant macrofossils for AMS (accelerator mass spectrometry) radiocarbon dating at the Poznan Radiocarbon Laboratory (Adam Mickiewicz University, Poznan, Poland). Six radiocarbon ages obtained by AMS dating on moss remains are the basis of the core chronology (Table 4.1). Ages were calibrated using “CALIB 6.0” [Stuiver and Reimer, 1993; Data set: IntCal09: Reimer *et al.*, 2009] and are denoted as calibrated thousand years before present (cal ka BP). We report the midpoint of the 2-sigma age ranges.

4.3.3 Sediment properties

The mass-specific magnetic susceptibility (MS) was measured on the halved core with a multi-sensor core logger (MSCL, GEOTEK) at 1-cm increments and is displayed using a 5-point running average. Core lithology was determined by detailed manual core logging including descriptions of sediment texture and structures, color, and biogenic features. The laboratory measurements and detailed core descriptions were used to characterize sediment units and transitions. Freeze-drying of the samples yielded estimates of the water content. A laser particle analyzer (Coulter LS 200) was used for grain-size analyses on organic-free (treated with 30 % H_2O_2) subsamples of the $<2\ \text{mm}$ fraction. The remaining particles greater than 2 mm were reintegrated into the grain-size statistics using the SediVision 2.0 software. Total carbon (TC), total organic carbon (TOC), total nitrogen (TN), and total sulfur (TS) contents were measured with a carbon-nitrogen-sulfur (CNS) analyzer (Elementar Vario EL III), and are given as weight percent (wt%). The C/N ratio (C/S ratio) is expressed as the quotient of TOC and TN (TS) values. Stable carbon isotope ratios ($\delta^{13}\text{C}$) of TOC were measured on carbonate-free (treated with 10 % HCl) samples with a combination of a mass spectrometer (DELTAplusXL, Finnigan) and an elemental analyzer (Carlo-Erba CN2500) at

the German Research Centre of Geosciences (GFZ) in Potsdam, Germany. The values are expressed in delta per mil notation (δ , ‰) relative to the Vienna Pee Dee Belemnite (VPDB) standard.

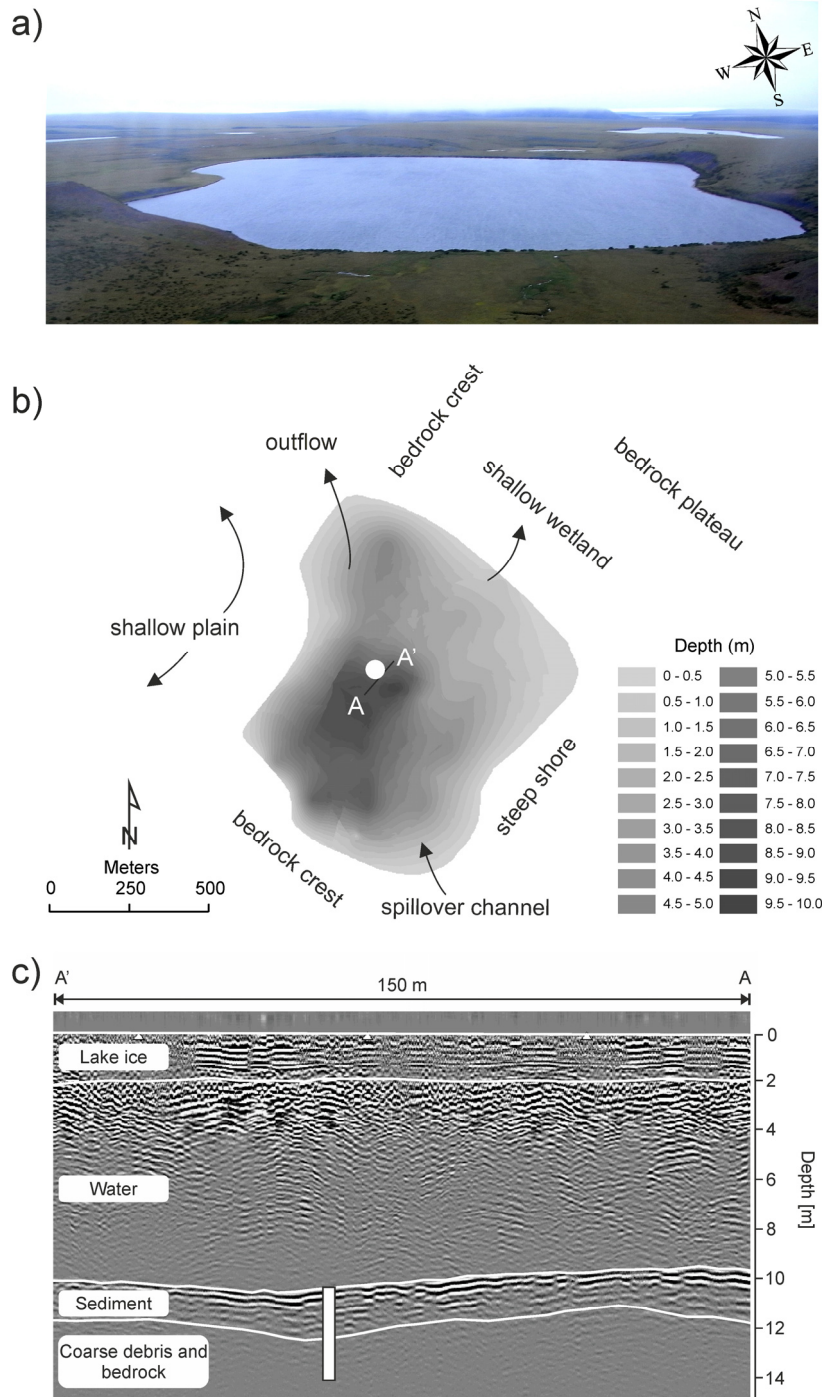


Figure 4.2: (a) Photograph showing the modern lake. (b) Trout Lake bathymetry and coring location (white circle) in April 2009. The bathymetry map is based on the ArcGIS TOPOGRID module using a series of different datasets including echosounding from boat surveys in summer, conventional depth sounding from holes drilled in the lake ice in winter, and depths extracted from ground penetrating radar (GPR) tracks collected on the lake ice in winter. (c) Interpreted GPR profile (100 MHz) across the coring location (white bar).

4.3.3 Pollen treatment and numerical methods

Preparation of the pollen samples included treatment with HCl, KOH, HF, acetolysis, sieving, and mounting in glycerin [Fægri and Iversen, 1989]. Two tablets of *Lycopodium* spores were added to calculate the pollen concentration. The sediment core was analyzed at 27 intervals in which at least 300 terrestrial pollen grains (excluding spores and aquatic taxa) were counted at each level. In the basal core sample, where pollen concentration was very low (2290 grains/cm³), 182 grains were counted. Pollen identifications were based on the relevant literature [McAndrews *et al.*, 1973; Moore *et al.*, 1991; Beug, 2004]. Pollen percentages were square-root transformed prior to all statistical analyses, and only pollen taxa that were present with an abundance of $\geq 0.5\%$ in at least three samples were included in further analyses. The definition of local pollen zone (PZ) boundaries within the pollen percentage diagram was based on a Constrained Incremental Sum of Squares cluster analysis (CONISS) using the Edwards and Cavalli-Sforza's chord distance measure with TILIA software [Grimm, 1991]. The main gradients of floristic variation were first assessed by using detrended correspondence analysis. Because the maximum gradient length of the first axis was 1.81 standard deviation units, the linear ordination technique principal components analysis (PCA) was chosen for subsequent statistical analysis [Lepš and Šmilauer, 2003]. PCA focused on inter-species distances. All multivariate ordinations were performed using the CANOCO 4.5 program for Windows [ter Braak and Šmilauer, 2002].

In order to gain quantitative information about mean July air temperature (T_{Jul}) in the past, pollen–climate transfer functions were applied to the fossil pollen spectra from Trout Lake. The modern pollen data set consists of 623 modern surface samples that we extracted from the North American Pollen Database [Grimm, 2000; Whitmore *et al.*, 2005, Version 1.7, updated until 2008] including sites located north of 50°N and west of 110°W. Sites with less than 150 terrestrial pollen grains and spores were excluded. Modern pollen spectra cover a wide range of T_{Jul} (2.9 to 16.7°C). Transfer functions were developed with weighted averaging partial least squares (WAPLS) regression (second-component model was chosen). Furthermore, modern analogue technique (MAT) with chord-distance as similarity measure was applied; the reconstructed T_{Jul} represents the average of the 5 closest analogues. Model performance was tested by leave-one-out cross-validation. The root mean square error of prediction (RMSEP) and the coefficient of determination (r^2) are $\pm 1.63^\circ\text{C}$ and 0.71 for WAPLS and $\pm 1.43^\circ\text{C}$ and 0.77 for MAT, respectively, and thus indicate that the modern data set is suitable for quantitative reconstructions. Calibrations were performed using C2 software [Juggins, 2003].

Table 4.1: Summary of Accelerator Mass Spectrometer (AMS) ^{14}C results and calibrated ages from Trout Lake, northern Yukon.

Core depth	Dated Material	Uncalibrated ^{14}C ages	Calibrated 2 σ -age range	Midpoint 2 σ -age	Lab no. ^a
[cm]		[yr BP]	[cal yr BP]	[cal yr BP]	
3	<i>Sphagnum</i> moss	930 \pm 30	925-782	852	Poz-36442
66	Moss remains	5760 \pm 40	6659-6465	6561	Poz-36443
176	Moss remains	9550 \pm 50	11,101-10,704	10,917	Poz-36455
225	Moss remains	12,770 \pm 70	15,641-14,714	15,164	Poz-36456
352	Moss remains	12,880 \pm 80	16,093-14,980	15,397	Poz-36445
373	Moss remains	13,140 \pm 80	16,533-15,242	15,961	Poz-36458

^a Poz = Poznan Radiocarbon Laboratory.

4.4 Results

4.4.1 Modern limnology

The limnological and water-chemistry data for 8 August 2008 and 21 April 2009 are summarized in Table 4.2. The oligotrophic Trout Lake is very weakly alkaline (pH 7.4 to 7.9) and has a low electrical conductivity, between 82 $\mu\text{S}/\text{cm}$ in August and 138 $\mu\text{S}/\text{cm}$ in April. The water column is well mixed to the bottom throughout the year; the dissolved oxygen content is high (>20 mg/l). With $\delta^{18}\text{O}$ values of about -17‰ and a deuterium excess ($d\text{-excess} = \delta\text{D} - 8\delta^{18}\text{O}$) that ranges from -5.8‰ in April to -7.4‰ in August, the hydrological system is rather closed; evaporation effects lead to enriched δ -values and a reduced $d\text{-excess}$ compared to modern precipitation data derived from Inuvik ($68^{\circ}18'\text{N}$, $133^{\circ}37'\text{W}$; IAEA, 2006), which is located about 150 km east of Trout Lake.

4.4.2 Chronostratigraphy and sediment properties

The age-depth model was constructed by linear interpolation between the lowermost three dates because these dates fall within an overlapping and narrow age range (Table 4.1). Age extrapolation to the bottom of the sediment core was done accordingly. A squared regression model was used between the uppermost four dated samples. Transferring the established age-depth relationship onto the lithostratigraphic units (Fig. 4.3), which are described in detail in the following, yields four chronostratigraphic periods (Fig. 4.3) that are discussed in the course of this study:

Basement (>16 cal ka BP; 405-386 cm)

The lowermost 20 cm of the core are composed of bedrock debris. Black shale and siltstone, typical of the Jurassic catchment rocks, showed shattered structures due to the coring process. Geochemical parameters measured within ground bedrock samples serve as background values for interpreting soft sediment values and their relationship to primary production within the lake or its catchment *versus* bedrock-derived components. Ancient organic carbon is present at about 1.6 to 2.0 % and with a $\delta^{13}\text{C}$ value of -24.2 ‰, together with moderate inorganic carbon (0.1 to 1.5 %) and high sulphur contents (0.4 to 8.7 %) leading to low C/S ratios (0.2 to 5.3; Fig. 4.3). Bedrock debris together with overlying coarse-grained material of unit 1 was mapped as a reflector in the GPR data (Fig. 4.2c) and provides insight into the basin morphology. This unit represents the basis of the basin; therefore, we can be sure that we covered the complete sediment record since sediment accumulation commenced.

Unit 1 (16.0 to 14.8 cal ka BP; 385-225 cm)

Black unbedded sand, gravel, and minor amounts of silt and clay make up this unit that covers the latest part of the full-glacial period. Sedimentological properties are homogenous throughout the whole segment and are comparable to the background values of the underlying bedrock in terms of TOC, $\delta^{13}\text{C}$, and C/S ratios, and therefore imply low organic matter production or preservation. At 381-366 cm and 347-330 cm greenish-gray silty clay lenses were visible. In both intervals the clay lenses can be recognized by a clay peak in the grain size diagram and a MS minimum (Fig. 4.3). A highly variable MS, between 13 and 68 SI, as well as the high and concurrently variable sand content of up to 81 % with gravel admixtures indicate a frequently-changing depositional environment during the rapid deposition of the lowermost 160 cm of sediment in a fluvial environment, or at least in a basin episodically traversed by running water. From 231 cm upwards, unit 1 grades into fine-clastic and compact material of unit 2.

Unit 2 (14.7 to 10.7ka; 224-150 cm)

Unit 2 encompasses the period of the late glacial–Holocene transition. The material is silty and clastic-dominated at the bottom. It becomes slightly finer and more organic-rich upwards, where clayey silt with some sand appears crumbly and compact without internal structure. Parallel bedding structures are visible in the upper part, and several moss and organic-rich layers are intercalated at 180-176, 172-171, and 160 cm. Sediments at the top of unit 2 are clayey, black, structureless, sticky, and greasy, and they gradually merge into unit 3. Water content rises sharply by 15 % at the transition between unit 1 and 2, where most sedimentological parameters including sedimentation rate change strongly. MS decreases to minimal values of 4 SI before it rises again

with secondary minima at organic-rich layers. TOC is constantly present above 3.5 % with maximum values of ca. 8 % where moss layers occur. Low C/N ratios (10 to 12) together with low C/S ratios (due to high sulfur contents, up to 3.7 %) and a $\delta^{13}\text{C}$ below -25‰ (Fig. 4.3), which is typical of terrestrial organic matter input, could point towards a preferential loss of organic carbon due to strong organic matter decomposition. At organic-rich layers, MS drops; moisture, TOC, and C/N ratios peak (Fig. 4.3), with concurrent minima in $\delta^{13}\text{C}$ (-28 to -27‰). This is typical of a dominance of terrestrial plants [Meyers, 1994]. The sedimentary record between 14.7 and 10.7 cal ka BP is characterized by episodically changing sedimentological parameters, and therefore indicates several shifts in the driving forces of deposition and organic matter accumulation. In contrast to unit 1, which is attributed to full-glacial conditions with a dominance of grain-size variability and high noise in the data, the variability within unit 2 is instead driven by changes in the biogeochemical parameters of Trout Lake and might be related to a response to climate forcing and fluctuating lake levels.

Table 4.2: Modern limnological, hydrochemical, and stable water isotope characteristics from Trout Lake, northern Yukon.

Parameter	Unit	August 2008	April 2009
Max water depth	m	10.2	
Surface water temperature	°C	11.0	0.7
Bottom water temperature	°C	11.1	2.8
O ₂ (dissolved)	mg/L	n.a.	21.9
pH		7.4	7.9
Electrical conductivity	µS/cm	82.1	138
Ca ²⁺	mg/L	9.65	15.3
K ⁺	mg/L	0.69	1.12
Mg ²⁺	mg/L	3.40	5.19
Na ⁺	mg/L	1.11	1.74
Cl ⁻	mg/L	0.67	1.17
SO ₄ ²⁻	mg/L	16.8	27.2
HCO ₃ ⁻	mg/L	24.9	37.8
$\delta^{18}\text{O}$	‰ VSMOW	-17.0	-17.7
δD	‰ VSMOW	-144	-147
<i>d</i> -excess	‰ VSMOW	-7.4	-5.8

Note:

Cation and anion contents were determined by inductively coupled plasma – optical emission spectrometry (ICP-OES, Perkin-Elmer Optima 3000 XL) and ion chromatography (IC, Dionex DX-320), respectively. Hydrogen carbonate concentrations were measured by titration (Metrohm 794 Basic Titrino). $\delta^{18}\text{O}$ and δD ratios were determined with a Finnigan MAT Delta-S mass spectrometer, using the equilibration technique [Horita *et al.*, 1989]. Deuterium excess (*d*-excess = $\delta\text{D} - 8\delta^{18}\text{O}$; Dansgaard, 1964) was calculated and provides insight into (i) the water source of the initial precipitation, and (ii) the presence or absence of secondary non-equilibrium fractionation processes.

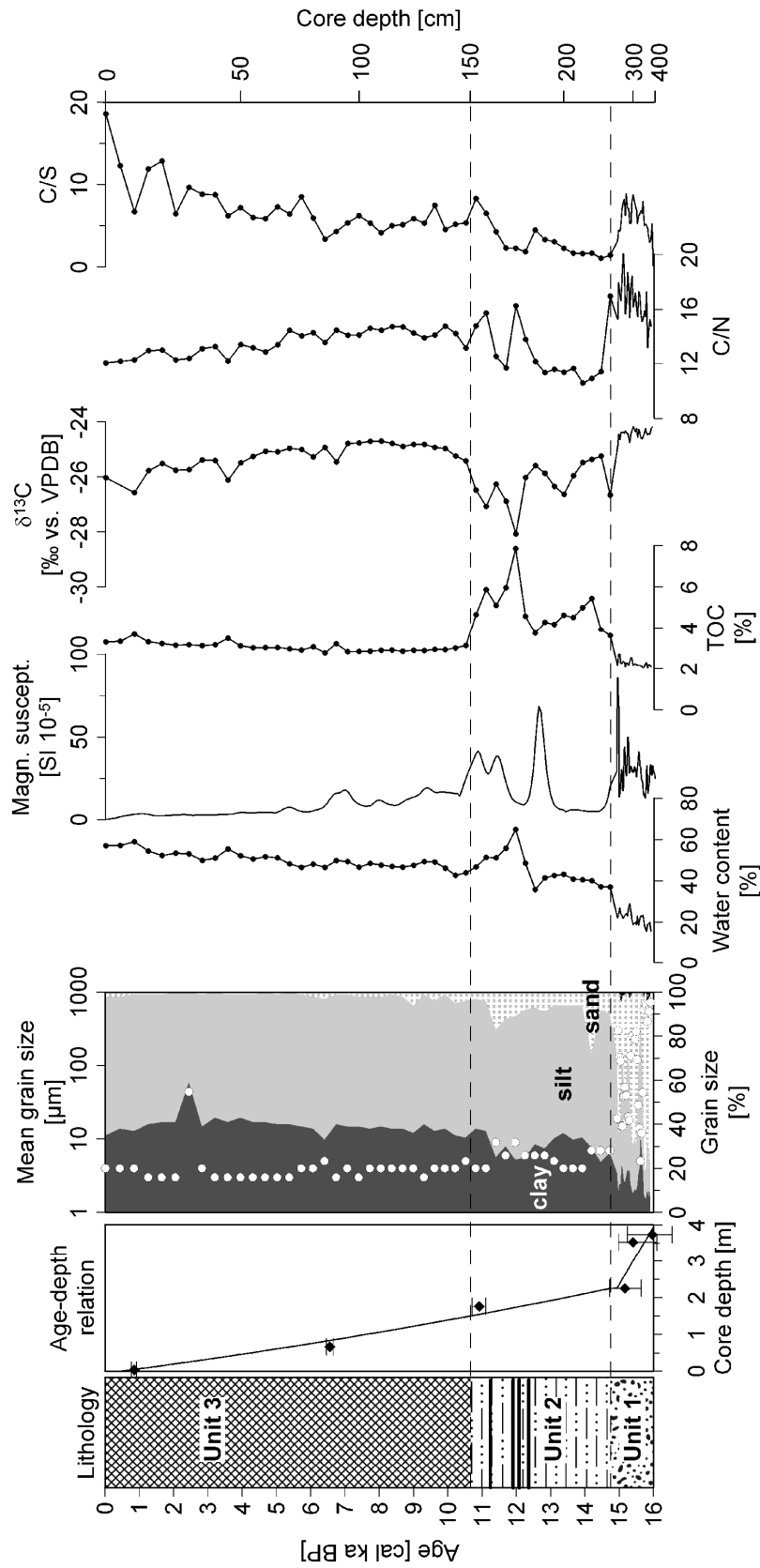


Figure 4.3: Summary plot of age-depth relationship and lithological, sedimentological, and biogeochemical parameters from Trout Lake, northern Yukon. Linear interpolation ($y = 0.158x - 2136.434$) between the lowermost three dates and a second order polynomial ($y = 2.536 \cdot 10^{-7}x^2 + 0.012x - 5.499$) between the uppermost dated samples was applied (see also Table 4.1).

Unit 3 (10.6 cal ka BP to present; 149-0 cm)

Deposits assigned to unit 3 cover the entire Holocene and appear black, structureless, water-saturated (46 to 59 % water content), and very soft. Most sedimentological properties are almost homogeneous throughout this segment (Fig. 4.3) as indicated by a constant low MS (0 to 9 SI). Very fine-grained and clayey to silty deposits with usually less than 5 % sand dominate, although single scattered clasts up to 0.5 cm in diameter are present at 58 and 54 cm. Thin organic-rich layers are visible at 135, 128, 111.5, 91, 87, 83, and 67 cm. A thin layer of *Sphagnum* moss covers the sediment surface. Carbonate shells are absent throughout the core except for one small fragment found at 142 cm. Values of inorganic carbon, calculated as the difference between measured TC and TOC, never exceed 0.4 %. Therefore, lake sediments are regarded as largely carbonate-free. TOC is only present at less than 2 % above the background value of the underlying bedrock, and shows a terrestrial carbon signature of -26.6 to -24.7 ‰ for $\delta^{13}\text{C}$. Low C/N ratios rise slightly, together with TOC contents, towards the surface (Fig. 4.3), and indicate strong decomposition of organic carbon and nitrogen fixation. Sedimentation rates were very low during the Holocene (≤ 0.17 mm/a) and partly explain the invariability in biogeochemical parameters. Well-aerated surface deposits exposed for a long time due to slow sedimentation rates in oxygen-rich lake water may have led to nearly complete oxidation of organic matter and unfavorable conditions for carbonate preservation in ion-poor lake water (e.g. depleted in HCO_3^-). Based on the homogeneity of sediment properties throughout the Holocene, we infer little changes in sediment input, sedimentation rate, or lake level; however, any such changes might be concealed because the sampling resolution, especially throughout the Holocene, is rather low, with a 300-to-400-year inter-sample resolution.

4.4.3 Pollen

Pollen zonation

The Trout Lake pollen percentage diagram is divided into four pollen zones (PZ) based on the information from CONISS (Fig. 4.4).

PZ 1 (16 to 15.1 cal ka BP): The pollen assemblages prior to ~15 cal ka BP indicates a dry herbaceous tundra as they are dominated by Poaceae (>37 %), *Artemisia* (~17 %), and Cyperaceae (5 to 9 %), high percentages of Brassicaceae (~4.5 %), and increasing values of *Betula* (10 to 24%) towards zone 2. PZ 1 exhibits the lowest pollen concentration, and low percentages of arboreal pollen, aquatic taxa, and spores.

PZ 2 (15.0 to 10.7 cal ka BP): In this zone *Betula* rises sharply, reaching maximum values of >70 % between ~14.0 and 12.9 cal ka BP. *Salix* is constantly present above 5 % while Cyperaceae slightly increases (8 to 20 %) and Poaceae drops to less than 15 %.

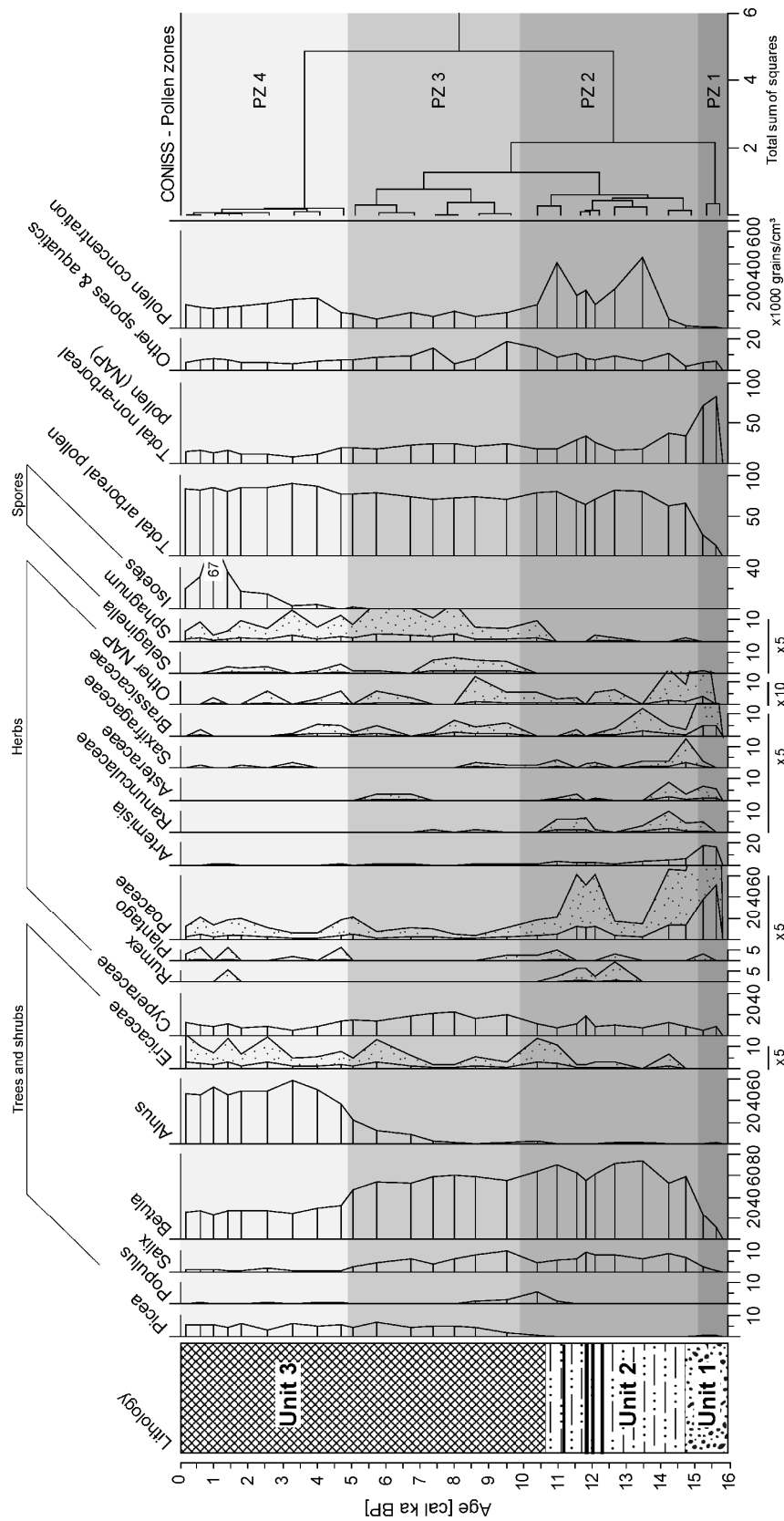


Figure 4.4: Pollen percentage diagram from Trout Lake, northern Yukon. Other non-arboreal pollen (NAP) comprise *Potentilla*, *Laminaceae*, *Papaveraceae*, *Fabaceae*, *Epilobium*, *Thalictrum*, *Caryophyllaceae*, *Chenopodiaceae*, *Rubus*, *Apiaceae*, and *Polygonum*. Other spores and aquatics comprise *Pteridium*, *Potamogeton*, *Myriophyllum*, *Equisetum*, *Bryidae*, *Pediastrum*, and *Botryococcus*. Note varying exaggeration factors for selected taxa.

Taxa that indicate disturbed ground or dry edaphic conditions like *Artemisia*, Brassicaceae, Asteraceae, Ranunculaceae, and Saxifragaceae are constantly present. A notable drop in *Betula* percentages with a parallel increase in Poaceae and Cyperaceae characterizes PZ 2 between 12.6 and 11.5 cal ka BP, which is probably coeval with the YD stadial (Fig. 4.4). By the end of PZ 2 towards the early Holocene at ~11.2 cal ka BP *Populus* occurs for the first time, although in small amounts.

PZ 3 (10.6 to 5.0 cal ka BP): *Betula* is still dominant with secondary influences of Cyperaceae, *Salix*, Ericaceae, and spores of *Sellaginella* and *Sphagnum*. *Populus* reaches its maximum of slightly more than 5 % and slowly decreases afterwards. *Picea* starts to occur at frequencies >1 % at 9.8 cal ka BP and exhibits constant values above 4 % after 8.9 cal ka BP, but never exceeds 7 % throughout the record. Towards the end of zone 3 *Alnus* occurs for the first time with values above 5 % at ~7.3 cal ka BP, followed by a rapid increase.

PZ 4 (4.9 cal ka BP to present): In this zone *Betula* and *Salix* decrease until ~4 cal ka BP and then remain constant at about 25 to 30 % and around 1 %, respectively. *Alnus* becomes dominant by ~5 cal ka BP, reaching maximum values of around 50 % after 4.3 cal ka BP. Ericaceae show a minor maximum in the last 3.0 cal ka BP. *Isoetes* spores begin to occur in PZ 3 at ~5.3 cal ka BP and remain the dominant aquatic taxon until present.

Principal component analysis and temperature reconstruction

The first two axes of the PCA explain 86.7 % of the variation in the pollen data (Fig. 4.5a). The length of a vector in the biplot indicates how strongly the variable is related to the displayed ordination [ter Braak and Šmilauer, 2002]. Hence, *Alnus*, *Isoetes*, *Picea*, and Ericaceae are positively correlated with the first axis in descending order of correlation, whereas *Salix*, *Artemisia*, and Ranunculaceae are negatively correlated. Taxa positively correlated with PCA axis 2 include Poaceae and *Artemisia*, whereas *Betula*, Cyperaceae, and *Sphagnum* are negatively correlated, and variations of *Populus* are badly represented in the plot. The separation of species into distinct groups in the PCA ordination relates to species-specific ecological preferences, most probably related to edaphic conditions and climate.

Sample scores on the first axis are negative until ~7 cal ka BP and show a generally increasing trend from 16.0 cal ka BP until 3.6 cal ka BP (Fig. 4.5b). Scores remain above unity after 4.3 cal ka BP. Sample scores on PCA axis 2 decrease from maximum values at 16.0 cal ka BP until ~13 cal ka BP and show a similar trend as sample scores on the first axis since ~10 cal ka BP. This is in contrast to the period between ~14 and 11 cal ka BP when sample scores on both axes run contrary to one another (Fig. 4.5b). Mean summer insolation (July, 60°N; Lasker et al., 2004) and the $\delta^{18}\text{O}$ record from the Greenland Ice Sheet Project 2 (GISP2) ice core [Grootes and Stuiver, 1997] since

16 cal ka BP as well as non-pollen palynomorphs (i.e. *Sphagnum* and *Isoetes* spores) and TOC are plotted in the PCA as inactive parameters (Fig. 4.5a) in order to enable qualitative assumptions about the relationship of regional vegetation response on changing supraregional environmental parameters represented by the supplement. In this context, GISP2 $\delta^{18}\text{O}$ reflects variations in northern hemisphere mean annual air temperatures, whereas summer insolation serves as a proxy for orbitally controlled summer temperature variations. Summer insolation is positively correlated to the first axis, the GISP2 record is negatively correlated to the first axis, and both parameters are slightly negatively correlated to the second axis. *Sphagnum* and *Isoetes* spores are positively related to the first axis; TOC is insignificant.

Pollen-inferred T_{Jul} were lowest during the late glacial between 16.0 and 13.7 cal ka BP but then rapidly ameliorated towards modern temperature conditions (Fig. 4.6). Results of both applied reconstruction methods indicate a sudden decrease in T_{Jul} of 1.5°C between 12.9 and 11.2 cal ka BP, followed by an increase to almost near-modern values at 7 cal ka BP. T_{Jul} has remained stable during the last 4.3 cal ka BP. Results based on WAPLS are similar to those based on MAT; however, the absolute reconstructed temperature range is larger (WAPLS: 5.8 to 11.5°C; MAT: 7.1 to 11.2°C). The temperature increase at the late glacial–Holocene transition is more pronounced in the applied WAPLS, whereas the MAT shows a more pronounced early Holocene warming between 11.2 and 8.9 cal ka BP with relatively stable conditions until today in both reconstructions (Fig. 4.6).

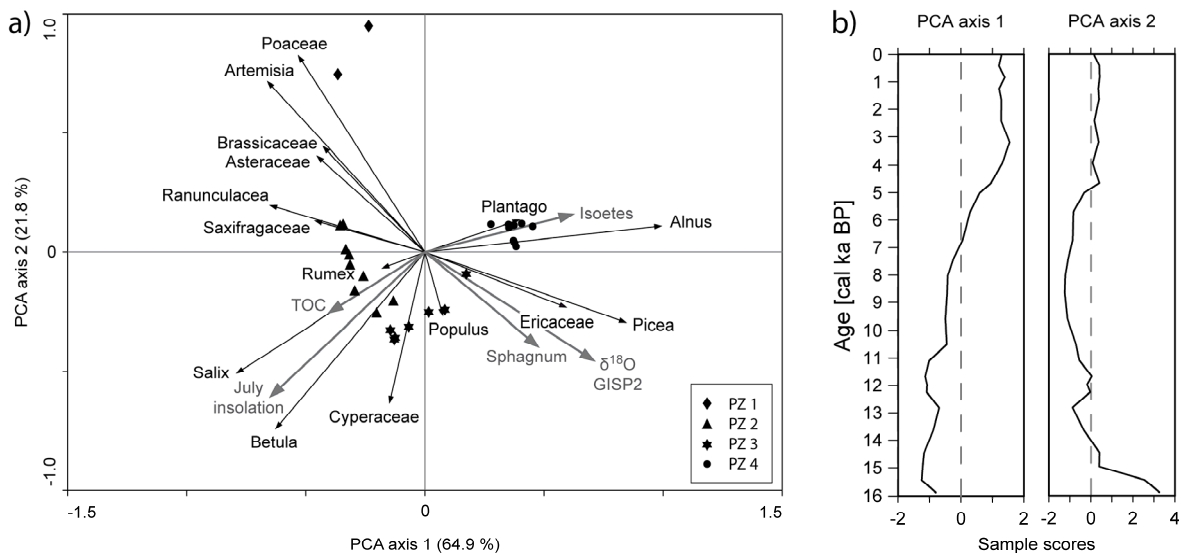


Figure 4.5: Summary of principal component analysis (PCA). **(a)** PCA biplot for pollen data. Inactive supplementary parameters (July insolation, $\delta^{18}\text{O}$ GISP2, TOC, *Sphagnum*, *Isoetes*) are shown in grey. Symbols are keyed to the Pollen Zones (PZ); see also Figure 4.4. **(b)** Time series of sample scores for PCA axes 1 and 2 from Trout Lake, northern Yukon.

4.5 Discussion

4.5.1 Formation and development of Trout Lake in ice-marginal east Beringia

Lake sediment accumulation in Trout Lake began around 16 cal ka BP during the waning stages of the late Wisconsin glaciation. Climate conditions and depositional processes were strongly influenced by the proximity of the LIS to the east that remained close to its northwestern limit until 15 to 14 cal ka BP [Dyke and Prest, 1987; Dyke et al., 2003]. Welsh and Rigby [1971] recognized that lakes are uncommon along the unglaciated parts of the YCP and in the adjacent foothills of the British Mountains. One exception is Trout Lake that may have formed as a plunge-pool lake in the ancient surface of the Babbage River drainage [Welsh and Rigby, 1971]. The Babbage River is entrenched 20 to 30 m below the pediment surface on Jurassic shale near Trout Lake with four distinct river terraces; the uppermost terrace is well above the proximate (eastern) lake shore and the current lake level.

Late glacial drainage diversion – initial sedimentation

The initial Trout Lake sedimentation at 16 cal ka BP was characterized by rapid input of sand with admixtures of clay, silt, and gravel of local provenance as indicated by the predominance of black shale particles. Rapid grain-size alternations with silty interbeds and intercalated clay lenses suggest frequently-changing water volumes and flow velocities. Bioproductivity and organic-matter input were low due to harsh climate conditions and sparse vegetation in the lake catchment. Depositional conditions during the waning stages of the full glacial were directly influenced by the proximity of the LIS, which crossed the Babbage River valley northeast of Trout Lake [Dyke and Prest, 1987; Dyke et al., 2002; Fig. 4.1b]. The LIS most likely blocked direct northern drainage into the Beaufort Sea, resulting in a drainage diversion that forced LIS meltwater and local drainage southward up the modern Babbage River and its confluences. Similarly, in the central Yukon, the LIS impounded the eastward drainage of the paleo-Porcupine River at McDougal Pass [e.g. Duk-Rodkin and Hughes, 1994] and caused westward drainage diversion into the Yukon River [e.g. Duk-Rodkin et al., 2004]. The southern slopes of the British Mountains all belonged to the paleo-Porcupine watershed [Duk-Rodkin and Hughes, 1995]; therefore, the Babbage River and its tributaries likely served as the major proglacial drainage path to the north along the oscillating LIS margin during the latest part of the full glacial. Dyke and Prest [1987] inferred asynchronous ice retreat for the northwest LIS margin that remained close to its limits until $\sim 15^{14}\text{C}$ ka BP while Murton et al. [2007] argued, on the basis of a series of optically-stimulated luminescence ages, that deglaciation on Tuktoyaktuk Peninsula commenced between 16 and 14 ka. This line of evidence provides reasonable support for the hypothesis that with the onset of substantial ice-margin recession, episodic spillovers may have entered the Trout Lake basin at its southeastern end via a

narrow valley incised into the uppermost Babbage River terrace and might also have filled the nearby smaller lakes (Figs. 4.1b and 4.2b).

Stabilizing lake environment

Beginning with the B/A interstadial, Trout Lake was a permanently water-filled basin with variable inputs of clay-, silt-, and sand-sized material. Coarser particles are probably wind-driven or derive from spring meltwater outwash from incompletely-vegetated slopes. For example, eolian transport of clasts up to 1.5 cm in diameter onto the Trout Lake ice was observed during a major windstorm in April 2009. Low C/S ratios point towards anoxic bottom water conditions in a shallow water body with still short ice-free periods under mats of plant detritus or algae, which inhibited surface sediment aeration. On millennial time scales, sedimentation history at Trout Lake is stable throughout the Holocene and is decoupled from the timing of vegetation succession as inferred from palynological results. The dominance of fine-grained deposits and low TOC contents account for high lake levels, densely-vegetated slopes that prevent mass-wasting events and low primary production in combination with low preservation capability of organic matter in an oligotrophic and well-aerated lake.

4.5.2 Environmental change during the late glacial–Holocene transition (~16 to 11.6 cal ka BP)

Latest full glacial

During the latest part of the full glacial (16.0 to 14.7 cal ka BP), a sparse vegetation, predominantly characterized as herb-dominated tundra, with communities indicating dry conditions and disturbed ground (Poaceae, *Artemisia*, Brassicaceae) together with low pollen concentrations (PZ 1), covered the ground in the direct vicinity of the Trout Lake basin. Inferred T_{Jul} of 6–7°C are the coldest of the whole record (Fig. 4.6). This is in good agreement with significantly lower-than-modern chironomid-inferred T_{Jul} from Hanging Lake [Kurek *et al.*, 2009] and up to 4°C cooler-than-modern T_{Jul} which lasted until ~15 cal ka BP based on a pollen-derived quantitative reconstruction using the MAT across eastern Beringia [Viau *et al.*, 2008].

Bølling/Allerød

The abrupt climate warming during the B/A (~14.7 to 13 cal ka BP) is well-recorded in the GISP2 ice-core record from central Greenland and matches the Trout Lake record (Fig. 4.6), where herbal taxa decline, whereas *Betula* and *Salix* percentages rise rapidly in the pollen record. We therefore infer a rapid change from herb-dominated alpine tundra to *Betula-Salix* shrub tundra and

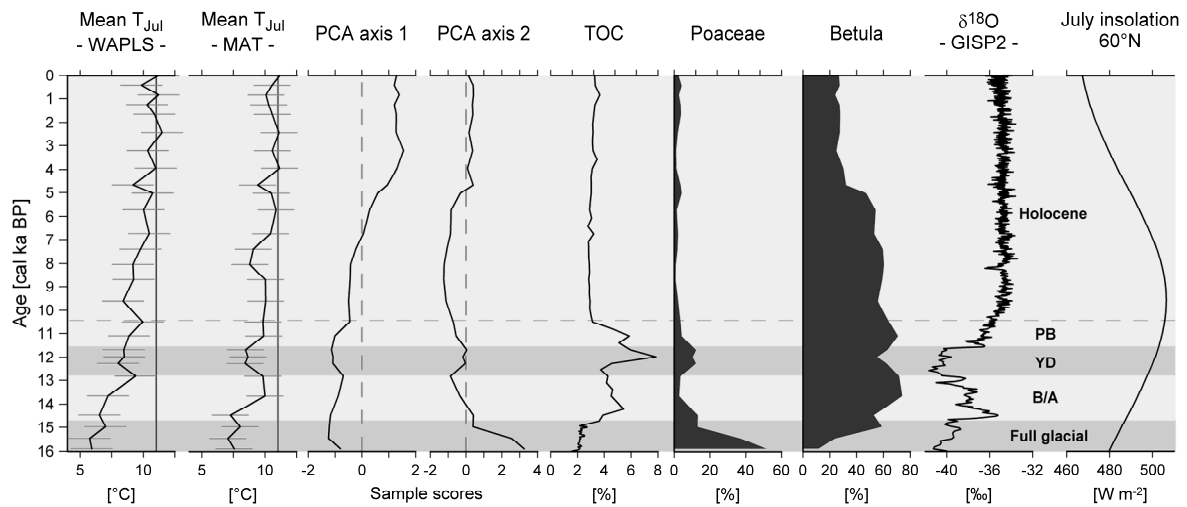


Figure 4.6: Summary plot of paleoclimate reconstructions, sample scores of principal component analysis (PCA), total organic carbon (TOC) of lake sediments, and selected pollen percentages (*Poaceae*, *Betula*) from Trout Lake compared with the oxygen isotope curve from GISP2 ice core (Greenland, 72°35'N, 38°28'W; Grootes and Stuiver, 1997) and mean summer insolation (July, 60°N; Laskar et al., 2004) of the last 16 cal ka BP. Reconstructed mean July air temperatures (T_{Jul}) are based on pollen using weighted averaging partial least squares regression (WAPLS) transfer function and the modern analogue technique (MAT). The root mean square errors of prediction (RMSEP: WAPLS $\pm 1.63^{\circ}\text{C}$; MAT $\pm 1.43^{\circ}\text{C}$) are shown as horizontal lines in the temperature reconstructions. Vertical lines represent modern mean July air temperature of 11.2°C at Shingle Point [Environment Canada, 2000].

increased vegetation coverage indicated by increasing pollen concentrations. High pollen concentrations between ~ 14 and 11 cal ka BP might also be related to a greater proximity of the coring site to the lake margin as a result of shallower water conditions and a smaller lake size.

T_{Jul} increased by about 3°C in east Beringia [Viau et al., 2008; Bunbury and Gajewski, 2009] most probably as a result of rising summer insolation, the retreating LIS front [Dyke and Prest, 1987; Dyke et al., 2002], and the still ~ 50 to 90 m lower (than present day) glacio-eustatic sea level of the Beaufort and Chukchi seas [Hill et al., 1985; Keigwin et al., 2006]. The LIS extent was probably still large enough to maintain an anticyclonic influence in east Beringia, especially under sustained split jet stream conditions [Bartlein, 1991], which, together with large exposed shelf areas and an almost permanent sea ice cover [Scott et al., 2009], support strong continentality effects. Similar to the Hanging Lake record [Kurek et al., 2009], T_{Jul} at Trout Lake rose during the B/A up to near-modern values, or are at least within the range of modern summer temperatures, taking into account a RMSEP of $\sim 1.5^{\circ}\text{C}$. Sediments show a concurrent increase in TOC content, probably due to increased vegetation cover in the catchment, low lake level, and dry climate conditions favoring organic matter preservation.

Younger Dryas

The temperature rise of the B/A interstadial at Trout Lake reverses abruptly at 12.9 cal ka BP (Fig. 4.6), which is coeval with the onset of the YD stadial in the GISP2 record [Grootes and Stuiver, 1997]. T_{Jul} dropped by about 1.5°C compared to the B/A interstadial and the subsequent Preboreal (PB) of the early Holocene and were roughly 2.5 to 3.0°C below modern conditions (Fig. 4.6). Cold- and dry-adapted non-arboreal pollen taxa (Poaceae, Ranunculaceae, *Rumex*, Asteraceae, *Artemisia*) briefly increase concurrently with a drop in pollen concentration mainly caused by a decreasing *Betula* input. A similar increase of *Artemisia*, which is indicative of a cold and dry climate, is documented during the YD in records from the southern Yukon [Cwynar, 1988; Bunbury and Gajewski, 2009]. Moreover, PCA sample scores of the first axis drop while those of the second axis rise during the YD. If we assume an explanatory potential of the first axis for moisture changes and a temperature signal expressed by variations along the second axis, it results in a significant YD cooling accompanied by dryer than modern conditions (Figs. 4.5 and 4.6).

Evidence for a YD stadial are known from lake sediments in southern and western Alaska [Engstrom *et al.*, 1990; Abbott *et al.*, 2000; Bigelow and Edwards, 2001; Hu *et al.*, 2002, 2006; Mann *et al.*, 2002] with the strongest impact on coastal sites close to the Pacific [Mikolajewicz *et al.*, 1997; Kokorowski *et al.*, 2008]. In addition, ice wedges [Meyer *et al.*, 2010] and fossil beetle assemblages [Elias, 2000] from northern Alaska have recorded a large-scale cooling of winter and summer temperatures, respectively, between 12.8 and 11.5 cal ka BP. In eastern Beringia, Viau *et al.* [2008] and Bunbury and Gajewski [2009] reconstructed a spatially-robust temperature decrease during the YD, whereas the Hanging Lake record does not show major temperature variations during the last 15 cal ka BP except for a neo-glacial cooling [Kurek *et al.*, 2009].

4.5.3 Environmental development since the early Holocene

(11.5 cal ka BP to present)

Early Holocene (thermal maximum?)

A summer insolation maximum during the early Holocene in combination with a further retreat of the LIS led to a warmer-than-modern period across the western Arctic known as the HTM, with maximum summer warmth in eastern Beringia between ca. 11 and 9 cal ka BP [Ritchie *et al.*, 1983; Kaufman *et al.*, 2004]. Pollen and plant macrofossil evidence (*Picea* and *Populus*) up to 75 to 100 km north of its present range indicate substantially warmer conditions than today [Cwynar, 1982; Ritchie, 1984; Nelson and Carter, 1987; Anderson, 1988; Vermaire and Cwynar, 2010]. Although *Populus* pollen occur briefly in the Trout Lake record, the early Holocene T_{Jul} reconstructed by both WAPLS and MAT approach modern values (within the range of error) but

do not exceed modern summer temperatures. A similar result emerges from *Viau et al.* [2008] for temperature reconstructions across eastern Beringia. However, if we assume that summer air temperature explains, to a certain degree, sample score variations for PCA axis 2, and that PCA axis 1 is related to moisture, we might be able to solve the issue of the missing HTM in the Trout Lake temperature record. Given that decreasing scores along axis 2 may point towards increasing temperatures, Trout Lake experienced maximum summer warmth after the YD termination until 8 cal ka BP, with slightly cooling [*Viau et al.*, 2008] but still warmer conditions until ~5 cal ka BP. Simultaneously, and as inferred from PCA axis 1, moisture availability probably remained low until ~8 cal ka BP as reported by *Pienitz et al.* [2000] for the central Yukon, and did not reach modern conditions before 5 to 4 cal ka BP [*Anderson et al.*, 2005; *Bunbury and Gajewski*, 2009]. We therefore infer that a moisture-limited spread of vegetation [*Cwynar*, 1988] dampened the reconstructed summer temperature signal and thereby obscured the Arctic-wide HTM in our pollen record.

Holocene moisture pattern and migration of key taxa (Picea, Alnus)

Continuously rising PCA sample scores of the first axis (Fig. 4.5b) indicate increasing moisture from the end of the YD until ~4.3 cal ka BP, and agree with rising *Alnus*, *Picea*, *Sphagnum*, *Ericaceae*, and *Isoetes* percentages. These taxa are positively correlated to PCA axis 1 and are known to reflect increased moisture [e.g. *Cwynar*, 1988; *Cwynar and Spear*, 1995; *Szeicz et al.*, 1995; *Lacourse and Gajewski*, 2000]. *Alnus-Betula* shrub tundra with wet heath communities (*Ericaceae*, *Cyperaceae*, *Sphagnum*) have covered the landscape around Trout Lake since ~5 cal ka BP (PZ 4, Fig. 4.4) indicating stable and near-modern moisture and temperature conditions on a millennial time scale. *Picea*, a frequently-studied example in terms of tree-line migration in the western Arctic, has been permanently present in the Yukon and the adjacent Northwest Territories (NWT) since ~9.5 ¹⁴C ka BP (~11 cal ka BP; e.g. *Ritchie*, 1984; *Wang and Geurts*, 1991; *Vermaire and Cwynar*, 2010). *Picea* has likely grown at a stable distance from Trout Lake since 9 cal ka BP but never in direct vicinity because *Picea* pollen percentages remain constantly low ($\leq 6\%$). *Picea* likely survived the LGM in eastern Beringia [*Brubaker et al.*, 2005], spread undirected, and arrived almost simultaneously in southwestern Alaska, the Yukon, and the Tuktoyaktuk Peninsula (NWT) [e.g. *Ritchie*, 1984; *Wang and Geurts*, 1991; *Brubaker et al.*, 2005]. Based on spatial analyses of pollen distribution patterns in east Beringia, *Brubaker et al.* [2005] concluded that low available moisture may have been responsible for the expansion lag of *Picea* during the HTM.

With a further lag of ~1000 years *Alnus* entered the northern Yukon by ~8 cal ka BP, as supported by the Hanging Lake pollen record [*Cwynar*, 1982], although its presence has been demonstrated in the southern Yukon since ~12 ¹⁴C ka BP [*Lacourse and Gajewski*, 2000] and *Alnus* likely survived the LGM in east Beringian refugia [*Brubaker et al.*, 2005]. *Alnus* is believed

to have been growing near Trout Lake by ~7 cal ka BP, and it has been the dominant pollen producer since ~5 cal ka BP. *Picea*, *Alnus*, and Ericaceae together with *Sphagnum* and *Isoetes* spores indicate substantially increasing moisture availability since the middle Holocene. Slowly-decreasing temperatures since the termination of the HTM [Ritchie, 1984; Kaufman *et al.*, 2004] may have led to paludification and a higher water table in response to increased permafrost aggradation that culminated in the middle Holocene [Cwynar and Spear, 1995; Vardy *et al.*, 1997]. Declining Beaufort Sea sea-ice coverage since ~9 cal ka BP [Schell *et al.*, 2008] in combination with a rising glacio-eustatic sea level approaching the modern coastline are likely to have favored enhanced moisture supply in summer to an area that became increasingly proximate to a moisture source, and thus evolved from a continental site during the late glacial and early Holocene into a maritime environment [Kaufman *et al.*, 2004]. Reconstructed T_{Jul} and PCA samples scores of second axis are relatively stable indicating that temperatures have been stable on a centennial to millennial timescale until today, with slightly decreasing temperatures between 7.0 and 4.5 cal ka BP as shown by PCA axis 2 (Fig. 4.6). This is consistent with decreasing summer insolation from 8 cal ka BP until present (Fig. 4.6).

4.6 Conclusions

Sedimentological and palynological studies together with multivariate statistics provide a detailed view on the sedimentation, vegetation, and temperature history from the northern Yukon Territory during the last ~16 cal ka BP. Using this approach, the following new findings could be derived:

1. As final deglaciation of the northwestern margin of the LIS commenced, the drainage diversion of the Babbage River caused spillovers of glacial meltwater to feed the bedrock basins close to the ice margin and initiated lake sedimentation in unglaciated northeastern Beringia.
2. Regional extralimital tree-line advances during the Holocene are reported in previous studies from northern Alaska and the Mackenzie Delta, but never reached the Trout Lake area.
3. Quantitative July air temperature reconstructions coincide with other paleoclimate records from Alaska and the Yukon and indicate a rapid climate warming by ~4°C, from cold full-glacial conditions towards the B/A interstadial, followed by a distinct YD stadial, which had not been reported for the northern Yukon so far.
4. Limited moisture availability in the northern Yukon during rising temperatures across the western Arctic in the early Holocene may have been responsible for a concealed HTM. A middle to late Holocene moisture increase throughout east Beringia with near-modern

temperatures supported the establishment of an extensive alder/birch shrub tundra north of the arctic tree line.

Acknowledgements

We thank the Parks Canada office (Ivvavik National Park) and the Aurora Research Institute – Aurora College (ARI) in Inuvik for administrative and logistical support. This study was partly funded by the German Science Foundation (DFG; Project No. LA 2399/3-1), the International Bureau of the German Federal Ministry of Education and Research (BMBF; Project No. CAN 08/A07, CAN 09/001), and by a doctoral fellowship awarded to M. Fritz by the German Federal Environmental Foundation (DBU). Analytical work at AWI received great help from C. Gebhardt, C. Funk, B. Plessen, H. Meyer, U. Bastian, A. Eulenburg, F. Günther, and J. Klemm. G. Müller and S. McLeod assisted in the field. We thank F. Kienast for plant identification and C. O'Connor for language revision.

5 Synthesis

The overarching aim of this thesis was to reconstruct the late Quaternary environmental dynamics along the easternmost margin of Beringia in northwest Canada using permafrost sequences, ground ice and lake sediments. Field studies have focused on three different sites (Fig. 1.1b):

- (1) Herschel Island in the southern Beaufort Sea is a push moraine located within the late Wisconsin glacial margin of the LIS and features glacial deposits, large bodies of tabular massive ground ice, ice wedges and ice-rich sediments.
- (2) Komakuk Beach is part of the YCP on the mainland coast and is located ~30 km beyond the limit of the LIS. This study site is representative for low-lying polygonal tundra with thick peat deposits, large Holocene ice-wedge systems and ice-wedge casts.
- (3) Trout Lake in the foothills of the British Mountains is ~40 km apart from the Beaufort Sea coast and only ~2 km beyond the LIS terminal limit. A number of environmental proxies obtained from a lake sediment core (~400 cm long) provide continuous paleoenvironmental information since the late Wisconsin.

Each of the above mentioned archives from three different locations contain distinct environmental proxy data with an archive-inherent spatial and temporal range for reconstruction. Working within and beyond the ultimate limit of the Wisconsin glaciation provided geographical coverage and regional representativity of environmental dynamics in order to reduce local bias. Furthermore, this study made it possible to compare spatially different stages in landscape dynamics in response to long-term climatic change and to elaborate dependencies amongst them. On the one hand, this thesis provides a qualitative perception of the landscape development of the YCP during the last ~16,000 years. It takes into account the influence of the glacial-deglacial history on depositional environments and on the buildup of massive ground-ice bodies as a particular element of ice-marginal permafrost regions. On the other hand, quantitative summer air temperature estimates based on pollen-temperature transfer functions provide new insights into the climate history of the northern Yukon close to the Beaufort Sea. Therefore, this study goes beyond a descriptive reconstruction of environmental change in easternmost Beringia since the last glacial–interglacial transition.

5.1 Main results in a Beringian context

5.1.1 Glacial chronology

Within this study, the youngest AMS radiocarbon age obtained from proglacially ice-thrust beds on Herschel Island, deposited directly above a massive ground-ice body, ranges between 16.8 and 15.6 cal ka BP (Poz-36441, chapter 2). The massive ice was assigned to have buried basal glacier ice origin (cf. chapter 3). The dating results suggest that glaciation occurred no earlier than 16.8 cal ka BP. This age, indeed, is conspicuously young but does not seem unlikely, given that a previous indication of Herschel Island deglacial age is based on a single date of a Yukon horse skull (*Equus lambei*, CMN 43815) with an age ranging from 19.6 to 18.9 cal ka BP (16.2 ± 0.15 ^{14}C ka; RIDDL-765) [Harington, 1989]. Other dates on allochthonous fossil vertebrates as young as 20.5-19.9 cal ka BP (17.1 ± 0.09 ^{14}C ka, Beta 185979) from Herschel Island coasts demonstrate that terrestrial mammals lived and died on the YCP (including the exposed shelf) and were incorporated into deposits that were later ice-thrust by a late Wisconsin advance of the LIS [Zazula *et al.*, 2009]. On the basis of dated postglacial lacustrine sediments and massive ground ice, Mackay and Dallimore [1992] suggested a short-lived regional ice advance to the Tuktoyaktuk Coastlands between ~17 to 15 cal ka BP. Taking these and other lines of evidence together, there is growing confirmation of a late Wisconsin maximum of the northwest LIS margin (see chapter 2). The existing chronology of the northwestern part of the LIS is still under debate, although it is essential for delineating the eastern margin of Beringia and for assessing the ice cap's climatic influence on east Beringian landscapes.

At the opposite margin of Beringia, the Barents-Kara Ice Sheet during MIS 2 did not reach the present-day mainland east of northern central Siberia, with the exception of the northwest margin of Taymyr Peninsula [Svendsen *et al.*, 1999, 2004] (Fig. 5.1). Model simulations indicate extremely low precipitation rates in the Kara Sea region [Siegert *et al.*, 2001]. Palynological records from the northern Taymyr Peninsula suggest annual precipitation was ~100 mm lower than today [Andreev *et al.*, 2003]. Consequently, pronounced aridity hampered the ice sheet growth in western Beringia during the LGM [Siegert *et al.*, 2001].

Regarding regional deglaciation, Trout Lake, located only slightly beyond the LIS limit, provides basal ages obtained from moss remains in coarse-grained debris overlying bedrock between 16.5 and 14.7 cal ka BP (Poz-36456, Poz-36445, Poz-36458, chapter 4). Proglacial meltwater input probably triggered rapid and coarse-grained sedimentation through a diversion of the Babbage River, which might have occasionally spilled over into the adjacent basins, and whose modern flow direction was blocked by the LIS. Dyke and Prest [1987] have inferred an



Figure 5.1: Map of northeast Asia and northwest North America showing the regions of western and eastern Beringia, the Bering land bridge, the adjacent seas and the exposed shelf areas during LGM sea level lowstand (-120 m). Modern coastline is white-rimmed. Light red striated area marks the extent of LGM glaciation. The extent of the Eurasian, the Laurentide, and the Cordilleran Ice Sheets as well as regional glaciations in Alaska are according to *Svendsen et al.* [2004], *Dyke et al.* [2003], and *Manley and Kaufman* [2002], respectively. Site numbers refer to lakes mentioned in the text and are keyed as follows: (1) Changeable Lake, (2) Lake Lama, (3) Lake Labaz, (4) Lake Taymyr, (5) Levinson-Lessing Lake, (6) Lake Billyakh, (7) Lake El'gygytgyn, (8) Zagoskin Lake, (9) Arolik Lake, (10) Kaiyak Lake, (11) Squirrel Lake, (12) Joe Lake, (13) Burial Lake, (14) Tukuto Lake, (15) Lake of the Pleistocene, (16) Ahaliarak Lake, (17) Antifreeze Pond, (18) Hanging Lake, (19) Trout Lake (this study).

asynchronous ice retreat for the northwest LIS margin that remained close to its limits until ~ 18 cal ka BP. This large-scale approximation is in good agreement with conclusions by *Murton et al.* [2007], based on combined AMS and luminescence chronologies, who showed that deglaciation of the Tuktoyaktuk Coastlands (western Canadian Arctic) had commenced by 14.3 cal ka BP and probably as early as ~ 16 cal ka BP.

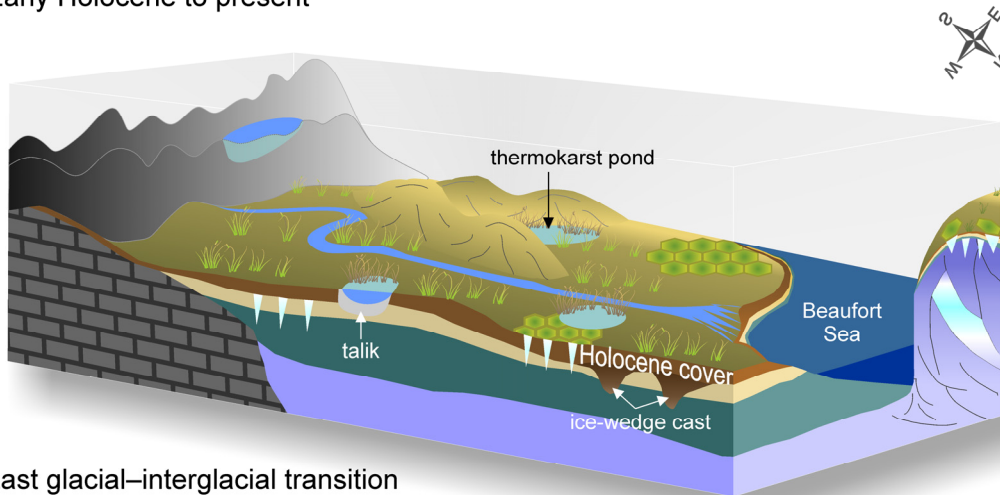
In westernmost Beringia, *Hubberten et al.* [2004] have presented manifold evidence for widespread climatic change around 15-13 ka BP that is consistent with the timing of general deglaciation and with the flooding of the Laptev Sea shelf [*Hubberten and Romanovskii*, 2001]. Major deglaciation of the Barents Sea shelf happened at this time, and the northwestern Taymyr Peninsula became rapidly ice-free (Fig. 5.1) [*Hubberten et al.*, 2004, and references therein].

5.1.2 Depositional environments

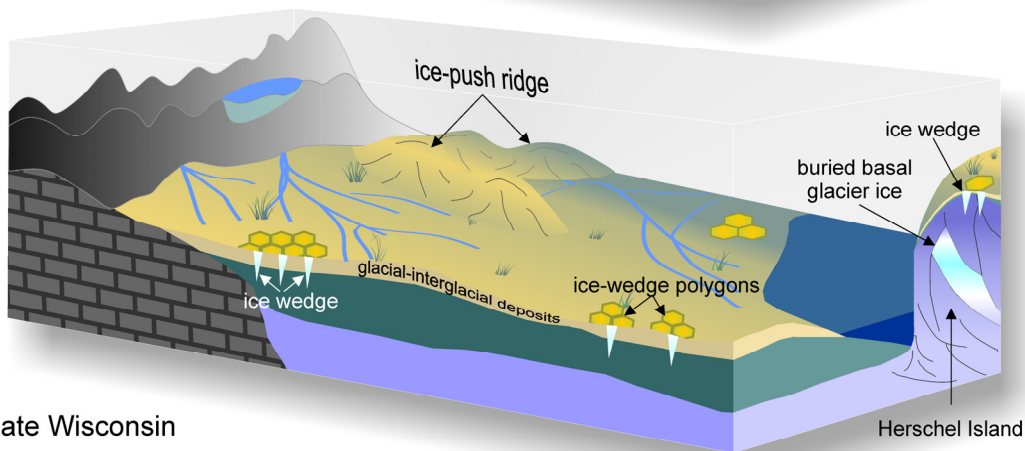
Late Wisconsin landscape development in the northern Yukon is strongly dependent on its glacial-deglacial history. Herschel Island is largely composed of proglacially ice-thrust sets of early to middle Wisconsin age and a relatively thin periglacial cover (Fig. 5.2). Terrestrial deposits of late Wisconsin age along the unglaciated YCP but concurrently close the LIS are poor in organic carbon and they do not exhibit a significant niveo-eolian sediment contribution. They rather have an alluvial and proluvial origin with meltwater contribution in very harsh and unfavorable conditions for life (chapter 2). The unglaciated Beringian landmass suffered sustained dryness until the Holocene [e.g. *Alfimov and Berman, 2001; Mann et al., 2002*], whereas ice-marginal zones benefited from large meltwater quantities of the waning ice sheets [e.g. *Mangerud et al. 2004*]. According to the results presented here, glacial meltwater started to feed lake basins and contributed to ground-ice development, either as massive ice or as non-massive intrasedimental ice (NMI) within ice-rich sediments (chapter 3).

The YCP does not exhibit Yedoma or muck deposits, which are typical for the Siberian lowlands [e.g. *Schirrmeister et al., 2011*], interior regions of Alaska [*Kanevskiy et al., 2011*] and the Yukon [e.g. *Fraser and Burn, 1997*], because of (i) the lack of large deflation areas due to the proximity of mountain ranges, (ii) a narrow continental shelf exposed [*Mathews, 1975*] while sea level was lowered and (iii) the predominance of cohesive tills in ablation zones [*Bateman and Murton, 2006*]. Therefore, depositional environments in coastal areas of Beringia are very different from inland sites during the LGM and late Wisconsin. This study shows that organic-rich sediments started to accumulate by ~11.2 cal ka BP on the lowlands of the YCP as a consequence of higher than modern air temperatures and increasing available moisture at the beginning of the Holocene; the latter not necessarily caused by increasing precipitation (chapters 2, 4). These results are consistent with an explosive peatland establishment between 11.5 and 9 ka BP in the Siberian lowlands [*Smith et al., 2004*] and as early as ~14.6 cal ka BP in central Alaska [*Mann et al., 2002*]. As detected on the YCP, melt-out of ice wedges and thermokarst lake development due to thaw subsidence promoted the establishment of ice-wedge casts filled with thaw lake deposits (chapter 2 and Fig. 5.2). Lake development stabilized on a high water level indicated by a homogeneous fine-grained sediment supply to Trout Lake (chapter 4). The limited peat thickness (~0.5 m) of middle to late Holocene age at Komakuk Beach is best explained by climate deterioration that led to reduced peat growth rates [e.g. *Vardy et al., 1997*], enhanced permafrost aggradation [e.g. *Eisner et al., 2005*] and resumed ice-wedge cracking [*Mackay, 1992*]. As the glacio-eustatic sea level approached modern conditions it led to extensive coastal erosion of ice-rich sediments and triggered coastal thermokarst in association with the exposure of massive ground-ice bodies on Herschel Island [*Lantuit and Pollard, 2005, 2008*].

Early Holocene to present



Last glacial–interglacial transition



Late Wisconsin

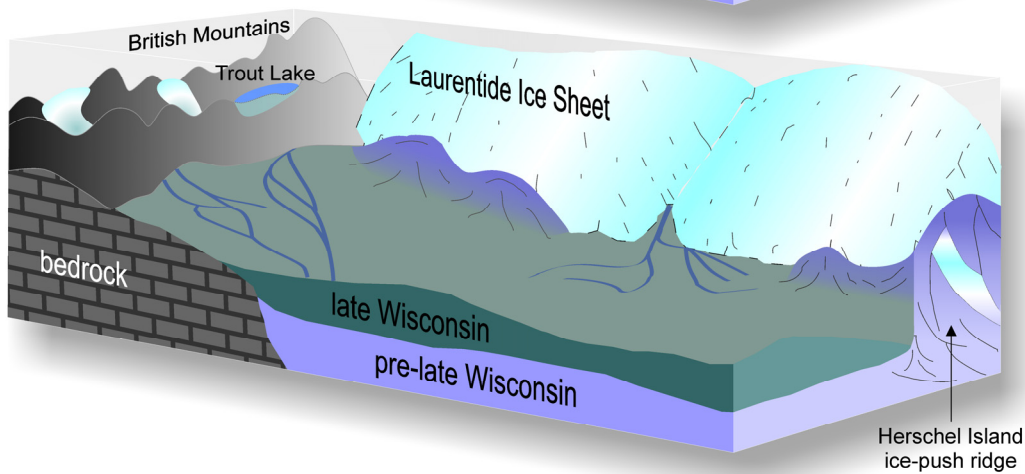


Figure 5.2: Schematic summary of the late Quaternary landscape evolution under glacial and periglacial conditions along the Yukon Coastal Plain. Note that the scheme does not follow a systematic scale.

5.1.3 Changes in hydrology and moisture

Although Beringia in its entirety is regarded as to have been a very dry subcontinent during glacial stages, coastal sites and ice-marginal areas may have experienced a significantly different

hydrological pattern. The YCP lacks topographic barriers for impounding proglacial lakes like the proglacial Lake Old Crow that occupied the Old Crow Flats until its final drainage about 18 cal ka BP [e.g. *Zazula et al.*, 2004]. Probably the YCP received a rather steady meltwater supply and a related delivery of fine material distal to the ice in combination with alluvial sediment supply from the northern foothills of the mountain ranges in the south, as concluded from the grain size composition and the paucity of organic material in late Wisconsin deposits (chapter 2 and Fig. 5.2). Decreasing meltwater supply in response to a receding ice margin during still harsh and dry climate conditions led to a decreasing sediment input during the last glacial–interglacial transition on the YCP (Fig. 5.2). Dry conditions and sustained low precipitation are also inferred from the palynological data from Trout Lake (chapter 4). This in turn might have favored permafrost aggradation in the study area, ice-wedge cracking and an increase in eolian sediment supply as indicated by higher sediment quantities in late Wisconsin ice wedges and a shift in grain size towards better-sorted silt-sized material (chapter 2, Fig. 2.4).

The onset of the Holocene thermal maximum (HTM) in east Beringia brought along wholesale changes in hydrology and atmospheric moisture availability. *Bartlein et al.* [1991, 1998] suggested that postglacial atmospheric circulation patterns in east Beringia were established by ~12 cal ka BP with a diminished influence of the remainder of the LIS. Tropospheric moisture content over east Beringia increased over the course of shoreline transgression, inundation of the Bering land bridge since ~13 cal ka BP [*Bradley and England*, 2008], and concurrently increasing summer insolation [*Kaufman et al.*, 2004]. However, the Trout Lake pollen record does not show a significant increase in precipitation or a vegetation response to it (chapter 4). It rather turns out that rising temperatures during the HTM led to extensive thermokarst and promoted changes in hydrology with higher water availability. Deep thaw together with thaw subsidence and standing water in thaw lakes favored the accumulation of lacustrine organic-rich deposits next to rapid peat growth on wet and plain surfaces (chapter 2).

A renewal of large-scale permafrost aggradation after the termination of the HTM led to extensive ice-wedge growth on the YCP [*Mackay*, 1992] and increasing precipitation [e.g. *Pienitz et al.*, 2000]; probably in winter, as the Aleutian Low intensified [*Anderson et al.*, 2005]. This together favored the establishment of a low-centered polygonal terrain on the mainland coast of the Yukon. Through the middle Holocene, low-centered polygons became high-centered due to the aggradation of segregated ice in polygon centers (chapter 2). Two-sided freezing with concurrent peat growth raised the polygon centers, improved their drainage towards the troughs and therefore led to reduced peat growth [e.g. *Vardy et al.*, 1997, 1998]. This was also supported by slightly decreasing air temperatures since the HTM termination [*Ritchie*, 1984].

5.1.4 Ground ice development and climatic implications

Three different types of ground ice (i.e. tabular massive ground ice, ice-wedge ice, and NMI) have been investigated within the scope of this study in order to reconstruct paleoenvironments in formerly ice-marginal areas since ground ice often comprises more than half of the near-surface permafrost volume in the western Canadian Arctic [e.g. *Mackay*, 1971]. The combination of stable water isotope analyses and hydrochemical investigations within the context of cryostratigraphic observations of host frozen deposits indicates that buried basal glacier ice contributes to the ground-ice inventory of Herschel Island (chapter 3). Strongly negative O-H isotope signatures ($\delta^{18}\text{O}$: -34 to -31 ‰) indicate a glacial origin of the water feeding the ice bodies (Figs. 3.4 and 5.3). Ice thrust and glaciotectonic deformation structures are similar to those from basal ice of contemporary glaciers or ice caps [e.g. *Knight*, 1997; *Murton et al.*, 2005]. Nevertheless, basal glacier ice and massive segregated ice might coexist in ice-marginal areas as emphasized by e.g. *French and Harry* [1990]. In addition to the dichotomy of buried glacier ice and massive segregated ice, another massive ground-ice type is observed within the late Wisconsin glacial limit. A pronounced freezing slope and ionic segregation demonstrate a postglacial freeze-through of proglacial ponds or lakes contributing to the local ground-ice inventory of Herschel Island and probably beyond (chapter 3).

Conspicuously, most relict massive ground-ice sites are located within the limits of Pleistocene glaciations, preserved in present-day permafrost [*Lacelle et al.*, 2009b]. Amongst other lines of evidence, their spatial distribution has led to the interpretation of a glacial ice (firnified or basal glacier ice) origin (West Siberia – *Astakhov and Isayeva*, 1988; *Ingólfsson and Lokrantz*, 2003, western Canadian Arctic – *Murton et al.*, 2005; *Lacelle et al.*, 2007, Canadian Arctic Archipelago – *Lorrain and Demeur*, 1985; *French and Harry*, 1988) or as having formed by segregation or intrusion during permafrost aggradation following deglaciation (northern Siberia – *Leibman et al.*, 2005, western Canadian Arctic – e.g. *Pollard and Dallimore*, 1988; *Lacelle et al.*, 2004). Large parts of the YCP may have been characterized by stagnant glacier ice and high pore water pressures in meltwater-saturated sediments, while the glacier front disintegrated. When permafrost re-aggrades beneath thinning stagnant basal ice, large amounts of meltwater are forced towards the freezing front forming large segregated ice bodies, which can occur close to buried basal glacier ice bodies, as observed in the western Canadian Arctic [*French and Harry*, 1990; *Rampton*, 1991].

Ice wedges from both sides of the late Wisconsin LIS limit serve as a palaeoenvironmental indicator of certain episodes of permafrost aggradation and basic winter temperature estimates, whereas ice-wedge casts, thaw unconformities, and truncated ice wedges have recorded permafrost degradation along the YCP (chapter 3). Low $\delta^{18}\text{O}$ and d -excess values of late Wisconsin ice

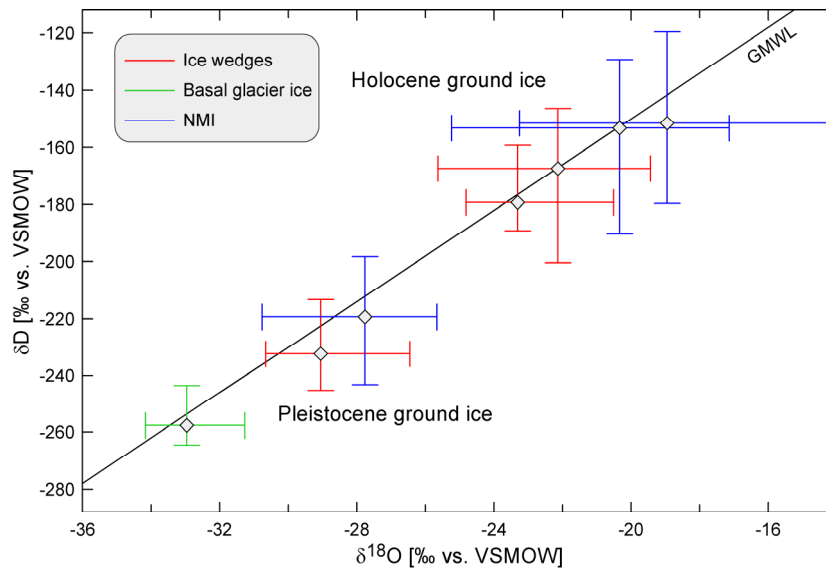


Figure 5.3: Summary $\delta\text{D}-\delta^{18}\text{O}$ diagram of ground ice sampled within and beyond the LIS limit. Ground-ice types comprise basal glacier ice, ice wedges and non-massive intrasedimental ice (NMI). Differentiation into Holocene and Pleistocene ground ice was supported by cryostratigraphic observations. GMWL: Global Meteoric Water Line.

wedges reflect greatly reduced winter temperatures and probably dryer conditions than those having occurred during formation of Holocene ice wedges (Figs. 2.9 and 5.3). Permafrost aggradation and extensive ice-wedge growth in the western Canadian Arctic probably resulted from the middle Holocene climate cooling, and locally ice wedges became recently renewed after a period of active layer deepening, which is undated so far (chapter 2). Isotope data from pre-Holocene ice wedges in east Beringia or at its margin are available from Herschel Island (Figs. 2.9 and 5.3) [Michel, 1990], Tuktoyaktuk Peninsula [Mackay, 1983], central Yukon [Burn *et al.*, 1986; Kotler and Burn, 2000], and from Barrow in Alaska [Meyer *et al.*, 2010]. They are characterized by $\delta^{18}\text{O}$ values between -31 and -26 ‰. A recent compilation of MIS 2 ice wedges by Wetterich *et al.* [2011] shows a similar range for west Beringia between the Taymyr Peninsula and the eastern Laptev Sea ($\delta^{18}\text{O}_{\text{mean}}$ between -31 and -26 ‰), except for Bol'shoy Lyakhovsky Island (East Siberian Sea, Fig. 5.1), where they indicate extremely cold winter temperatures ($\delta^{18}\text{O}_{\text{mean}}$: -37 ‰), probably accompanied by a different moisture source for winter precipitation.

A growing number of studies show that some relict ground-ice bodies in east Beringia have survived the HTM [e.g. Lacelle *et al.*, 2004, 2007] or even multiple glacial-interglacial cycles [e.g. Froese *et al.*, 2008] with summer temperatures several degrees Celsius warmer than the present-day [e.g. Kaufman *et al.*, 2004]. This knowledge adds to our understanding of the preservation of relict Pleistocene-age permafrost and its resilience to climate warming [e.g. Lacelle *et al.*, 2009b; Reyes *et al.*, 2010].

Hydrochemical considerations provide additional information on the water source of different types of ground ice. The Herschel Island NMI record reveals a prolonged contact of LIS meltwater with pre-glacial marine sediments enriched in chloride and potassium ions (chapter 3 and Fig. 5.4). Mixing, ion exchange processes, and debris incorporation produced a mixed hydrochemical signal within NMI and basal glacier ice. Besides a distinct isotope signature, late Wisconsin and Holocene ice wedges differ in their hydrochemical composition. Most conspicuous is a surplus in SO_4^{2-} within late Wisconsin ice wedges that cannot be explained by their larger amount of sediment inclusions, as even the NMI record does not show similar proportions of SO_4^{2-} (Fig. 5.4). One hypothesis is the incorporation of sulfate-rich ash particles from late Wisconsin Dawson tephra (~27 cal ka BP), although its northernmost range (i.e. a minimum range) is supposed to be several hundred kilometers south of the study area [Froese *et al.*, 2002]. A second possibility would be the increased transport of sea-salt-sulfur from the Arctic Ocean during periods of strong winds like the late Wisconsin, when Herschel Island was less than ~20 km inland [Fig. 2.1]. Both ways of SO_4^{2-}

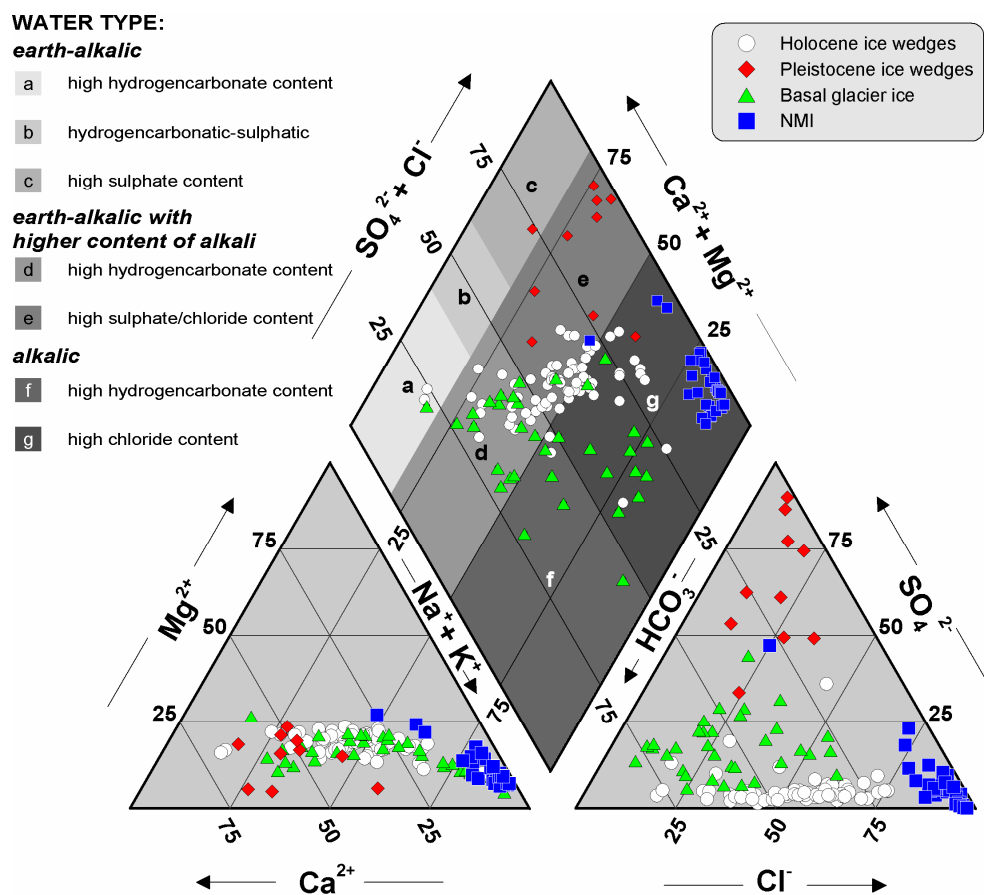


Figure 5.4: Piper plot [Piper, 1944] of major ion concentrations of different ground-ice types from Herschel Island. The two ternary plots show the percentage of the major cations and anions. The rhomb plot combines anion and cation concentrations and adds a water type classification [cf. Hölting and Coldewey, 2009]. Note that the non-massive intrasedimental ice (NMI) displays only samples below the Holocene thaw unconformity.

enrichment in ice wedges would probably not leave a significant imprint in the sedimentary record due to already high absolute sulfate contents in upthrust marine sediments (chapter 3, supplementary material).

5.1.5 Vegetation and temperature history

There is general acceptance that cold and dry conditions characterized MIS 2 environments throughout Beringia. In this study, fossil pollen assemblages from Trout Lake (chapter 4) suggest that a sparse and herb-dominated tundra dominated the landscape of ice-marginal east Beringia until ~14.7 cal ka BP with mean July air temperatures ~5°C colder than today. Numerous palynological studies across Beringia have reconstructed a graminoid-herb tundra during MIS 2 (ca. 26-16 cal ka BP). Cold- and dry-adapted taxa with minor admixtures of birch and willow dominated throughout west Beringia (Laptev Sea area, Fig. 5.1) [e.g. *Andreev et al.*, 2011], central Beringia (St. Michael Island, western Alaska) [*Ager*, 2003], central east Beringia (Kotzebue Sound area, northwestern Alaska) [e.g. *Anderson*, 1985, 1988], and in east Beringia (central Alaska and northern Yukon) [e.g. *Ritchie*, 1984; *Bigelow and Edwards*, 2001].

The pollen record from Trout Lake indicates rapid warming occurred in east Beringia during the Bølling/Allerød (B/A) interstadial with a vegetation that changed into a *Betula-Salix* shrub tundra together with herb communities. This is consistent with palynological evidence from west Beringia between ~16 and 12 cal ka BP that show a dominance of grass-sedge communities indicative of significantly warmer and moister conditions than during the full glacial [*Andreev et al.*, 2011]. Across the Bering land bridge and Alaska, tundra communities spread rapidly between ~17 and 15 cal ka BP [*Ager*, 2003] and were dominated by low shrubs, sedges, and mosses. In northwest Alaska, *Betula* increased ~17 cal ka BP and indicates the presence of a birch-dominated shrub tundra [*Anderson*, 1985]. Similar to modern temperatures have been suggested during the B/A interstadial in east Beringia by *Bunbury and Gajewski* [2009] and *Kurek et al.* [2009]. *Edwards and Barker* [1994] correlated the successive expansion of *Salix*, *Betula*, and *Populus* in northeastern Alaska between ~17 and 13 cal ka BP with the crossing of temperature thresholds that might be determined by the position of the LIS.

A distinct backfall from near-modern summer air temperatures during the B/A interstadial into dry and cold climate conditions, contemporaneous with the Younger Dryas stadial, is evident in the Trout Lake record by an increase in herb and grass pollen percentages on the expense of shrubs (chapter 4). The same event is probably preserved in capped ice wedges on Herschel Island featuring low $\delta^{18}\text{O}$ values indicative of cold winter temperatures and a low *d*-excess suggesting dry conditions and/or a different moisture source than during the Holocene (chapter 2). *Bigelow and Edwards* [2001] have suggested that after an abrupt shift to shrubby tundra at ~14 cal ka BP, herb

communities became re-established during the Younger Dryas as a result of climate deterioration in central east Beringia. Numerous pollen records from across southern Alaska generally indicate colder conditions during the Younger Dryas [Kokorowski *et al.*, 2008, and references therein]. The reconstructed shift in vegetation communities and the inferred summer temperatures, presented in chapter 4, highlight first evidence of a Younger Dryas stadial in the northern Yukon. So far, its prominence was thought to be restricted to sites closer to the North Pacific Ocean [Mathewes, 1993; Kokorowski *et al.*, 2008], where sites could respond more directly to decreasing sea surface temperatures that were triggered by teleconnections associated with the shutdown of the North Atlantic meridional overturning [e.g. Mikolajewicz *et al.*, 1997; Tarasov and Peltier, 2005].

Beringia experienced warmer summer temperatures than present during the HTM. Areas farthest from the ice sheets and ocean waters with their cooling effects experienced maximum warmth before other parts of the Arctic and began to warm around 11.5 cal ka BP in western Alaska [Kaufman *et al.*, 2004]. Summer climate was influenced by a strong positive insolation anomaly [Ritchie *et al.*, 1983]. *Alnus fruticosa*, *Betula nana*, Poaceae, and Cyperaceae dominate early Holocene pollen spectra in western Beringia and reconstructed air temperatures of the warmest month were up to 12°C and therefore ~4°C warmer than present [Andreev *et al.*, 2011]. Latitudinal range extensions of several invertebrate and plant taxa on the Arctic Coastal Plain of Alaska indicate summer temperatures increased by 2-3°C [Nelson and Carter, 1987; Elias, 2000]. *Picea glauca* was present on Seward Peninsula as early as ~9.5 cal ka BP [Wetterich *et al.*, submitted], spread along major river valleys at ~9 cal ka BP and slightly later at upland sites in the Brooks and Alaska ranges [Edwards and Barker, 1994] (Fig. 5.1). In northwest Canada, the tree line advanced ~75 km northward of its present-day limit [e.g. Ritchie, 1984] into the Tuktoyaktuk Coastlands and increased in elevation in the Mackenzie Mountains [Szeicz and MacDonald, 2001]. Elias [2001b] reconstructed a mean July air temperature 5.6°C warmer than modern on the basis of a small insect fauna assemblage (dated at ~12.8 cal ka BP) from the Yukon coast near the international border [Matthews, 1975]. However, this result remains puzzling, because the radiometric date is of Younger Dryas age and the corresponding pollen assemblage indicates cool conditions with an almost complete lack of shrubs in the sedge tundra with the exception of *Salix*. The Trout Lake pollen assemblage and the inferred July air temperatures during the early Holocene do not reveal a pronounced positive temperature anomaly (chapter 4). In contrast, permafrost sequences along the YCP exhibit thermokarst features like ice-wedge casts, deeply truncated ice wedges and other cryostructures, assigned to the early Holocene thaw unconformity (chapter 3) [cf. Burn *et al.*, 1986; Burn, 1997]. This dichotomy between clear evidence of warmer than modern temperatures and the largely missing response of vegetation communities might be explained by sustained dryness on well-drained sites. Summer precipitation was probably still low like in the southern Yukon [Anderson *et al.*, 2005] and evaporation rates increased in response to rising

summer temperatures. On lowlands, melting ground ice and waterlogging provided enough moisture for extensive peat growth and thaw-lake development (chapter 3), whereas upland sites like the Trout Lake area experienced sustained dry conditions (chapter 4).

An early mid-Holocene expansion of *Alnus crispa* and *Picea mariana* suggests the development of moister conditions, which have continued until present, although temporal patterns in the *Picea* treeline position during the Holocene are different across Beringia [Edwards and Barker, 1994]. In easternmost Beringia, Cwynar and Spear [1995] reconstructed a decline in *Picea glauca* between 6.5 and 6.0 cal ka BP as *Picea mariana* and *Alnus crispa* became the dominant tree species. The latter indicate increasing moisture, but probably not solely because of increased precipitation [Pienitz et al., 2000] but also in combination with rising water tables as the permafrost table rose subsequently to slowly decreasing summer temperatures (chapters 2 and 4) [Cwynar and Spear, 1995].

5.2 Potentials and limitations of the studied paleoenvironmental archives within and beyond the eastern Beringian edge

5.2.1 Permafrost and ground-ice archives

The general potential of permafrost archives includes its presence on spatial and temporal environmental gradients. This includes its circum-arctic distribution from the high Arctic to boreal zones and the local persistence of permafrost since the early Pleistocene until present in Beringia. Absolutely dated permafrost records were found to cover at least the last 200 ka in east Siberia [Schirrneister et al., 2002a; Hubberten et al., 2004] and up to 800 ka in Alaska [Froese et al., 2008]. Coastal permafrost cliffs like the ones studied within this thesis often naturally expose large cross sections through modern and ancient landscapes. Contrary to cores, which are highly localized records and often problematic when extrapolating horizons in inhomogeneous and ground ice-deformed permafrost sequences, coastal bluffs provide an opportunity to study the wider context of depositional environments and ground-ice features. Due to the relatively easy access to coasts and the recurring natural exposure of cliffs by thermo-abrasive wave action [Aré, 1988] they are convenient study objects for regional comparisons and the correlation of past environmental conditions. The spatial reconstruction of ancient landscapes is possible using detailed studies of kilometer-long coastal exposures.

Multidisciplinary approaches can be applied to permafrost sequences in order to comprehensively make use of the rich paleoenvironmental information stored in this frozen archive. Cryostratigraphical analysis describing both sediment and ice structures [Murton and French, 1994; French and Shur, 2010] allows the interpretation of freezing conditions, thaw

events, and local accumulation conditions. Ground ice within permafrost sequences can be studied and sampled simultaneously to the analysis of its host sediments (see chapter 5.2.2). The stratigraphy of permafrost sequences can be determined by lithostratigraphical classifications and geochronological results. Numerous sediment parameters can be determined to differentiate between horizons in individual exposures, for local and regional stratigraphic correlation as well as for the reconstruction of accumulation and transport conditions [e.g. *Schirrmeister et al.* 2002b, c, 2003; *Schwamborn et al.* 2002, 2008]. Age determinations, carried out by radiocarbon analyses on organic remains, isochron uranium–thorium disequilibria technique on peats [*Schirrmeister et al.*, 2002a], optically stimulated luminescence of periglacial structures [e.g. *Bateman*, 2008], and tephrochronology of volcanic ash layers [e.g. *Westgate et al.*, 1983, 1985; *Preece et al.*, 1992] can integrate paleoenvironmental results into the geological record. For paleoecological reconstructions, various fossil bioindicators can be studied, including pollen, plant macro-remains, insects, ostracods, testate amoebae, diatoms, chironomids, and mammal bones. Proxy–climate transfer functions provide the possibility for quantitative reconstructions of climate parameters such as air temperature and precipitation [e.g. *Birks*, 1998]. By combining these data sets, it is possible to derive a complex picture of climate, landscape and vegetation dynamics of the studied regions since the late Quaternary.

The main limitations of permafrost archives are the frequent lack of continuous sequences due to erosion or thermokarst [e.g. *Murton and Kolstrup*, 2003]. Local stratigraphies are sometimes difficult to correlate on a regional scale because of permafrost degradation or neotectonic influence on the accumulative/erosive environment in some regions [*Kienast et al.*, 2008]. As of yet, there are still uncertainties when comparing different geochronological methods. Some of them are related to unknown influences of permafrost processes on chemical and physical parameters important to the age determination technique [*L. Schirrmeister, personal communication*, 2011]. Due to cryoturbation processes and sometimes challenging sampling situations on near-vertical frozen exposures, the geochronological resolution in permafrost sequences is usually lower than in lacustrine sequences or ice cores.

This study has shown that the analyses of stable O-H isotopes in ground ice, its hydrochemical composition and cryostructures provide valuable information on past temperatures, hydrological conditions, freezing processes and on the water source feeding ice structures (chapters 2 and 3). For example, tabular massive ground-ice bodies identified as buried basal ice can help in delineating the spatial extent of glaciations in the Arctic; and if dated accurately, they could provide further evidence for the age of glaciation. Datasets on massive ground-ice bodies with consistent analytical treatment probably have the potential to enable analogue studies in areas of ambiguous glacial

chronology such as the New Siberian Islands (Fig. 5.1) or Banks Island (Canadian Arctic Archipelago).

Ice wedges from west Beringia have been frequently used to characterize climate and environmental conditions during the late Pleistocene and the Holocene, especially to derive overview temperature trends [e.g. *Vasil'chuk and Vasil'chuk*, 1997, 1998; *Meyer et al.*, 2002a, b; *Opel et al.*, 2011]. However, the derivation of continuous time series to link climate information from ice wedges to the geological record has proved to be problematic because of sometimes inconsistent AMS dating results [e.g. *Opel et al.*, 2011]. The assumption of a continuously increasing age of individual frost cracks from the ice-wedge center towards its edges [*Lachenbruch*, 1962] is complicated by the occurrence of temporal as well as geometrical irregular frost cracking [*Mackay*, 1974, 1992]. Despite the mentioned limitations, they have the potential to serve as an important climate archive, as was recently shown by stable-isotope records of the Younger Dryas cold period in Barrow, northern Alaska [*Meyer et al.*, 2010]. Further efforts should strive for using stable water isotopes in ice wedges as temperature and moisture proxies in regions without current glaciation. This approach should be accompanied by involving the Global Network of Isotopes in Precipitation (GNIP) hosted by the International Atomic Energy Agency (IAEA) that provides modern climate information related to stable O-H isotopes in order to derive isotope-temperature transfer functions as the basis for reconstructing absolute (past) winter temperatures.

Studying the water cycle is a precondition for the interpretation of the NMI isotope record, since NMI formed in the active layer consists of refrozen soil water, which is a mixture of summer and winter precipitation, surface waters, and last winter's ice [*Schwamborn et al.* 2006]. Several atmospheric and terrestrial sources of H₂O collected year-round could help to generate a set of end members in order to enable mixing calculations of the relative proportions of water types that contribute to permafrost ice. Furthermore, isotope fractionation during freezing must be considered for NMI that takes place when soil water turns slowly into ice [*Michel*, 1982]. In that case the heavy isotopes crystallize first and thus become depleted in the remaining liquid phase. Repeated seasonal freeze and thaw adds numerous cycles of phase change and mixes the isotopic composition in the active layer. Fractionation during slow freezing should also be noticeable in the *d*-excess, because freezing occurs along a slope different from the global meteoric water line (GMWL) (i.e. much lower than 8). A shift in the *d*-excess is, however, not solely dependent on kinetic fractionation during freezing but could be related to several other processes determining the initial *d*-excess of the water involved, such as (1) a change in the moisture source, (2) different proportions of winter and summer precipitation, (3) different humidity in the area of precipitation, or (4) a variable amount of recycled water [*Schwamborn et al.*, 2006].

5.2.2 Lake sediment archives

Lake sediments provide the only continuous records of environmental change across Beringia. Environmental proxies contained in lake sediments are eligible for quantitative climate reconstructions, so that most terrestrial absolute temperature inferences are derived from lacustrine archives. Despite the ubiquity of lakes from a circum-arctic perspective, very few ancient lakes exist that have survived as permanently water-filled basins throughout several glacial–interglacial cycles. Lakes in Beringia were particularly prone to dry-out. Hitherto, only nine lakes in Alaska have been reported with records that are of LGM age or older (Fig. 5.1): Ahaliorak [Eisner and Colinveaux, 1990], Arolik [Kaufman *et al.*, 2003], Burial [Abbott *et al.*, 2010], Joe [Anderson, 1988; Anderson *et al.*, 1994], Kaiyak [Anderson, 1985], Lake of the Pleistocene [Mann *et al.*, 2002], Tukuto [Oswald *et al.*, 1999], Squirrel [Anderson, 1985; Berger and Anderson, 1994], and Zagoskin [Ager, 2003].

Comparably old lake records in west Beringia (Fig. 5.1) are known from the wider Taymyr area (Lake Lama – Hahne and Melles, 1997, Lake Labaz – Andreev *et al.*, 2002, Lake Taymyr – Andreev *et al.*, 2003, Levinson-Lessing Lake – Ebel *et al.*, 1999), from Severnaya Zemlya (Changeable Lake – Raab *et al.*, 2003), and the Verkhoyansk Mountains (Lake Billyakh – Müller *et al.*, 2010). Although obvious for the most simple reason but still noteworthy because of the archive's age, Beringia (as devoid of ice) hosts the oldest lake in the Arctic. The El'gygytgyn crater lake (Fig. 5.1), located in eastern central Beringia (Chukotka), is one of the most promising paleoclimate archives of the northern hemisphere. Based on preliminary paleomagnetic dating results, the lake sediment record extends back through the whole Quaternary into the Pliocene [Melles *et al.*, 2011] and thus through most of the life and times of the Bering land bridge.

Accurate absolute age control is essential for interpreting paleoenvironmental findings. However, chronologies developed from radiocarbon dates of bulk sediments in Arctic lakes are often problematic because of low bioproductivity rates [Abbott and Stafford, 1996] and the high potential for preservation of organic matter that might become frequently reworked [Nelson *et al.*, 1988]. In northwest Canada, Hanging Lake [Cwynar, 1982] and Antifreeze Pond [Rampton, 1971] (Fig. 5.1) were believed to contain sediments as old as ~34 cal ka BP, based on conventional bulk-sediment radiocarbon dates. However, based on new AMS radiocarbon chronologies, their records have been recently revised to be significantly briefer, with ~17 ka for Hanging Lake [Kurek *et al.*, 2009] and with ~19 ka for Antifreeze Pond [Vermaire and Cwynar, 2010]. Moreover, data from arctic lake systems often suffer low temporal resolution due to low sedimentation rates. Northerly sites tend to have, on average, lower sedimentation rates than temperate sites (Webb and Webb, 1988; Edwards and Whittington, 2001). It is expected to observe higher sediment accumulation

rates in shallow and nutrient-rich lake systems with a larger catchment area to lake area ratio [Brothers *et al.*, 2008].

Trout Lake has demonstrated its ability to provide paleoenvironmental information since the late Wisconsin with centennial resolution (chapter 4). It records changes in sedimentation history in vicinity to the LIS and enables the reconstruction of vegetation communities as well as temperature changes inferred from its fossil pollen record. Finally, it turns out that lacustrine records in the easternmost part of Beringia do not exceed timescales beyond the LGM (Fig. 2.1, Table 2.1). It is therefore recommended to conduct complementary permafrost studies from a paleoenvironmental perspective.

5.3 Outlook

This thesis has shown that a combined approach of studying different paleoenvironmental archives and proxy data at multiple sites provides an encompassing view of environmental changes in the western Canadian Arctic since the late Wisconsin and enabled the comparison of landscape and climate evolution within and beyond the eastern margin of Beringia. The paleoenvironmental implications presented herein are valid on millennial to sub-millennial time scales, however short-term climate fluctuations (annual to centennial) probably remain obscured and represent one perspective of further environmental reconstructions. High-resolution climate reconstructions should be extended to thermokarst lakes and to deposits from peatlands, as these are rapidly accumulating archives and they are widespread on the Arctic coastal plain. Furthermore, they usually contain numerous ecological proxies for absolute temperature and precipitation reconstruction such as fossil pollen, plant macrofossils, chironomids, and /or ostracods. The onset and progression of Holocene thermokarst, the development of thermokarst lakes and peatlands, and the sequestration of organic carbon under consideration of a time-transgressive warming in the Arctic are still poorly understood. Evaluating the processes and spatial-temporal trends of thermokarst development in the western Arctic will have to take into account the shift of Pleistocene to Holocene climate modes with regard to atmospheric circulation patterns that modify hydrological conditions and determine available moisture, regional sea level history, and permafrost dynamics. Terrestrial paleoenvironmental studies complemented by investigations of near-shore marine archives could help answering the question of which response mechanisms are predominant in the coastal zone. This approach would add knowledge about climate-related coastal thermokarst amplitudes and about the release of organic matter into the sea. High-resolution archives that enable to resolve decadal climate variations especially would help to better constrain the periodicity and magnitude of future changes along the coast.

Today, many environmental reconstructions focus on paleoecological proxy data. These studies have provided benchmark datasets on past summer temperatures, precipitation, and the succession of habitats. Knowledge of paleo-winter temperature magnitudes and of the pathways of moisture transport is, however, largely unavailable. Besides ice caps, ice wedges have shown their potential for winter paleothermometry [*Nikolayev and Mikhalev, 1995*] as they are mainly fed by winter snowmelt and they are largely unaffected by secondary fractionation [*Michel, 1982*]. Transfer functions derived from stable water isotopes in wedge ice and modern precipitation monitoring programmes, together with emerging dating methods of small particulate and dissolved carbon quantities in the ice, would foster climate reconstructions in Beringian environments. However, accurate dating in permafrost terrain is still challenging [cf. *Murton et al., 1998*] for reasons that are related to the occurrence of frequent freeze and thaw (i.e. cryoturbation), thermokarst and thermoerosion, cryogenic weathering, and ground-ice aggradation. Advances in absolute dating techniques should take into account the specific physical and chemical processes in permafrost archives. Concerning radiocarbon dating, these processes are for instance low bioproductivity, long residence times of carbon in terrestrial landscapes, and microbial activity even below 0°C. In terms of luminescence age determinations, polar night has an influence on zeroing the luminescence signal and inhomogeneous ground-ice aggradation around individual soil particles probably attenuates radiation during nuclear decay.

In spite of its relevance to the various fields of polar research, the modeling of permafrost dynamics has remained the domain of individuals and small groups of scientists and hence has attracted little attention for a direct interaction between the permafrost and climate modeling community. Future directions in modeling permafrost response to climate change projections should consider the interaction between permafrost, snow cover, vegetation and other environmental factors at various timescales. Recent modeling advances include the incorporation of permafrost directly within global circulation models (GCMs) [*Riseborough et al., 2008*] and face the challenge of considering the final direction of feedback mechanisms to permafrost behavior in response to environmental change.

Finally, further knowledge of the northern Yukon environmental history is of special public interest since Ivvavik National Park of Canada, Vuntut National Park of Canada, and Herschel Island (Qikiqtaruk) Territorial Park are together designated to become Canada's next UNESCO World Heritage Site.

6 Bibliography

- Abbott, M.B., Edwards, M.E., Finney, B.P., 2010. A 40,000-yr record of environmental change from Burial Lake in Northwest Alaska. *Quaternary Research* **74**, 156-165.
- Abbott, M.B., Finney, B.P., Edwards, M.E., Kelts, K.R., 2000. Lake-level reconstruction and paleohydrology of Birch Lake, central Alaska, based on seismic reflection profiles and core transects. *Quaternary Research* **53**, 154-166.
- Abbott, M.B., Stafford Jr, T.W., 1996. Radiocarbon geochemistry of modern and ancient Arctic lake systems, Baffin Island, Canada. *Quaternary Research* **45**, 300-311.
- ACIA, 2004. Impacts of a warming Arctic: Arctic Climate Impact Assessment. Cambridge University Press, Cambridge, 146p.
- Ager, T.A., 2003. Late Quaternary vegetation and climate history of the central Bering land bridge from St. Michael Island, western Alaska. *Quaternary Research* **60**, 19-32.
- Alfimov, A.V., Berman, D.I., 2001. Beringian climate during the Late Pleistocene and Holocene. *Quaternary Science Reviews* **20**, 127-134.
- Anderson, L., Abbott, M.B., Finney, B.P., Edwards, M.E., 2005. Palaeohydrology of the Southwest Yukon Territory, Canada, based on multiproxy analyses of lake sediment cores from a depth transect. *The Holocene* **15**, 1172-1183.
- Anderson, P.M., 1985. Late quaternary vegetational change in the Kotzebue Sound area, northwestern Alaska. *Quaternary Research* **24**, 307-321.
- Anderson, P.M., 1988. Late quaternary pollen records from the Kobuk and Noatak river drainages, northwestern Alaska. *Quaternary Research* **29**, 263-276.
- Anderson, P.M., Bartlein, P.J., Brubaker, L.B., 1994. Late Quaternary history of tundra vegetation in Northwestern Alaska. *Quaternary Research* **41**, 306-315.
- Anderson, P.M., Lozhkin, A.V., 2001. The Stage 3 interstadial complex (Karginskii/middle Wisconsinan interval) of Beringia: variations in paleoenvironments and implications for paleoclimatic interpretations. *Quaternary Science Reviews* **20**, 93-125.
- Andreev, A.A., Schirrmeister, L., Tarasov, P.E., Ganopolski, A., Brovkin, V., Siebert, C., Wetterich, S., Hubberten, H.-W., 2011. Vegetation and climate history in the Laptev Sea region (Arctic Siberia) during Late Quaternary inferred from pollen records. *Quaternary Science Reviews* **30**, 2182-2199.
- Andreev, A.A., Siebert, C., Klimanov, V.A., Derevyagin, A.Y., Shilova, G.N., Melles, M., 2002. Late Pleistocene and Holocene vegetation and climate on the Taymyr lowland, northern Siberia. *Quaternary Research* **57**, 138-150.
- Andreev, A.A., Tarasov, P.E., Siebert, Ch., Ebel, T., Klimanov, V.A., Melles, M., Bobrov, A.A., Dereviagin, A.Yu., Lubinski, D.J., Hubberten, H.-W., 2003. Late Pleistocene and Holocene vegetation and climate on the northern Taymyr Peninsula, Arctic Russia. *Boreas* **32**, 484-505.
- Aré, F.E., 1988. Thermal abrasion of sea coast (parts I and II). *Polar Geography and Geology* **12**, 1-157.
- Astakhov, V.I., Isayeva, L.L., 1988. The "Ice Hill": An example of 'retarded deglaciation' in Siberia. *Quaternary Science Reviews* **7**, 29-40.
- Ayles, G.B., Snow, N.B., 2002. Canadian Beaufort Sea 2000: the environmental and social setting. *Arctic* **55** (suppl. 1), 4-17.
- Barendregt, R.W., Duk-Rodkin, A., 2004. Chronology and extent of Late Cenozoic ice sheets in North America: A magnetostratigraphic assessment, in: Ehlers, J., Gibbard, P.L. (Eds.), *Quaternary Glaciations - Extent and Chronology, Part II: North America*. Elsevier, Amsterdam, pp.1-7.
- Bartlein, P.J., Anderson, K.H., Anderson, P.M., Edwards, M.E., Mock, C.J., Thompson, R.S., Webb, R.S., Webb, T., Whitlock, C., 1998. Paleoclimate simulations for North America over the past 21,000 years: features of the simulated climate and comparisons with paleo-environmental data. *Quaternary Science Reviews* **17**, 549-585.
- Bartlein, P.J., Anderson, P.M., Edwards, M.E., McDowell, P.F., 1991. A framework for interpreting paleoclimatic variations in Eastern Beringia. *Quaternary International* **10-12**, 73-83.
- Bateman, M.D., 2008. Luminescence dating of periglacial sediments and structures. *Boreas* **37**, 574-588.
- Bateman, M.D., Murton, J.B., 2006. Late Pleistocene glacial and periglacial aeolian activity

- in the Tuktoyaktuk Coastlands, NWT, Canada. *Quaternary Science Reviews* **25**, 2552-2568.
- Beget, J.E., 2001. Continuous Late Quaternary proxy climate records from loess in Beringia. *Quaternary Science Reviews* **20**, 499-507.
- Berger, G.W., Anderson, P.M., 1994. Thermoluminescence dating of an Arctic lake core from Alaska. *Quaternary Science Reviews* **13**, 497-501.
- Beug, H.-J., 2004. Leitfaden der Pollenbestimmung für Mitteleuropa und angrenzende Gebiete. Dr. Friedrich Pfeil Verlag, Munich, 542p. (in German).
- Bigelow, N.H., Edwards, M.E., 2001. A 14,000 yr paleoenvironmental record from Windmill Lake, Central Alaska: Lateglacial and Holocene vegetation in the Alaska range. *Quaternary Science Reviews* **20**, 203-215.
- Birks, H.J.B., 1998. Numerical tools in palaeolimnology – Progress, potentialities, and problems. *Journal of Paleolimnology* **20**, 307-332.
- Black, R.F., 1964. Gubik Formation of Quaternary age in northern Alaska. U.S. Geological Survey Professional Paper 302-C, pp.59-91.
- Bouchard, M., 1974. Géologie des dépôts meubles de l'île Herschel, territoire du Yukon. M.Sc. (maitrise) thesis. Université de Montréal, 70p. (in French).
- Bradley, R.S., 1999. Paleoclimatology. Reconstructing climates of the Quaternary. 2nd edition. Academic Press, San Diego, 613p.
- Bradley, R.S., England, J.H., 2008. The Younger Dryas and the sea of ancient ice. *Quaternary Research* **70**, 1-10.
- Brezgunov, V.S., Derevyagin, A.Y., Chizhov, A.B., 2001. Using natural stable hydrogen and oxygen isotope for studying the conditions of ground ice formation. *Water Resources* **28**, 604-608.
- Brigham-Grette, J., 2001. New perspectives on Beringian Quaternary paleogeography, stratigraphy, and glacial history. *Quaternary Science Reviews* **20**, 15-24.
- Brigham-Grette, J., Gualtieri, L., 2004. Response to Grosswald and Hughes (2004), Brigham-Grette et al. (2003). "Chlorine-36 and ¹⁴C chronology support a limited last glacial maximum across central Chukotka, northeastern Siberia, and no Beringian ice sheet," and, Gualtieri et al. (2003), "Pleistocene raised marine deposits on Wrangel Island, northeastern Siberia: implications for Arctic ice sheet history". *Quaternary Research* **62**, 227-232.
- Brigham-Grette, J., Gualtieri, L.M., Glushkova, O.Y., Hamilton, T.D., Mostoller, D., Kotov, A., 2003. Chlorine-36 and ¹⁴C chronology support a limited last glacial maximum across central Chukotka, northeastern Siberia, and no Beringian ice sheet. *Quaternary Research* **59**, 386-398.
- Brigham-Grette, J., Hopkins, D.M., 1995. Emergent marine record and paleoclimate of the last interglaciation along the northwest Alaskan coast. *Quaternary Research* **43**, 159.
- Brigham-Grette, J., Hopkins, D.M., Ivanov, V.F., Basilyan, A.E., Benson, S.L., Heiser, P.A., Pushkar, V.S., 2001. Last interglacial (isotope stage 5) glacial and sea-level history of coastal Chukotka Peninsula and St. Lawrence Island, Western Beringia. *Quaternary Science Reviews* **20**, 419-436.
- Brigham-Grette, J., Lozhkin, A.V., Anderson, P.M., Glushkova, O.Y., 2004. Paleoenvironmental conditions in Western Beringia before and during the Last Glacial Maximum, in: Madsen, D.B. (Ed.), Entering America: Northeast Asia and Beringia before the Last Glacial Maximum. University of Utah Press, Salt Lake City, pp.29-61.
- Briner, J.P., Kaufman, D.S., Werner, A., Caffee, M., Levy, L., Manley, W.F., Kaplan, M.R., Finkel, R.C., 2002. Glacier readvance during the late glacial (Younger Dryas?) in the Ahklun Mountains, southwestern Alaska. *Geology* **30**, 679-682.
- Brothers, S., Vermaire, J., Gregory-Eaves, I., 2008. Empirical models for describing recent sedimentation rates in lakes distributed across broad spatial scales. *Journal of Paleolimnology* **40**, 1003-1019.
- Brown, J., O.J. Ferrians Jr., J.A. Heginbottom, and E.S. Melnikov. 1998. revised February 2001. Circum-Arctic map of permafrost and ground-ice conditions. Boulder, CO: National Snow and Ice Data Center/World Data Center for Glaciology.
- Brubaker, L. B., Anderson, P. M., Edwards, M. E., Lozhkin, A. V., 2005. Beringia as a glacial refugium for boreal trees and shrubs: New perspectives from mapped pollen data. *Journal of Biogeography* **32**, 833-848.
- Brubaker, L.B., Anderson, P.M., Hu, F.S., 2001. Vegetation ecotone dynamics in southwest Alaska during the Late Quaternary. *Quaternary Science Reviews* **20**, 175-188.
- Bunbury, J., Gajewski, K., 2009. Postglacial climates inferred from a lake at treeline, southwest Yukon Territory, Canada. *Quaternary Science Reviews* **28**, 354-369.

- Burgess, M.M., Smith, S.L., 2003. 17 years of thaw penetration and surface settlement observations in permafrost terrain along the Norman Wells pipeline, Northwest Territories, Canada, *in*: Phillips, M., Springman, S.M., Arenson, L.U. (Eds.), Eighth International Conference on Permafrost. Balkema, Zürich, Switzerland, 21-25 July 2003, pp.107-112.
- Burn, C.R., 1997. Cryostratigraphy, paleogeography, and climate change during the early Holocene warm interval, western Arctic coast, Canada. *Canadian Journal of Earth Sciences* **34**, 912-925.
- Burn, C.R., Michel, F.A., Smith, M.W., 1986. Stratigraphic, isotopic, and mineralogical evidence for an early Holocene thaw unconformity at Mayo, Yukon Territory. *Canadian Journal of Earth Sciences* **23**, 794-801.
- CAPE – Last Interglacial Project Members, 2006. Last Interglacial Arctic warmth confirms polar amplification of climate change. *Quaternary Science Reviews* **25**, 1383-1400.
- Cardyn, R., Clark, I.D., Lacelle, D., Lauriol, B., Zdanowicz, C., Calmels, F., 2007. Molar gas ratios of air entrapped in ice: A new tool to determine the nature and origin of relict massive ground ice bodies in permafrost. *Quaternary Research* **68**, 239-248.
- Carter, L.D., 1981. A Pleistocene sand sea on the Alaskan Arctic Coastal Plain. *Science* **211**, 381-383.
- Carter, L.D., 1983. Fossil sand wedges on the Alaskan Arctic Coastal Plain and their paleoenvironmental significance. Proceedings of the Fourth International Conference on Permafrost, 17-22 July 1983, Fairbanks, USA. National Academy Press, Washington D.C., pp.109-114.
- Chen, J.H., Curran, A.H., White, B., Wasserberg, G.J., 1991. Precise chronology of the last interglacial period: 234U-238Th data from fossil coral reefs in the Bahamas. *Geological Society of America Bulletin* **103**, 82-97.
- Clark, I.D., Lauriol, B., 1997. Aufeis of the Firth River basin, Northern Yukon insights to permafrost hydrogeology and karst. *Arctic and Alpine Research* **29**, 240-252.
- Cohen, A.S., 2003. Paleolimnology: The history and evolution of lake systems. Oxford University Press, New York, 500p.
- Craig, H., 1961. Isotopic variations in meteoric waters. *Science* **133**, 1702-1703.
- Cwynar, L.C., 1982. A Late-Quaternary vegetation history from Hanging Lake, northern Yukon. *Ecological Monographs* **52**, 1-24.
- Cwynar, L.C., 1988. Late Quaternary vegetation history of Kettlehole Pond, southwestern Yukon. *Canadian Journal of Forest Research* **18**, 1270-1279.
- Cwynar, L.C., Spear, R.W., 1995. Paleovegetation and paleoclimatic changes in the Yukon at 6 ka BP. *Géographie physique et Quaternaire* **49**, 29-35.
- Dallimore, S.R., Wolfe, S.A., Matthews, J.V. Jr., Vincent, J.-S., 1997. Mid-Wisconsinan eolian deposits of the Kittigazuit Formation, Tuktoyaktuk Coastlands, Northwest Territories, Canada. *Canadian Journal of Earth Sciences* **34**, 1421-1441.
- Dansgaard, W., 1964. Stable isotopes in precipitation, *Tellus* **16**, 436-468.
- Dansgaard, W., Tauber, H., 1969. Glacier oxygen-18 content and Pleistocene ocean temperatures. *Science* **166**, 499-502.
- Delorme, L.D., 1968. Pleistocene freshwater ostracoda from Yukon, Canada. *Canadian Journal of Zoology* **46**, 859-876.
- Delorme, L.D., Zoltai, S.C., Kalas, L.L., 1977. Freshwater shelled invertebrate indicators of paleoclimate in northwestern Canada during late glacial times. *Canadian Journal of Earth Sciences* **14**, 2029-2046.
- Dinter, D.A., Carter, D.L., Brigham-Grette, J., 1990. Late Cenozoic geological evolution of the Alaskan North Slope and adjacent continental shelves, *in*: Grantz, A., Johnson, L., Sweeney, J.F. (Eds.), The Arctic Ocean Region, The Geology of North America. Geological Society of America, Boulder, pp.459-490.
- Dredge, L.A., Thorleifson, L.H., 1987. The middle Wisconsinan history of the Laurentide Ice Sheet. *Géographie physique et Quaternaire* **41**, 215-235.
- Duk-Rodkin, A., Barendregt, R.W., Froese, D.G., Weber, F., Enkin, R., Smith, I., Zazula, G.D., Waters, P., Klassen, R., 2004. Timing and extent of Plio-Pleistocene glaciations in northwestern Canada and east-central Alaska. *in*: Ehlers, J., Gibbard, P.L. (Eds.), Quaternary Glaciations - Extent and Chronology, Part II: North America. Elsevier, Amsterdam, pp.313-345.
- Duk-Rodkin, A., Barendregt, R.W., Tarnocai, C., Phillips, F.M., 1996. Late Tertiary to late Quaternary record in the Mackenzie Mountains, Northwest Territories, Canada: Stratigraphy,

- paleosols, paleomagnetism and chlorine-36. *Canadian Journal of Earth Sciences* **33**, 875–895.
- Duk-Rodkin, A., Hughes, O.L., 1994. Tertiary-quaternary drainage of the pre-glacial Mackenzie basin. *Quaternary International* **22-23**, 221-241.
- Duk-Rodkin, A., Hughes, O.L., 1995. Quaternary geology of the northwest part of the central Mackenzie Valley corridor, Northwest Territories. *Geological Survey of Canada Bulletin* **458**, 45p.
- Dyke, A.S., Andrews, J.T., Clark, P.U., England, J.H., Miller, G.H., Shaw, J., Veillette, J.J., 2002. The Laurentide and Innuitian ice sheets during the Last Glacial Maximum. *Quaternary Science Reviews* **21**, 9-31.
- Dyke, A.S., Moore, A., Robertson, L., 2003. Deglaciation of North America, Geological Survey of Canada Open File 1574.
- Dyke, A.S., Prest, V.K., 1987. Late Wisconsinan and Holocene history of the Laurentide Ice Sheet. *Géographie Physique et Quaternaire* **41**, 237-263.
- Ebel, T., Melles, M., Niessen, F., 1999. Laminated sediments from Levinson-Lessing Lake, northern central Siberia—a 30,000 years record of environmental history? *in*: Kassens, H., Bauch, H.A., Dmitrenko, I.A., Eicken, H., Hubberten, H.W., Melles, M., Thiede, J., Timokhov, L.A. (Eds.), Land–ocean systems in the Siberian Arctic: Dynamics and history. Springer, Berlin, pp.425-435.
- Edwards, K.J., Whittington, G., 2001. Lake sediments, erosion and landscape change during the Holocene in Britain and Ireland. *Catena* **42**, 143-173.
- Edwards, M.E., Barker Jr, E.D., 1994. Climate and vegetation in northeastern Alaska 18,000 yr B.P.-present. *Palaeogeography, Palaeoclimatology, Palaeoecology* **109**, 127-135.
- Eisner, W.R., 1991. Palynological analysis of a peat core from Innavait Creek, the North Slope, Alaska. *Arctic* **44**, 279-282.
- Eisner, W.R., Bockheim, J.G., Hinkel, K.M., Brown, T.A., Nelson, F.E., Peterson, K.M., Jones, B.M., 2005. Paleoenvironmental analyses of an organic deposit from an erosional landscape remnant, Arctic Coastal Plain of Alaska. *Palaeogeography, Palaeoclimatology, Palaeoecology* **217**, 187-204.
- Eisner, W.R., Colinvaux, P.A., 1990. A long pollen record from Ahaliarak Lake, Arctic Alaska. *Review of Palaeobotany and Palynology* **63**, 35-52.
- Eisner, W.R., Hinkel, K.M., Bockheim, J.G., Nelson, F.E., 2003. Late-Quaternary paleoenvironmental record from a palsa-scale frost mound in arctic Alaska. Proceedings of the Eighth International Conference on Permafrost, 21-25 July 2003, Zürich, Switzerland. A.A. Balkema Publishers, Lisse, pp.229-234.
- Elias, S.A., 2000. Late Pleistocene climates of Beringia, based on analysis of fossil beetles. *Quaternary Research* **53**, 229-235.
- Elias, S.A., 2001a. Beringian paleoecology: results from the 1997 workshop. *Quaternary Science Reviews* **20**, 7-13.
- Elias, S.A., 2001b. Mutual climatic range reconstructions of seasonal temperatures based on Late-Pleistocene fossil beetle assemblages in Eastern Beringia. *Quaternary Science Reviews* **20**, 77-91.
- Elias, S.A., Brigham-Grette, J., 2007. Late Pleistocene events in Beringia, *in*: Elias, S.A. (Ed.), Encyclopedia of Quaternary Science, Elsevier, Oxford, pp.1057-1066.
- Elias, S.A., Short, S.K., Birks, H.H., 1997. Late Wisconsin environments of the Bering Land Bridge. *Palaeogeography, Palaeoclimatology, Palaeoecology* **136**, 293-308.
- Elias, S.A., Short, S.K., Nelson, C.H., Birks, H.H., 1996. Life and times of the Bering land bridge. *Nature* **382**, 60.
- England, J.H., Furze, M.F.A., Douppé, J.P., 2009. Revision of the NW Laurentide Ice Sheet: Implications for paleoclimate, the northeast extremity of Beringia, and Arctic Ocean sedimentation. *Quaternary Science Reviews* **28**, 1573-1596.
- Engstrom, D.R., Fritz, S.C., Almendinger, J.E., Juggins, S., 2000. Chemical and biological trends during lake evolution in recently deglaciated terrain. *Nature* **408**, 161-166.
- Engstrom, D.R., Hansen, B.C.S., Wright, H.E., Jr., 1990. A possible Younger Dryas record in southeastern Alaska. *Science* **250**, 1383-1385.
- Environment Canada, 2000. <http://climate.weatheroffice.ec.gc.ca>. (accessed June 2011).
- Fægri, K., Iversen, J., 1989. Textbook of pollen analysis. The Blackwell Press, New Jersey, 328p.
- Fairbanks, R.G., 1989. A 17,000-year glacio-eustatic sea level record: Influence of glacial melting rates on the Younger Dryas event and deep-ocean circulation. *Nature* **342**, 637-642.
- Fitzpatrick, J.J., Alley, R.B., Brigham-Grette, J., Miller, G.H., Polyak, L., White, J.W.C., 2010.

- Arctic paleoclimate synthesis thematic papers. *Quaternary Science Reviews* **29**, 1674-1678.
- Forbes, D.L. (editor). 2011. State of the Arctic Coast 2010 – Scientific Review and Outlook. International Arctic Science Committee, Land-Ocean Interactions in the Coastal Zone, Arctic Monitoring and Assessment Programme, International Permafrost Association. Helmholtz-Zentrum Geesthacht, Geesthacht, Germany, 178 p., [<http://arcticcoasts.org>]
- Fraser, T.A., Burn, C.R., 1997. On the nature and origin of "muck" deposits in the Klondike area, Yukon Territory. *Canadian Journal of Earth Sciences* **34**, 1333-1344.
- French, H.M., 1998. An appraisal of cryostratigraphy in north-west Arctic Canada. *Permafrost and Periglacial Processes* **9**, 297-312.
- French, H.M., 2007. The periglacial environment, 3rd ed. Longman, Harlow, 341p.
- French, H.M., Harry, D.G., 1988. Nature and origin of ground ice, Sandhills Moraine, southwest Banks Island, Western Canadian Arctic. *Journal of Quaternary Science* **3**, 19-30.
- French, H.M., Harry, D.G., 1990. Observations on buried glacier ice and massive segregated ice, western Arctic coast, Canada. *Permafrost and Periglacial Processes* **1**, 31-43.
- French, H.M., Harry, D.G., 1992. Pediments and cold-climate conditions, Barn Mountains, unglaciated northern Yukon, Canada. *Gegrafiska Annaler, Series A, Physical Geography* **74**, 145-157.
- French, H., Shur, Y., 2010. The principles of cryostratigraphy. *Earth-Science Reviews* **101**, 190-206.
- Fritz, M., Wetterich, S., Meyer, H., Schirrmeister, L., Lantuit, H., Pollard, W.H., 2011. Origin and characteristics of massive ground ice on Herschel Island (western Canadian Arctic) as revealed by stable water isotope and hydrochemical signatures. *Permafrost and Periglacial Processes* **22**, 26-38.
- Fritz, M., Herzschuh, U., Wetterich, S., Lantuit, H., De Pascale, G.P., Pollard, W.H., Schirrmeister, L., (*under review*). Late glacial and Holocene sedimentation, vegetation, and temperature history from easternmost Beringia (Northern Yukon Territory, Canada). *Quaternary Research*.
- Fritz, M., Wetterich, S., Schirrmeister, L., Meyer, H., Lantuit, H., Preusser F., Pollard, W.H., (*under review*). At the eastern Beringian edge: Late Wisconsinan and Holocene landscape dynamics along the Yukon Coastal Plain, Canada. *Palaeogeography, Palaeoclimatology, Palaeoecology*.
- Froese, D.G., Westgate, J.A., Preece, S.J., Storer, J., 2002. Age and significance of the Late Pleistocene Dawson tephra in eastern Beringia. *Quaternary Science Reviews* **21**, 2137-2142.
- Froese, D.G., Westgate, J.A., Reyes, A.V., Enkin, R.J., Preece, S.J., 2008. Ancient permafrost and a future, warmer Arctic. *Science* **321**, 1648.
- Gat, J.R., 1996. Oxygen and hydrogen isotopes in the hydrologic cycle. *Annual Review of Earth and Planetary Sciences* **24**, 225-262.
- Grimm, E.C., 1991. TILIA and TILIAGRAPH Software. Illinois State Museum, Springfield.
- Grimm, E.C., 2000. North American Pollen Database. IGBP PAGES/World Data Centre for Paleoclimatology. NOAA/NGDC Paleoclimatology Program, Boulder, USA, <http://www.ngdc.noaa.gov/paleo/pollen.html> (accessed June 2011).
- Groottes, P.M., Stuiver, M., 1997. Oxygen 18/16 variability in Greenland snow and ice with 10⁻³- to 10⁻⁵-year time resolution. *Journal of Geophysical Research* **102**, 26455-26470.
- Guthrie, R.D., 1968. Paleoecology of the large mammal community in interior Alaska during the late Pleistocene. *American Midland Naturalist* **79**, 346-363.
- Guthrie, R.D., 2001. Origin and causes of the mammoth steppe: a story of cloud cover, woolly mammal tooth pits, buckles, and inside-out Beringia. *Quaternary Science Reviews* **20**, 549-574.
- Hahne, J., Melles, M., 1997. Late- and post-glacial vegetation and climate history of the southwestern Taymyr Peninsula, central Siberia, as revealed by pollen analysis of a core from Lake Lama. *Vegetation History and Archaeobotany* **6**, 1-8.
- Hamilton, T.D., Ashley, G.M., 1993. Epiguruk: A late Quaternary environmental record from northwestern Alaska. *Geological Society of America Bulletin* **105**, 583-602.
- Hamilton, T.D., Ashley, G.M., Reed, K.M., Schweger, C.E., 1993. Late Pleistocene vertebrates and other fossils from Epiguruk, Northwestern Alaska. *Quaternary Research* **39**, 381-389.
- Harington, C.R., 1989. Pleistocene vertebrate localities in the Yukon, in: Carter, L.D., Hamilton, T.D., Galloway, J.P., (Eds.), Late Cenozoic history of the interior basins of Alaska

- and the Yukon. U.S. Geological Survey Circular 1026, pp.93-98.
- Harris, S.A., 1989. Landforms and ground ice as evidence of the source of H₂O in permafrost. *Progress in Physical Geography* **13**, 367-390.
- Harry, D.G., French, H.M., Pollard, W.H., 1985. Ice wedges and permafrost conditions near King Point, Beaufort Sea coast. Yukon Territory, Geological Survey of Canada, Paper 85-1A, pp.111-116.
- Harry, D.G., French, H.M., Pollard, W.H., 1988. Massive ice and ice-cored terrain near Sabine Point, Yukon Coastal Plain. *Canadian Journal of Earth Sciences* **25**, 1846-1856.
- Hill, P.R., Mudie, P.J., Moran, K., Blasco, S.M., 1985. A sea-level curve for the Canadian Beaufort Shelf. *Canadian Journal of Earth Sciences* **22**, 1383-1393.
- Hölting, B., Coldewey, W.G., 2009. Hydrologie – Einführung in die allgemeine und angewandte Hydrogeologie. Spektrum, Heidelberg, 384p. (in German).
- Hooke, R.L., Clausen, H.B., 1982. Wisconsin and Holocene $\delta^{18}\text{O}$ variations, Barnes Ice Cap, Canada. *Geological Society of America Bulletin* **93**, 784-789.
- Hopkins, D.M., 1967. The Bering Land Bridge. Stanford University Press, Stanford, California, 495p.
- Hopkins, D.M., 1982. Aspects of the paleogeography of Beringia during the Late Pleistocene, in: Hopkins, D.M., Matthews, J.V. Jr, Schweger, Ch.E., Young, S.B. (Eds.), *Paleoecology of Beringia*. Academic Press, New York, pp.3-28.
- Hopkins, D.M., Matthews Jr, J.V., Schweger, C.E., Young, S.B., 1982. *Paleoecology of Beringia*. Academic Press, New York, 489p.
- Horita, J., Ueda, A., Mizukami, K., Takaton, I., 1989. Automatic δD and $\delta^{18}\text{O}$ analyses of multi-water samples using H₂- and CO₂-water equilibration methods with a common equilibration set-up. *Applied Radiation and Isotopes* **40**, 801-805.
- Hu, F.S., Lee, B.Y., Kaufman, D.S., Yoneji, S., Nelson, D.M., Henne, P.D., 2002. Response of tundra ecosystem in southwestern Alaska to Younger-Dryas climatic oscillation. *Global Change Biology* **8**, 1156-1163.
- Hu, F.S., Nelson, D.M., Clarke, G.H., Rühland, K.M., Huang, Y., Kaufman, D.S., Smol, J.P., 2006. Abrupt climatic events during the last glacial-interglacial transition in Alaska. *Geophysical Research Letters* **33**, L18708.
- Hubberten, H.-W., Andreev, A., Astakhov, V.I., Demidov, I., Dowdeswell, J.A., Henriksen, M., Hjort, C., Houmark-Nielsen, M., Jakobsson, M., Kuzmina, S., Larsen, E., Lunkka, J.P., Lyså, A., Mangerud, J., Möller, P., Saarnisto, M., Schirmer, L., Sher, A.V., Siegert, C., Siegert, M.J., Svendsen, J.I., 2004. The periglacial climate and environment in northern Eurasia during the Last Glaciation. *Quaternary Science Reviews* **23**, 1333-1357.
- Hubberten, H.-W., Romanovskii, N.N., 2001. Terrestrial and offshore permafrost evolution of the Laptev Sea region during the last Pleistocene–Holocene glacial-eustatic cycle. In: Paepe, R., Melnikov, V. (Eds.), *Permafrost response on economic development, environmental security and natural resources*. Proceedings of the NATO-ARW, Novosibirsk. Kluwer, Dordrecht, 1998, pp.43-60.
- Hughes, O., 1972. Surficial geology of northern Yukon Territory and northwestern District of Mackenzie, Northwest Territories, Geological Survey of Canada, Paper 69-36. Map 1319 A.
- Hultén, E., 1937. Outline of the history of Arctic and boreal biota during the Quaternary period. Bokförlags Aktiebolaget Thule, Stockholm, 168p.
- IAEA (International Atomic Energy Agency), 2006. Isotope Hydrology Information System. The ISOHIS Database. <http://www.iaea.org/water>. (accessed January 2011)
- Ingólfsson, Ó., Lokrantz, H., 2003. Massive ground ice body of glacial origin at Yugorski Peninsula, arctic Russia. *Permafrost and Periglacial Processes* **14**, 199-215.
- Inman, D.L., 1952. Measures for describing the size distribution of sediments. *Journal of Sedimentary Petrology* **22**, 125-145.
- IPCC, 2007. Climate Change 2007: The physical science basis. Contribution of Working Group I to the Fourth Assessment Report of the Intergovernmental Panel on Climate Change. Cambridge University Press, Cambridge.
- Jakobsson, M., Macnab, R., Mayer, L., Anderson, R., Edwards, M., Hatzky, J., Schenke, H.W., Johnson, P., 2008. An improved bathymetric portrayal of the Arctic Ocean: Implications for ocean modeling and geological, geophysical and oceanographic analyses. *Geophysical Research Letters* **35**, L07602.
- Jansen, E., Sjøholm, J., 1991. Reconstruction of glaciation over the past 6 Myr from ice-borne

- deposits in the Norwegian Sea. *Nature* **349**, 600-603.
- Jouzel, J., Souchez, R., 1982. Melting and refreezing at the glacier sole and the isotopic composition of the ice. *Journal of Glaciology* **28**, 35-42.
- Juggins, S., 2003. C2 User Guide. Software for ecological and palaeoecological data analysis and visualisation. University of Newcastle, Newcastle upon Tyne, UK.
- Kanevskiy, M., Shur, Y., Fortier, D., Jorgenson, M.T., Stephani, E., 2011. Cryostratigraphy of late Pleistocene syngenetic permafrost (yedoma) in northern Alaska, Itkillik River exposure. *Quaternary Research* **75**, 584-596.
- Kaplina, T.N., 1981. Permafrost history of north Yakutia during late Cenozoic time. Nauka, Moscow, pp.153-181 (in Russian).
- Kaplanskaya, F.A., Tarnogradskiy, V.D., 1986. Remnants of the Pleistocene ice sheets in the permafrost zone as an object for paleoglaciological research. *Polar Geography* **10**, 257-266.
- Kaufman, D.S., Ager, T.A., Anderson, N.J., Anderson, P.M., Andrews, J.T., Bartlein, P.J., Brubaker, L.B., Coats, L.L., Cwynar, L.C., Duvall, M.L., Dyke, A.S., Edwards, M.E., Eisner, W.R., Gajewski, K., Geirsdottir, A., Hu, F.S., Jennings, A.E., Kaplan, M.R., Kerwin, M.W., Lozhkin, A.V., MacDonald, G.M., Miller, G.H., Mock, C.J., Oswald, W.W., Otto-Bliesner, B.L., Porinchu, D.F., Rühland, K., Smol, J.P., Steig, E.J., Wolfe, B.B., 2004. Holocene thermal maximum in the western Arctic (0–180°W). *Quaternary Science Reviews* **23**, 529-560.
- Kaufman, D.S., Manley, W.F., 2004. Pleistocene Maximum and Late Wisconsinan glacier extents across Alaska, U.S.A., in: Ehlers, J., Gibbard, P.L. (Eds.), *Quaternary Glaciations - Extent and Chronology, Part II: North America*. Elsevier, Amsterdam, pp.9-27.
- Kaufman, D.S., Sheng Hu, F., Briner, J.P., Werner, A., Finney, B.P., Gregory-Eaves, I., 2003. A ~33,000 year record of environmental change from Arolik Lake, Ahklun Mountains, Alaska, USA. *Journal of Paleolimnology* **30**, 343-361.
- Keigwin, L., Donnelly, J.P., Cook, M.S., Driscoll, N.W., Brigham-Grette, J., 2006. Rapid sea-level rise and Holocene climate in the Chukchi Sea. *Geology* **34**, 861-864.
- Kennedy, K.E., Froese, D.G., Zazula, G.D., Lauriol, B., 2010. Last Glacial Maximum age for the northwest Laurentide maximum from the Eagle River spillway and delta complex, northern Yukon. *Quaternary Science Reviews* **29**, 1288-1300.
- Kienast, F., Tarasov, P., Schirmermeister, L., Grosse, G., Andreev, A.A., 2008. Continental climate in the East Siberian Arctic during the last interglacial: Implications from palaeobotanical records. *Global and Planetary Change* **60**, 535-562.
- Kienast, F., Wetterich, S., Kuzmina, S., Schirmermeister, L., Andreev, A.A., Tarasov, P., Nazarova, L., Kossler, A., Frolova, L., Kunitsky, V.V., 2011. Paleontological records indicate the occurrence of open woodlands in a dry inland climate at the present-day Arctic coast in western Beringia during the Last Interglacial. *Quaternary Science Reviews* **30**, 2134-2159.
- Knight, P.G., Patterson, C.J., Waller, R.I., Jones, A.P., Robinson, Z.P., 2000. Preservation of basal-ice sediment texture in ice-sheet moraines. *Quaternary Science Reviews* **19**, 1255-1258.
- Knight, P.G., 1997. The basal ice layer of glaciers and ice sheets. *Quaternary Science Reviews* **16**, 975-993.
- Kokelj, S.V., Burn, C.R., 2005. Geochemistry of the active layer and near-surface permafrost, Mackenzie delta region, Northwest Territories, Canada. *Canadian Journal of Earth Sciences* **42**, 37-48.
- Kokelj, S.V., Smith, C.A.S., Burn, C.R., 2002. Physical and chemical characteristics of the active layer and permafrost, Herschel Island, western Arctic coast, Canada. *Permafrost and Periglacial Processes* **13**, 171-185.
- Kokorowski, H.D., Anderson, P.M., Mock, C.J., Lozhkin, A.V., 2008. A re-evaluation and spatial analysis of evidence for a Younger Dryas climatic reversal in Beringia. *Quaternary Science Reviews* **27**, 1710-1722.
- Kotler, E., Burn, C.R., 2000. Cryostratigraphy of the Klondike "muck" deposits, west-central Yukon Territory. *Canadian Journal of Earth Sciences* **37**, 849-861.
- Kurek, J., Cwynar, L.C., Vermaire, J.C., 2009. A late Quaternary paleotemperature record from Hanging Lake, northern Yukon Territory, eastern Beringia. *Quaternary Research* **72**, 246-257.
- Kuzmina, S., Lister, A.M., Edwards, M.E., 2011. Andrei Sher and Quaternary science. *Quaternary Science Reviews* **30**, 2039-2048.
- Lacelle, D., 2011. On the $\delta^{18}\text{O}$, δD and D-excess relations in meteoric precipitation and during equilibrium freezing: theoretical approach and

- field examples. *Permafrost and Periglacial Processes* **22**, 13-25.
- Lacelle, D., Bjornson, J., Lauriol, B., Clark, I.D., Troutet, Y., 2004. Segregated-intrusive ice of subglacial meltwater origin in retrogressive thaw flow headwalls, Richardson Mountains, NWT, Canada. *Quaternary Science Reviews* **23**, 681-696.
- Lacelle, D., Lauriol, B., Clark, I.D., Cardyn, R., Zdanowicz, C., 2007. Nature and origin of a Pleistocene-age massive ground-ice body exposed in the Chapman Lake moraine complex, central Yukon Territory, Canada. *Quaternary Research* **68**, 249-260.
- Lacelle, D., Lauriol, B., Clark, I.D., 2009a. Formation of seasonal ice bodies and associated cryogenic carbonates in Caverne de l'Ours, Quebec, Canada: Kinetic isotope effects and pseudobiogenic crystal structures. *Journal of Cave and Karst Studies* **71**, 48-62.
- Lacelle, D., St-Jean, M., Lauriol, B., Clark, I.D., Lewkowicz, A., Froese, D.G., Kuehn, S.C., Zazula, G., 2009b. Burial and preservation of a 30,000 year old perennial snowbank in Red Creek valley, Ogilvie Mountains, central Yukon, Canada. *Quaternary Science Reviews* **28**, 3401-3413.
- Lachenbruch, A.H., 1962. Mechanics of thermal contraction cracks and ice-wedge polygons in permafrost. Special Geol. Soc. of Am. Papers 70. New York, 69p.
- Lachenbruch, A.H., Marshall, B.V., 1986. Changing climate: Geothermal evidence from permafrost in the Alaskan Arctic. *Science* **234**, 689-696.
- Lacourse, T., Gajewski, K., 2000. Late Quaternary vegetation history of Sulphur Lake, Southwest Yukon Territory, Canada. *Arctic* **63**, 27-35.
- Lambeck, K., Esat, T.M., Potter, E.-K., 2002. Links between climate and sea levels for the past three million years. *Nature* **419**, 199-206.
- Lantuit, H., Pollard, W.H., 2005. Temporal stereophotogrammetric analysis of retrogressive thaw slumps on Herschel Island, Yukon Territory. *Natural Hazards and Earth System Science* **5**, 413-423.
- Lantuit, H., Pollard, W.H., 2008. Fifty years of coastal erosion and retrogressive thaw slump activity on Herschel Island, southern Beaufort Sea, Yukon Territory, Canada. *Geomorphology* **95**, 84-102.
- Lantuit, H., Pollard, W.H., Couture, N., Fritz, M., Schirmer, L., Meyer, H., Hubberten, H.-W. (under review) Modern and Late Holocene retrogressive thaw slump activity on the Yukon Coastal Plain and Herschel Island, Yukon Territory, Canada. *Permafrost and Periglacial Processes*.
- Laskar, J., Robutel, P., Joutel, F., Gastineau, M., Correia, A.C.M., Levrard, B., 2004. A long-term numerical solution for the insolation quantities of the Earth. *Astronomy and Astrophysics* **428**, 261-285.
- Lauriol, B., Cabana, Y., Cinq-Mars, J., Geurts, M.-A., Grimm, F.W., 2002. Cliff-top eolian deposits and associated molluscan assemblages as indicators of Late Pleistocene and Holocene environments in Beringia. *Quaternary International* **87**, 59-79.
- Leibman, M.O., Arkhipov, S.M., Perednya, D.D., Savvichev, A.S., Vanshtein, B.G., Hubberten, H.-W., 2005. Geochemical properties of the water-snow-ice complexes in the area of Shokalsky glacier, Novaya Zemlya, in relation to tabular ground-ice formation. *Annals of Glaciology* **42**, 249-254.
- Lepš, J., Šmilauer, P., 2003. Multivariate analysis of ecological data using CANOCO. Cambridge University Press, Cambridge, 269p.
- Lorrain, R.D., Demeur, P., 1985. Isotopic evidence for relic Pleistocene glacier ice on Victoria Island, Canadian Arctic Archipelago. *Arctic and Alpine Research* **17**, 89-98.
- Mackay, J.R., 1959. Glacier ice-thrust features of the Yukon Coast. *Geographical Bulletin* **13**, 5-21.
- Mackay, J.R., 1971. The origin of massive icy beds in permafrost, western arctic coast, Canada. *Canadian Journal of Earth Sciences* **8**, 397-422.
- Mackay, J.R., 1972a. Offshore permafrost and ground ice, southern Beaufort Sea, Canada. *Canadian Journal of Earth Sciences* **9**, 1550-1561.
- Mackay, J.R., 1972b. The world of underground ice. *Annals of the Association of American Geographers* **62**, 1-22.
- Mackay, J.R., 1973. Problems in the origin of massive ice beds, western Arctic, Canada., in: Permafrost: North American contribution to the second international conference, Yakutsk, U.S.S.R. National Academy of Sciences, Washington, DC, Publication 2115., pp.223-228.
- Mackay, J.R., 1974. Ice-wedge cracks, Garry Island, Northwest Territories. *Canadian Journal of Earth Sciences* **11**, 1366-1383.
- Mackay, J.R., 1976. Ice-wedges as indicators of recent climatic change, western Arctic coast.

- Current Research, Geological Survey of Canada Paper 76-1A, 233-234.
- Mackay, J.R., 1983. Oxygen isotope variations in Permafrost, Tuktoyaktuk peninsula area, Northwest Territories. Geological Survey of Canada, Current Research Part B (Paper 83-1B), 67-74.
- Mackay, J.R., 1989. Massive ice: some field criteria for the identification of ice types. Geological Survey of Canada, Current Research Part G (Paper 89-1G), 5-11.
- Mackay, J.R., 1992. The frequency of ice-wedge cracking (1967-1987) at Garry Island, western Arctic coast, Canada. *Canadian Journal of Earth Sciences* **29**, 236-248.
- Mackay, J.R., Dallimore, S.R., 1992. Massive ice of the Tuktoyaktuk area, western Arctic coast, Canada. *Canadian Journal of Earth Sciences* **29**, 1235-1249.
- Mangerud, J., Jakobsson, M., Alexanderson, H., Astakhov, V., Clarke, G.K.C., Henriksen, M., Hjort, C., Krinner, G., Lunkka, J.-P., Möller, P., Murray, A., Nikolskaya, O., Saarnisto, M., Svendsen, J.I., 2004. Ice-dammed lakes and rerouting of the drainage of northern Eurasia during the Last Glaciation. *Quaternary Science Reviews* **23**, 1313-1332.
- Manley, W.F., Kaufman, D.S., 2002. Alaska PaleoGlacier Atlas. Institute of Arctic and Alpine Research (INSTAAR), University of Colorado [http://instaar.colorado.edu/QGISL/ak_paleoglacier_atlas].
- Mann, D.H., Hamilton, T.D., 1995. Late Pleistocene and Holocene paleoenvironments of the North Pacific coast. *Quaternary Science Reviews* **14**, 449-471.
- Mann, D.H., Peteet, D.M., Reanier, R.E., Kunz, M.L., 2002. Responses of an arctic landscape to Lateglacial and early Holocene climatic changes: The importance of moisture. *Quaternary Science Reviews* **21**, 997-1021.
- Mason, O.K., Bowers, P.M., Hopkins, D.M., 2001. The early Holocene Milankovitch thermal maximum and humans: Adverse conditions for the Denali complex of eastern Beringia. *Quaternary Science Reviews* **20**, 525-548.
- Mathewes, R.W., 1993. Evidence for Younger Dryas-age cooling on the North Pacific coast of America. *Quaternary Science Reviews* **12**, 321-331.
- Matthews, J.V. Jr., 1975. Incongruence of macrofossils and pollen evidence: A case from the late Pleistocene of the northern Yukon Coast. Geological Survey of Canada, Report of Activities, Part B, Paper 75-1B, 139-146.
- Matthews, J.V. Jr., Schweger, C.E., Hughes, O.L., 1990. Plant and insect fossils from the Mayo Indian Village section (Central Yukon): New data on Middle Wisconsinan environments and glaciation. *Géographie physique et Quaternaire* **44**, 15-26.
- McAndrews, J.H., Berti, A.A., Norris, G., 1973. Key to the Quaternary pollen and spores of the Great Lakes region. The University of Toronto Press, Toronto, 61p.
- Melles, M., Brigham-Grette, J., Minyuk, P., Koeberl, C., Andreev, A., Cook, T., Fedorov, G., Gebhardt, C., Haltia-Hovi, E., Kukkonen, M., Nowaczyk, N., Schwamborn, G., Wennrich, V., and the El'gygytgyn Scientific Party., 2011. The Lake El'gygytgyn Scientific Drilling Project – Conquering Arctic Challenges through Continental Drilling. *Scientific Drilling* **11**, 15-40.
- Merlivat, L., Jouzel, J., 1979. Global climatic interpretation of the deuterium-oxygen-18 relationship for precipitation. *Journal of Geophysical Research* **84**, 5029-5033.
- Meyer, H., Dereviagin, A.Y., Siegert, C., Hubberten, H.-W., 2002a. Paleoclimate studies on Bykovsky Peninsula, North Siberia – Hydrogen and oxygen isotopes in ground ice. *Polarforschung* **70**, 37-51.
- Meyer, H., Dereviagin, A.Y., Siegert, C., Schirrmeister, L., Hubberten, H.-W., 2002b. Paleoclimate reconstruction on Big Lyakhovsky Island, north Siberia – Hydrogen and oxygen isotopes in ice wedges. *Permafrost and Periglacial Processes* **13**, 91-105.
- Meyer, H., Schirrmeister, L., Yoshikawa, K., Opel, T., Wetterich, S., Hubberten, H.-W., Brown, J., 2010. Permafrost evidence for severe winter cooling during the Younger Dryas in northern Alaska. *Geophysical Research Letters* **37**, L03501.
- Meyer, H., Schönicke, L., Wand, U., Hubberten, H.-W., Friedrichsen, H., 2000. Isotope studies of hydrogen and oxygen in ground ice – Experiences with the equilibration technique. *Isotopes in Environmental and Health Studies* **36**, 133-149.
- Meyer, H., Yoshikawa, K., Schirrmeister, L., Andreev, A., 2008. The Vault Creek Tunnel (Fairbanks Region, Alaska) – A late Quaternary palaeoenvironmental permafrost record. Ninth International Conference on Permafrost (NICOP), Fairbanks, Alaska, pp.1191-1196.
- Meyers, P.A., 1994. Preservation of elemental and isotopic source identification of sedimentary organic matter. *Chemical Geology* **114**, 289-300.

- Michel, F.A., 1982. Isotope investigations of permafrost waters in Northern Canada. PhD thesis, Dept. of Earth Sciences, University of Waterloo, Canada. 227p.
- Michel, F.A., 1986. Isotope geochemistry of frost-blister ice, North Fork Pass, Yukon, Canada. *Canadian Journal of Earth Sciences* 23, 543-549.
- Michel, F.A., 1990. Isotopic composition of ice-wedge ice in Northwestern Canada. Proceedings of the Fifth Canadian Permafrost Conference. Collection Nordicana, Quebec City, pp.5-9.
- Michel, F.A., Fritz, P., 1978. Environmental isotopes in permafrost related waters along the Mackenzie Valley corridor. *in: Proceedings of the Third International Conference on Permafrost*, National Research Council of Canada, Edmonton, Canada, pp.252-255.
- Michel, F.A., Fritz, P., 1982. Significance of isotope variations in permafrost waters at Illisarvik, NWT. Proceedings of the Fourth Canadian Permafrost Conference, pp.173-181.
- Michel, F.A., Fritz, P., 1983. Isotope variations in permafrost waters along the Dempster Highway Pipeline corridor. *in: Proceedings of the Fourth International Conference on Permafrost*, French HM (Ed.). National Research Council of Canada: Fairbanks, Alaska, pp.843-848.
- Mikolajewicz, U., Crowley, T.J., Schiller, A., Voss, R., 1997. Modelling teleconnections between the North Atlantic and North Pacific during the Younger Dryas. *Nature* 387, 384-387.
- Moore, P.D., Webb, J.A., Collinson, M.E., 1991. Pollen analysis. Blackwell Science, Oxford, 216p.
- Moorman, B.J., Michel, F.A., Wilson, A.T., 1996. ¹⁴C dating of trapped gases in massive ground ice, western Canadian Arctic. *Permafrost and Periglacial Processes* 7, 257-266.
- Moorman, B.J., Michel, F.A., Wilson, A.T., 1998. The development of tabular massive ground ice at Peninsula Point, N.W.T., Canada. *in: Proceedings of the Seventh International Conference on Permafrost*, Lewkowicz AG, Allard M (Eds.). Collection Nordicana No. 57. Yellowknife, Canada, June 1998, pp.757-762.
- Morlan, R.E., Cinq-Mars, J., 1982. Ancient Beringians: Human occupation in the Late Pleistocene of Alaska and the Yukon Territory. *in: Hopkins, D.M., Matthews, J.V. Jr, Schweger, Ch.E., Young, S.B. (Eds.), Paleoecology of Beringia*. Academic Press, New York, pp.353-381.
- Muhs, D.R., Ager, T.A., Begét, J.E., 2001. Vegetation and paleoclimate of the last interglacial period, central Alaska. *Quaternary Science Reviews* 20, 41-61.
- Müller, S., Tarasov, P.E., Andreev, A.A., Tütken, T., Gartz, S., Diekmann, B., 2010. Late Quaternary vegetation and environments in the Verkhoyansk Mountains region (NE Asia) reconstructed from a 50-kyr fossil pollen record from Lake Billyakh. *Quaternary Science Reviews* 29, 2071-2086.
- Murton, J.B., 1996. Morphology and paleoenvironmental significance of Quaternary sand veins, sand wedges, and composite wedges, Tuktoyaktuk Coastlands, Western Arctic Canada. *Journal of Sedimentary Research* 66, 17-25.
- Murton, J.B., 2001. Thermokarst sediments and sedimentary structures, Tuktoyaktuk Coastlands, western Arctic Canada. *Global and Planetary Change* 28, 175-192.
- Murton, J.B., 2005. Ground-ice stratigraphy and formation at North Head, Tuktoyaktuk Coastlands, western Arctic Canada: a product of glacier-permafrost interactions. *Permafrost and Periglacial Processes* 16, 31-50.
- Murton, J.B., 2009. Stratigraphy and palaeoenvironments of Richards Island and the eastern Beaufort Continental Shelf during the last glacial-interglacial cycle. *Permafrost and Periglacial Processes* 20, 107-125.
- Murton, J.B., Bateman, M.D., 2007. Syngenetic sand veins and anti-syngenetic sand wedges, Tuktoyaktuk Coastlands, western Arctic Canada. *Permafrost and Periglacial Processes* 18, 33-47.
- Murton, J.B., Bateman, M.D., Dallimore, S.R., Teller, J.T., Yang, Z., 2010. Identification of Younger Dryas outburst flood path from Lake Agassiz to the Arctic Ocean. *Nature* 464, 740-743.
- Murton, J.B., Frechen, M., Maddy, D., 2007. Luminescence dating of mid- to Late Wisconsinan aeolian sand as a constraint on the last advance of the Laurentide Ice Sheet across the Tuktoyaktuk Coastlands, western Arctic Canada. *Canadian Journal of Earth Sciences* 44, 857-869.
- Murton, J.B., French, H.M., 1994. Cryostructures in permafrost, Tuktoyaktuk Coastlands, western Arctic Canada. *Canadian Journal of Earth Sciences* 31, 737-747.
- Murton, J.B., French, H.M., Lamothe, M., 1997. Late Wisconsinan erosion and eolian deposition, Summer Island area, Pleistocene Mackenzie Delta, Northwest Territories: Optical dating and implications for glacial chronology. *Canadian Journal of Earth Sciences* 34, 190-199.

- Murton, J.B., French, H., M., Lamothe, M., 1998. The dating of thermokarst terrain, Pleistocene Mackenzie Delta, Canada, *in*: Lewkowicz, A.G., Allard, M. (Eds.), Seventh International Permafrost Conference. Nordicana, Yellowknife, NWT, Canada, 23-27 June 1998, pp.777-782.
- Murton, J.B., Kolstrup, E., 2003. Ice-wedges casts as indicators of paleotemperatures: precise proxy or wishful thinking? *Progress in Physical Geography* **27**, 155-170.
- Murton, J.B., Waller, R.I., Hart, J.K., Whiteman, C.A., Pollard, W.H., Clark, I.D., 2004. Stratigraphy and glaciotectonic structures of permafrost deformed beneath the northwest margin of the Laurentide ice sheet, Tuktoyaktuk Coastlands, Canada. *Journal of Glaciology* **50**, 399-412.
- Murton, J.B., Whiteman, C.A., Waller, R.I., Pollard, W.H., Clark, I.D., Dallimore, S.R., 2005. Basal ice facies and supraglacial melt-out till of the Laurentide Ice Sheet, Tuktoyaktuk Coastlands, western Arctic Canada. *Quaternary Science Reviews* **24**, 681-708.
- NCDC National Climatic Data Center. [<http://www.ncdc.noaa.gov/oa/ncdc.html>] (accessed 5 Sept. 2011)
- Nelson, R.E., Carter, L.D., 1987. Paleoenvironmental analysis of insects and extralimital *Populus* from an early Holocene site on the Arctic slope of Alaska, U.S.A. *Arctic and Alpine Research* **19**, 230-241.
- Nelson, R.E., Carter, L.D., Robinson, S.W., 1988. Anomalous radiocarbon ages from a Holocene detrital organic lens in Alaska and their implications for radiocarbon dating and paleoenvironmental reconstructions in the arctic. *Quaternary Research* **29**, 66-71.
- Nikolayev, V.I., Mikhalev, D.V., 1995. An oxygen-isotope paleothermometer from ice in Siberian permafrost. *Quaternary Research* **43**, 14-21.
- Norris, K., 1977. Blow River and Davidson Mountains, Yukon Territory–District of Mackenzie. Geological Survey of Canada, Map 1516A.
- Oechel, W.C., Hastings, S.J., Vourlitis, G., Jenkins, M., Riechers, G., Rulke, N., 1993. Recent change of Arctic tundra ecosystems from a net carbon dioxide sink to a source. *Nature* **361**, 520-523.
- Opel, T., Dereviagin, A.Y., Meyer, H., Schirrmeister, L., Wetterich, S., 2011. Palaeoclimatic information from stable water isotopes of Holocene ice wedges on the Dmitrii Laptev Strait, northeast Siberia, Russia. *Permafrost and Periglacial Processes* **22**, 84-100.
- Osterkamp, T.E., 2005. The recent warming of permafrost in Alaska. *Global and Planetary Change* **49**, 187-202.
- Oswald, W.W., Brubaker, L.B., Anderson, P.M., 1999. Late Quaternary vegetational history of the Howard Pass Area, northwestern Alaska. *Canadian Journal of Botany* **77**, 570-581.
- Otto-Bliesner, B.L., Marshall, S.J., Overpeck, J.T., Miller, G.H., Hu, A., CAPE Last Interglacial Project members, 2006. Simulating Arctic climate warmth and icefield retreat in the last interglaciation. *Science* **311**, 1751-1753.
- Overpeck, J., Hughen, K., Hardy, D., Bradley, R., Case, R., Douglas, M., Finney, B., Gajewski, K., Jacoby, G., Jennings, A., Lamoureux, S., Lasca, A., MacDonald, G., Moore, J., Retelle, M., Smith, S., Wolfe, A., Zielinski, G., 1997. Arctic environmental change of the last four centuries. *Science* **278**, 1251-1256.
- PARCS, 1999. The Arctic paleosciences in the context of global change research - PARCS Paleoenvironmental Arctic sciences. American Geophysical Union, Earth System History, Education & Research Directorate, Washington, D.C., 95p.
- Pienitz, R., Douglas, M.S.V., Smol, J., 2004. Paleolimnological research in polar regions: an introduction, *in*: Pienitz, R., Douglas, M.S.V., Smol, J. (Eds.), Long-term environmental change in Arctic and Antarctic lakes. Springer, Dordrecht, pp.1-17.
- Pienitz, R., Smol, J.P., Last, W.M., Leavitt, P.R., Cumming, B.F., 2000. Multi-proxy Holocene palaeoclimatic record from a saline lake in the Canadian subarctic. *The Holocene* **10**, 673-686.
- Piper, A.M., 1944. A graphic procedure in the geochemical interpretation of water-analyses. *Transactions of the American Geophysical Union* **25**, 914-923.
- Pollard, W.H., 1990. The nature and origin of ground ice in the Herschel Island area, Yukon Territory. *in*: Proceedings of the Fifth Canadian Permafrost Conference. Collection Nordicana, No. 54. Centre d'études Nordiques, Université Laval, Québec, Nordicana Québec; 23-30.
- Pollard, W.H., 1998. Arctic Permafrost and Ground Ice. In: Weatherhead, E., Morseth, C.M. (Eds.) Chapter 11: Climate change, ozone and ultraviolet radiation. Arctic Monitoring and Assessment Program Report.
- Pollard, W.H., 1990. The nature and origin of ground ice in the Herschel Island area, Yukon Territory. Proceedings of the Fifth Canadian

- Permafrost Conference. Collection Nordicana, Québec, pp.23-30.
- Pollard, W.H., Dallimore, S.R., 1988. Petrographic characteristics of massive ground ice, Yukon Coastal Plain, Canada. Proceedings of the Fifth International Conference on Permafrost, 2-5 August 1988, Trondheim, Norway. Tapir Publishers, pp.224-229.
- Preece, S.J., Westgate, J.A., Gorton, M.P., 1992. Compositional variation and provenance of Late Cenozoic distal tephra beds, Fairbanks area, Alaska. *Quaternary International* **13-14**, 97-101.
- Preusser, F., 2003. IRSL dating of K-rich feldspars using the SAR protocol: Comparison with independent age control. *Ancient TL* **21**, 17-23.
- Preusser, F., Kasper, H.U., 2001. Comparison of dose rate determination using high-resolution gamma spectrometry and inductively coupled plasma-mass spectrometry. *Ancient TL* **19**, 17-21.
- Raab, A., Melles, M., Berger, G.W., Hagedorn, B., Hubberten, H.-W., 2003. Non-glacial paleoenvironments and the extent of Weichselian ice sheets on Severnaya Zemlya, Russian High Arctic. *Quaternary Science Reviews* **22**, 2267-2283.
- Rachold, V., Eicken, H., Gordeev, V.V., Grigoriev, M.N., Hubberten, H.-W., Lisitzin, A.P., Shegchenko, V.P., Schirrmeister, L., 2004. Modern terrigenous organic carbon input to the arctic Ocean. in: Stein, R., Macdonald, R.W. (Eds.) *Organic Carbon Cycle in the Arctic Ocean: Present and Past*. Springer. Berlin, pp.33-55
- Rampton, V.N., 1971. Late Quaternary vegetational and climatic history of the Snag-Klutlan area, southwest Yukon Territory, Canada. *Geological Society of America Bulletin* **82**, 959-978.
- Rampton, V.N., 1982. Quaternary geology of the Yukon Coastal Plain. *Geological Survey of Canada Bulletin* **317**, 49 p.
- Rampton, V.N., 1988. Quaternary geology of the Tuktoyaktuk coastlands, Northwest Territories. *Geological Survey of Canada Memoir* **423**, 98p.
- Rampton, V.N., 1991. Observations on buried glacier ice and massive segregated ice, Western Arctic Coast, Canada: Discussion. *Permafrost and Periglacial Processes* **2**, 163-165.
- Rampton, V.N., 2001. Major end moraines of Younger Dryas age on Wollaston Peninsula, Victoria Island, Canadian Arctic: implications for paleoclimate and for formation of hummocky moraine: Discussion. *Canadian Journal of Earth Sciences* **38**, 1003-1006.
- Reimer, P.J., Baillie, M.G., Bard, E., Bayliss, A., Beck, J.W., Blackwell, P.G., Bronk Ramsey, C., Buck, C.E., Burr, G.S., Edwards, R.L., Friedrich, M., Grootes, P.M., Guilderson, T.P., Hajdas, I., Heaton, T.J., Hogg, A.G., Hughen, K.A., Kaiser, K.F., Kromer, B., McCormac, F.G., Manning, S.W., Reimer, R.W., Richards, D.A., Southon, J.R., Talamo, S., Turney, C.S.M., van der Plicht, J., Weyhenmeyer, C.E., 2009. Intcal09 and marine09 radiocarbon age calibration curves, 0–50,000 years cal BP. *Radiocarbon* **51**, 1111-1150.
- Reyes, A.V., Froese, D.G., Jensen, B.J.L., 2010. Permafrost response to last interglacial warming: field evidence from non-glaciated Yukon and Alaska. *Quaternary Science Reviews* **29**, 3256-3274.
- Riseborough, D., Shiklomanov, N., Etmüller, B., Gruber, S., Marchenko, S., 2008. Recent advances in permafrost modelling. *Permafrost and Periglacial Processes* **19**, 137-156.
- Ritchie, J.C., 1984. Past and Present Vegetation of the Far Northwest of Canada. University of Toronto Press, Toronto, 251p.
- Ritchie, J.C., Cwynar, L.C., 1982. The late-Quaternary vegetation of the north Yukon, in: Hopkins, D.M., Matthews, Jr. J.V., Schweger, C.E., Young, S.B. (Eds.), *Paleoecology of Beringia*. Academic Press, New York, pp.113-126.
- Ritchie, J.C., Cwynar, L.C., Spear, R.W., 1983. Evidence from north-west Canada for an early Holocene Milankovitch thermal maximum. *Nature* **305**, 126-128.
- Ritchie, J.C., Hare, F.K., 1971. Late-quaternary vegetation and climate near the arctic tree line of northwestern North America. *Quaternary Research* **1**, 331-342.
- Rozanski, K., Araguas-Araguas, L., Giofanti, R., 1993. Isotopic patterns in modern global precipitation. *Geophysical Monograph* **78**, 1-36.
- Schell, T.M., Scott, D.B., Rochon, A., Blasco, S., 2008. Late Quaternary paleoceanography and paleo-sea ice conditions in the Mackenzie Trough and Canyon, Beaufort Sea. *Canadian Journal of Earth Sciences* **45**, 1399-1415.
- Schirrmeister, L., Grosse, G., Schwamborn, G., Andreev, A.A., Meyer, H., 2003. Late Quaternary history of the accumulation plain north of the Chekanovsky ridge (Lena delta, Russia): A multidisciplinary approach. *Polar Geography* **27**, 277-319.
- Schirrmeister, L., Grosse, G., Wetterich, S., Overduin, P.P., Strauss, J., Schuur, E.A.G., Hubberten, H.-W., 2011. Fossil organic matter

- characteristics in permafrost deposits of the northeast Siberian Arctic. *Journal of Geophysical Research* **116**, G00M02.
- Schirrneister, L., Oezen, D., Geyh, M.A., 2002a. ²³⁰Th/^U Dating of frozen peat, Bol'shoy Lyakhovsky Island (Northern Siberia). *Quaternary Research* **57**, 253-258.
- Schirrneister, L., Siegert, C., Kunitzky, V., Grootes, P., Erlenkeuser, H., 2002b. Late Quaternary ice-rich permafrost sequences as a paleoenvironmental archive for the Laptev Sea Region in northern Siberia. *International Journal of Earth Sciences* **91**, 154-167.
- Schirrneister, L., Siegert, C., Kuznetsova, T., Kuzmina, S., Andreev, A., Kienast, F., Meyer, H., Bobrov, A., 2002c. Paleoenvironmental and paleoclimatic records from permafrost deposits in the Arctic region of Northern Siberia. *Quaternary International* **89**, 97-118.
- Schwamborn, G., Fedorov, G., Schirrneister, L., Meyer, H., Hubberten, H.-W., 2008. Periglacial sediment variations controlled by late Quaternary climate and lake level change at Elgygytgyn crater, Arctic Siberia. *Boreas* **37**, 55-65.
- Schwamborn, G., Meyer, H., Fedorov, G., Schirrneister, L., Hubberten, H.-W., 2006. Ground ice and slope sediments archiving late Quaternary paleoenvironment and paleoclimate signals at the margins of El'gygytgyn impact crater, NE Siberia. *Quaternary Research* **66**, 259-272.
- Schwamborn, G., Rachold, V., Grigoriev, M.N., 2002. Late Quaternary sedimentation history of the Lena Delta. *Quaternary International* **89**, 119-134.
- Schweger, C.E., Matthews, J.V., 1985. Early and Middle Wisconsinan environments of Eastern Beringia: Stratigraphic and paleoecological implications of the Old Crow Tephra. *Géographie physique et Quaternaire* **39**, 275-290.
- Scott, D.B., Schell, T., St-Onge, G., Rochon, A., Blasco, S., 2009. Foraminiferal assemblage changes over the last 15,000 years on the Mackenzie-Beaufort Sea Slope and Amundsen Gulf, Canada: Implications for past sea ice conditions. *Paleoceanography* **24**, PA2219.
- Serreze, M.C., Barrett, A.P., Stroeve, J.C., Kindig, D.N., Holland, M.M., 2009. The emergence of surface-based Arctic amplification. *The Cryosphere* **3**, 11-19.
- Serreze, M.C., Francis, J., 2006. The Arctic amplification debate. *Climatic Change* **76**, 241-264.
- Sher, A.V., Kuzmina, S.A., Kuznetsova, T.V., Sulerzhitsky, L.D., 2005. New insights into the Weichselian environment and climate of the East Siberian Arctic, derived from fossil insects, plants, and mammals. *Quaternary Science Reviews* **24**, 533-569.
- Siegert, M.J., Dowdeswell, J.A., Hald, M., Svendsen, J.-I., 2001. Modelling the Eurasian Ice Sheet through a full (Weichselian) glacial cycle. *Global and Planetary Change* **31**, 367-385.
- Smith, A.J., Delorme, L.D., 2010. Chapter 19 - Ostracoda, in: Thorp, J.H., Covich, A.P. (Eds.), Ecology and classification of North American freshwater invertebrates (Aquatic Ecology). Elsevier, London, pp.725-771.
- Smith, C.A.S., Kennedy, C.E., Hargrave, A.E., McKenna, K.M., 1989. Soil and vegetation of Herschel Island, Yukon Territory. Yukon Soil Survey Report No. 1. Land Resource Research Centre, Agriculture Canada, Ottawa, 101p.
- Smith, L.C., MacDonald, G.M., Velichko, A.A., Beilman, D.W., Borisova, O.K., Frey, K.E., Kremenetski, K.V., Sheng, Y., 2004. Siberian peatlands a net carbon sink and global methane source since the early Holocene. *Science* **303**, 353-356.
- Smith, S.L., Burgess, M.M., 2000. Ground temperature database for northern Canada. Geological Survey of Canada Open File Report 3954, 57p.
- Smol, J.P., 2002. Pollution of lakes and rivers: A paleoenvironmental perspective. Arnold Publishers, London, 280p.
- Smol, J.P., Cumming, B.F., 2000. Tracking long-term changes in climate using algal indicators in lake sediments. *Journal of Phycology* **36**, 986-1011.
- Souchez, R.A., Jouzel, J., Lorrain, R., Sleewaegen, S., Stiévenard, M., Verbeke, V., 2000. A kinetic isotope effect during ice formation by water freezing. *Geophysical Research Letters* **27**. 1923-1926.
- Souchez, R.A., Lemmens, M., Lorrain, R., Tison, J.L., Jouzel, J., Sugden, D., 1990. Influence of hydroxyl-bearing minerals on the isotopic composition of ice from the basal zone of an ice sheet. *Nature* **345**, 244-246.
- Spear, R.W., 1993. The palynological record of Late-Quaternary arctic tree-line in northwest Canada. *Review of Palaeobotany and Palynology* **79**, 99-111.
- St-Jean, M., Lauriol, B., Clark, I.D., Lacelle, D., Zdanowicz, C., 2011. Investigation of ice-wedge

- infilling processes using stable oxygen and hydrogen isotopes, crystallography and occluded gases (O₂, N₂, Ar). *Permafrost and Periglacial Processes* **22**, 49-64.
- Stuiver, M., Reimer, P.J., 1993. Extended ¹⁴C data base and revised CALIB 3.0 ¹⁴C age calibration program. *Radiocarbon* **35**, 215-230.
- Suzuoki, T., Kimura, T., 1973. D/H and ¹⁸O/¹⁶O fractionation in ice-water systems. *Mass Spectroscopy* **21**, 229-233.
- Svendsen, J.I., Alexanderson, H., Astakhov, V.I., Demidov, I., Dowdeswell, J.A., Funder, S., Gataullin, V., Henriksen, M., Hjort, C., Houmark-Nielsen, M., Hubberten, H.-W., Ingólfsson, Ó., Jakobsson, M., Kjær, K.H., Larsen, E., Lokrantz, H., Lunkka, J.P., Lyså, A., Mangerud, J., Matiouchkov, A., Murray, A., Möller, P., Niessen, F., Nikolskaya, O., Polyak, L., Saarnisto, M., Siegert, C., Siegert, M.J., Spielhagen, R.F., Stein, R., 2004. Late Quaternary ice sheet history of northern Eurasia. *Quaternary Science Reviews* **23**, 1229-1271.
- Svendsen, J.I., Astakhov, V.I., Bolshiyakov, D.Y., Demidov, I., Dowdeswell, J.A., Gataullin, V., Hjort, C., Hubberten, H.W., Larsen, E., Mangerud, J., Melles, M., Möller, P., Saarnisto, M., Siegert, M.J., 1999. Maximum extent of the Eurasian ice sheets in the Barents and Kara Sea region during the Weichselian. *Boreas* **28**, 234-242.
- Swain, F.M., 1963. Ostracoda from the Gubik Formation, Arctic Coastal Plain, Alaska. *Journal of Paleontology* **37**, 798-834.
- Szeicz, J.M., MacDonald, G.M., 2001. Montane climate and vegetation dynamics in easternmost Beringia during the Late Quaternary. *Quaternary Science Reviews* **20**, 247-257.
- Szeicz, J.M., MacDonald, G.M., Duk-Rodkin, A., 1995. Late Quaternary vegetation history of the central Mackenzie Mountains, Northwest Territories, Canada. *Palaeogeography, Palaeoclimatology, Palaeoecology* **113**, 351-371.
- Tarasov, L., Peltier, W.R., 2005. Arctic freshwater forcing of the Younger Dryas cold reversal. *Nature* **435**, 662-665.
- ter Braak, C.J.F., Šmilauer, P., 2002. CANOCO reference manual and CANODRAW for Windows user's guide: Software for canonical community ordination (Version 4.5). Microcomputer Power, New York, 500p.
- Vaikmäe, R., 1989. Oxygen isotopes in permafrost and in ground ice - A new tool for paleoclimatic investigations, 5th Working Meeting Isotopes in Nature, Leipzig, September 1989, pp.543-551.
- Vaikmäe, R., 1991. Oxygen-18 in permafrost ice, in: IAEA (Ed.), International Symposium of the Use of Isotope Techniques in Water Resources Development. International Atomic Energy Agency, 11-15 March 1991. Vienna.
- van Everdingen, R.O. (Ed.), 1998. Multi-language glossary of permafrost and related ground-ice terms. National Snow and Ice Data Center/World Data Center for Glaciology, Boulder. (available at <http://nsidc.org/fgdc/glossary>)
- Vardy, S.R., Warner, B.G., Aravena, R., 1997. Holocene climate effects on the development of a peatland on the Tuktoyaktuk Peninsula, Northwest Territories. *Quaternary Research* **47**, 90-104.
- Vardy, S.R., Warner, B.G., Aravena, R., 1998. Holocene climate and the development of a subarctic peatland near Inuvik, Northwest Territories, Canada. *Climatic Change* **40**, 285-313.
- Vardy, S.R., Warner, B.G., Turunen, J., Aravena, R., 2000. Carbon accumulation in permafrost peatlands in the Northwest Territories and Nunavut, Canada. *The Holocene* **10**, 273-280.
- Vasil'chuk, Y.K., 1991. Reconstruction of the paleoclimate of the late Pleistocene and Holocene on the basis of isotope studies of subsurface ice and waters of the permafrost zone. *Water Resources* **17**, 640-674.
- Vasil'chuk, Y.K., van der Plicht, J., Jungner, H., Sonninen, E., Vasil'chuk, A.C., 2000. First direct dating of Late Pleistocene ice-wedges by AMS. *Earth and Planetary Science Letters* **179**, 237-242.
- Vasil'chuk, Y.K., Jungner, H., Vasil'chuk, A.C., 2001. ¹⁴C dating of peat and δ¹⁸O-δD in ground ice from northwest Siberia. *Radiocarbon* **43**, 527-540.
- Vasil'chuk, Y.K., Vasil'chuk, A.C., 1997. Radiocarbon dating and oxygen isotope variations in Late Pleistocene syngenetic ice-wedges, Northern Siberia. *Permafrost and Periglacial Processes* **8**, 335-345.
- Vasil'chuk, Y.K., Vasil'chuk, A.C., 1998. Oxygen-isotope and C¹⁴ data associated with Late Pleistocene syngenetic ice-wedges in mountains of Magadan region, Siberia. *Permafrost and Periglacial Processes* **9**, 177-183.
- Vermaire, J.C., Cwynar, L.C., 2010. A revised late-Quaternary vegetation history of the unglaciated southwestern Yukon Territory, Canada, from Antifreeze and Eikland ponds. *Canadian Journal of Earth Sciences* **47**, 75-88.

- Viau, A.E., Gajewski, K., Sawada, M.C., Bunbury, J., 2008. Low- and high-frequency climate variability in eastern Beringia during the past 25000 years. *Canadian Journal of Earth Sciences* **45**, 1435-1453.
- von Toll EV. 1897. Iskopaemye ledniki Novo-Sibirskikh ostrovov, ikh otnoshenie k trupam mamontov i k lednikovomu periodu (Ancient glaciers of New Siberian Islands, their relation to mammoth corpses and the Glacial period). *Zapiski Imperatorskogo Russkogo Geograficheskogo obshestva po obshei geografii* (Notes of the Russian Imperial Geographical Society) **32**, 1-137 (in Russian).
- Wahl, H.E., Fraser, D.B., Harvey, R.C., Maxwell, J.B., 1987. Climate of Yukon. Environment Canada, Atmospheric Environment Service, *Climatological Studies* **40**, 1-323.
- Walter, K.M., Zimov, S.A., Chanton, J.P., Verbyla, D., Chapin, F.S., 2006. Methane bubbling from Siberian thaw lakes as a positive feedback to climate warming. *Nature* **443**, 71-75.
- Wang, X.-C., Geurts, M.-A., 1991. Late Quaternary pollen records and vegetation history of the southwest Yukon Territory: A review. *Géographie physique et Quaternaire* **45**, 175-193.
- Ward, B.C., Bond, J.D., Froese, D., Jensen, B., 2008. Old Crow tephra (140 ± 10 ka) constrains penultimate Reid glaciation in central Yukon Territory. *Quaternary Science Reviews* **27**, 1909-1915.
- Washburn, A.L., 1979. *Geocryology. A survey of periglacial processes and environment*. London, 406p.
- Webb, R.S., Webb III, T., 1988. Rates of sediment accumulation in pollen cores from small lakes and mires of eastern North America. *Quaternary Research* **30**, 284-297.
- Welsh, S. L., Rigby, J.K., 1971. Botanical and physiographic reconnaissance of northern Yukon. *Biological Series* **14**, 64p.
- Westgate, J.A., Hamilton, T.D., Gorton, M.P., 1983. Old Crow tephra: A new Pleistocene stratigraphic marker across north-central Alaska and Western Yukon Territory. *Quaternary Research* **19**, 38-54.
- Westgate, J.A., Walter, R.C., Pearce, G.W., Gorton, M.P., 1985. Distribution, stratigraphy, petrochemistry, and palaeomagnetism of the late Pleistocene Old Crow tephra in Alaska and the Yukon. *Canadian Journal of Earth Sciences* **22**, 893-906.
- Wetterich, S., Grosse, G., Schirrmeyer, L., Andreev, A.A., Bobrov, A., Kienast, F., Bigelow, N.H., Edwards, M.E., (submitted to *Quaternary Science Reviews*) Late Quaternary environmental and landscape dynamics revealed from a pingo sequence on the northern Seward Peninsula, Alaska.
- Wetterich, S., Rudaya, N., Tumskey, V., Andreev, A.A., Opel, T., Schirrmeyer, L., Meyer, H., 2011. Last Glacial Maximum records in permafrost of the East Siberian Arctic. *Quaternary Science Reviews* **30**, 3139-3151.
- Whitmore, J., Gajewski, K., Sawada, M., Williams, J.W., Minckley, T., Shuman, B., Bartlein, P.J., Webb III, T., Viau, A.E., Shafer, S., Anderson, P., Brubaker, L.B., 2005. A North American modern pollen database for multi-scale paleoecological and paleoclimatic applications. *Quaternary Science Reviews* **24**, 1828-1848.
- Yokoyama, Y., Lambeck, K., De Deckker, P., Johnston, P., Fifield, L.K., 2000. Timing of the Last Glacial Maximum from observed sea-level minima. *Nature* **406**, 713-716.
- Yu, Z., Walker, K.N., Evenson, E.B., Hajdas, I., 2008. Lateglacial and early Holocene climate oscillations in the Matanuska Valley, south-central Alaska. *Quaternary Science Reviews* **27**, 148-161.
- Zazula, G.D., Duk-Rodkin, A., Schweger, C.E., Morlan, R.E., 2004. Late Pleistocene chronology of glacial Lake Old Crow and the north-west margin of the Laurentide Ice Sheet, in: Ehlers, J., Gibbard, P.L. (Eds.), *Quaternary Glaciations - Extent and Chronology, Part II: North America*. Elsevier, Amsterdam, pp.347-362.
- Zazula, G.D., Hare, P.G., Storer, J.E., 2009. New radiocarbon-dated vertebrate fossils from Herschel Island: Implications for the palaeoenvironments and glacial chronology of the Beaufort Sea coastlands. *Arctic* **62**, 273-280.
- Zdanowicz, Ch., Fisher, D.A., Clark, I., Lacelle, D., 2002. An ice-marginal ^{18}O record from Barnes Ice Cap, Baffin Island, Canada. *Annals of Glaciology* **35**, 145-149.
- Zhang, T., Barry, R.G., Knowles, K., Heginbottom, J.A., Brown, J., 1999. Statistics and characteristics of permafrost and ground - ice distribution in the Northern Hemisphere. *Polar Geography* **23**, 132-154.

Note: The reference list has been updated and arranged according to the structure of the thesis. Therefore, slight differences to citations in the already published original paper may occur.

Acknowledgements

This thesis would not exist in this form without the scientific and private support of so many people over the last years. My warmest thanks to all of you!

Lutz Schirrmeister – Thank you for your steady guidance through the thicket people call a doctorate, for your never-ending scientific ideas, for your extraordinary problem-solving competence, for the plethora of fatherly advice, and for your enormous efforts for each of your PhD students.

Hans-Wolfgang Hubberten – I thank you for your excellent and continuous support and for the treasure of possibilities and resources I was able to use. Moreover, I very much enjoyed the working atmosphere in your department.

Hugues Lantuit – Conducting joint expeditions, writing numerous third-party applications, hanging out together on conferences, having completely fanciful ideas that suddenly become reality. All this could fill pages and I have learned so much.

Hanno Meyer and **Thomas Opel** – Without you, stable water isotopes and deuterium excess considerations would remain a mystery, probably for ever.

Ulrike Herzsuh – Thank you for numerous joint strategic reflections and most notably for your guidance while learning palynology and multivariate statistical methods.

Sebastian Wetterich – You are/were the structure-giving constant in all manuscripts and I thank you for the great time in the Canadian Arctic.

Georg Schwamborn – I am impressed of your fatalistic attitude in life that helped me to sharpen the personal view on the essentials in life.

And many thanks to all the young enthusiastic **AWI-colleagues** (Lars Ganzert, Mathias Ulrich, Andreas Borchers, Josefine Lenz, Jens Strauß, Frank Günther, Boris Biskaborn, Stephan Opitz, Mare Pit, Liv Heinecke, Juliane Klemm) for the great time together during scientific discussions, at BBQs, in the Waschbar, and during numerous coffee breaks.

I also highly acknowledge the technical support in the lab and friendship provided by **Antje Eulenburg** and **Ute Bastian**. Strongly appreciated is the help during lab work by **Christiane Funk**, **Dennis Bunke**, **George Tanski**, and **Cordula Teschner**.

I am very grateful to **Bernd Wagner**, **Sabrina Ortlepp**, **Sonja Berg**, and **Hendrik Vogel** from the working group for Quaternary geology at the University of Cologne, led by **Martin Melles**. I had so much fun and learned a lot during our drilling campaigns and in Cologne.

The most gorgeous part of such a PhD project is, without any doubt, the field component. I am highly indebted to **Wayne Pollard** (McGill University of Montréal) for his scientific and logistical support of our joint projects in Canada and to **Nicole Couture** (Geological Survey of Canada) for managing big chunks of our expeditions. I enjoyed the time and inspiring moments being in the Arctic together with **Michael Angelopoulos**, **Gregory De Pascale**, **Nicolas Arkell**, and **Samuel McLeod**. Mein besonderer Dank gilt **Gerald Müller** für das technische Geschick am Uwitec und für die unglaublichen Geschichten aus Natur, Alltag und bislang ungeschriebener deutsch-deutscher Expeditionsgeschichte.

Furthermore, I am delighted by the helpfulness provided by **Pippa Secombe-Hett**, **William Hurst**, and **Donald Ross** (Aurora Research Institute –ARI) in Inuvik and the help we received on Herschel Island from chief Ranger **Richard Gordon** and his colleagues **Lee-John Meyook**, **Edward McLeod** and **Jordan McLeod**.

I thank **Julian Murton**, **Reinhard Pienitz**, **John England**, **Chris Burn**, **Steve Blasco**, **Don Forbes**, **Steve Solomon**, **Scott Dallimore**, **Tanja Giberien**, **Inga May**, **Nicolas Rolland**, and **Dave Fox** for the inspiring discussions about the Arctic in Inuvik and on conferences. And I thank **Martin Jakobsson** for sending me data on the Eurasian Ice Sheet at the very last minute.

I am highly indebted to the **German Federal Environmental Foundation (DBU)** for granting me a PhD fellowship; especially to **Nicole Freyer**, **Hans-Christian Schaefer** and **Maximilian Hempel**, who were always within reach for me.

Special thanks go to the Graduate School for Polar and Marine Research (**POLMAR**), primarily to **Claudia Hanfland** and **Claudia Sprengel** for the plethora of supplementary academic education possibilities. This graduate program is a true enrichment for every PhD.

Der größte Dank gilt meinem familiären Umfeld, insbesondere meinen Eltern, die mich nicht nur immer finanziell unterstützt, sondern es auch geschafft haben, die Alltagsorgen von mir zu nehmen.

Zum Glück hat meine kleine Familie ganz andere Aspekte des täglichen Lebens zum Mittelpunkt. So war an den Abenden und Wochenenden, abseits der Arbeit, kein Platz und keine Zeit, um sich über so vermeintlich wichtige Dinge wie eine Promotion Gedanken zu machen.

Alex und Janne, vielen Dank dafür!

Eidesstattliche Erklärung

Hiermit erkläre ich, die vorliegende Dissertation selbständig verfasst und keine anderen als die angegebenen Quellen und Hilfsmittel verwendet zu haben. Die Dissertation wird erstmalig und nur an der Universität Potsdam eingereicht.

Die dem Verfahren zugrunde liegende Promotionsordnung ist mir bekannt.

Potsdam, 18. Oktober 2011

Michael Fritz